G29–38 AND THE ADVENT OF COOL DAV ASTEROSEISMOLOGY

by

SCOT JAMES KLEINMAN, B.S., M.A.

DISSERTATION

Presented to the Faculty of the Graduate School of

The University of Texas at Austin

in Partial Fulfillment

of the Requirements

for the Degree of

DOCTOR OF PHILOSOPHY

THE UNIVERSITY OF TEXAS AT AUSTIN

August 1996

G29–38 AND THE ADVENT OF COOL DAV ASTEROSEISMOLOGY

APPROVED BY
DISSERTATION COMMITTEE:

Supervisor: _____

_____

_____

_____

_____

In the memory of Art Smothers who taught me the beauty and the value of words, carefully chosen and slyly taught me to enjoy math through dominoes; Raymond Kleinman whom I am grateful to have met, but sorry it was so late in his life; Martha Kleinman, who constantly encouraged me to explore my interest in science and the world around us, and Maria Good who helped make the daily bureaucracy of the University transparent to many a clueless graduate student.

I also dedicate this work to my family and friends who give these words true meaning.

Acknowledgements

I need a miracle every day.
— Bob Weir & John Barlow, *I Need a Miracle*

There are many people whose help, knowledge, time, generosity, and simply kindness, have if not directly contributed to the science of this work, have kept me sane in the process. I can only attempt to offer them all appropriate thanks here.

I have been blessed by a truly supportive family. Grandma may have not bothered to correct her friends when they heard her saying *Harvard Med* instead of *Harvey Mudd*, but she never questioned her grandson's strange desire (or attire, for that matter) to spend nearly an eternity to study something seemingly so far removed from daily life. Grandad always asked about my work and both of them (and Uncle Bill) read all the astronomy articles that appeared in the paper, so they could stump me whenever I found my way home.

Mom has always been there, offering support in any way it was needed, whether it was requested or not. She always seemed to understand what was important to me without really asking. I am grateful for such support, love, and understanding.

Dad, too, has encouraged me, even as a child, to pursue my interests and succeed. He has taught me to do the best you can in whatever you do. Both Mom and Dad have lead by example. Dad's other $upport was also deeply appreciated and made life possible when it often seemed not.

Brothers Bret and Craig were out earning a real living, living real lives, while their younger brother remained in school. They accepted this role and have always lived up to the reputations of big brothers.

Sovanna Lieou deserves special recognition for her unquestioning acceptance of my work and tacit support. Her family also provided a (large) local family, while my blood relatives were far away.

I could not have asked for better advisors than Ed and Don. Ed was my official advisor, but the two are a package deal, and I am grateful to have received support from Don as a co-advisor throughout this work. Both men are wonderful scientists who need only to teach by example. Ed's attention to detail, careful mental modelling (being careful to always distinguish the model form the observations), and use of the English language will always remain with me. I can only strive to improve myself in these areas.

Don's enthusiasm and zest for science is contagious. His ability to create models and be personally unattached to them is a rare and gifted talent. He inspires confidence and an effort to always proceed as true to the scientific method as possible.

The other WET members around the world are too numerous to mention, but my interactions with them are treasured and have significantly

contributed to this work.

The WET lab forms an incredible working unit. Old students helping new students who eventually end up helping the old students in turn. Even after they graduate, the ex-WET-students stay in touch and have never turned down a request for help. Their help is just as often philosophical as it is scientific. Topics discussed can vary from how to talk to an advisor in a bad mood to what exactly is a $C_{\ell,k}$. Thanks to all of these students including Butler Hine, Matt Wood, Chris Clemens, Paul Bradley, Chuck Claver, Judi Provencal, Antonio Kanaan, Mike Montgomery, Atsuko Nitta, and Todd Watson.

In particular, Chris has been a continuing source of inspiration and an early mentor and I am grateful for all his help and discussions. It's just too bad we didn't get that stock a year earlier.... I thank Paul especially for the models and calculations he helped with towards the end of this thesis. He was also an invaluable source of references, as was Gerald Handler, visiting from Vienna. Chuck has also provided continuing encouragement and was an invaluable resource during the design of the *phatphot*. His spaghetti isn't bad, either. Judi taught me the fundamentals of data reduction when I first started working with the lab. She also shrivelled in Mexico and has shared many good times since. Antonio, besides being a VI wizard (now using emacs in VI-emulation mode — go figure) always knew something about whatever I asked him. When he didn't know exactly what I needed, he (or we) looked it up and we learned together. You can't ask for much better help than that.

Mike, despite being a fairly serious theorist (with a foosball in his pocket), was usually able to explain things in a way even an observer could understand and never tired in trying if I at first did not get it. Atsuko, too, helped me learn answers to questions we did not know and was always encouraging, even when I felt little enthusiasm myself. She has made the lab a brighter place, and has kept me alive in these last difficult years. Todd's love of observing was refreshing and his willingness to discuss anything were greatly appreciated. I thank him, along with Ed, Don, Chris, Paul, Judi, and Chuck for helping me with the user interface of the phatphot. Many of this WET crew also helped me collect data. I mention them by name in Chapter 3 but want to thank them again here. All of them made working in the lab fun. I was rarely seen in my office because of it!

My class was a class of 13 entering students in 1987. Paul, Chuck, and Judi, I have already mentioned. This group of 13 was remarkably cohesive and we all helped each other through the process. Dean was a good friend and offered not only diversion, but an ideal and an attitude about science. Bob never tired of doing things right and always listened when I needed to talk. Jay never really appreciated the Velvet Elvis, but I appreciate his putting up with my antics. Kim listened to a lot more than she really wanted to, probably, but offered sound advice and needed insight. She has helped me a lot through difficult times and I am indeed grateful. I hope we all can continue our friendship despite the different circumstances in which we will all find ourselves. Seeing as how I am the last one left, and I am still corresponding with the others, I suspect we will, and I am happy to say it.

Through the WET, I have had the pleasure of meeting and working with such now-friends as Jurek "goraco" Krzesinski, Kouji Yanagida, Gerald Handler and Jiang Xiaojun. Many good times, both here, and in their home country were had and I am grateful for the insights in to the world they have offered me. Their help and friendship mean a lot to me. I also should mention Lori Allen, whom I met while working at NASA/Ames. She is to blame for my intense, but fun, observing schedule. Radio!

Tom Phillips, Jimmy Welborn, George Barczak, David Boyd, and John Booth have all contributed immensely to my instrumental work. Never too busy to help, they have given me excellent teachings and equally excellent work. Mark Cornell deserves thanks for tirelessly solving computer problems. He is a valuable department resource.

Dave Way's contribution goes beyond his computer knowledge to include many stress-relieving, life-enjoying, breeze-shooting boat rides and water skiing. Water sports are an important part of life. Dave Nelson also lives by this motto and his spontaneous trips to the lake were always welcomed.

Maria Good helped in almost every way possible and I know I am not alone when I say she is sorely missed.

Gil Reinin, Mike Kang, Tom "Frank Bob" Mahnke, and Matt Schlegel, whose friendships predate my arrival in Austin, helped me stay balanced and in tune to the rest of the world. Their friendships have been eternal lights.

Finally, I thank Elvis Presley, James Brown, Otis Redding, Muddy Waters, Robert Cray, Jerry Garcia and the Grateful Dead, Pete Townshend,

and Paul Weller (amongst thousands of others) for helping to provide life's musical accompaniment.

Preface

Science is rarely an individual effort. Ideas and work often originate, and are almost always improved, by collaboration with others. In this sense, the pronoun *I* is almost never an accurate reflection all the effort going into a scientific endeavor. Nonetheless, individuals do generate ideas and perform tasks, and in these cases, the use of *I* is appropriate. I also find the general abuse of the royal *we* to be very annoying. In this work, I have adhered to no convention and freely use both pronouns. Where I was clearly able to separate things that I did or initiated primarily by myself, I describe them with *I*. Where ideas or work were helped or improved significantly by group effort, I use *we*. The actual group of people implied by each *we*, of course, varies. It may be we, the Whole Earth Telescope; we, my advisors (Ed and Don) and I; we, another student an I; or we, any possible other group. Where neither *I* or *we* flowed freely from my fingertips, I simply chose one nearly at random. I made no effort to be consistent in my usage of these terms and am not offering an apology for it here.

My position in the Whole Earth Telescope operations center at the University of Texas Astronomy department, dating from the first (Xcov1) WET campaign, means I have insights and information about the WET and its results that may not have been previously published. I have sprinkled such tidbits of information throughout this text, citing no reference for the

information, because there are not any.

G29–38 AND THE ADVENT OF COOL DAV ASTEROSEISMOLOGY

Publication No. _____

Scot James Kleinman, Ph.D.
The University of Texas at Austin, 1996

Supervisor: R.E. Nather

The history of our galaxy and a record of stellar evolution is hidden within the white dwarf stars. The white dwarfs are the most numerous members of the stellar graveyard, stars whose luminosity is no longer powered by nuclear processes. They are simple stars. They cool and radiate away their heat. The coolest observed white dwarf is also the oldest. They take time to cool: the coolest are not any cooler because the Universe has not been around long enough for them to cool any further. If we can measure their rate of cooling, we can measure their age. By choosing the coolest observed stars to measure, we can get a lower limit for the age of the galaxy.

The white dwarfs have a very narrow mass distribution, yet their progenitors must have a wide range of initial masses. Somehow, they must lose a substantial portion of their mass in the process, yet still end up with the same final mass. Inside the white dwarfs are the products of stellar evolution and previous nucleosynthesis. Uncertain nuclear reaction rates aside, were we to measure the composition and structure of the white dwarfs, we would gain

great insights into the processes of nucleosynthesis and the mechanisms of mass loss.

Fortunately, the white dwarfs give us ample opportunity to make such measurements. At three places along the white dwarf cooling track, they become unstable to non-radial, g-mode pulsations. Performing asteroseismology, analogous to terrestrial seismology, we can reveal the innards of the white dwarfs through their oscillations. Secular cooling also changes the pulsation properties. Measure these changes and we have measured their cooling rates.

The Whole Earth Telescope, a new tool designed to make these measurements on the variable white dwarfs, has enjoyed remarkable successes with two of the three white dwarf instability strips. The remaining strip, the cool DAVs, proved mysterious. Clemens has recently shown the hotter members of the DAVs can be solved by studying their group properties. The cooler DAVs, whose modes are more numerous, though unstable, could not be included in this picture. Their unstable nature made us wonder if they could ever be used for asteroseismological measurements.

By gathering multiple years of data on one DAV, G29–38, I show there is indeed an underlying stable structure of modes that can be used for asteroseismological measurements. I also use data on additional DAVs similar to G29–38 that show they are all remarkably alike: they share the same modes of oscillation. Although existing theoretical models to match with the data are few and incomplete, I use what is available to derive preliminary parameters

of these cool white dwarfs. I find them consistent with having thick (near $10^{-4}M_{\star}$) H layers, although then the asteroseismological and spectroscopic masses for G29–38 disagree.

The result of this effort opens the last major frontier of white dwarf asteroseismology. All the DAVs, the coolest and the oldest of the known white dwarf variables, are open and available for asteroseismological analysis.

Table of Contents

Table of Tables

List of Figures

Chapter 1

Introduction

Bound to cover just a little more ground.
—Jerry Garcia & Robert Hunter, *The Wheel*

1. Who?

Perhaps the most fundamental questions of all astronomy, if not all mankind, question our very existence: how and why did we get here? It is not at all obvious, unfortunately, how to find answers to such questions. Where do we start?

Imagine a group of aliens visiting Earth and wanting to understand humans. If they are here for a short time, they will not have time to watch us being born, grow, live, and die. What then would be the most efficient way for them to learn about our life cycle?

They could sneak into a hospital's maternity ward and kidnap a number of new-borns, seeing us in our newly born state, but without the knowledge and abilities that we develop and use in the rest of our lives.

Perhaps taking off with a classroom of Astronomy 301 students (as long as they accelerated the classroom at 9.8 m/s^2 they wouldn't notice) for further laboratory analysis would be useful. The aliens would know the undergraduates were in a transition state, but which way they were evolving would be uncertain. Or perhaps they would invade a few funeral homes and capture some recently-deceased corpses. Here, they would not be misled by temporary transitions in life (do all human females wear large bows?) and would see the end-product of the human life. Sure, they would not learn about the stages of human life, but they would have boundary conditions. They would see the accumulation of a lifetime, not just the initial ingredients. Whatever theory they develop from their studies must end up as their stolen corpses.

In our quest for knowledge of the Universe, we are a bit more fortunate[1] than the visiting aliens in that we have some idea at least of the ordering of the cosmos. We can distinguish young stars from old stars. But we still have problems with the intermediate stars. How exactly do they work and where do they go?

At least some of the clues to these questions lie in the white dwarf stars, the equivalent of stellar corpses. Uncomplicated by such worrisome problems as nucleosynthesis, they are simple objects, relatively easy to understand. They are dense objects with a very large surface gravity and hence, are nearly as spherical as a theoretician's cow. This spherical symmetry allows other

[1]But only because we have been studying the stars for a long time. Our advantage is hard won.

complications such as rotation and magnetic fields to be treated as simple perturbations.

They are the end points of stellar evolution: if we could learn the secrets of their interiors, we would know the products of the nuclear burning that took place in more lively days of the stars' lives. They are old; there are no older stars than the coolest white dwarfs.[2] Their age, then, tells us how long ago star formation began. We can date the Universe by dating the white dwarfs within it.

2. What?

The aliens take off with their corpses, and we are left with the white dwarfs. But this is where our similarity ends for how do we cut open a white dwarf for investigation? Short of a binary white dwarf supernova explosion (in which case we are learning about specific white dwarfs — only those in binaries — and not the more general case of the single white dwarf), astronomical observations are limited to the surfaces of stars. How then to probe the interior?

It is here we will make another analogy, this time closer to Earth. Seismologists explore the earth's interior with earthquakes. By studying how the waves of displacement travel through the Earth after an earthquake, they learn about the internal structure and composition of the planet.

---

[2]The local observed white dwarf luminosity function, the number of observed white dwarfs of a given luminosity (or, equivalently, temperature) per volume of space, has a sharp drop-off at low luminosities. This is most directly interpreted as a measurement of the age of the local galactic disk. The white dwarfs simply have not had time to cool any farther.

A bell-maker knows the same physics as the seismologist, although perhaps at a more practical level. Take two bells, identical except for the material from which they are made, and they will sound different. The different harmonics and overtones produced by each bell give it a distinct sound. Each material we could choose for our bells would have a different sound. Analyze the sound, and learn about the material. The Stradivarius violin is another example; its structure and material directly affect its sound.

White dwarfs do not have earthquakes (or even starquakes) so far as we know, but they do something even better. As they cool (which is what white dwarfs do best), they pass through four instability regions, four regions where they become unstable to pulsations. It is through the study of these pulsations, and how they propagate through the star, that the analogy to Earthly seismology is made. The field of asteroseismology, studying pulsations on stars as a means to explore their internals, takes over.

The goal of asteroseismology is simple: use the pulsations as probes beneath the surface of the white dwarf. From there, we can determine a star's composition and structure while making precise measurements of mass, rotation, and magnetic field at the same time. With this information, we have a detailed picture of one of the endpoints of stellar evolution. With any luck, we will address such problem areas as nuclear reaction rates, mass loss, and the evolutionary path to, and within, the white dwarf cooling track. In addition, we can make measurements which will allow observational calibrations of the white dwarf cooling curve. In time, this will provide a completely observational answer to a very fundamental astronomical question: how old are we? In order for all this to work, however, we must first isolate

and identify the individual pulsations.

3. White Dwarf Asteroseismology (Where? When? and How?)

There are four classes of pulsating white dwarfs, with no fundamental difference between the pulsating dwarfs of each subclass and the neighboring white dwarfs just outside of the class except for their temperatures. The pulsating white dwarfs, therefore, are otherwise normal stars; they pulsate when they have cooled enough to reach an instability strip. In at least the hottest two instability strips, there are stars inside the strip that do not pulsate. Evidence is now mounting that this may be true in the coolest strip, too. So, things may not be quite as rosy as the picture just painted. This is an active area of current research (See Kepler 1993, Dolez Vauclair & Koester 1991, Bradley & Winget 1994, and Bergeron et al. 1995, for discussion.)

The four white dwarf instability strips are the PNNVs (the planetary nebula nuclei variables), the DOVs (the hot DO pre-white dwarf variables), the DBVs (with a helium-dominated spectrum) and the DAVs (with hydrogen, and no helium spectral lines). The recent discovery of a pulsating transition object between the PNNVs and the DOVs, RX J2117.1+34.12 (Watson, T.K. 1992, Vauclair et al. 1993) suggests the PNNVs and the DOVs may actually be a single class, but since there are observed differences in the gross pulsational properties of these two groups, we continue to keep them separate. The effective temperatures of each strip are near 100,000K for the PNNVs and DOVs, 30,000K for the DBVs, and 13,000K for the DAVs.

Because of their condensed state (a typical white dwarf is about as

massive as the sun[3], but only as large as the Earth) and large gravities, we can exploit the white dwarfs' spherical symmetries to model their pulsations as spherical harmonics on each star's surface. The study of the stars' pulsations, therefore, proceeds very similarly to the study of normal modes, or eigenmodes, in atomic physics. Each pulsation mode is described by three quantized numbers representing the number of nodes in each normal direction within the star. k represents the number of nodes in the radial direction (and is alternatively called n in the literature), while ℓ and m, respectively, are the total number of nodal lines on the surface of the star and the number of nodal lines along a line of latitude. The radial wave function is represented by some function R(r,k), while the surface deformations are modelled by the spherical harmonics, $\{Y_\ell^m(\theta,\phi)\}$.[4] Much as in atomic physics, every pulsation mode is characterized by these three quantum numbers, k, ℓ, and m, and its frequency, ν.

3.1. The Fourier Transform and Spectral Window

The non-radial modes are easily visualized as sloshing motions on the surface of the star. When material sloshes together, it becomes hotter and thence, brighter. It is these brightness variations that we measure with high-speed photometers. Sampling every 10s or so, we get a continuous set of readings

[3]The average single white dwarf mass is near $0.6M_\odot$

[4]An important distinction here is that any surface deformation on the white dwarf (or any sphere) can be approximated by a *sum* over ℓ and m of spherical harmonics; in practice, we ignore the summation and treat the individual spherical harmonics as the pulsation modes. This is what is meant by normal mode analysis since each mode, in the linear case, is independent of, or normal to, each other.

throughout the observing night.

After obtaining these lightcurves, we use a Fourier transform (FT) to search them for coherent periodicities. The FT is very good at identifying well-sampled, isolated, periodic signals, but has problems (through no fault of its own) when there are many modes close together. The reason for this is simple: a periodic gap in the observations is nearly the same as a periodic signal to the FT. Thus, spurious modes always accompany the real mode in a pattern indicative of the data sampling. The pattern a single sinusoidal signal makes in the FT is called the spectral window and is often just abbreviated as the "window". For data taken from a single site, the dominant feature in the spectral window is a set of one-day aliases, peaks separated in frequency from the real peak by integer multiples of d^{-1} (11.6μHz). We call each spurious peak an alias of the real one and ignore them once the real peak has been identified. The presence of many aliases (aliai?), however, can make that identification difficult or impossible.

We make spectral windows for each data set by taking a continuous sine curve and sampling it exactly as the data were sampled. The resulting FT then shows the pattern produced by a single noise-free sine curve in our data. A sample single-site window is shown in Figure 1.1 and is from a 20 night run at McDonald Observatory. The one-day aliases are dominant and obvious. The spectral window is designed to show us exactly what a single mode in our data would look like in the FT. While it comes close to doing just that, there are some subtle problems with it which we have not been able to address. First of all, the window is noise-free whereas our data (unfortunately) are not. This problem becomes worse when combining data from multiple sites, each with a

different signal to noise ratio. Is the pattern produced by three 4m telescopes and one 24" telescope spaced around the globe the same as one produced only by 24" telescopes? Somehow, the data should be weighted according to their relative noise, but currently are not. The spectral window is made with sine curves; our real pulsations may or may not be accurately modeled by simple sine curves. Also, our measurements are integrated measurements of light intensity over some sampling interval; our current window algorithm makes no attempt to reproduce the integral samplings (although this would be an easy thing to add if we felt it were important to do so.) The fortunate thing however, is that we have been able to work well with our current, perhaps limited, window. One that solves some of these problems may be essential when we really start pushing on our observations for different kinds of measurements, but for now, what we have works quite well.

The Fourier transform uses sine curves as its set of basis functions. This is great if the underlying intensity variations are sinusoidal (or nearly so), but not so good if they aren't. In an attempt to fit a strictly periodic, but non-sinusoidal function, the Fourier transform will produce a series of periodicities (harmonically related) whose sum approximates the actual pulse shape. Instead of a single peak in the FT representing the single period in the data, we will have a series of peaks, masquerading as a series of unique sinusoidal variations. When we see harmonics or combination modes (modes whose frequencies are linear combinations of frequencies of other modes) in an FT, we do not immediately know if they are real modes or if they are simply artifacts of not having strictly sinusoidal variations. Many of the lightcurves presented here are decidedly not sinusoidal, although the

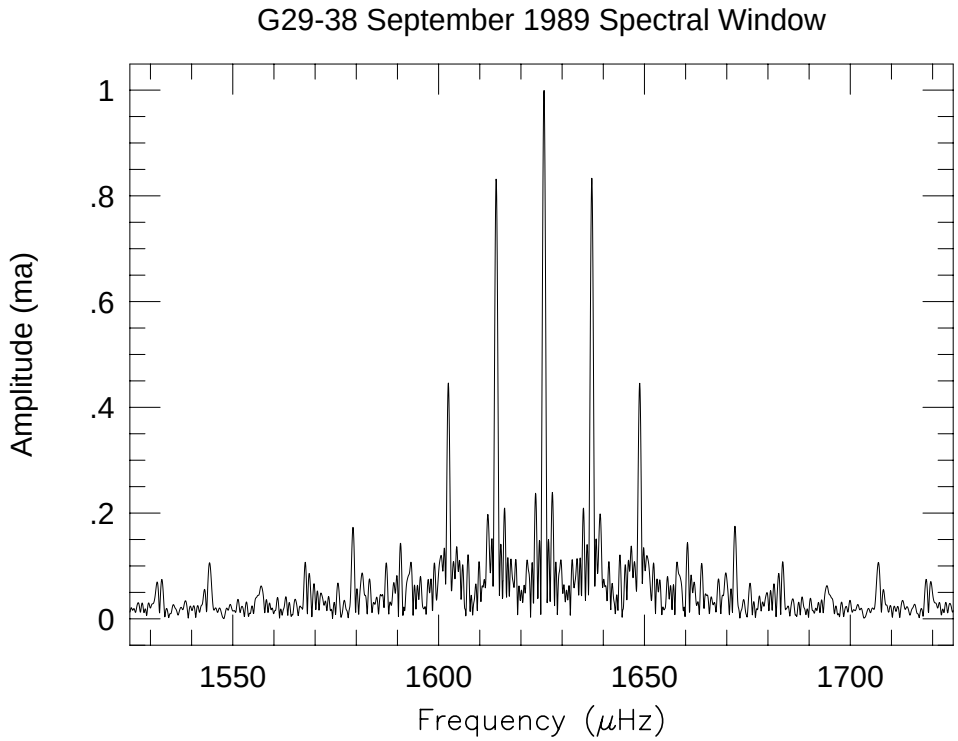

Fig. 1.1.— A sample single-site spectral window.

pulse shapes (produced by folding, or binning, the lightcurve on a given period) may actually be. Once the harmonics and combination modes are identified, however, they are discarded and treated no more in the subsequent normal-mode analysis. If they are spurious modes produced by the sine-fitting process, throwing them away is a good thing; if, on the other hand, they represent real non-linearities in the star itself, perhaps signs of resonant coupling (Dziembowski 1982), we are undoubtedly throwing away a lot of additional information when these modes are discarded.[5] There is a fundamental confusion here: the difference between non-linearities in the system and non-sinusoidal variations. For now, we generally treat them both as the same thing, but we will someday, I'm sure, be able to distinguish the two effects and will probably laugh at ourselves for being confused for so long. Haha.

3.2. Theory (Why?)

The theorists generally believe[6] the pulsations seen in white dwarfs are driven by partial ionization (at least in the DBVs and DAVs; the jury is still out on the hotter variables) and the restoring force is gravity. The pulsations are non-radial gravity-modes, or more simply g-modes.[7] They are *not* pressure-modes (p-modes) such as those seen in the Cepheid variables.

---

[5]This is *additional* information we are discarding here. The asteroseismological analysis depends only on the linear, normal g-modes and is independent of the existence of these combination modes.

[6]And therefore it must be true.

[7]This was proved fairly conclusively by Robinson, Kepler, & Nather (1982) and Winget et al. (1991) in their analysis of the PG 1159–035.

The white dwarfs are particularly rewarding objects for asteroseismology. The gains of asteroseismology are proportional to the number of identified modes. (Modes are identified by specifying the values of the three integers, k, ℓ, m, along with ν or P, the frequency or period.) Cepheids pulsate in one or two modes; the Delta-Scuti star with the most known modes has around 20 (Handler 1995). The white dwarfs, however, can pulsate in hundreds of modes. Each normal mode probes a slightly different region of the stellar interior, so having 100 modes is like having 100 probes, all going to different depths and/or locations in the star's interior.

Another particularly satisfying quality of the white dwarf pulsations is their timescale. The periods are generally between 100—1000s and thus many cycles can be observed in a fairly short period of time. The periods are long enough, however, that except for the dimmest targets, there usually are plenty of photons available to be counted within each integration. While we can always improve our signal to noise ratio, we are, in general, not photon-starved.

The advantages of white dwarfs as asteroseismological laboratories quickly become their biggest disadvantage as well: they are very complicated. With so many modes active at the same time, we need extended data sets to be able to resolve and identify closely-spaced modes (the resolution, or ability to resolve two closely-spaced modes, of an FT is proportional to one over the length, in time, of the lightcurve). This problem is worsened by the typical white dwarf rotation of one day, which causes closely-spaced modes, separated roughly by $1\mathrm{d}^{-1}$ in frequency — the exact place where daily gaps in coverage put spurious peaks in the FT.

While it is difficult to add additional pulsations to a star that does not have enough for asteroseismological analysis, it is much easier to change where alias peaks appear in a spectral window. In order to minimize (or ideally, eliminate) the dominant one day aliases, we simply eliminate the one day gap in our data. To do this, we set up a network of collaborating astronomers around the globe, all observing the same star over the same time period with similar tools and observing techniques. This network is called the Whole Earth Telescope[8] (WET) and is discussed more in Chapter 3. For now, the important point is that the network can obtain lightcurves uninterrupted by the daily rising of the sun and hence can produce vastly improved windows, with few aliases surrounding the real peaks. A sample WET-produced window[9] is shown in Figure 1.2. A comparison with Figure 1.1, a very good single-site window, shows a near-complete lack of the one day aliases dominant in the single-site data. With such a window, we can now identify the closely-spaced modes we expect the non-radial pulsations to produce.

Once the WET has allowed us to obtain near alias-free transforms, we can search them for identifiable peaks. This is the difficulty in asteroseismological analysis: mode identification. We must first determine if an observed peak in the FT is a real normal mode of oscillation, a linear combination mode, an artifact in the data, or something else entirely. If it is a normal mode, we need to identify at least its k and ℓ to proceed with

---

[8]An actual run of the WET is commonly called an XCOV (for eXtended COVerage) run and in keeping with the C language, are intuitively numbered successively from 0.

[9]In keeping with time-honored tradition, I have chosen the best WET window yet obtained (XCOV10 on GD 358), labelled it typical, and published.

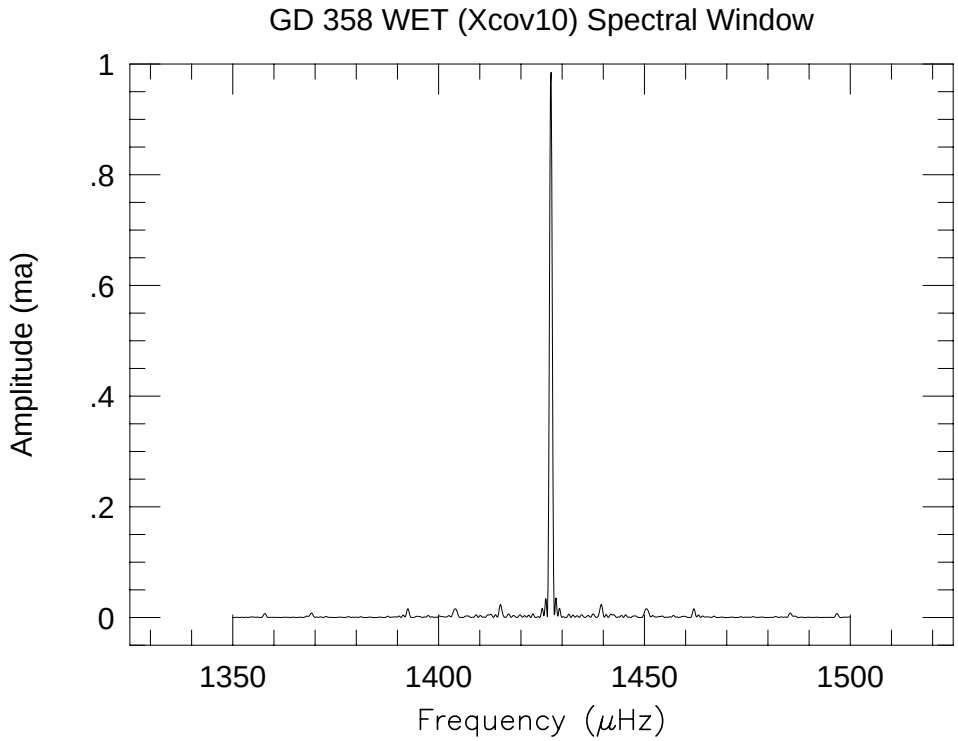

Fig. 1.2.— A sample WET spectral window.

our analysis. Luckily, the stars provide many clues which can be used in this process. If a full set of modes (say all the possible m values for a couple values of ℓ over a consecutive series of k values) are present in the star, the job is relatively easy. If not, then clues must be taken whenever available and pieced together for a consistent final picture. The clues involve the spacings between modes of same k and ℓ but different m, and those between modes of same ℓ and m, but different k.

As long as the spherical harmonics are valid representations of the observed surface distortions (they are as valid as our assumption of spherical symmetry), their underlying symmetry implies that the period of each mode depends only on k, and ℓ, the total number of surface nodal lines: it does not depend on how the nodes are arranged on the surface (i.e. m). When the underlying symmetry is broken, however, the observed periods become a function of m as well. Rotation breaks the symmetry and splits each mode of a given k and ℓ into a multiplet of modes with $2\ell + 1$ components with m running from $-\ell$ to ℓ.

The m-splittings can be thought of as due to travelling waves either with or against rotation. Under the slow rotation limit, (so long as $\Delta\sigma/\sigma \ll 1$), the frequency difference ($\Delta\sigma$) for each m mode is given by:

$$\Delta\sigma = m(1 - C_{\ell,k})\Omega \tag{1.1}$$

where Ω is the constant stellar rotation frequency and $C_{\ell,k}$ is, in general, a complicated function of the star's density and modal displacements, but in the asymptotic (large k) limit, approaches the value $\frac{1}{\ell(\ell+1)}$. Thus, modes of

same k and ℓ, but different m will be uniformly spaced in frequency and barring radially differential rotation (which changes the effective value of Ω, which should therefore be called Ω_k, for each mode), all modes with the same ℓ will have the same frequency spacings. If differential rotation is present, we will see a corresponding systematic pattern in the m-splittings as a function of k. Since the white dwarf rotations so far measured with the Whole Earth Telescope are near one day, we expect the ℓ=1 m-spacing to be on the order of 6μHz, much smaller than the typical period spacing which is close to 150μHz in the region of main power. Since such spacings are small, we expect to find closely-spaced triplets for ℓ=1 modes, and quintuplets for ℓ=2, etc. We have never identified an observed ℓ=3 mode. Geometric cancellation effects, where many small cells of brightness variations cancel each other out on the surface of the star, predict we won't see much beyond ℓ=3 anyhow (Dziembowski 1977). Our observations say not to worry past ℓ=2.

m values are assigned differently according to two different conventions. Here, I will adopt what I consider to be more physically intuitive: modes with a positive m are prograde modes (and therefore have a slightly higher frequency) and modes with a negative m are retrograde and have slightly smaller frequencies. (The first edition of the non-radial pulsation bible by Unno et al. (1979) uses this convention, while the second edition (1989) uses the opposite. They also changed their convention for the radial node number from k to n. Be warned.)

As the number of radial nodes (k) increases, the frequency of a g-mode decreases (there is less of a restoring force since the wavelength of the oscillation decreases). In the asymptotic limit, the modes with same ℓ are

equally spaced in period. The periods of a such modes are given by:

$$P = \frac{k\Delta\Pi}{\sqrt{\ell(\ell+1)}} + constant \tag{1.2}$$

where $\Delta\Pi$ is related to the period spacing and the constant is small. $\Delta\Pi$ itself is a function of the mass of the star and is truly constant only for stars of uniform composition. Adding compositionally stratified layers, or any other radial discontinuity, to a model star (remember, white dwarf stars have a very high gravity which separates and stratifies the constitute elements) makes the value of $\Delta\Pi$ vary for each mode, but maintain a mean that is indicative of the total stellar mass. The deviations of $\Delta\Pi$ measure the layering present in the star. This effect is called mode-trapping as modes with nodes near the composition transition boundaries will have their periods shifted slightly so the nodes correspond as closely as possible to the transition discontinuities. Carl Hansen was the first to realize this possibility as published in Winget, Van Horn, and Hansen (1981).

Note that both the period spacing and m-splitting are only a function of ℓ in the asymptotic limit and thus ℓ=1 and ℓ=2 modes have different spacings, but with a constant ratio. The period spacing ratio for ℓ=1 to ℓ=2 is $\sqrt{3}$, or 1.73. The multiplet spacing ratio is 0.60. If we have a series of observed multiplets in a star, we can use these ratios to help distinguish the different ℓs, in this case ℓ=1 from ℓ=2. Each set of ℓs provide an independent set of asteroseismological probes.

The physics comes out of asteroseismology by matching the observed set of frequencies to a model set of frequencies, ks, ℓs, and ms calculated by varying the physical parameters of the model star, In this way, the

observed frequencies have a one-to-one correspondence to the star's physics. Initial attempts at this matching failed because the investigators could not unambiguously identify enough modes to make a reasonable match. The WET changed all this by observing a star nearly continuously for up to two weeks, eliminating three problems that plagued mode identification: aliases in the transforms which makes peak isolation difficult, if not impossible; low frequency resolution that blended distinct modes closely spaced in frequency; and low signal to noise ratios which effectively hid real modes in the "grass" of the FT.

Once we have accurately isolated and measured the frequencies of the pulsations, we, with a long timebase of observations, can actually observe stellar evolution in progress. The period of a mode will change slightly as the star cools and/or contracts. The contraction process (presumably dominating only in the hottest of the white dwarf pulsators) tends to decrease the period with time while cooling increases it. This is a very difficult measurement, as the rates of change (or $\dot{P}$s) are very small (of order 10^{-15} for an average DAV), but an extremely important one. For once we can measure the rate at which a star is cooling (Winget et al. 1991, Kepler 1993), we can apply it directly to the white dwarf cooling curve, and hence luminosity function (Liebert, Dahn & Monet 1988) to measure the age of the white dwarfs (Winget et al. 1987). If we pick which white dwarfs' ages to measure (the oldest, coolest) we get the age of the local galactic disk, or globular cluster, or whatever object we choose to study.

4. Asteroseismology Success Stories

4.1. The DOVs

The first star successfully analyzed by the WET was a textbook example of asteroseismology. It fit the existing theory almost to the letter, crossing every t and dotting every i. It was the DOV, PG 1159–035 (Winget et al. 1991). In it, we clearly saw evidence of both ℓ=1 and ℓ=2 with their associated triplets and quintuplet structure. The observed frequency and period spacings surprised us: they were nearly exactly what theory predicted (well, the observers were surprised; the theorists, of course, expected the match). The ℓ=1 m-splittings were what theory predicted; the ℓ=2 m-splittings were what theory predicted; the ℓ=1/ℓ=2 m-splitting ratios were exactly what theory predicted. The spacing between adjacent (successive k) ℓ=1 modes was what theory predicted. Again, so too were the ℓ=2 spacings (given the mass) and the ℓ=1/ℓ=2 spacing ratio (this last value being independent of the mass). The ℓ=1 modes were triplets; the ℓ=2 modes, quintuplets. Everything matched the existing theory and mode identification was rock-solid. 125 individual modes were resolved in the power spectrum. The resulting physical parameters were remarkably precise. The principal results from the initial analysis and that of Kawaler & Bradley (1994) are:

1. Most, and probably all, the observed pulsations are due to nonradial g-modes (a nice check of theory in itself).

2. Only ℓ=1 and ℓ=2 are seen; there is no sign of ℓ=3 or higher.

3. The mass of PG 1159–035 is $0.59 \pm 0.01 M_{\odot}$.

4. The uniform rotation period is 1.38 ± 0.01d.

5. PG 1159–035 is compositionally stratified.

6. PG 1159–035 has a surface He-rich layer of $\approx 0.004 M_\star$.

7. The surface He abundance is ≈ 0.27 by mass.

8. The distance to PG 1159–035 is 440 ± 40pc; the previously measured parallax was 800 ± 400pc (Werner, Heber & Hunger 1991).

The first seven results were expected kinds of results from asteroseismology, but the last was not. Until, that is, we realized (Paul Bradley gets the credit here) the absolute stellar luminosity is a model parameter, determined by the pulsations. When combined with a bolometric correction and observed magnitudes, then, we have a fairly accurate distance-determination method. This idea initially arose in dealing with the DBV, GD 358, whose power spectrum showed only a single set of ℓs. Assuming they were ℓ=1 was the simplest assumption, but we were not forced to that conclusion until Paul rather nonchalantly offered that either the modes were ℓ=1, or the parallax was wrong. What he meant was if the modes were all ℓ=2, then the models gave an absolute luminosity inconsistent with the available parallax measurements. What was born at that time, were two things: a new way to identify pulsation modes, and a new way to probe the distance scale of the Universe.

4.2. The DBVs

GD 358 was the first DBV successfully explored with the Whole Earth Telescope's application of asteroseismology (Winget et al. 1994). Analysis of

its data set took longer than did PG 1159–035's. The basic features seen in PG 1159–035 were also seen in GD 358, but with enough differences that only hindsight shows how similar they actually are.

There were no observed quintuplets in GD 358, only triplets. The m-splittings were slightly asymmetric (that is the m=–1 to m=0 splitting was a bit less than the m=0 to the m=+1 splitting) and varied from one triplet to the next, with the higher period mode having a larger splitting. There were many modes at low and high frequencies which did not fit any known period-spacing patterns. In short, the redundant, self-checking, method of mode identification developed for PG 1159–035 did not work here and new tools had to be developed.

The solution eventually came. All the dominant modes are ℓ=1 (ℓ=2 would have produced the wrong absolute luminosity). The different m-splittings within a triplet are consistent with the presence of a small magnetic field. (A perturbing magnetic field acts as an additional restoring force and shifts modes to higher frequency by an amount proportional to m^2 [Jones et al. 1989].) The increase in m-splittings with period is due to the presence of differential rotation in the star. Most of the modes whose periods did not fit into any obvious pattern were found to be linear combination modes. Once they were identified and removed, all the remaining high-power modes were completely explained by a series of ℓ=1 multiplets.

Quantitatively, the main results were:

1. GD 358's mass is $0.61 \pm 0.03 M_{\odot}$.

2. The outer He envelope is $2.0 \pm 1.0 \times 10^{-6} M_{\star}$.

3. The results are consistent with a magnetic field of 1300 ± 300G.

4. The core rotation rate is 1.6d.

5. The outer envelope of GD 358 is rotating 1.8 times faster than the core.

6. The distance to GD 358 is 42 ± 3pc; the previously measured parallax was 36 ± 4pc (Harrington etal. 1985).

4.3. The DAVs

We had actually looked at some DAVs with the WET prior to the PG 1159–035 and GD 358 observations and had not managed any of the successes that came later with these other stars. The problem was fundamental. The DAVs are divided into two camps: the hotter, lower-amplitude, shorter-period pulsators and the cooler, large-amplitude, longer-period pulsators. The hot DAVs have very few modes while the cooler DAVs have many modes, but most are unstable and seem to come and go without much rhyme or reason.

In his thesis, Chris Clemens (1994) solved the hotter DAVs by looking at the ensemble of individual pulsators. He was able to determine the individual properties of each of the hot DAVs he analyzed by seeing how it fit in with group properties he discovered global to all the hot DAVs. He found the modes present in the hot DAVs are mostly ℓ=1 modes, although only a few modes are present in any given star. When he added the modes of all the stars together and treated them as if they came form a single star, a nice understandable pattern of successive-k, ℓ=1 modes emerged. That this worked at all means the overall structure of the hot DAVs are all very similar:

their masses are near $0.6M_{\odot}$, and their Hydrogen envelopes near $10^{-4}M_{\star}$. The remarkable similarities of the hot DAVs he analyzed support the common asteroseismology credo that the pulsators are "otherwise normal stars," but Chris could not put the cool DAVs with their complex, variable power spectra on the same grounds; they, for the time-being, remained an enigma.

What Chris's work once again highlighted, however, is our lack of understanding of the mode selection process. The theoretical spectrum of available g-modes for pulsation is much more dense than the spectra we see. Why should some stars show some modes and not others? There are general arguments based on the timescales in the driving region which explains general trends seen in mode selection, but not the wide variety of behavior we have witnessed. Why do we not always see multiplets? And when we do, why are the amplitudes not all the same? Or indeed, should they be the same?[10] There are also many instances when a mode, seen one time in a star, disappears a short time later. We do not understand such changes, but fortunately, the modes that have appeared and disappeared do so in locations still consistent with the set of expected normal-modes. For example, a "missing k" may suddenly appear one year later exactly where we expected to see it.

5. Remaining Asteroseismology Questions (and the Purpose of this Work)

[10]Actually, we expect the star's inclination angle to alter the relative amplitudes of a multiplet (Pesnell 1985), but the amplitude patterns we see cannot be explained solely due to inclination effects.

Two (and only two) subclasses of white dwarf pulsators have been left out of the above success stories: the PNNVs and the cool DAVs. The PNNVs' pulsation spectra did not look anything like those of the DOVs; there were few modes and no identifiable pattern existed amongst the modes that were present. The question was unanswered: are these stars normal mode pulsators like the other white dwarf variables?

The WET run on RX J2117.1+34.12 provided the last clues to answer that question. All we are seeing in the PNNVs are the trapped modes, modes with radial nodes near the chemical[11] transition zones. The theory for trapped modes is basically this: it is easier for a mode to oscillate if it has a node at or near the chemical composition boundaries. Thus modes with a node that happens to fall close to such a transition zone, will have its node (and hence frequency) shifted slightly so it is as close as possible to the desired boundary. If, as theory predicts, trapped modes are thus easier to excite, we expected to see trapped modes with larger amplitudes than neighboring modes in all the white dwarf pulsators, but we didn't. What we did see, however, were mode frequencies being pulled to be closer to a trap than it would otherwise have been. We could not explain why the amplitudes of the modes weren't also significantly affected, but the fact is, they weren't. In the PNNVs however, it appears the trapped modes are so efficient that nothing else is seen; amplitudes *are* affected. The ratios between observed periods were exactly what theory predicted would exist for trapped modes. (See Bradley (1993) for example.)

---

[11] Actually, all we really know from asteroseismology is that there is a discontinuity in the star someplace; we do not know for sure if it is the expected chemical transition zones, or perhaps something else like a degeneracy boundary providing the discontinuity.

The PNNVs, then, are "otherwise normal stars" whose pulsations can now be exploited for asteroseismological analysis.

The remaining mystery then, were the cool DAVs. With such wildly varying pulsation spectra, no obvious pattern within them, and few observed multiplets, the question was still open: are the cool DAVs normal-mode pulsators like the other white dwarf variables? Despite one of its class, HL Tau 76, being the first variable white dwarf discovered (Landolt 1968), we did not really know if the cool DAVs were "otherwise normal stars" with normal-mode pulsations. We did not know if they held any hope for asteroseismology.

With the evidence I present here, we now know the answer to this last question: yes, the cool DAVs *are* normal-mode pulsators. We *can* use their pulsations to learn the inner secrets of the DA white dwarfs. The last remaining "is it even fruitful" question surrounding white dwarf asteroseismology has been removed and we can now continue to tear apart the insides of all the white dwarfs and place them into the evolutionary context where they belong. The aliens could not learn anything about human evolution if they stole a kennel full of barking dogs; we couldn't learn anything about the cool DAVs through asteroseismology if they were not normal-mode pulsators. They are. We can.

6. The Rest of this Work

In reaching the above conclusions, I concentrated primarily on a single DAV, G29–38. I first became aware of its existence during the second WET run in

November, 1988. Observing with my (at that time) new advisor and our first three-channel photometer (it, too, was seeing first light during this run) in Australia, Ed and I marvelled for hours at the lightcurve's strange behavior (see Figure A.3, for example). Seven years and hundreds of runs later, I can now explain a part of G29–38's behavior. That I say "a part" and not "all" is not to be considered discouraging, but rather a promise of what is to come from the field. That we know anything at all, that we can say it is a normal-mode pulsator, means our time is not wasted in continuing study.

6.1. G29–38 Vital Statistics

G29–38 was first discovered as a variable by Shulov & Kopatskaya (1974) and confirmed by McGraw & Robinson (1975). Holm et al. (1985) took pulsationally-phased spectrophotometric IUE (International Ultraviolet Explorer) observations and found the results consistent with g-mode pulsations. There was little additional information published on the star until the discovery of an infrared excess above 2μm by Zuckerman & Becklin (1987). This prompted a flurry of activity and the discovery of an additional excess above 10μm (Tokunaga et al. 1988, Telesco et al. 1990, Tokunaga et al. 1990). Continuous debate emerged over the source of the excess: brown dwarf or dust (Greenstein 1988, Liebert, Saffer, & Pilachowski 1989, Stringfellow et al. 1990, & Graham et al. 1990a)? Zuckerman (1993) summarizes most of this work and concludes dust is the most likely explanation, but the exact circumstances remain uncertain. He also states there are no other such anomalous variations in other white dwarfs, particularly (Zuckerman, private communication) other cool DAVs.

Prompted by the brown dwarf possibility, in addition to its unusual pulsation spectrum, Winget et al. (1990) (and Kleinman 1990) report on WET observations on G29–38, finding an unexpected phase change of the dominant pulsation unaccompanied by any amplitude variability. The natural explanation was reflex orbital motion, this time due to a *massive* companion. Measurements of the only other resolvable mode during the run did not show a similar variation — meaning there was no reflex orbital motion. Radial velocity measurements (Graham et al. 1990b)[12] agreed with these results, showing no significant radial velocity variation to within 10 km/s.

Later evidence for a radial velocity variation, this time near 10 km/s came from Barnbaum & Zuckerman (1992). Kleinman et al. (1994) were able to use the same stable peak that disproved the initial binary model to show the observed radial velocity variations were not due to reflex orbital motion. Their nature, then, still remains a mystery.

Basic data on the star has come from many sources. Shipman (1979) derives an optical temperature of 11,900K and a mass of $0.84 M_{\odot}$. The IUE measurements of Holm et al. (1985) derived a temperature of 11040 ± 555K while those of Kepler & Nelan (1991) yield a temperature near 11400 or 11800, depending on the photometric calibration used. The most recent vital

[12]The radial velocity measurements were initiated by a preprint of the WET work. During the referee process, however, we found the second stable peak which did not show the same variation. The published WET paper, therefore, did not claim the system was a binary. The radial velocity paper made it to the presses before the WET paper, disproving something that was not suggested in the upcoming final version. The two groups worked independently, but shared results. We were searching for additional peaks as the initial manuscript was sent to the ApJ, but did not discover it in time to deny the need for the radial velocity measurements.

statistic determinations come from Bergeron et al. (1995). Their best values for G29–38 are a temperature of 11820K and a mass of $0.69 M_{\odot}$. The USNO (United States Naval Observatory) parallax is $0".071 \pm 0".004$ (Harrington & Dahn 1980). Its V magnitude is ≈ 13.0. G29–38's many aliases include WD 2326+0.49, ZZ Psc, Gl 895.2, EG 159, and LTT 16907.

6.2. Further Outline

In addition to the observations on G29–38, I observed other cool DAVs to show that G29–38's features were not unique to it, but applied to the entire subclass of objects. My analysis (and the data) on these stars is not as complete as it is on G29–38, but is sufficient enough to show universality of my conclusions.

In the next chapter, I discuss an instrumental project I undertook to help with these investigations. It involves an improvement to existing two-channel photometers that allows more accurate measurements of pulsation amplitudes and permits our target stars to be observed longer each night and each season, and on smaller telescopes than were otherwise possible. This last advantage was important for this work because the volume of data I needed for this analysis (see Figure 1.3) meant I had to use the smaller telescopes available to me at McDonald Observatory. I simply could not have gotten the needed amount of time on the larger telescopes. Many of my target stars have V magnitudes near 16. To get useful data on such objects from a 1-m telescope meant I had to have these capabilities.

In Chapter 3, I discuss the observations themselves and the tools used for reduction and analysis. The remaining chapters detail the analysis of

Fig. 1.3.— The amount of data I gathered for this thesis.

G29–38 and the other cool DAVs I observed. Chapter 7 discusses some of the remaining mysteries brought to light by this work. Finally, in the two appendices, I include the FTs of nearly all the data collected for this work.

Chapter 2

The Instrument

If the thunder don't get you
then the lightning will.
—Jerry Garcia & Robert Hunter, *The Wheel*

This chapter is nearly identical to a paper submitted to the PASP entitled "The WET Standard Photometer." The paper has three authors: Scot Kleinman, R. Ed Nather and Tom Phillips. Ed provided background on the history of the WET photometer and decreed the requirements an instrument must have to be WET approved. He also came up with the initial idea for an add-on third channel to our standard two-star photometers. Tom Phillips, while working at the machine shop in the UT Astronomy department, helped me with the design of the instrument and did most of the machining. I was responsible for the design and testing of the instrument and wrote the paper.

The PASP has suggested we trim the manuscript. Much of our discussion concerning photometer fundamentals is already in the literature, they say. While this is true, we have seen recently-built photometers which

have ignored some of the basic rules discussed here. I have not been able to find all these items in a single reference. It is my hope to provide them here, if not in the final published paper.

1. Introduction

In the beginning of the modern era of time-series photometry, there was the one-channel photometer adopted unchanged from the traditional UBV photometrists: a single phototube continuously measuring the brightness of a single star. Unfortunately, the single detector made it difficult, or impossible, to distinguish true variability from such local effects as clouds. Thus, the two-channel photometer was developed (Nather 1973, Grauer & Bond 1981) to measure two stars simultaneously. If the second star was chosen to be a non-variable, then any variability that showed up in both channels was an artifact and not intrinsic to the observed stars.

Initially, these two-channel devices were adopted for the Whole Earth Telescope (WET) for its observations of variable white dwarfs. For uniformity, each WET participant uses similar equipment, software, and observing procedures wherever possible (Nather et al. 1990). Uniformity of observations is one of the WET's most important requirements, permitting it to produce a wealth of new information on its targets (Winget et al. 1990).

For the high-speed work required by the WET observers, however, even the addition of the second channel can leave artifacts in the data. In order to measure the sky background, the data are interrupted by offsetting the telescope to a clear patch of sky. Measurements are taken as often as

conditions demand, but rarely more frequently than thirty minutes, so not to lose too much data on the target star. We have found, however, the night sky often varies on similar timescales as do the variable white dwarfs (as quickly as a few minutes). Since the white dwarfs are intrinsically faint, measured pulsation mode amplitudes can therefore be inaccurate without a continuous subtraction of the sky background. Having accurate amplitudes is particularly important in understanding the modes which seem to change their frequencies and power on short timescales. We need to know if the amplitude changes seen are real, or simply consistent with instrumental noise. We therefore realized the need for a three-channel photometer to monitor not only the target and comparison stars, but the sky as well — its purpose, to measure accurate pulsation amplitudes. Other groups had independently come to the same conclusion; see for example Vauclair et al. (1989).

Our first three-channel instrument was a complete re-design and required collaborators to replace their current photometers with the new one in order to get three channels. While this solution was acceptable to our well-funded collaborators with lots of shop time (only one other instrument has been built to date), it was not the solution we needed to outfit a complete network with three-channel instruments. We needed to design a new instrument that would easily work with the existing two-channel photometers, upgrading them to include a third channel with as little modification to the base instrument as possible. We report here on the design of just such an instrument; we call it the *dual-beam miniphot*. The new instrument has been used in four WET runs and many supplementary observations as well. We consider the instrument a prototype, in that there are a few areas we feel could

be improved, but as is, it is certainly capable of recording scientifically valuable data and has already demonstrably done so. The planned improvements are mainly conveniences and do not significantly affect the quality of the data.

While the primary motivation for the instrument was to obtain more accurate measurements of pulsation amplitudes, observing with three channels has other advantages, many of which we had not anticipated. We have often been able to take useful data with three channels when we would have otherwise been forced to close the dome and yield the night to the spectroscopists. In particular, we gain nearly an hour and a half extra observing time each night by starting before, and continuing after, astronomical twilights. We can extend our monthly observing time, often competing with spectroscopists for grey and bright time, because the sky channel allows an accurate subtraction of varying levels of moonlight. The WET has allowed us to remove the single-day gap that used to occur in our measurements due to the inevitable rising of the sun; the sky channel allows us to remove the periodic one-month gap that comes from avoiding the moon. Because of our increased ability to measure and subtract the sky brightness, we find we can observe dimmer stars (where sky typically dominates the signal) on smaller telescopes than were previously useful. This capability is crucial in extending the WET's eyes to dimmer objects — it is very difficult to get two weeks of overlapping time on many large telescopes around the globe. We have been able to take good data during a variety of adverse weather conditions such as intense Northern Lights (they do occasionally make it to Texas) and active lightning storms on the horizon. The proven ability of the instrument to measure variable sky brightness also makes it ideal for

extracting photometric data from small telescopes located near cities with less than ideal observing conditions.

2. The Design

The photometer we now call the "WET Standard" did not just spring into being, but evolved slowly. Rather than spend all our time building and improving the instrument, we *used* it as soon as it was capable of the measurements we sought. The modifications to the initial design have taken decades, which may prompt some to wonder how good data were ever taken in the "old days" with such an obvious dinosaur. The point is the instrument worked, and until the desired science *demanded* an instrumental improvement, observers lived with a few inconveniences in the instrument. The addition of the second channel to measure a comparison star was just such a demand; so, too is the recent addition of the third sky-measuring channel described here. The history of the instrument tracks well the history of the science done with it and is instructive to understanding how we got to where we are now.

2.1. The Design History

The photometer we are about to describe [1] has its roots in the photometers used by Harold Johnson as he developed the UBV photometry system while at the University of Texas (Johnson 1962). The electronics Johnson described are largely out of date, but the offset guiding photometer he described lives

[1]This section is a summary of material to appear in a book by one of us (REN) titled *Techniques of Asteroseismology*

on as the basis of the standard WET instrument. The original design had a single phototube for one-channel operation and an offset guider for visual guiding on a nearby star. The offset guider was fed by light coming off a large 45°mirror in the guider box. The mirror had a central hole in it, allowing the on-axis light to travel to the phototube below, while the periphery field was sent to the guiding eyepiece. The guiding eyepiece itself was mounted on an XY stage with facilities for both large, quick movements and more careful, precise motion. An experienced observer could set the XY positions with a 100 micron precision.

Under the traditional cyclical mode of observing (comparison star 1, sky, target, sky, comparison star 2, sky, target, sky, comparison star 1,...) the standard filter photometrist could *usually* determine if the night was photometric while later reducing the data. Since the study of rapid variable stars requires the observer to remain on the target star without interruption as much of the night as possible, this method of quality control would not work.

Starting with the Johnson offset guider, an evolutionary step was taken with the addition of a second (miniature) photometer to the offset guiding eyepiece. An additional mirror, hinged on one edge, was placed between the large 45°mirror and the eyepiece so that it can be flipped in and out of the light beam, intercepting (when flipped in) the light headed to the guiding eyepiece and directing it to the new miniature photometer. The comparison star measurements are thus occasionally interrupted for guiding, but most seasoned astronomers can do this very quickly and are often heard boasting about how quickly they can "get in and out" while guiding. An eyepiece

on the new second channel for viewing the apertures was initially thought redundant: careful observers could center the star electrically, watching the light curves of both stars (the target star apertures have always had a viewing eyepiece) while blindly adjusting the position of the flip mirror. This approach worked, but was, in a word, inconvenient. Eighteen years later (during which time we were busy using the instrument), an aperture viewing eyepiece was added to the basic design of the second channel. With this new addition to the miniature photometer, the "miniphot" was born and soon replaced the target channel photometer attached to the bottom of the offset guider, being much smaller and housing the more modern, more sensitive Hamamatsu R647 phototube. Thus equipped with two miniphots and other small modifications, the original Johnson guider became the instrument of choice for high-speed photometry (and the WET) until we realized the need for a third channel — to measure sky.

2.2. Criteria of the Design

The criteria for a WET instrument are different from those for a standard single-site instrument. At observatories where we don't have collaborators with suitable instruments, an observer and instrument are often sent from elsewhere to make the observations. The photometer is traditionally carried as checked-baggage and must therefore be relatively light, yet still able to survive the abuse of aggressive baggage handlers. Because we want to equip the entire network with identical instruments, it must also be fairly simple to manufacture and as inexpensive as possible. It could potentially be used on a variety of telescopes, so it must be able to handle a wide range of focal

ratios. Since we are talking about an upgrade, it would be nice if it could be easily integrated into the current two-channel photometers, requiring no modifications to the base instrument, and if its use required little change in current operating procedures. The list is a tough one: the instrument needs to be light, rugged, easy to make and operate, flexible, and low-cost.

The scientific requirements of the instrument are equally numerous. It must have a motor-controlled filter wheel with at least 4 available filters to allow for multi-color work. We require a complete set of apertures to accommodate a large variety of seeing conditions and telescope plate scales. So that the chosen patch of sky is not contaminated by nearby stars, there must be an acceptable way of changing the location at which we measure sky. We must also meet the standard photometer requirements that it have illuminated apertures and optics with which to view them, a set of Fabry lenses to provide uniform measurements despite small image drift (Michlovic (1972) gives a simple discussion on this crucial photometer element), and a dark slide to protect the tubes from light. All mating surfaces must be stepped to provide a labyrinth that ensures no light leaks.

There are two additional requirements that we consider so basic that they are usually left unsaid, but as the saying goes, "if it goes without saying, say it twice." The lightpath from the telescope to the ch1 phototube must have nothing in its way other than the Fabry lens. Additional mirrors are often inserted in the lightpath to make the instrument more compact, but at the expense of losing light to the ch1 phototube. Coated mirrors come with 90% or more reflection guarantees, but add a little dust and a few fingerprints and you can easily lose even 50% of the light. We are in the business of

counting photons; why throw even one away unnecessarily?

The apertures we use also function as a knife-edge for focussing. By removing the eyepiece, and moving the star across the sharp edge of a large aperture, a precise focus can be obtained at the start of each run. If you cannot see the apertures, or they do not have sharp edges, then you lose the ability to accurately focus the telescope to the instrument.

2.3. The Dual-Beam Miniphot: Overall Design

Figure 2.1 is a photograph of the Texas two-channel guider box with the dual-beam miniphot attached at the bottom. Figure 2.2 is a schematic of the major components of the new instrument only. The guider box described in the previous sections and seen in Figure 2.1 is widely available to most WET collaborators. The miniphot is shown on the offset guider in Figure 2.1 and is used for comparison star (ch2) measurements. For two-channel use, a miniphot is also mounted at the bottom of the instrument for measuring the target star (ch1). The new three-channel instrument simply replaces the ch1 miniphot with the dual-beam miniphot, adding the sky channel (ch3) without affecting the rest of the instrument.

The main feature of the dual-beam miniphot design is that two lightbeams are being measured by the instrument at the same time. It has two sets of apertures and filters, two Fabry lenses, and of course two phototubes all housed in a single unit. When looking through the eyepiece, the observer sees a pair of illuminated apertures: one for the target star and one for a clear region of sky. Since the sky aperture is fixed relative to the target aperture,

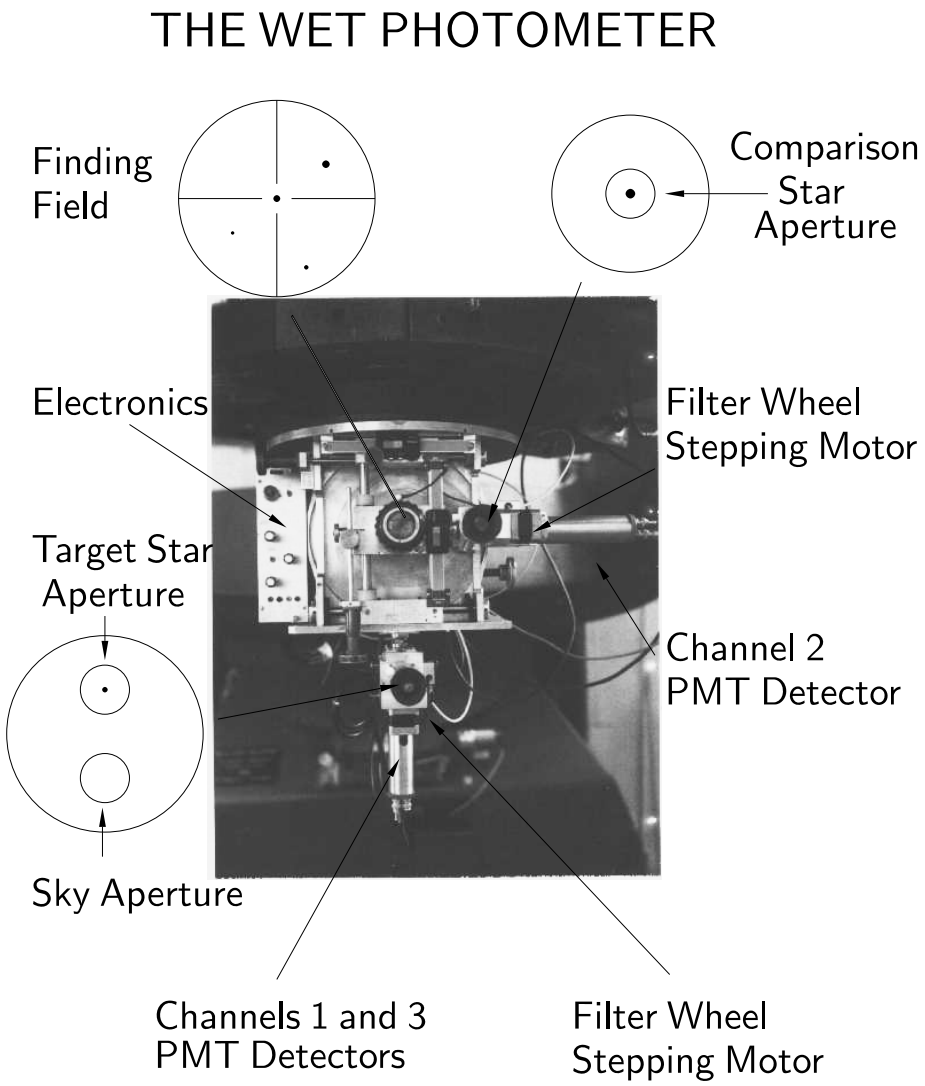

Fig. 2.1.— The WET Photometer mounted on the McDonald 36" Telescope and the view from each eyepiece.

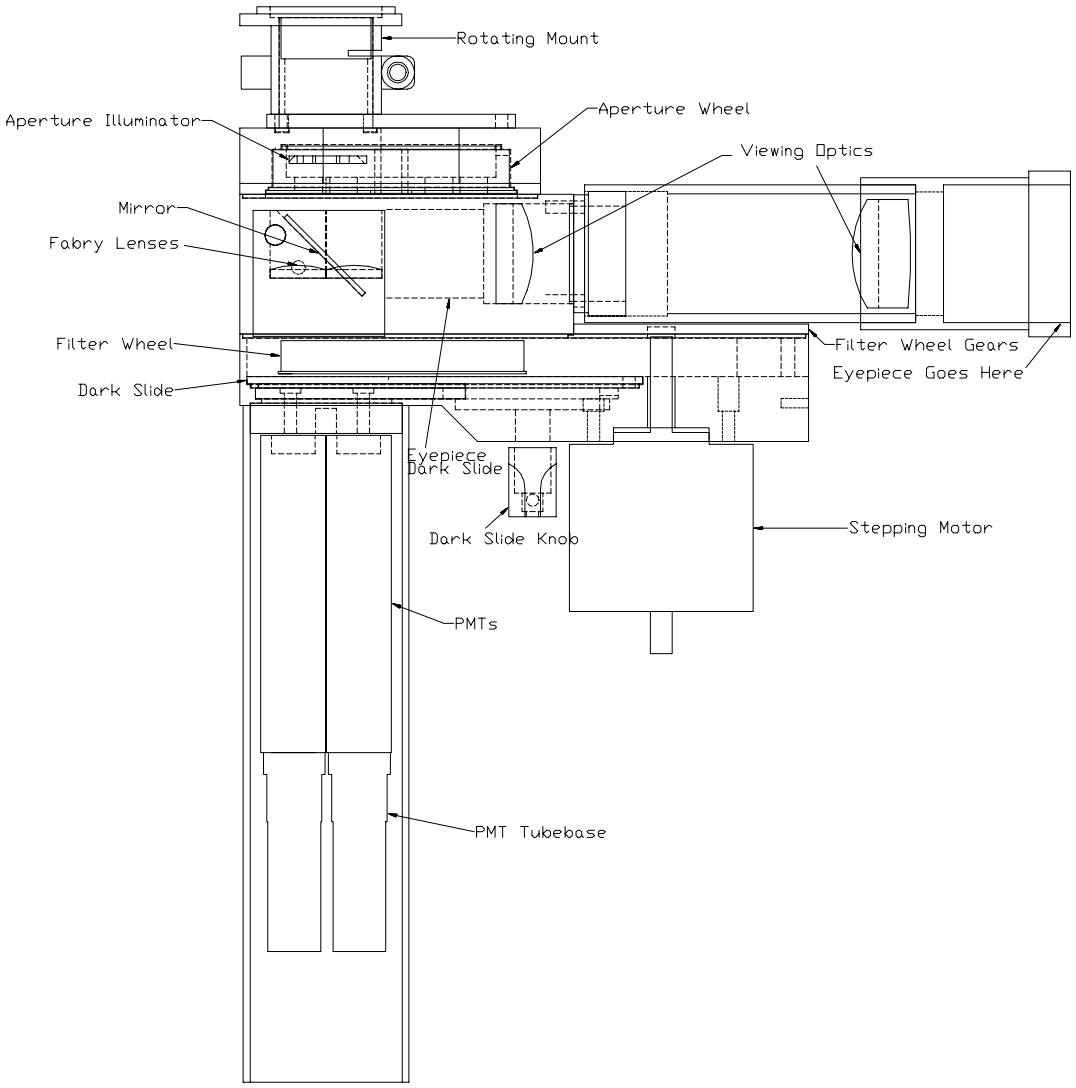

Fig. 2.2.— A layout diagram of the new dual-beam miniphot.

it could be contaminated by a random field star. In all but a few percent of these cases, we can simply swap the star and sky positions. In this way, there are two spots to find an uncontaminated area of sky and a problem only arises when both positions contain a contaminated sky. The dual-beam miniphot therefore has a rotating, detented mount, allowing 360°of rotation and thus, the ability to select a patch of sky anywhere within a fixed radius of the target star. The detents allow the position to be accurately reproduced for further observations, but do not preclude selecting a spot in between detents.

The Hamamatsu R647 bi-alkali phototubes have been used successfully in the miniphots for many years now. Their small size makes them equally suitable for the new dual-beam unit. We are able to fit two of these phototubes side by side in the same sized cylinder we used in the miniphots. Actually, the phototube cylinder is one of only two parts identically reproduced from the miniphot, although the appearance and operation of the two instruments are quite similar.

The constraining factor in the design was the size of the available unvignetted field from the guider box (section 2.4 explains this constraint). Because this field is so small, and we want to be able to run on a variety of F ratios (we had aimed for F8 as our fastest), we could not space the apertures far enough apart to center them over the phototubes. We therefore centered the Fabry lenses over the phototubes and use them to translate the light beam to the phototubes from the apertures (see Figure 2.4 to see the schematic lightpath through the system). While this approach is unconventional, certainly, we note no ill-effects by its use. Fabry lenses are traditionally equally spaced between the apertures and the phototubes. While

this arrangement provides a uniformly-sized beam, no losses are incurred by changing this placement (except when sending non-parallel light through interference filters, which we do not do here). The space constraints in the system did not allow such an equi-distant placement (although it is close to it) of the Fabry lens, but it nonetheless performs quite well without it.

Additionally, Fabry lenses are usually fixed in place so no movement is possible. Due to the same constraints described above, there was simply not enough room in this design to permit this luxury. Instead, the Fabry lenses are in an assembly with the viewing optics pickoff mirror, sliding into place on a heavily detented shaft when data are being taken, and sliding out when the pickoff mirror is in place to view the apertures. With a carefully constructed, loaded detent, the Fabry lenses' position is precisely reproducible. While unconventional, this arrangement works and was the best solution, given the available space.

2.4. Unique Features

Besides the rotating base and offset optical axes, this design has several unique features. Aperture illumination has proverbially been a problem in most photometers. Achieving bright, uniform illumination is difficult, at best, with one aperture, but all that much harder with two. What we would like to see through the eyepiece is a cleanly illuminated aperture edge with no light coming from within the aperture itself. To aid in focusing on the aperture, some people prefer to have the walls of the aperture illuminated as well, providing an out-of-focus "tunnel" culminating in the sharp edge of the aperture. The original two-channel photometer apertures were illuminated

by a circle of 4 LEDs placed around an opening above the apertures which provided adequate, but uneven lighting, with four "hot spots" around the apertures. The miniphot uses an LED-fed fiber optic cable, carefully scored and wrapped around an aperture to improve the clarity of the illumination, at the expense of much time and finesse needed to make it. We decided to take a different approach that is much simpler to produce and equally effective. Figure 2.3 is a drawing of the resulting illumination design. We took a piece of clear plastic and machined an oval with the same end-radii as the biggest apertures we use, added to it a 45°bevel, and attached a single LED to the side of it with Epoxy cement. We leave the 45°bevel of the oval alone, but cover the rest of the illuminator (and LED) with white paint, to provide some internal reflection, then apply a coat of black paint so light will only escape from the unpainted surface of the oval. The illuminator is fed with a single LED, although we did leave provision for a second one should more light be needed (we find the single LED sufficient). The assembly is mounted above the apertures, aiming down. The brightness is controlled through a potentiometer on the electronics box mounted on the left of the instrument (see Figure 2.1). Without the white paint, the illumination was very uneven, being brighter on the LED side than on the far side. Without the black paint, stray light was escaping from all over the illuminator and scattering within the aperture housing of the instrument. The two coats in tandem are both necessary and sufficient.

Another feature requiring a new approach was the dark slide. Ideally, we would like two dark slides, one for each tube, each operated similarly to the existing miniphot dark slides. We had the same amount of space for the slide

as we did in the miniphot and could not find a way to fit in two slides. We did get twice as much travel from the same size slide, however, by adding a second track in the slide and a corresponding second drivepin in the actuating cam. This solution was a compromise: it does not allow the isolation of each tube for testing and debugging, but it does permit the observer to uncover (and cover) first one tube, then the other. In practice, there are only rare instances when we wish we had a second slide. Although the two slide tracks were machined with a computer-controlled milling machine, we believe they can be reproduced accurately enough with a set of X-Y coordinates, and some patience, on an ordinary mill.

Where light can get out, it can also get in. Initially, there was a light leak into the system through the viewing eyepiece. We added a dark slide which blocks the opening in the eyepiece tube while the Fabry lenses are in place and solved the problem quite effectively (see Figure 2.2).

Where possible, the components of the dual-beam miniphot were designed to be easy (and therefore inexpensive) to build. The aperture illuminator is an example of this effort; the dark slide and the rotating mount are examples of where this effort failed. Nonetheless, the McDonald machinists have estimated it actually costs less to machine the dual-beam unit than it does a single-beam miniphot.

2.5. Design Limitations

As stated earlier, the biggest constraint in the instrument design was trying to fit two independent lightbeams into the unvignetted field made available by the

existing guider boxes. It is the size of this field which dictated the separation of the apertures (8 mm center-to-center) and the resulting length-scale of the instrument, required the Fabry Lenses to be slightly off-axis (see Figure 2.4), and limits the workable F ratios. The observer can use the largest apertures (4mm) at F ratios up to F10.1, but is limited to smaller apertures at faster F ratios. At F9 all but the largest aperture are usable. The internal lightpath makes anything faster than about F8 unusable.

It would be possible to avoid both the need to bend the lightpath and the limitations at fast F ratios by increasing the unvignetted field size from the guider box. The limiting element determining the field size is the central hole of the large 45°mirror in the guider box. Were we to relax our criteria and allow modifications to the existing equipment, we could slightly enlarge this hole and increase our available field at the expense of comparison star search area, although the loss here would be unimportant. With such a modification, the apertures in the dual-beam miniphot could be further separated, keeping the entire lightpath in the instrument on-axis and allowing enough room to operate at smaller F ratios. This is a possible modification for the next generation instrument, although an increased aperture separation is not without problems of its own — such as fitting both apertures comfortably into the field of view of the aperture eyepiece with enough magnification to make centering a star in the smallest aperture possible.

One last piece that could be redesigned in a future version of the instrument is the rotating mount. Its combination of round and square features make machining it very difficult, which while not ideal, would be acceptable were its performance completely satisfactory. It is not. The

current detents are not strong enough to be easily felt and the mount itself is prone to flexure if a force (like an abnormally tight cable) pulls on it. It is capable of rotation, and under normal conditions does not flex, but its overall performance does not match the difficulty of machining it. A likely alternative will be a simpler system based on a circular bearing and a stronger detent.

2.6. Electronics and Software

Ask a physicist to provide a set of electronics for your new phototube and you will likely get something very pleasing to the physicist, but completely inappropriate for astronomical applications. Astronomy is traditionally photon-starved; the typical physics application is not. The physicist, as most phototube specification sheets will tell you, often use the phototube in a current-measuring mode whereas the astronomer *counts* each individual photon as if it were a rare gold coin. It is no surprise, then, the ensuing electronics are vastly different and cannot be interchanged with good results.

Each photoelectron liberated at the photocathode is amplified by the dynode chain inside the phototube, a stochastic process. Therefore, the number of electrons reaching the anode, and hence the height of the output pulse, varies wildly from pulse to pulse. The amplifying electronics must therefore have a discriminator to separate noise pulses from the photon-produced pulses and must be able to accommodate a variety of incoming pulse heights while producing uniform-height peaks at the output for easy counting later. There is no need for pulse amplitude normalization in current-measuring mode. It must be done here.

Another likely point of difference is the high voltage used to operate the tube. Either the photocathode is at ground and each successive dynode is at an increasingly higher positive potential, or the anode is at ground and each dynode working up to the photocathode is increasingly negatively charged. The first case uses positive high voltage; the latter, negative. When using negative high voltage, not only is the photocathode at a high negative potential, but the glass window at the surface of the phototube must be also or the photocathode material will wander through the glass surface and find itself outside the tube — clearly an undesirable situation. Also undesirable, however, is having a highly charged outer phototube surface. Using a grounded anode and positive high voltage eliminates all of these undesirables and has been in successful use for many years by WET observers.

In general, the electronics needed to operate a two-star photometer have changed little since those described in 1971 by Nather and Warner (Nather & Warner 1971), although the components have been updated. The additional electronics needed to power a third channel are simply replicas of those required for a single channel. The box that houses the electronics we use with the WET photometer is mounted on the left of the photometer as seen in Figure 1. The box contains a custom-designed interface (Clemens & Nather 1987) that counts the pulses from the amplifier/discriminators and sends them to an IBM-compatible PC for display and manipulation via a standard serial port connection, a driver board for the stepping motors, a high voltage power supply for the phototubes, and a low voltage supply for everything else.

The PC runs a program written by one of us (REN) called Quilt9. Originating from a version that ran on Data General NOVA computers,

Quilt9 communicates with the interface controlling such things as integration times, filter cycling and start/stop timings. It also graphically displays the lightcurves in real time, allowing the user to manipulate the display in a variety of ways and save the data to disc. The real-time display is critical for efficient data taking. We monitor the lightcurves continuously as the data arrive, so any problem can be quickly spotted and handled by the observer, avoiding the risk of discovering only after the run that bad equipment or poor technique had adversely affected the data. A very accurate, temperature-compensated crystal oscillator in the interface provides the fundamental timing signals used by both the interface and Quilt9. The photometric package is completed with a separate program called QED (also written by REN) for reducing the data. With a user-interface similar to that in Quilt9, QED runs on IBM-compatible computers and provides the standard tools for high-speed photometry data reduction (Nather et al. 1990).

3. Results

Our primary goal in building the dual-beam miniphot was to increase our ability to measure pulsation amplitudes. Having used the earlier three-channel photometer, we knew this goal would be easily reached. To demonstrate this effect, we used the data set from the May, 1994 WET run on the DB white dwarf variable, GD 358 where we had a pair of these new WET Standard photometers in operation: one at the 24" telescope at Siding Spring Observatory in Australia, and one used on the 36" and 82" telescopes at McDonald Observatory. Selecting only runs long enough to resolve neighboring pulsation modes, we took one fairly isolated mode and measured its amplitude

in each run. Figure 2.5 has the WET photometer data plotted as $\times$s (and offset 40mma for clarity [2]) and all other data (which includes some other 3-channel instruments) as $\circ$s. Most of the telescopes in the network are 1 – 2m in diameter. We determined the mode's amplitude by a linear least-squares fit to each lightcurve of a sine curve with a fixed period, taken from the overall Fourier transform of the data set. The formal uncertainties on each point are roughly equal and usually of the same order as the size of the plotted points. The results show the data from the new instruments to have a mean of 13.9 ± 6mma compared to 17.7 ± 9mma for the rest of the data set. The new instruments produced measured pulsation amplitudes 50% more accurate than the other WET photometers. Note, however, the scatter in Figure 2.5 is not entirely random; indeed it appears to be periodic with a period of roughly four days, likely caused by the beating of two closely-spaced frequencies. The mode we chose to measure is actually one member of a multiplet of closely-spaced modes with an intra-mode spacing of about 6μHz, corresponding to a beat period of almost two days. Since there may be more than one such spacing, the period we see (four days) is quite consistent with the expected beating due to low-power nearby modes. A hint of this beating process is also seen in the upper panel of Figure 2.5, but it is quite obvious in the WET photometer data. At any rate, the scatter is not random and is likely to be intrinsic to the star, making the WET photometer amplitudes even more precise than the standard deviation would suggest.

We have often claimed that with two channels on our photometer,

---

[2]The unit *mma* refers to milli-modulation amplitude of the observed variation. 1000mma is equivalent to 100% modulation.

we could correct for thin clouds simply by dividing the ch1 lightcurve by ch2. In practice, however, it never really worked well. Whereas transparency variations such as clouds and extinction affect both lightcurves the same percentage, sky adds directly to the light measured and depending on the brightness of the observed stars, is a different percentage of the actual number of photons counted. In general then, dividing two lightcurves with unequal sky-to-star ratios is ineffective. The sky background can be considered a DC offset and therefore division does not completely remove it. The results are particularly bad with moonlit clouds if the stars are of unequal brightnesses. With the sky channel accurately removing the sky background from the data, however, some cloud correction is now possible.

Figure 2.6 is a run taken with the new WET photometer at the 24" telescope at Siding Spring Observatory, Australia. The run was started about 20 minutes before evening twilight and continued roughly 30 minutes past morning twilight. The top panel is the unreduced lightcurve from the target star, PG1159–035, showing both the effects of twilight and of occasional passing clouds. The middle panel is the same lightcurve, just with the sky subtracted. The bottom panel is a semi-reduced lightcurve, with the sky subtracted, atmospheric extinction corrected, and our cloud correction routines applied. The y-scale of each plot is different to accommodate the true range in the data. The onset of twilight is now undetectable and some of the clouds have been effectively removed. Note that where the cloud is not completely corrected, the original counts had fallen nearly 85%; we can't correct for that much cloud extinction. The increase in noise at each end of the lightcurve is due primarily to the heavy atmospheric extinction correction

needed, and partly to the noise that accompanies the large sky counts during twilight. In practice, we would not use all these data, but the figure shows that some corrections can be made with the third channel that are not possible without it.

Two more figures show some of the conditions under which we have taken data with the new instrument we couldn't have otherwise. Both Figures 2.7 and 2.8 are from runs taken with three-channel instruments on the 36" telescope at McDonald Observatory in Texas. The target object in Figure 2.7 is PG1351+489, a low-amplitude, Bmag $\approx$ 16, DB pulsator. The left-half of the top three panels of the figure are the raw data for each channel: PG1351, comparison star, and sky. Note it is nearly impossible to spot which curve is the real variable. The bottom two panels show the reduced channel 1 and channel 2 data (with the sky subtracted), leaving a nearly flat comparison star and an obvious variable in channel 1. To the right of each lightcurve is a Fourier transform (FT) of the data (in the first and second panels, the data are reduced normally, except a constant equal to the mean value of sky is subtracted from the data in lieu of the continuous sky subtraction performed in the last two panels). Since the mean sky value is a factor of three times the mean ch1 counts and one third the ch2 counts, the size of the noise introduced in the FT differs in each panel; for ch1, the noise goes off scale to nearly 170mma. The reduced ch1 FT clearly shows the expected periodicity near 2000μHz(500s) which is also present in the uncorrected FT, but almost lost in the noise. A peak half this amplitude would be completely lost in the noise: present, but not detected.

The data shown in Figure 2.8 are of the DA pulsator G29–38, taken

in clear skies (starting shortly before twilight), but surrounded by lightning. The top panel is the raw target data, while the lower panel shows the sky-subtracted data. Without the sky channel, most of the run would simply be too noisy to be of much scientific value. As in the case of the data in Figure 2.7, an occasional measurement of the sky taken every 20 minutes would leave the artifacts in the data. The lightning, however, is nicely removed from the data by subtracting the continuous sky channel. So, too, are other occurrences of scattered light, like moonlight reflecting off a rotating dome, car headlights, and stray flashlight beams.

4. Conclusion

The Whole Earth Telescope has made remarkable instrumental progress that has made the asteroseismological studies of white dwarfs possible. One further instrumental step was required that would allow the WET to obtain more accurate pulsation amplitude information, extend available observing time to include grey and bright time, and allow useful data to be obtained on dimmer stars with smaller telescopes. Adding a sky channel to the existing two-channel photometers meets all the above objectives. We therefore designed a new dual-beam miniature photometer that is a bolt-on upgrade to turn existing two-channel photometers into three-channel photometers that have the new ability to measure the sky brightness continuously. We will make the plans of the new instrument (including the electronics, computer interface, and software) available to all interested parties on request.

To summarize, we present here the principal characteristic of the WET photometer and those that any other photometer must also have to be

considered an acceptable replacement:

1. Three counting channels: target star, comparison star and sky
2. No reflection optics in channel 1 (coated Fabry lens only)
3. Mu-metal shielded Bi-alkali PMT detectors in all channels (Hamamatsu R647)
4. Adjustable apertures in all channels, concentric, identical in size
5. Independent filters in all channels, after Fabry lens, motor-driven
6. Provision for guiding without interrupting the data channels
7. Precise telescope focussing method (e.g. knife-edge)
8. Unitized TTL pulse output from PMT preamplifier/discriminator
9. Live, real-time graphical display of the 3 incoming light curves
10. Portability

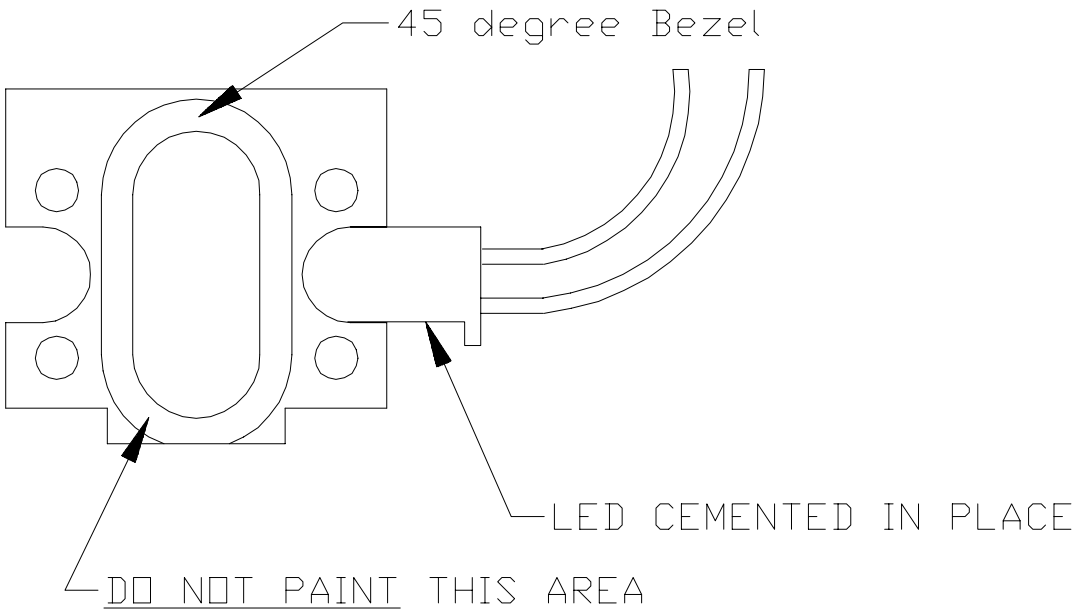

Fig. 2.3.— The new aperture illuminator design.

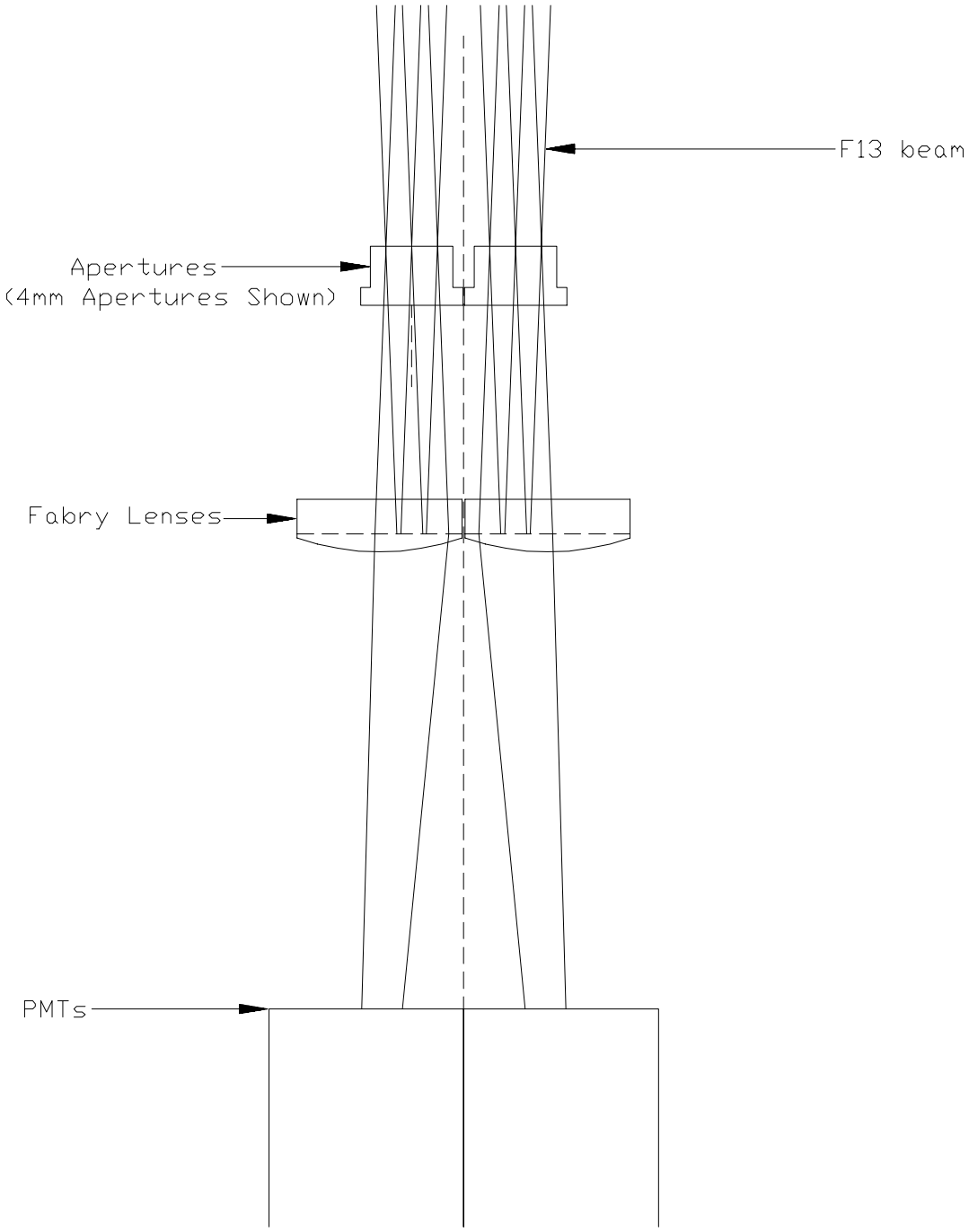

Fig. 2.4.— The lightpath through the dual-beam miniphot.

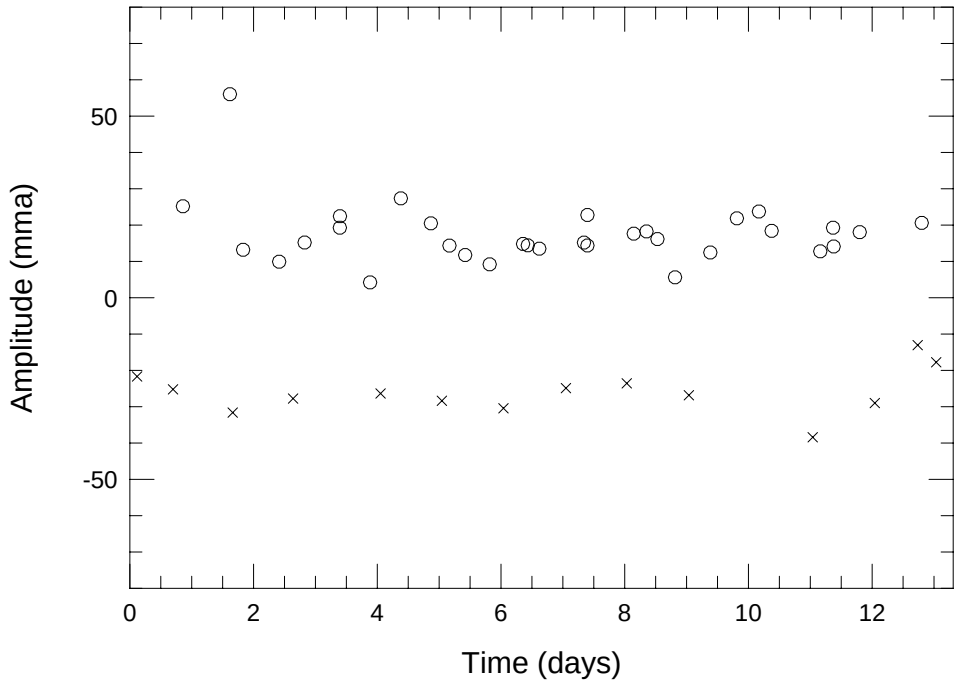

Fig. 2.5.— Amplitudes of a pulsation mode measured in a WET run by standard WET photometers (× — displaced -40mma) and all others in the network (○).

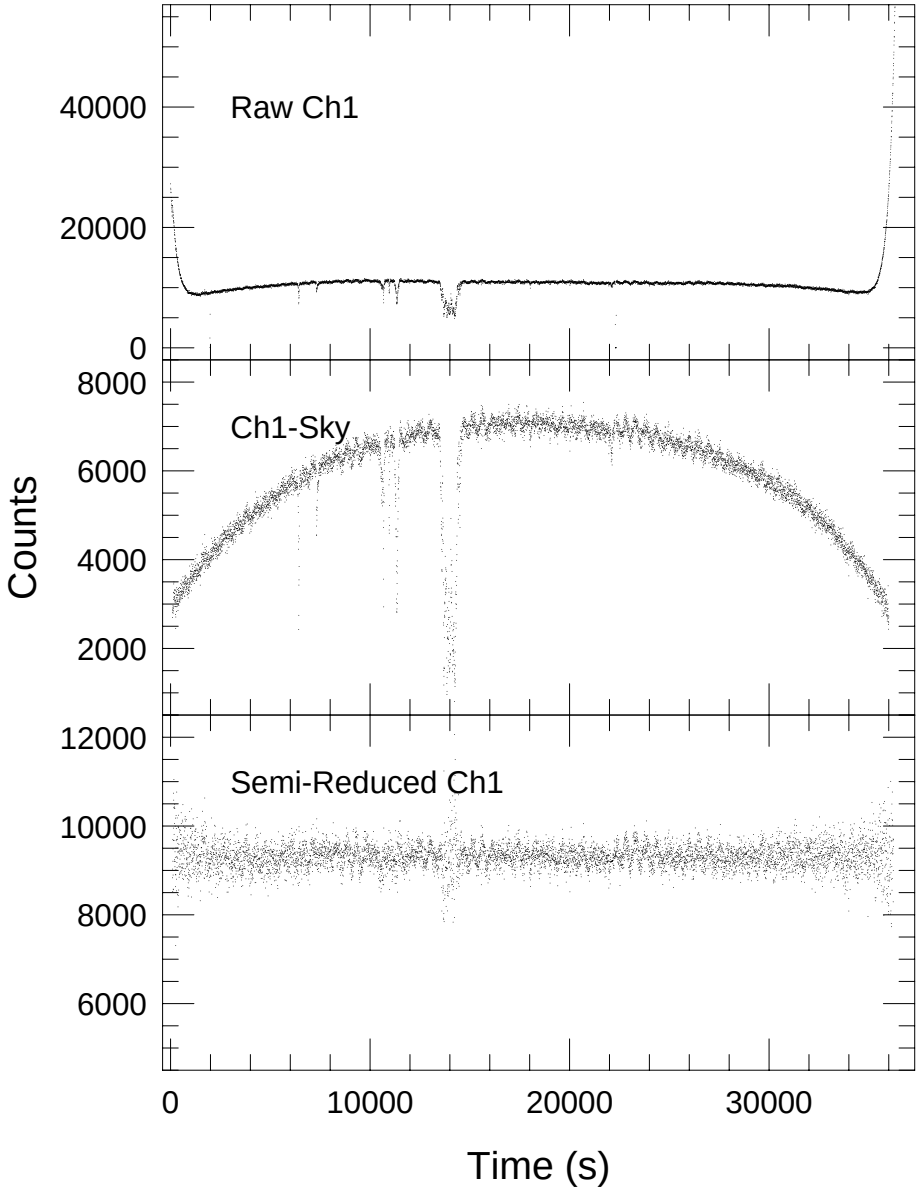

Fig. 2.6.— Observing in twilight and cloud with the WET photometer.

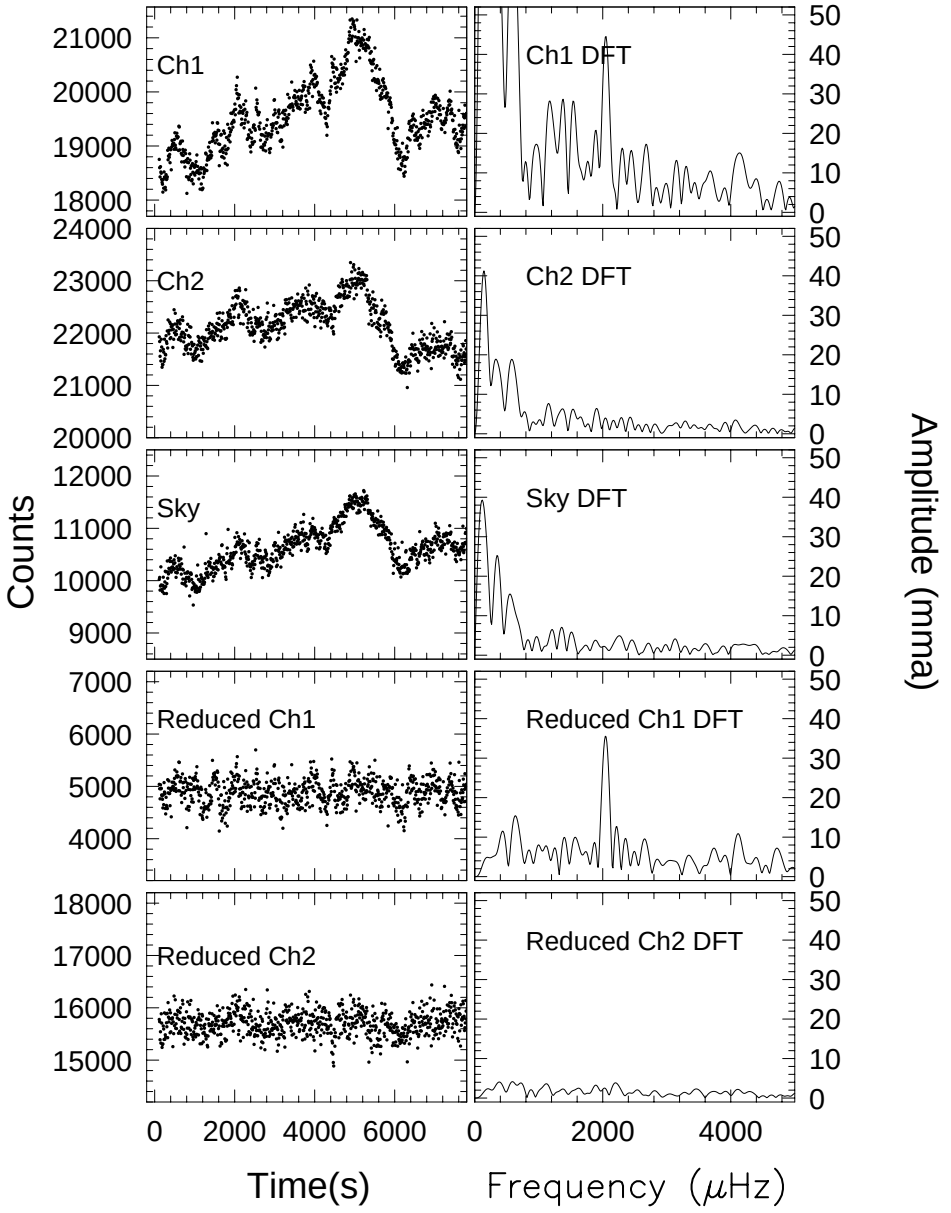

Fig. 2.7.— Three channel data taken during extreme sky variations.

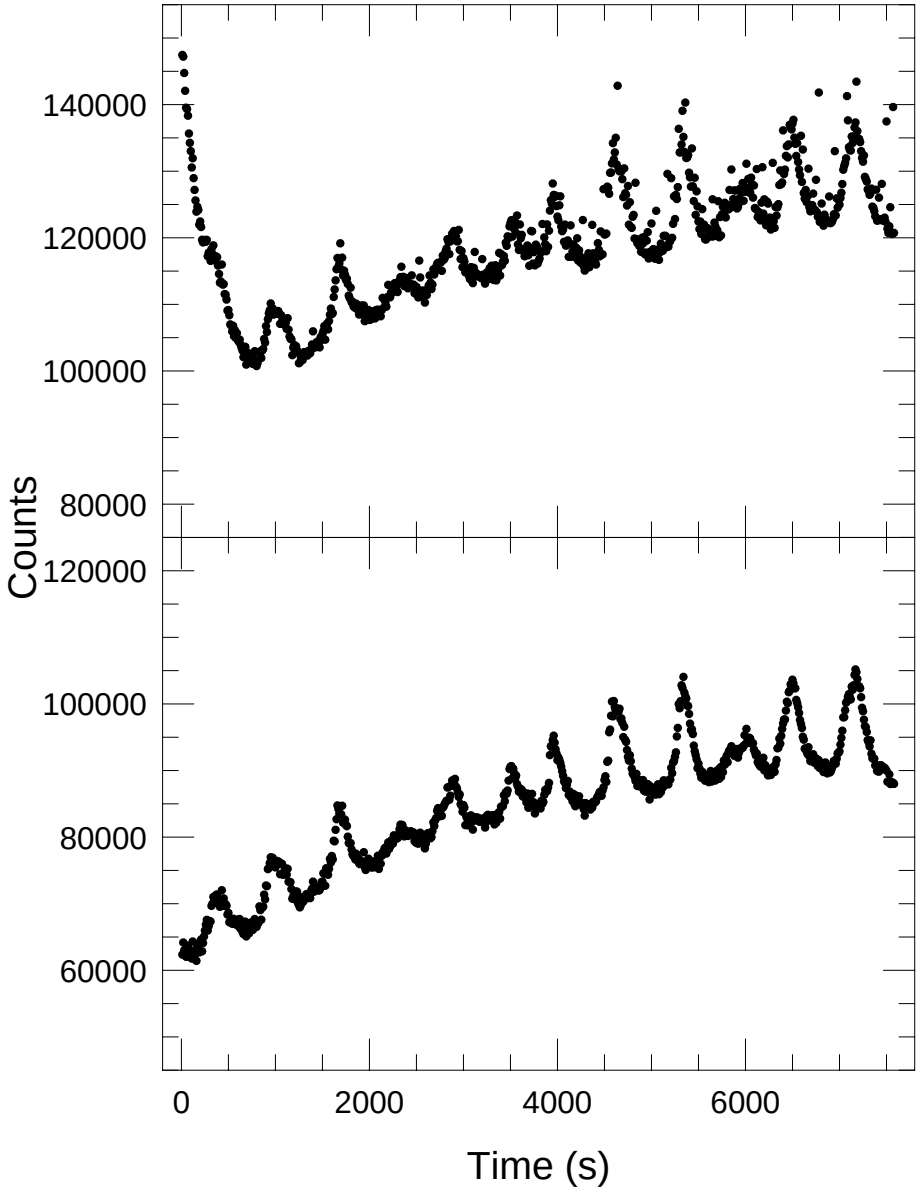

Fig. 2.8.— Three channel data taken with surrounding lightning.

Chapter 3

Observations and Techniques

Didn't get to sleep last night
'til the morning came around.
—Jerry Garcia, J. Dawson, & Robert Hunter, *Friend of the Devil*

The purpose of this chapter is not only to describe the observations discussed here and how they were obtained, but also to describe the extraction process from lightcurves to asteroseismology.

1. Introduction

Asteroseismology depends on mode identification. Mode identification depends on the ability to recognize patterns in the data: the m-splittings and k-(period-) spacings discussed earlier are the two main keys. Accurate pulsation frequencies, combined with the assigned k, ℓ, and m values form our set of observables, to be matched to theoretical models. Adjusting the physics going into the models until the match is made, we derive the physical properties of the star which are as accurate as the physics we include in the models. Where

we have been able to verify asteroseismological measurements, we find the included physics appears to be quite good.

The search for mode identification begins in the Fourier transform of the observed lightcurves. The lightcurves, therefore, serve mainly to feed the FT where most of the analysis is performed. The domain of some of our analysis tools is in the lightcurve space, but the most crucial work of mode identification is always done in the transformed space. To this end, the spectral window plays a very important role: our ability to measure modes accurately depends directly on the quality of our spectral window. Early on, we found the spectral windows provided by conventional observations were not good enough for asteroseismological measurements. As with the instrument described in the previous chapter, designed to increase modal amplitude measurement precision, we developed another instrument (actually done before the dual-beam miniphot was born) to improve our spectral window. This instrument is of course the Whole Earth Telescope (WET), not that we are claiming credit for the Earth, or any of the single telescopes on it, just for the combination we use for our measurements. In keeping with astronomical tradition, we named the telescope after its mounting.

Unfortunately, even the WET was not the only required tool to investigate the cool DAVs. Here, since modes come and go from one observing season to another, we needed a long baseline of observations; extensive single-site data were needed to supplement the intense, but short, WET observations. Were the WET available all the time, we would have employed it to look continuously at our objects over many observing seasons, but since it is a rather burdensome tool, best used only for things that can be solved

no other way, we could only use the WET to establish a baseline on which seasonal single-site data could continue to expand. In theory, once a star is resolved with the WET, single-site data can continue to monitor things even without being able to independently separate modes from spectral window aliases. In practice, however (at least with the stars discussed here), the observed modes change so much that the WET data does little to improve mode identification from single-site data. The single-site data, therefore, have to be of exceptionally good quality to be useful.

2. Temporal Spectroscopy

Since most of our analysis is done in FT, or frequency, space and since our observing techniques have little to do with conventional filter-photometry, we call our observing technique, *temporal spectroscopy.* Our goal is to analyze the frequencies (in time) of oscillations in the stars we observe; our final product is a temporal spectrum, an FT, of the object under study.

Single-site observations mean we will be left with unavoidable coverage gaps in our data. We can only minimize them by observing as long as possible each night, observing quite literally from treetop to treetop (or sometimes dome to dome) and as far into each astronomical twilight as possible. We observe at large airmasses, even though all good photometrists know no useful data can be taken past an airmass of two or three. Still, nothing we can do from a single site will remove the inevitable one day alias in the resultant FT. We can only minimize its effect by obtaining a long baseline, so the FT resolution is high enough to distinguish the aliases from any nearby modes

and has a high enough signal to noise ratio so the window pattern of each peak is clearly evident.

The WET strives to eliminate aliases in the FT by eliminating gaps in observational coverage of the lightcurve. To do this, we employ a network of collaborating astronomers observing at various sites around the world, so there is always one telescope under darkness. Ideally, each collaborator observes at their home institution's site, but in reality, there are some sites in the network without local collaborators, and hence we must send observers there from other places, often with a standard instrument brought along as checked baggage.

It has often been said, even in print (Schwarzschild 1995), that only three, or even two, sites, if they are spaced correctly, are needed for continuous coverage. Ignoring for the moment the availability of three such sites equally spaced around the globe, there are other problems with this arrangement: weather, accessibility of the target object for the full 8 hours from each site, and the availability and assignment of precisely concurrent telescope time. We typically run with 12–13 sites, split almost equally between the Northern and Southern hemispheres. In this way, the WET as an instrument enjoys better weather than any one of its sites, and we do not require the longest nights of the year to ensure our data overlap each other.

We find that data overlap, where two sites are observing the same star at the same time, is useful on many grounds. For one, we can calibrate extinction models (the data must look the same no matter which site at which airmass took it) and verify timings of each run. The overlap also increases our signal to noise ratio, temporarily forming a bigger telescope from two

smaller ones. Instead of obtaining overlapping data, we can, at the discretion of the PI at headquarters, use two clear sites to observe two different stars at the same time. With our redundancy of sites and clear weather, we have occasionally gone around the globe with continuous coverage on two target stars at the same time. The decision on which stars to observe at which site comes from the command center which operates continuously during the run.

One reason for coining the new term, *temporal spectroscopy*, was to clearly separate it from the preconceived biases associated with the term *photometry*. If you are a filter photometrist observing a dim object, you just integrate longer; you don't need a bigger telescope. In our case, however, the stars themselves (by their rapid variability) set the maximum allowable integration times and therefore the minimum telescope aperture needed to observe them. In addition, we do not care about the mean brightness of our targets — only their excursions above and below the mean. Thus, the amplitude of the variations present also determine the telescope aperture needed to measure them. It is not simply a matter determined by the stars' mean magnitudes. These are all concepts unfamiliar to many telescope allocation committees.

3. The Data

What if our aliens[1] tried to study the Earth from their home planet before coming here and stealing a mortuary-load of corpses? On their home planet, they had multiple suns, so nighttime was extremely rare. Whenever it did

[1]See Chapter 1.

come, however, they rushed to their telescopes to gaze upon our planet. They only had very high-powered telescopes (their technology was very advanced, perhaps too much for their own good in this case) and could only see a small part of the the Earth at once, although at very high magnification. They were shocked to realize every time they looked at us, we appeared different. They never saw the same land, the same buildings, the same people. While their best theorists could easily come up with three ways to explain this, they never really succeeded in making any successful predictions; they only explained the observations in retrospect. Debate was endless: were they seeing some underlying pattern that would eventually repeat and make itself clear with extended observations that might eventually cover the entire range of observable states, or were these Earthlings very chaotic, constantly changing and electing new leaders every four years?

While the debate raged on our alien world, a similar one took place here on Earth, this one concerning our observations of the cool DAVs. We already knew each seasonal cool DAV power spectra contained mostly linear combination modes. Many of the non-combination modes were unstable, varying from one seasonal observation to the next. We had occasionally seen them disappear, but did not know if they would ever reappear. We had seen new modes appear, but did not know if they were just previously unseen ks or ℓs of a constant underlying structure, or a never-ending stream of randomly-placed power. By gathering data over many seasons and searching for this underlying structure, if it existed, we hoped to address these issues by answering a fundamental question: are the pulsations seen in the cool DAVs normal modes or not?

The cool DAVs change their power spectra on yearly timescales, so I needed a number of years of intense observations to obtain the desired data set. In the interest of brevity (of my career as a graduate student,[2] not of this thesis), I concentrated on one star, G29–38, obtaining a smaller data set on each of the other stars studied. All totaled, I have over 1100 hours of data on G29–38 alone. Many people contributed to this data set. I could not have done this work without them and their data.

The run names in Table 3.1 tell who took the data. sjk* runs are mine. The s* and r* runs from 1985 were taken by Darragh O'Donoghue, Don Kurtz, Butler Hine, Ed Nather, Brian Warner, and J. Allen Hill. jcc* runs, throughout the span of the data set, are from J. Chris Clemens. Chuck Claver (cfc*), Paul Bradley (pab*), Marian Frueh (mlf*), and Al Grauer (a*) provided runs immediately after the Xcov2 WET campaign. Paul Bradley, Judi Provencal (jlp*), and Todd Watson (tkw*) provided additional data outside of WET campaigns. The WET participants (as listed in Winget et al. 1990 & Kleinman et al. 1994) are many and include, in addition to the above, D.E. Winget, E.L. Robinson, G. Fontaine, N. Achilleos, T.M.K. Marar, S. Seetha, B.N. Ashoka, P. Martinez, G. Vauclair, M. Chevreton, A. Kanaan, S.O. Kepler, T. Augusteijn, J. Van Paradijs, C.J. Hansen, J. Liebert, K. Yanagida, J.S. Dixson, D.J. Sullivan, E. Meštas, E.M. Leibowitz, P. Moskalik, S. Zola, G. Pajdosz, J. Krzesinski, J.-E. Solheim, A. Bruvold, M. Katz, N. Dolez, M.A. Barstow, O. Giovannini, and S.D. Kawaler.

The G29–38 table of observations is presented in Table 3.1. In it are

[2] Oops, too late!

the name, site, date, and time of each run used in this work. Much of the data are single-site taken from McDonald. In addition, there are two WET campaigns (Nov, 1988, and Sep, 1992) where G29–38 was one of several target objects and a dual-site (SAAO and McDonald) campaign in 1985.

Table 3.1. Journal of Observations for G29–38.

Telescope	Run Name	Date (UT)	Runstart (UT)
SAAO 74"	s3598	1985 Aug 8	0:54:04
SAAO 74"	s3606	1985 Aug 10	22:23:42
SAAO 30"	s3615	1985 Aug 13	20:56:20
SAAO 30"	s3618	1985 Aug 14	20:23:40
SAAO 30"	s3621	1985 Aug 15	20:24:00
SAAO 30"	s3624	1985 Aug 16	19:51:20
SAAO 30"	s3628	1985 Aug 17	20:14:20
SAAO 30"	s3631	1985 Aug 19	20:42:20
SAAO 40"	s3634	1985 Aug 20	21:05:16
SAAO 40"	s3638	1985 Aug 21	22:21:45
McDonald 36"	r3084	1985 Aug 22	6:37:26
McDonald 36"	r3085	1985 Aug 23	7:43:21
SAAO 40"	s3642	1985 Aug 23	20:54:18
SAAO 40"	s3645	1985 Aug 24	20:59:43
SAAO 40"	s3647	1985 Aug 25	20:06:20
McDonald 36"	r3086	1985 Aug 26	7:19:19
SAAO 40"	s3651	1985 Aug 26	20:20:03
SAAO 30"	s3654	1985 Sep 10	18:44:20
SAAO 30"	s3655	1985 Sep 13	17:42:00
SAAO 30"	s3656	1985 Sep 14	17:43:00
SAAO 30"	s3658	1985 Sep 15	0:42:40

Table 3.1—Continued

Telescope	Run Name	Date (UT)	Runstart (UT)
SAAO 30"	s3660	1985 Sep 15	17:39:20
SAAO 30"	s3663	1985 Sep 16	17:39:20
McDonald 82"	r3088	1985 Oct 22	2:58:37
McDonald 82"	r3094	1985 Oct 31	3:02:00
McDonald 82"	r3095	1985 Nov 1	1:56:30
McDonald 30"	jcc-55	1988 Oct 24	2:00:00
McDonald 30"	jcc-57	1988 Oct 25	1:50:00
McDonald 30"	jcc-59	1988 Oct 26	4:50:00
SAAO 0.75m	s4453	1988 Nov 4	18:38:0
McDonald 82"	maw-0017	1988 Nov 6	1:42:20
SAAO 0.75m	s4455	1988 Nov 6	18:23:0
McDonald 82"	maw-0019	1988 Nov 7	1:31:00
SidingSpring 40"	ren-0040	1988 Nov 7	11:12:30
SidingSpring 40"	ren-0042	1988 Nov 8	9:41:00
McDonald 82"	maw-0023	1988 Nov 9	1:21:10
McDonald 82"	maw-0024	1988 Nov 9	4:54:40
SidingSpring 40"	ren-0044	1988 Nov 9	9:41:10
SAAO 0.75m	s4456	1988 Nov 9	18:53:3
McDonald 82"	maw-0026	1988 Nov 10	1:23:00
SidingSpring 40"	ren-0045	1988 Nov 10	9:28:50
SAAO 0.75m	s4457	1988 Nov 10	18:33:5

Table 3.1—Continued

Telescope	Run Name	Date (UT)	Runstart (UT)
McDonald 36"	cfc-0001	1988 Nov 11	1:51:00
OHP 1.93m	gv37	1988 Nov 11	18:59:20
McDonald 82"	maw-0029	1988 Nov 12	1:24:10
McDonald 36"	cfc-0002	1988 Nov 12	3:41:01
MaunaKea 24"	a91	1988 Nov 12	5:12:00
SidingSpring 40"	ren-0049	1988 Nov 12	9:30:10
SAAO 0.75m	s4458a	1988 Nov 12	19:41:5
McDonald 82"	maw-0031	1988 Nov 13	0:51:20
McDonald 36"	cfc-0005	1988 Nov 13	3:03:50
MaunaKea 24"	a93	1988 Nov 13	8:04:00
SidingSpring 40"	ren-0053	1988 Nov 13	9:28:20
OHP 1.93m	gv39	1988 Nov 13	18:12:30
McDonald 82"	maw-0033	1988 Nov 14	1:04:00
McDonald 36"	cfc-0009	1988 Nov 14	3:22:30
McDonald 36"	cfc-0010	1988 Nov 15	3:46:30
McDonald 82"	maw-0036	1988 Nov 16	1:07:20
MaunaKea 24"	a97	1988 Nov 16	6:29:00
McDonald 82"	maw-0038	1988 Nov 17	0:58:20
McDonald 82"	maw-0039	1988 Nov 17	2:47:20
SAAO 0.75m	s4466	1988 Nov 17	18:43:0
McDonald 82"	maw-0040	1988 Nov 18	6:05:40

Table 3.1—Continued

Telescope	Run Name	Date (UT)	Runstart (UT)
SAAO 0.75m	s4468	1988 Nov 18	18:43:0
McDonald 82"	maw-0042	1988 Nov 19	0:52:20
McDonald 30"	mlf-0001	1988 Nov 20	1:19:28
SAAO 0.75m	s4472a	1988 Nov 21	18:52:0
McDonald 30"	mlf-0003	1988 Nov 22	1:04:03
McDonald 30"	sjk-0004	1988 Nov 23	1:42:50
McDonald 30"	sjk-0005	1988 Nov 24	1:29:40
McDonald 30"	cfc-0016	1988 Nov 26	1:01:40
McDonald 30"	cfc-0017	1988 Nov 27	0:50:00
McDonald 30"	cfc-0018	1988 Nov 28	0:57:50
SAAO 0.75m	s4480	1988 Nov 28	19:29:1
McDonald 30"	pab-0002	1988 Nov 29	1:14:50
McDonald 36"	pab-0003	1988 Nov 29	3:24:20
McDonald 36"	pab-0004	1988 Dec 1	0:44:30
MaunaKea CFHT	jcc-0063	1988 Dec 1	5:54:30
MaunaKea CFHT	jcc-0066	1988 Dec 2	4:59:10
McDonald 36"	pab-0009	1988 Dec 3	0:54:10
McDonald 36"	pab-0011	1988 Dec 4	0:56:20
McDonald 36"	mlf-0004	1988 Dec 14	1:21:21
McDonald 36"	mlf-0005	1988 Dec 15	1:17:04
McDonald 36"	jcc-0069	1988 Dec 21	1:25:00

Table 3.1—Continued

Telescope	Run Name	Date (UT)	Runstart (UT)
McDonald 36"	jcc-0071	1988 Dec 22	1:24:00
KPNO 1.3-m	a100	1988 Dec 30	2:47:00
KPNO 1.3-m	a104	1988 Dec 31	1:57:00
KPNO 1.3-m	a107	1989 Jan 1	1:57:00
KPNO 1.3-m	a112	1989 Jan 6	1:49:00
KPNO 1.3-m	a118	1989 Jan 9	1:56:00
McDonald 36"	jcc-0087	1989 Jun 5	9:42:00
McDonald 36"	jcc-0091	1989 Jun 8	8:45:00
McDonald 36"	jcc-0095	1989 Jun 12	8:46:30
McDonald 36"	jcc-0097	1989 Jun 13	8:35:00
McDonald 36"	jcc-0100	1989 Jul 1	7:22:00
McDonald 36"	jcc-0102	1989 Jul 2	7:10:30
McDonald 36"	jcc-0104	1989 Jul 3	7:21:30
McDonald 36"	sjk-0008	1989 Jul 4	7:10:00
McDonald 36"	sjk-0010	1989 Jul 5	7:12:30
McDonald 36"	sjk-0012	1989 Jul 6	7:00:00
McDonald 36"	jcc-0112	1989 Jul 13	6:31:00
McDonald 36"	jcc-0114	1989 Aug 1	5:38:00
McDonald 36"	jcc-0116	1989 Aug 2	5:36:00
McDonald 36"	jcc-0117	1989 Aug 6	5:36:00
McDonald 36"	sjk-0015	1989 Aug 9	5:47:30

Table 3.1—Continued

Telescope	Run Name	Date (UT)	Runstart (UT)
McDonald 36"	sjk-0016	1989 Aug 10	8:26:00
McDonald 36"	sjk-0018	1989 Aug 11	6:39:00
McDonald 36"	jcc-0119	1989 Aug 30	5:30:27
McDonald 36"	jcc-0120	1989 Sep 3	3:10:00
McDonald 36"	jcc-0122	1989 Sep 4	2:40:00
McDonald 30"	sjk-0021	1989 Sep 17	2:46:30
McDonald 30"	sjk-0022	1989 Sep 18	2:29:30
McDonald 30"	sjk-0023	1989 Sep 19	2:46:00
McDonald 30"	sjk-0024	1989 Sep 19	8:14:30
McDonald 30"	sjk-0025	1989 Sep 20	2:42:00
McDonald 30"	sjk-0027	1989 Sep 21	2:20:30
McDonald 30"	sjk-0029	1989 Sep 22	2:25:00
McDonald 30"	sjk-0030	1989 Sep 23	4:38:00
McDonald 30"	sjk-0031	1989 Sep 24	2:07:00
McDonald 30"	sjk-0032	1989 Sep 25	2:09:30
McDonald 36"	sjk-0033	1989 Sep 26	2:27:30
McDonald 36"	sjk-0035	1989 Sep 27	2:10:30
McDonald 36"	sjk-0036	1989 Sep 28	2:04:00
McDonald 36"	sjk-0037	1989 Sep 29	2:03:30
McDonald 36"	sjk-0038	1989 Sep 30	2:04:00
McDonald 36"	sjk-0039	1989 Oct 1	1:57:00

Table 3.1—Continued

Telescope	Run Name	Date (UT)	Runstart (UT)
McDonald 36"	sjk-0046	1989 Oct 4	1:55:30
McDonald 36"	jcc-0124	1989 Oct 24	4:29:00
McDonald 36"	jcc-0126	1989 Oct 25	1:37:00
McDonald 36"	jcc-0130	1989 Oct 29	1:31:30
McDonald 36"	pab-0014	1989 Oct 31	1:24:30
McDonald 36"	pab-0016	1989 Nov 1	3:26:00
McDonald 36"	pab-0019	1989 Nov 3	1:10:00
McDonald 36"	sjk-0048	1989 Nov 19	4:20:30
McDonald 36"	sjk-0049	1989 Nov 22	3:54:00
McDonald 36"	sjk-0051	1989 Nov 23	4:40:30
McDonald 36"	sjk-0053	1989 Nov 26	0:56:00
McDonald 36"	sjk-0055	1989 Nov 27	1:03:00
McDonald 36"	sjk-0056	1989 Dec 9	1:40:00
McDonald 36"	sjk-0058	1989 Dec 10	1:21:00
McDonald 36"	sjk-0060	1989 Dec 13	1:21:30
McDonald 36"	sjk-0064	1989 Dec 15	1:22:30
McDonald 36"	sjk-0103	1990 Jun 20	7:46:30
McDonald 36"	sjk-0105	1990 Jun 21	7:43:10
McDonald 36"	pab-0051	1990 Aug 25	6:43:30
McDonald 36"	pab-0053	1990 Aug 26	6:36:30
McDonald 36"	pab-0054	1990 Aug 26	9:59:30

Table 3.1—Continued

Telescope	Run Name	Date (UT)	Runstart (UT)
McDonald 36"	pab-0056	1990 Aug 27	6:44:30
McDonald 36"	pab-0058	1990 Aug 28	6:45:30
McDonald 36"	pab-0060	1990 Aug 29	9:08:30
McDonald 36"	pab-0062	1990 Aug 30	5:51:30
McDonald 36"	pab-0064	1990 Aug 31	5:26:00
McDonald 30"	pab-0065	1990 Sep 1	5:01:00
McDonald 36"	sjk-0106	1990 Sep 9	6:58:00
McDonald 36"	sjk-0107	1990 Sep 10	2:28:30
McDonald 36"	sjk-0108	1990 Sep 11	2:37:30
McDonald 36"	sjk-0109	1990 Sep 12	2:28:30
McDonald 36"	sjk-0110	1990 Sep 18	3:55:00
McDonald 36"	jcc-0159	1990 Sep 28	3:40:30
McDonald 36"	jcc-0163	1990 Oct 9	1:50:00
McDonald 36"	jcc-0164	1990 Oct 10	2:01:00
McDonald 36"	jcc-0166	1990 Oct 11	2:32:00
McDonald 82"	g293020	1990 Oct 20	1:59:28
McDonald 82"	g293027	1990 Oct 22	1:46:13
McDonald 82"	g293034	1990 Oct 23	1:40:29
McDonald 36"	sjk-0112	1990 Oct 24	2:22:30
McDonald 36"	sjk-0114	1990 Oct 25	1:20:00
McDonald 36"	sjk-0116	1990 Oct 26	1:22:30

Table 3.1—Continued

Telescope	Run Name	Date (UT)	Runstart (UT)
McDonald 36"	sjk-0118	1990 Oct 27	1:14:00
McDonald 36"	sjk-0121	1990 Oct 29	1:15:00
McDonald 36"	sjk-0123	1990 Nov 10	1:08:00
McDonald 36"	sjk-0125	1990 Nov 11	1:04:00
McDonald 36"	sjk-0129	1990 Nov 14	1:04:30
McDonald 36"	sjk-0130	1990 Dec 18	2:55:00
McDonald 36"	sjk-0132	1990 Dec 19	1:21:30
McDonald 36"	sjk-0134	1990 Dec 20	2:24:00
McDonald 36"	sjk-0136	1990 Dec 21	3:02:30
McDonald 36"	sjk-0143	1991 Jan 16	1:19:00
McDonald 36"	jcc-0185	1991 Jul 18	7:44:00
McDonald 36"	sjk-0156	1991 Sep 4	3:01:00
McDonald 36"	sjk-0158	1991 Sep 8	7:38:00
McDonald 82"	jcc-188	1991 Oct 16	1:47:00
McDonald 82"	jcc-190	1991 Oct 17	1:46:00
McDonald 36"	sjk-0164	1991 Oct 17	3:11:00
McDonald 36"	sjk-0166	1991 Nov 4	1:51:00
McDonald 36"	sjk-0168	1991 Nov 5	1:51:30
McDonald 36"	sjk-0171	1991 Nov 6	1:28:00
McDonald 36"	sjk-0173	1991 Nov 7	1:27:30
McDonald 36"	sjk-0175	1991 Nov 9	1:29:00

Table 3.1—Continued

Telescope	Run Name	Date (UT)	Runstart (UT)
McDonald 36"	sjk-0177	1991 Nov 10	1:25:00
McDonald 36"	sjk-0179	1991 Dec 11	2:31:00
McDonald 36"	sjk-0180	1991 Dec 13	2:09:00
McDonald 36"	sjk-0182	1991 Dec 14	1:22:00
McDonald 82"	tkw-0017	1992 Aug 23	9:13:30
LNA 1.6m	ro018	1992 Sep 22	3:24:30
LaPalma INT	int-0009	1992 Sep 22	3:54:40
LaPalma INT	int-0013	1992 Sep 23	2:42:50
CTIO 1.5m	jlp-0114	1992 Sep 23	6:25:45
CTIO 1.5m	jlp-0117	1992 Sep 24	6:28:35
Maidanak 1.0m	jesem-07	1992 Sep 24	21:51:00
LaPalma INT	int-0016	1992 Sep 25	2:09:10
McDonald 82"	pab-0154	1992 Sep 25	9:26:00
Maidanak 1.0m	jesem-09	1992 Sep 25	20:53:20
CTIO 1.5m	jlp-0122	1992 Sep 26	6:30:10
McDonald 82"	pab-0158	1992 Sep 26	9:26:00
OHP 1.93m	gv-0236	1992 Sep 26	1:56:30
CTIO 1.5m	jlp-0124	1992 Sep 27	6:31:40
McDonald 82"	pab-0161	1992 Sep 27	9:55:30
Maidanak 1.0m	jesem-13	1992 Sep 27	22:49:50
LaPalma INT	int-0023	1992 Sep 28	3:49:50

Table 3.1—Continued

Telescope	Run Name	Date (UT)	Runstart (UT)
CTIO 1.5m	jlp-0127	1992 Sep 28	6:17:00
McDonald 82"	pab-0164	1992 Sep 28	10:01:30
McDonald 82"	pab-0167	1992 Sep 29	9:48:30
MaunaKea 24"	maw-0110	1992 Sep 29	12:21:10
OHP 1.93m	gv-0244	1992 Sep 29	23:24:40
McDonald 82"	pab-0169	1992 Sep 30	9:45:00
MaunaKea 24"	maw-0112	1992 Sep 30	12:19:20
SSO 40"	sjk-0209	1992 Sep 30	14:39:30
OHP 1.93m	gv-0247	1992 Sep 30	23:52:30
McDonald 82"	pab-0172	1992 Oct 1	9:44:00
MaunaKea 24"	maw-0115	1992 Oct 1	12:41:40
McDonald 82"	pab-0174	1992 Oct 2	9:36:30
McDonald 36"	sjk-0220	1992 Oct 26	1:05:30
McDonald 36"	sjk-0223	1992 Oct 27	1:42:30
McDonald 36"	jlp-0130	1992 Nov 23	0:45:00
McDonald 36"	jlp-0133	1992 Nov 25	0:38:10
McDonald 36"	tkw-0019	1993 Jan 11	2:09:00
McDonald 36"	tkw-0021	1993 Jan 12	1:26:30
McDonald 36"	tkw-0025	1993 Jan 14	1:09:00
McDonald 36"	sjk-0264	1993 Jul 21	9:16:30
McDonald 36"	tkw-0034	1993 Aug 11	8:23:00

Table 3.1—Continued

Telescope	Run Name	Date (UT)	Runstart (UT)
McDonald 36"	tkw-0040	1993 Aug 16	4:16:00
McDonald 36"	sjk-0265	1993 Sep 14	2:04:00
McDonald 36"	sjk-0266	1993 Sep 14	9:24:30
McDonald 36"	sjk-0267	1993 Sep 15	1:53:30
McDonald 36"	sjk-0268	1993 Sep 16	2:03:30
McDonald 36"	sjk-0269	1993 Sep 17	2:34:00
McDonald 82"	sjk-0270	1993 Sep 18	3:52:30
McDonald 82"	sjk-0276	1993 Sep 19	3:39:30
McDonald 82"	sjk-0277	1993 Sep 20	3:39:00
McDonald 82"	sjk-0278	1993 Sep 20	5:05:30
McDonald 82"	sjk-0279	1993 Sep 20	10:32:30
McDonald 82"	sjk-0281	1993 Sep 21	4:38:30
McDonald 36"	sjk-0282	1993 Nov 4	1:11:30
McDonald 36"	sjk-0283	1993 Nov 5	1:12:30
McDonald 36"	sjk-0285	1993 Nov 6	0:54:00
McDonald 36"	sjk-0287	1993 Nov 7	0:55:30
McDonald 36"	sjk-0288	1993 Nov 8	2:17:00
McDonald 36"	sjk-0289	1993 Nov 8	5:45:00
McDonald 36"	sjk-0293	1993 Dec 14	1:57:30
McDonald 36"	sjk-0295	1993 Dec 15	0:38:00
McDonald 36"	sjk-0297	1993 Dec 16	2:05:30

Table 3.1—Continued

Telescope	Run Name	Date (UT)	Runstart (UT)
McDonald 36"	sjk-0299	1993 Dec 17	1:01:30
McDonald 36"	sjk-0302	1993 Dec 18	0:49:00
Siding Spring 24"	sjk-0363	1994 May 14	18:44:00
Siding Spring 24"	sjk-0368	1994 May 15	18:44:30
Siding Spring 24"	sjk-0373	1994 May 16	18:43:30

4. Data Reduction and Analysis

The standard reductions for this kind of data are discussed in many places (Nather et al. 1990, for example), so I will only briefly describe them here. The fundamental purpose, of course, is to remove the instrumental signature from the data. To do this, we first remove the sky background from each lightcurve (after getting rid of any bad points: flashlights, dome obscurations, etc.), then correct for extinction with standard extinction/air mass formulae. If additional long-period transparency (or extinction) effects are still in the data, they are removed by division with a low-order polynomial. In addition, we can correct the variable light curve for extreme transparency variations by dividing by the comparison star lightcurve. The lightcurves are then normalized to represent the relative deviation from a mean light level of zero. Amplitudes of oscillation at this point use the unit *mmi*, for milli-modulation intensity, where a value of 1000 means 100% peak to peak modulation. Amplitudes in the FT space are referred to in *mma* units, milli-modulation amplitude, and measure root mean square amplitude variations. Power in FT space is the square of amplitude and is most conveniently measured in μmp, micro-modulation power units. Times are put on a uniform timebase relative to the solar system's barycenter. Leap seconds are taken into account. Table 3.2 lists the number of leap seconds and when they were added. The next leap second is schedule to be added 1 Jan 1996. The International Earth Rotation Service Bulletin[3] carries the current and upcoming leap second information.

---

[3]The IERS Bulletin is a publication of the United States Naval Observatory (USNO), 3450 Massachusetts Ave. NW, Washington, DC 20392-5420, navobsy@usno01.usno.navy.mil.

Table 3.2. Complete list (up to 31 Dec 1995) of added leap seconds needed to convert UTC to international atomic time (TAI)

Date	Leap Seconds
1 Jan 1972	10
1 Jul 1972	11
1 Jan 1973	12
1 Jan 1974	13
1 Jan 1975	14
1 Jan 1976	15
1 Jan 1977	16
1 Jan 1978	17
1 Jan 1979	18
1 Jan 1980	19
1 Jul 1981	20
1 Jul 1982	21
1 Jul 1983	22
1 Jul 1985	23
1 Jan 1988	24
1 Jan 1990	25
1 Jan 1991	26
1 Jul 1992	27
1 Jul 1993	28
1 Jul 1994	29

The FT, as already discussed, is the primary analysis tool. Here, I have used a simple discrete Fourier transform algorithm (Deeming 1975). While not as fast nor as clever as many newer modified FFT programs, it handles data gaps quite easily, works well in all appropriate frequency ranges, and is accurate and easily understood. With today's fast computers, I see no reason to settle for a technique that may be quicker, but less accurate. The particular code I use always calculates a spectral window along with the data FT. Do an FT, get a window.

Once the location (frequency) of a peak is identified in an FT, I use least-squares fitting algorithms to determine its phase. The fitting routines simply fit a sine curve to the reduced lightcurve, varying period, amplitude and phase. They are, in essence, a single-point FT (Scargle 1982). Applying trigonometric identities, a linear least-squares algorithm can fit the phase and amplitude, given a fixed period. The non-linear routine fits period, phase, and amplitude and requires initial guesses for each parameter (which are routinely provided by the FT and/or linear least squares program.) Both sets of routines have their uses and will be used throughout this work.

4.1. The $O-C$ Diagram

The $O-C$ diagram is a diagnostic used to measure period and phase stability (or lack thereof) of a single mode. Based on an initial time of zero (phase) and period, subsequent times of zeroes are calculated (C) and compared to the observed (O) values. The difference between the two, the $O-C$, is plotted as a running function of time. An incorrect period results in a linear trend in the $O-C$ diagram; a constant change in period ($\dot{\mathrm{P}}$) enters in as a parabolic trend

in the plot. $\dot{\mathrm{P}}$s in the pulsating white dwarfs can be dominated by contraction (in which case $\dot{\mathrm{P}}$ would be negative) or cooling (producing a positive $\dot{\mathrm{P}}$). Reflex orbital motion of a pulsator in a binary would also be seen in the $O-C$ diagrams, which can thus be used to search for unseen companions (Greenstein 1988, Kleinman et al. 1994).

4.2. The ΔP vs. P Diagram

A useful way to look for equal period spacing (and the variations caused by mode trapping) is the ΔP *vs.* P diagram which plots the difference in period from mode to mode versus the periods themselves. I will discuss five different methods for such a plot, three of which are already used in the literature, and two more just to be complete:

1. Predict the location of each mode based on an initial zero point and the mean spacing, and plot the difference between it and the observed period versus the observed period of each mode.

2. Make the same prediction as above, but use the median of the period spacings instead of the average in the prediction ephemeris.

3. Plot the period difference between a mode and its neighbor to the right (higher period) versus its period. This is forward differencing.

4. Plot the backward difference: the period difference between one mode and its neighbor to the left.

5. Plot the average of the forward and backward difference: a sort of "zone-centered" diagram.

The advantage of the first two methods (which can either be plotted as calculated period vs. observed period, or as an $O - C$ diagram of the observed period) is that each mode is plotted independent of all other modes; the disadvantage is that the period spacing is a required parameter. For exploratory work (as is done here), this value may not be well known. The modes to be used may not even all be of the same ℓ. The other three methods do not depend on any pre-calculated quantity, but because each point depends on two mode periods, they are more affected by errors from incorrect mode identifications.

Figure 3.1 is a ΔP *vs.* P diagram made using the first method listed above and plotted as calculated period vs. observed period. The dotted line shows an exact fit. The zero-point is arbitrary and the data can be slid up or down on the graph to make a better fit. The general trend, that equal-period spacing is a reasonable fit to the data, is obvious from the figure; the exact deviations from the mean are not so obvious.

The following figure (Figure 3.2) shows all five ΔP *vs.* P plotting methods listed above, with the first two plotted as an $O - C$ diagram. The mean period spacing, and deviations from it, are best seen in the lower two panels: the forward and backward differences. The zone-centered difference, being an average, tends to smear out the deviations. The data used in these diagrams, by the way, will be presented in the next chapter and is from the combined G29–38 observations presented here. The gap is where we suspect a missing mode (k) in the sequence.

5. Tricks of the Trade

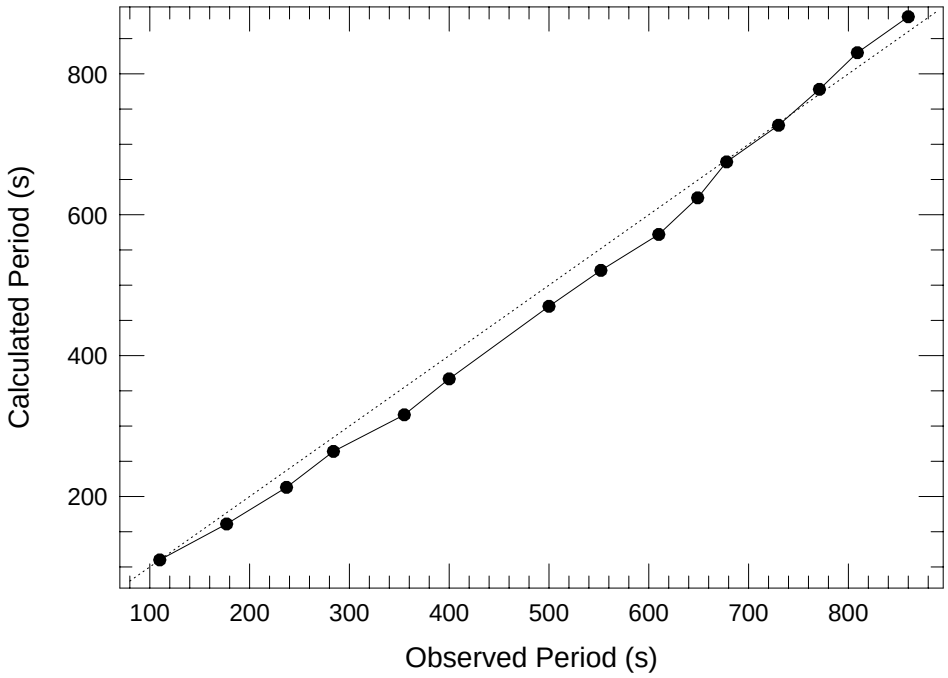

Fig. 3.1.— A sample (G29–38) ΔP *vs.* P diagram plotted as predicted period vs. observed period.

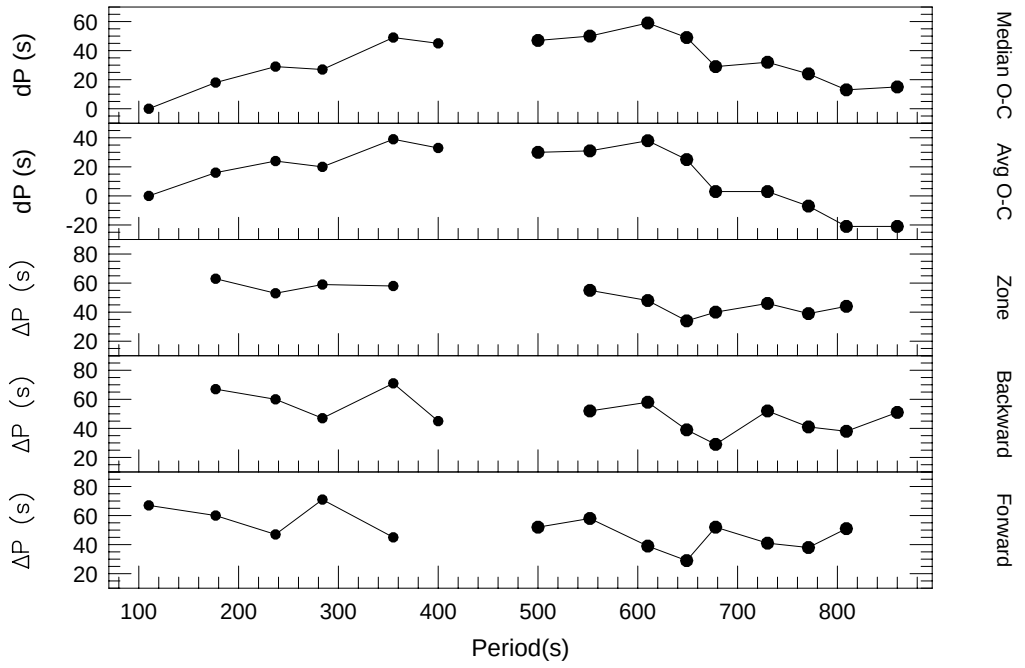

Fig. 3.2.— Five ways to plot a ΔP *vs.* P diagram.

Despite the way observational papers (and this chapter) are written, data reduction is often not an exact science; it is also an art form. What constitutes a bad data point? Should bad data points be bridged over or left out entirely? How much twilight and cloud correction is tolerable? When is a peak a real peak? How much should I oversample the FT?

There is so much more to data reduction (even of our relatively simple one-dimensional data streams discussed here) than is ever explained to the new data reducer. Tests to explore different aspects of data analysis are probably performed again and again by each observer as they all, in turn, realize the need for them. Some of this redundancy is good, as it aids in understanding the details of one's data. On the other hand, sometimes these tests are thought of too late, and a lot of prior work is compromised because of it. It is not my place here to decide how much about data reduction should be told and how much should be rediscovered, but I do feel it worthwhile to share some secrets that I, and probably countless others, have learned along the way. This section, therefore, is a hodgepodge of data reduction tricks I think may be useful to future data reducers.[4] They are discussed in no particular order and are certainly not complete.

Most of what is written about temporal spectroscopy data reduction concentrates on arriving from the raw data to the FT. While a lot of analysis takes place with the FT, it is not the final tool in the analysis. We have found that for almost every star we "solve," we must first develop a new tool. In this case, it was the accurate removal of linear combination modes. In the

[4]I could have said observers here, but there have been a few theorists known to reduce data from time to time.

Clemens et al. (1992) work on V 471 Tau, forming pulse shapes of the observed periodicities proved to be the key. It is impossible, therefore to describe all the tools necessary to solve an asteroseismological problem. We can, however, do a more complete job than what has already been written on some of the other analysis tools we use.

The most used tools, besides the FT, are the least-squares fits mentioned earlier. These fit a sine-curve to the reduced data, determining its period, phase, and amplitude. A mode's stability can be determined by running a series of these fits over a sequential set of data. We can then look for drifts of phase or period.

For non-WET data, deciding when a peak is real is often a difficult challenge. To help, we have two different approaches. The first involves subtracting the known variations (with parameters determined from the least-squares fitting routines) from the lightcurve (called *pre-whitening* the data) and making an FT of the result. Ideally, the alias structure from the known peaks are now gone, leaving any nearby low-amplitude peaks more visible. Pre-whitening is risky business as the noise in the data affects what is removed. The effective noise, therefore, is increased with every pre-whitening attempt. Clemens (1994) has a good discussion of the dangers looming in this technique.

The second method for determining when peaks are real and when they aren't is a reverse pre-whitening approach; it relies on synthesizing the lightcurve from known periods, adding more periods only as needed to see what peaks are really needed to match the observed lightcurve and FT. An FT of the synthetic lightcurve is computed and the process is iterated until a

satisfactory fit is found.

With the wide availability of the Internet to most astronomers, I feel no reason to append any of the source codes for data reduction tools to this thesis, but I will gladly provide any of the discussed routines to anyone who requests them. Some are solid, user-friendly programs; others are short and dirty routines, designed just to get the job done, requiring adjustment for each new application. In the course of this work, most of the codes used have been upgraded to the first class, but remember, you get what you pay for.

5.1. Why is the $O - C$ Scatter More Than the Fits' Uncertainties?

We have long noted the scatter in an $O - C$ phase diagram is nearly always a factor of four or so larger than the individual least-squares uncertainties on each data point would suggest. This is not really a problem, so long as you quote the scatter as the true uncertainty instead of the formal fit value, but it is certainly curious.

To figure out where this factor of 4 was coming from, I generated some synthetic lightcurves and corresponding $O - C$ diagrams from them. I started with a good channel 2, the comparison star channel, and added various sine curves to it. In this way, I was simulating the noise properties inherent in real stellar data. With no noise, there was no discrepancy between the least-squares errors and the $O - C$ scatter; with the channel 2 noise, the scatter increased by a factor of two. The additional factor of two enters if there is additional power nearby the mode being fit.

5.2. How Do the Timebase and Time Sequence Affect the Least-Squares Fits?

When fitting a lightcurve (time vs. amplitude) for the phase of a mode in the FT, for example, the least-squares algorithms calculate a phase that is essentially phased back to zero time, thus accumulating error if the input times are vastly different form zero. I have addressed this problem by calculating an internal time of zero within each program. This renormalizes each input timebase to start near zero.

Since the zero point of the fit is relative to the first data points read (at least in the routines I have used) the signal to noise ratio of the first data set, in a multi-data-set fit, directly affects the precision of the resultant fit. I have found improved fits come from ordering the data sets in order of decreasing signal to noise ratio. I do not do this on a nightly basis, but when grouping monthly data sets for a yearly fit, I order each month accordingly.

5.3. How Does the Phase Affect Multiple-Period Windows?

The spectral windows presented in Chapter 1 were all of single sinusoids. While these are the most commonly used windows, many times it is useful to construct a window with more than one period. This is particularly useful when forming a synthetic lightcurve to try and resolve multiplets in single-site data. Clearly, the relative phases of the component periodicities will affect the way the sinusoids beat together and hence, the pattern produced in the spectral window. While we could use the phases given by the least squares fitting routines, these are often very uncertain for closely-spaced peaks and

could be off entirely if additional power, not fit, is present. Since we are often looking for such power, phase becomes a free parameter.

The tool I used to address this problem takes the input periods and systematically varies their phases, sampling the full range of possibilities as densely as practical.[5] I then do an FT of each of these phase-varied data sets and plot the minimum and maximum of all the simulations for each point. The result is a band of power that represents (approximately) the worst case in the range of power consistent with input peaks of completely unknown phases. Any observed power that falls within this band is consistent with the input peaks at some phase. An example of one of these plots is shown in Figure 3.3. The arrows point to the two peaks used in the simulation.

5.4. How Much Data do I Need For a Given Precision Measurement?

The answer to this question, of course, varies depending on the particular measurement desired as well as the star's and pulsation's magnitudes. We are more often interested in phase and period measurements than we are in amplitude, mainly because we don't fully understand, yet, why modes have the amplitudes they do. For $O-C$ timings and $\dot{\mathrm{P}}$ measurements, the most time-consuming measurements of asteroseismology, precision is a particular concern. Presented in Figure 3.4 are the number of nights, observationally determined, needed to reach a given precision measurement of period and

[5]The current incarnation of this tool accepts any number of periods and produces a set of 12 possible phase orientations.

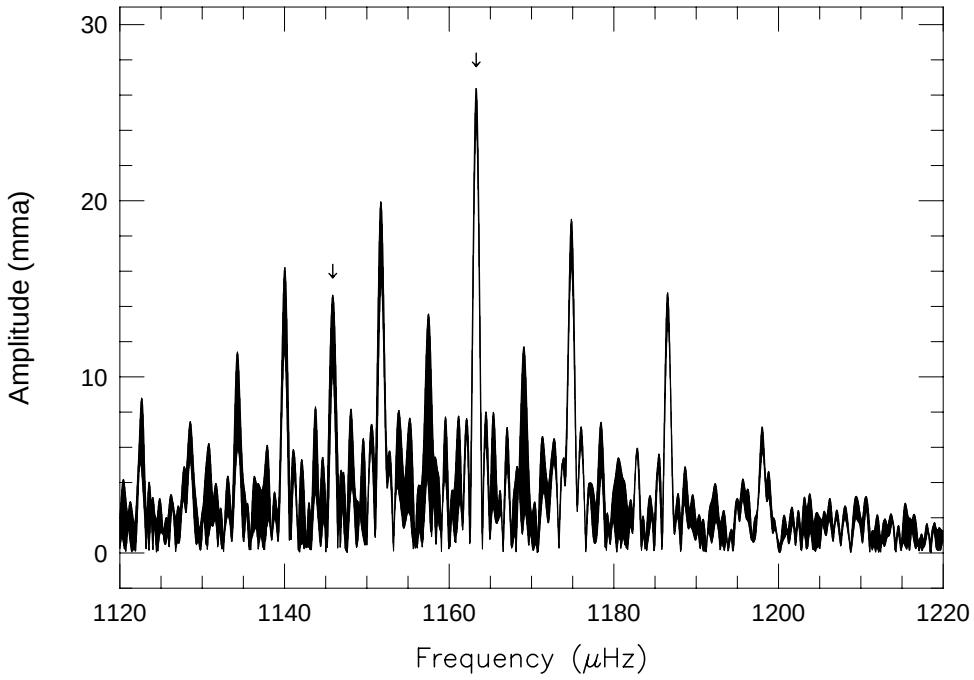

Fig. 3.3.— A multiple period, multiple phase window.

phase for the 284s mode in G29–38. The data are from my extended McDonald observing run on the 36" telescope in September, 1989. The 284s mode had an amplitude of 6.4mma; G29–38 's V magnitude is ≈ 13. G29–38 was visible and observed nearly all night each night. For most of my work, I could easily justify a two-week run, simply based on this plot.

5.5. How do I Identify Combination Modes?

Searching through a list of observed frequencies for sums and differences is a tedious and tiresome task, ideally suited for a computer. But when initially pondering the complexities of the problem, the thought of writing the computer code was more overwhelming than just going through another list of data. Do you look for just two-mode combinations, or 3- and 4-mode combinations as well? What about harmonics? How do you code the search efficiently? What about aliases?

Upon further reflection, however, I realized that a simple (stupid) straight-ahead brute force algorithm would probably work fine; there was no need to be frugal with computer cycles. The resulting code goes through the lists of modes and searches (as simply as you could imagine) for combinations that may occur. It accepts a user-defined equality criteria and dominant alias value (e.g. 11.6μHz) to account for the data resolution and possible peak mis-identification due to aliasing. The question regarding how many component modes to search for in a combination answered itself when I realized that most, if not all observed three mode combinations had two mode combinations embedded within them. That is, if there is a mode such that A+B+C=D, then there is usually another mode that is just the sum of A+B.

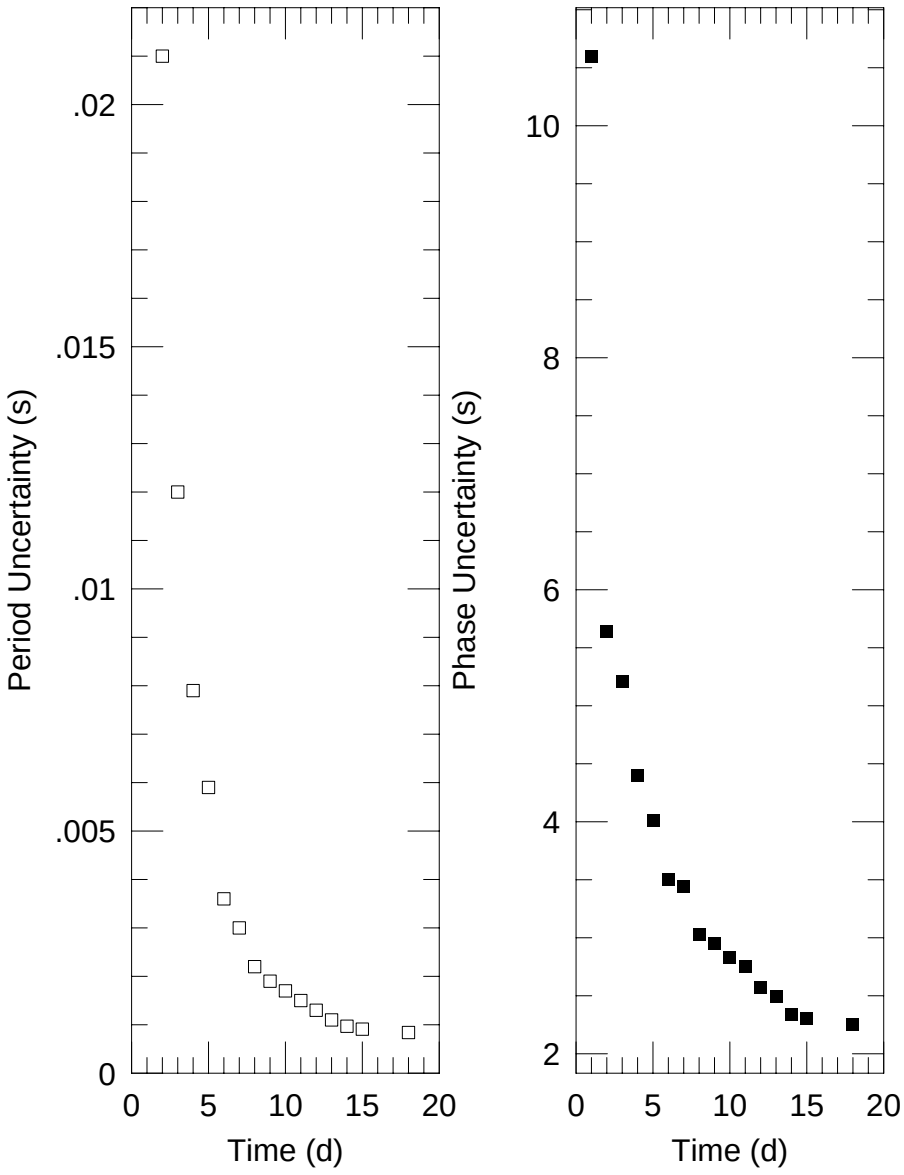

Fig. 3.4.— Observing nights needed to reach an arbitrary precision.

Thus, A+B+C, a three-mode combination, would be found as (A+B)+C. After writing the program, I ran it on the data I had already searched for combination modes and it found every combination I did, plus some I didn't. In addition, while I stopped upon finding one possible combination, the program kept on going and sometimes found more exact combinations than ones I had found myself. Sometimes, there is more than one screwdriver.[6]

[6] You always find the missing screwdriver the last place you look for it. . . .

Chapter 4

The Pulsation Spectrum of G29–38

Skippin' through the lily fields, I came across an empty space.
It trembled and exploded, left a bus stop in its place.
—Bob Weir & Bill Kreutzmann, *Other One*

1. Radial Modes

The observed oscillations of the white dwarf variables are non-radial g- (or gravity-) modes. This is in contrast to the radial- (pressure-) modes that occur in the more well-known pulsators, the Cepheids. White dwarfs are collapsed objects and therefore their intense gravity ($\log(g)$[1] ≈ 8 for a DAV) very effectively inhibits radial motion. As a matter of fact, we may be able to explain the amplitude limiting mechanism of the observed g-modes as due to the small radial motion that occurs along with the dominant surface motion. The star's available energy is taken up by the small radial motions that accompany the g-mode oscillations.

[1] In cgs units.

Were the white dwarf stars to pulsate radially, such modes would be extremely low amplitude and of very high frequency. The radial mode timescale is simply the freefall time for the star, that is, the time for a unit mass to fall through the radius, R, of a star under the local gravitational force given by $\frac{GM}{R^2}$ which, ignoring factors of two or so, is $\approx (G\rho)^{(-\frac{1}{2})}$ where G is the gravitational constant, M, R, and ρ are the star's mass, radius and density respectively. For a white dwarf with a mass on the order of $1 M_\odot$ and a radius of 10^7m, the timescale is on the order of a few seconds — much quicker than the observed pulsations near 1000s.

While we have not looked at G29–38 with the the short integration times and large telescopes needed to detect radial modes, there has been some recent work by Kawaler et al. (1994) to search for radial modes in the DB variables. Previous work was done by Robinson (1985) for the DA variables. Neither group was able to detect any radial modes in their search. Were such modes to exist, they would aid vastly in probing these stars, providing a new set of modes that reveal more of the stars' interiors and probing distinctly different regions. But since there is no evidence for their observable existence in the DAVs, I will not discuss them or their associated timescales any further.

The g-mode pulsations, however, occur at a much longer timescale than the radial modes. Their characteristic frequency is the Brunt-Väisälä frequency, the frequency with which a blob of material oscillates in pressure equilibrium and under the force of gravity (Unno et al. 1989). For a DAV white dwarf, this characteristic frequency corresponds to periods near 600s.

When pulsars were discovered, the non-radial g-modes, although known in principle (Ledoux & Walraven 1958), were not widely understood

or accepted as important in stellar environments. Radial modes were the mainstay of pulsation theory and their timescales were much too short to be the cause of the pulsar variations. The g-mode neutron star timescales, however, match pretty well. Imagine what directions this field might have taken had this avenue been considered.

2. The Ensemble Approach

Of all the variable white dwarfs, the DAVs have been the hardest to study with asteroseismology. The hotter DAVs have only a few modes — too few to make a believable mode identification. The cooler DAVs show many modes, but most are unstable and many are combination modes (modes whose frequencies are linear combinations of other modes) which greatly complicate mode identification. Clemens (1993, 1994) showed that by treating the ensemble of the hot DAVs as a single star, he could make consistent mode identifications. Here, I will use data from many different observing seasons on G29–38 to search for normal modes. Where Clemens used many different stars, I will use many different observing seasons. The goals, however, are similar: search the resulting set of modes for a sensible set of normal mode oscillations.

Figure 4.1 is reproduced from Clemens (1993, 1994). Plotted in each box are the location of the observed modes in each star. The bottom box is the union of all the modes observed in all the stars. Clemens claims the groupings represent same-k, ℓ=1 modes. The deviation of each star from the union's mean is caused, at least in part, by slight variations of mass. Indeed, when a "mass correction" (plotting the periods where they would be if all the stars had the same mass) is applied to each star, the result is

a tighter grouping, confirming both the initial hypothesis and existing mass measurements (Figure 4.2). Actually, the correction applied in the figure is not derived from mass, but is empirical and was found to be an accurate predictor of mass.

The implications of this result are astounding: the essential structure and composition of all the hot DAVs are the same regardless of the wide mass range in their progenitors. Since we believe the only thing distinguishing a DAV from a non-variable DA is its temperature (with the exceptions noted in Chapter 1), the similarity applies to all the DAs throughout the white dwarf cooling track (with the exception of those which become non-DAs by the time they reach the DAV instability strip).

With such an astonishing result in hand from a multitude of different stars, I looked at the modes of G29–38 in a similar, although not identical way. G29–38's power spectra change dramatically from year to year, with less dramatic changes occurring even during a given season. Thus, if we think of each season as a different star in the above example, and considering that in reality we have only one star with a presumably set structure and composition, the resulting "union" of modes should show very tight groupings. If the star oscillates in normal g-modes, but picks and chooses which particular modes to oscillate in at any given time, we should see modes that recur and definite gaps where there are no normal modes. Amidst the wealth of modes that come and go with each observing season, we are searching for an underlying stable structure that might shed some light on the nature of the variations. Unfortunately, with the richness of the g-mode spectra, we can get a mode just about anywhere; as long as we remain in model space, we can simply

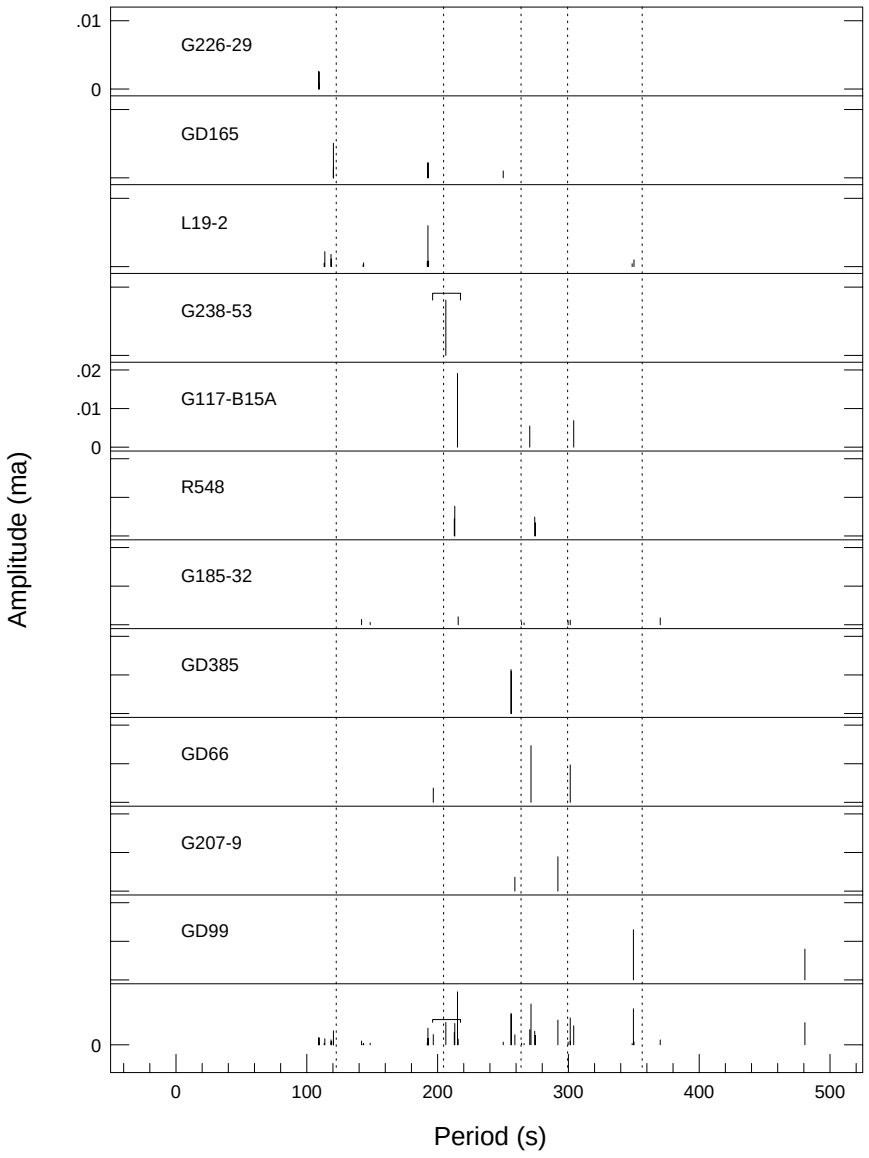

Fig. 4.1.— Pulsation modes of the hot DAVs from Clemens (1993, 1994).

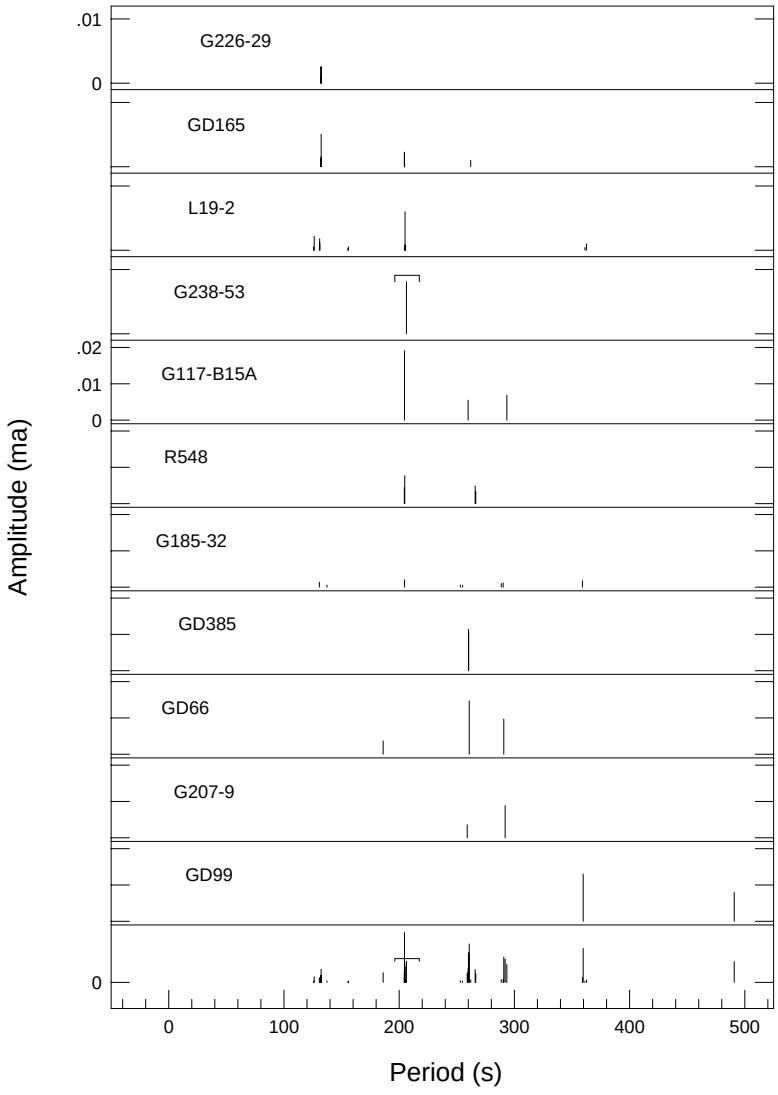

Fig. 4.2.— Pulsation modes of the hot DAVs empirically adjusted for mass from Clemens (1993, 1994).

choose from an infinite (although discrete) set of ℓ, k, and m values to get a mode nearly anywhere we want. Fortunately, however, the stars are simpler than our models, seeming only to select modes with ℓ less than 3.

Figure 4.3 is a schematic mode plot for our G29–38 data. The amplitude information has been ignored here and every mode is plotted with the same amplitude to better highlight the possible groupings. Following the work of Clemens, the X-axis is period, not frequency. A wealth of information is contained within this plot, but for now, note the bottom *Sum* panel and the conspicuous lack of groupings like those seen in Clemens's figures. The obvious conclusion here is that the modes we see are not explainable by single-ℓ, normal-mode pulsations. Remember that g-mode theory says that same-ℓ, successive-k pulsation modes are nearly equally spaced in period. While there appear to be some gaps in G29–38's schematic mode plot, there are few concise groupings.

Given the results of this ensemble test, we have to answer the question: what are these modes? There are at least 3 possibilities: 1) They are not normal g-modes of the system; we may be seeing a majority of linear combination modes or transient, impulse modes. 2) They are normal modes of many different ℓs. 3) The star is a rapid rotator so multiplet component spacings are of the same order as the same-ℓ, k-spacing, confusing mode identifications and obliterating any groupings.

Since it is already known that this star (and others of its class) have linear combination modes, we will start by removing the linear combinations and see what the remaining modes look like. If we are indeed seeing normal g-mode pulsations, we expect to find series of nearly equally spaced

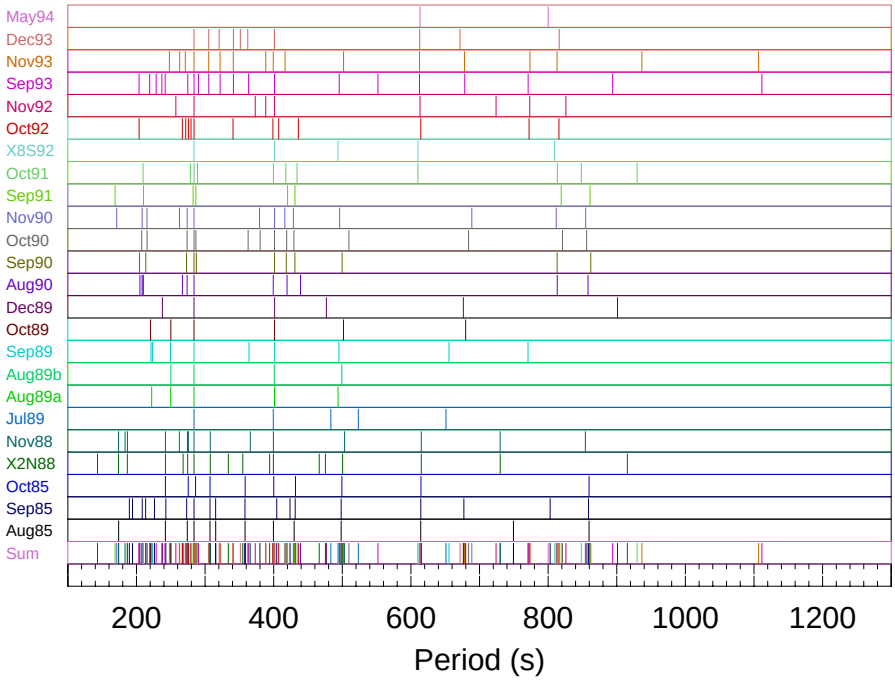

Fig. 4.3.— Schematic diagram of G29–38's periodicities for the entire data set.

periodicities, representing a succession of different-k, same-ℓ modes. If there is more than one ℓ present, we expect to see two such patterns. More likely, however, is a set of ℓ=1 only pulsations with perhaps, but not necessarily, a mode or two of ℓ=2. The simplest approach is to assume only ℓ=1 modes and see what, if anything, cannot be explained as either an ℓ=1, or a linear combination mode. If there is a lot left over, we will have to consider the second two possibilities.

Our ability to identify (and hence remove) the linear combinations depends greatly on the signal to noise ratio and the resolution of each transform. To help avoid uncertain and incorrect identifications, I now restrict my analysis to the best data sets available — one per year: Aug85 is the August, 1985 data set from a combined campaign by South Africa and McDonald. X2N88 is the data from the WET Xcov2 campaign on G29–38 in November, 1988. Sep89 is a 20-night data set from McDonald from September, 1989. Oct90, and Sep93 are also single-site data sets from McDonald during October, 1990 and September, 1993 respectively. X8S92 is the data from the second WET run (Xcov8) on G29–38 in September, 1992.

Figure 4.4 is the schematic period diagram minus the identified linear combinations from this selected data subset. This new schematic period diagram is substantially cleaner and qualitatively shows the mode groupings we would expect for normal-mode pulsations. The roughly equally-spaced groups seen in the *Sum* row suggest a mean period of roughly 50s. We see a near complete set of modes from 110s to 900s with two more at longer periods. With few exceptions, the groups are tight and have distinct gaps between them.

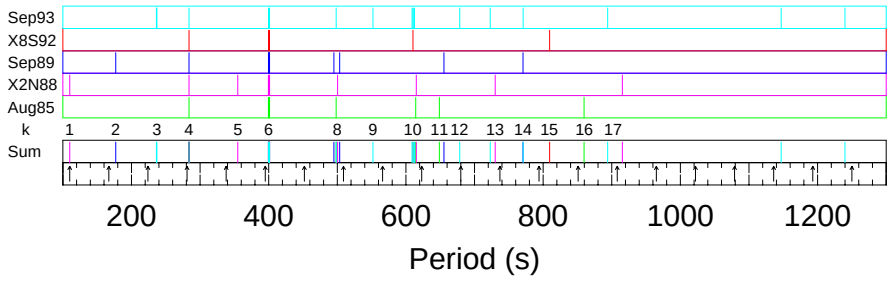

Fig. 4.4.— Schematic diagram of G29–38's periodicities minus the linear combination modes. The arrows in the bottom panel show where precisely equally-spaced modes would lie.

The data from September, 1993 have the most modes and nicely reproduce the expected $\approx$ 50s spacing. This season is unique in that there appear to be six consecutive ks in one period range. The other seasons also show roughly equally spaced groups, but are often missing one or more ks in between each observed mode. Most notable in this respect are the X2N88, Sep89, and X8S92 data sets. We now have evidence for a series of successive-k, same-ℓ modes. Earlier, we mentioned three possibilities for the lack of groupings in Figure 4.3. It looks like the first possibility, an abundance of linear combinations, is the right one. There is no reason to continue along the other two paths.

Instead of going in detail through each individual season here, I have placed the lightcurve, FT and list of modes for each season in Appendix A. Since there are a few notes of interest in each season, I will discuss those briefly here, but will concentrate on the result of Figure 4.4 that there does appear a recurring, underlying structure behind the plethora of unstable modes in G29–38. To keep things in perspective during the discussion, I have reproduced the appropriate rows and k assignments of Figure 4.4 on the top of each page.

3. Seasonal G29–38 Mode Structure

As Figure 4.4 readily shows,[2] the power spectrum of G29–38 changes dramatically from year to year. It appears, however, to make its most dramatic changes when the star is behind the sun and we are not watching

[2]It would be even more obvious were the amplitude information kept in that plot.

it. While this predisposition means we do not get to watch the star change, the advantage is the FT of each individual year provides a relatively stable set of modes that may be used for asteroseismological analysis. In order to have a simple model to compare to our observations (and not get lost in parameter space of purely theoretical model pulsation spectra), I plot in the bottom panel of Figure 4.4 a set of equally spaced arrows (the spacing is 57s) to simulate a series of successive k, ℓ=1 modes. Warning. Warning. We are *not* in asymptopia here. We do not expect to see strictly uniform period spacing. Rather, we have have identified modes starting at k=1 which is certainly *not* in the high-k limit. Our search for equal period spacing should not be too strict; we expect to see significant departures until we get to the higher-k modes. We also expect deviations on the order of 10s or so due to mode-trapping effects. In some cases, however, models of Bradley (1995) show deviations of as much as 20 — 30s. Under the assumption that each group is a different k, ℓ=1 mode, I provide a running k assignment for each group as shown in Figure 4.4.

August 1985

Of the 20 periodicities identified in the Aug85 data, only 8 do not appear to be linear combination modes although it is sometimes difficult to decide exactly which modes are the combinations, and which are the fundamental modes which make up the combination. In general, I have decided based on relative mode amplitudes (component modes generally have larger amplitudes), number of combinations with each mode (combinations with combination modes are less likely than first order combinations), the existence of multiplet

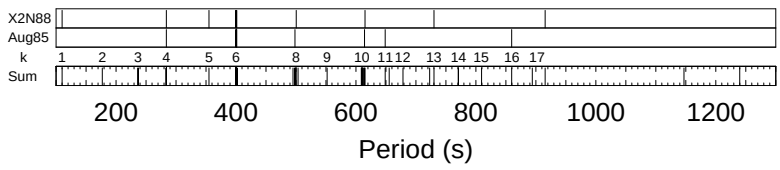

structure (two multiplets adding together produce distinctly different structure in the combination), and the way modes and their combinations disappear and recur in the various data sets (a component mode can appear without its combinations, but not vice. versa). Still, though, there are occasions when I cannot decide without resort to a model that predicts normal modes. In this case, I assume modes with periods near the expected groups are real and not combinations. Any modes that are still ambiguous are marked with a *?* in the table of modes (Appendix A).

We see in this data set the k=4, 6, 8, and 10 modes (we will be seeing a lot of these guys), a mode at k=11, and the only occurrence of the mode labelled k=16.

Xcov2: November 1988

The WET run in November 1988 (Winget et al. 1990) is what prompted this extended investigation. Despite the intensive coverage provided by the WET, there are few non-combination modes. With the exception of only two modes, we see only every other (or every fourth) k in this data set. We see this predisposition for every other k again in this star, and in many other variable white dwarfs as well. There is undoubtedly information in this preference, but we do not yet know how to interpret it.

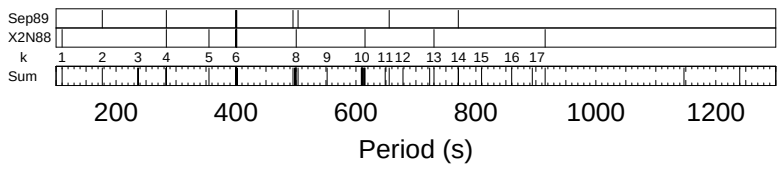

We see the repeating k=4, 6, 8, and 10 along with a very low period (the lowest observed) at k=1, and new modes at k=5, 13, and a mode just past k=17, probably k=18. There is also a hint of some power near 6220μHzthat may be interesting. A plot of the region is shown in Figure 4.5. The signal to noise ratio of the biggest peak here is clearly low enough that I would ordinarily not even consider calling it real. The reason why I can't just leave it at that, however, is what looks like a sequence of 5 (five) evenly spaced peaks. Could this be a low-amplitude ℓ=2? Unfortunately, I really cannot say, but I do want to point it out for future observations.

September 1989

Although the Sep89 data suffer from prominent aliases in the power spectrum resulting from single-site coverage, the extended baseline of long runs provides an excellent signal to noise ratio, the best of each individual data set. The low noise in this data set means we can identify a larger number of linear combinations and harmonics than in the other data sets. Unfortunately, however, G29–38 was in a low-amplitude state during this time and did not pulsate with many modes. Compare its lightcurve with that of the X2N88 and Aug85 data sets (see Appendix A) and note the plot scales are the same. What changed was the y-scale of G29–38 itself.

Despite the low-amplitude, however, we see the usual k=4, 6, and 8

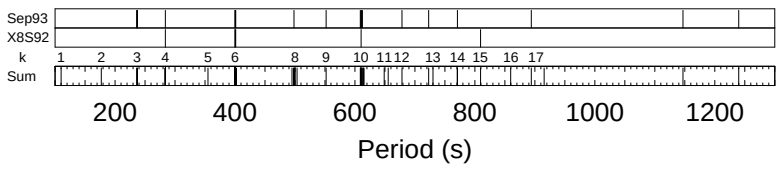

(the k=10 mode is sitting out this time) in addition to a new mode at k=2, a repeat of the mode at k=11, and a new mode at k=14.

Xcov8: September 1992

Of the recognized modes this season, three of the four have been seen before: the usual k=4, and 6 (but no k=8) modes and a return of the once dominant k=10 mode near 610s after a three year absence. At this point, the 610s mode's amplitude was rather small and it only grew in the following observing season, its frequency changing slightly (about 8 μHz total) as the amplitude grew. For now, it seems safe to call it the same k as the previous modes near this period. The only new mode is one at k=15.

September 1993

The transform of the Sep93 data set is the richest of all. The striking regular pattern of modes in this data set was what first suggested to us that the idea of only ℓ=1, successive k modes might actually work. We see the usual k=4, 6, 8, and 10 modes along with new modes at k=12 and 17, and repeats of the k=13 mode from X2N88 and the k=14 mode from Sep89. Two very long period modes appear for the first time. Since they are so far from the rest of the modes, their ks are uncertain, but they are consistent with k=22 and 24.

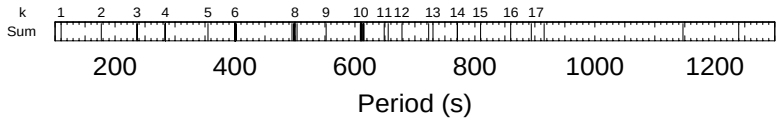

4. Period Spacing Analysis

The remarkable pattern of Figure 4.4 means our initial guess that the linear combination modes were responsible for obscuring the normal mode structure is probably right. Almost half of the observed non-combination modes repeat at least once in the data set; four are present in four of the five data sets. We have indeed uncovered the stable structure underlying all our observations of G29–38 and now, for the first time, have a hope of making detailed asteroseismological measurements on a DAV.

All the observed modes fit well with an ℓ=1 model and their expected period spacing. The most likely possible exception are the two modes near k=17, but they could also be k=17 and k=18 without much problem. These two modes, the 894s mode in Sep93 and the 915s mode in X2N88 are separated by 21s, a little too close, but not completely impossible, to be different ks (17 and 18), same-ℓ pulled closer by mode trapping. Models of Bradley (1995) do show some spacings this low for models with parameters near what we expect for G29–38. In frequency, the separation is 26 μHz, too far to be easily explained by the kind of multiplets we have so far seen, although, once again, not completely out of the realm of possibility.

In Sep93, we have labeled the 894s mode and the mode at 498s as real modes and labeled the 1125s mode their difference. It is possible the

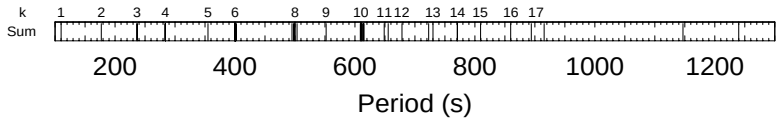

distribution of these assignments is in error. The 498s mode, however, is one that repeats over the years so it is unlikely that this mode is a combination. The 1125s mode, were it labelled real, would also present a problem in our identifications. There is no clear choice here, but the current assignment leaves the fewest things unexplained. We probably have the sum and difference assignments correct.

The X2N88 915s mode is easily identified and uncluttered with excess power. There is no power in this data set corresponding to the Sep93 mode (and vice. versa). There is little chance of a sum and difference confusion with this mode. We do note, however, that the ratio of this period with the dominant period in the data set, the 615s modes is 1.49 — a number that repeatedly occurs in observations of these stars.

Based on these arguments, we cannot say with certainty what these two modes are. However, because of the Bradley models, we cannot say they have to be different ℓs. I will therefore consider them as ℓ=1, k=17 and k=18, but to be safe, will offer an alternative explanation of k=17 and something else.

The observed non-combination modes are consistent with our ℓ=1 model. To explore this in more detail is Figure 4.6, the corresponding ΔP *vs.* P diagram for which I have adopted the following assumptions and conventions:

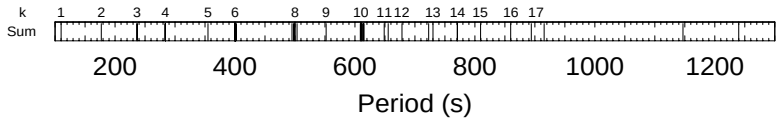

- Each mode in the sum panel of Figure 4.4 is the same ℓ (presumably ℓ=1).
- Where obvious multiplets are present, I take either the period of the middle mode (presumably m=0) or the largest amplitude mode where only two members of the multiplet are seen.
- The gap between what we have identified as k=6 and k=8 is a missing mode we will call k=7. I will tentatively plot the spacings for these modes (with dotted squares) as 1/2 the k=6 to k=8 spacing. This is done only to show the mean spacing agrees with the rest of the data. I do the same for the two long-period modes.
- There will be unavoidable uncertainties in the modes' periods (and differences) since the m values are uncertain.
- I use forward differences. The data, however, are the same as those used in Chapter 3 where all five discussed ΔP *vs.* P methods were shown.

In the interest of completeness, I have plotted some alternative identifications in Figure 4.6. With the exception of the two modes near k=17, there is no reason to suspect any of these modes are a different ℓ. On the other hand, there is nothing besides Occam's razor to forbid having a mode or two of a different ℓ. Based on the previous WET observations and the

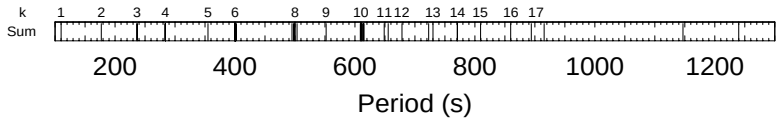

work of Clemens with the hot DAVs, it seems unlikely that the majority of the modes are anything other than ℓ=1. (Evidence from Chapter 5 and 6 also supports this conclusion.) However, since it is possible to have a mode or two of a different-ℓ sneak into our identifications, I have plotted some likely alternatives to the the ℓ=1 only model by dotted lines and circles. Where I have plotted such alternatives, the only ℓ=1 interpretation is plotted with thinner lines and slightly smaller filled circles. The data represented by the solid line plot is also plotted in Chapter 3, Figure 3.2. The bottom panel of the plot is an enlarged plot of the familiar sum row of Figure 4.4 with arrows showing which modes were used to calculate the differences shown above it. The line type of each conforms with the convention used in the first panel. Above this plot are ℓ=1 k assignments.

There are few published models for DAVs since until just recently, we have not had many observed modes to test them with. Those models that we do have are almost certainly incomplete since they have not yet been faced with many observational tests. Nonetheless, there are some interesting model comparisons to make. In Chapter 6, I discuss the cool DAV group modal properties and derive a set of modes common to all the cool DAVs which I use to place constraints on the H-layer of these stars. The advantage of using this subset of modes (the "class modes" of the cool DAVs) is that they are unlikely to be a mixture of ℓs given the power spectra similarities found in

Chapter 6. The ΔP *vs.* P diagram for the model fit to these modes is shown in Figure 4.7.

The model is not a good fit. More serious than the misalignment of the trapping cycles (as this may be corrected through adjustments of the H-layer and total stellar masses) is the mismatch of the overall shape of the two diagrams (Figures 4.6 and 4.7). G29–38's period spacings show a trend which decreases with period, whereas the model has maxima that decrease and minima that increase. That these overall shapes do not agree is no big surprise;[3] this is the first time we have had an observational DAV ΔP *vs.* P diagram with which to compare the models. The observers have opened the ranch gate — let the theoretical herd out!

4.1. Mass Estimates and Mode-Identification Implications

The mean period spacing, P_o, of a set of successive-k, same-ℓ g-modes is a direct function of the stellar mass. Few detailed mode calculations of this correlation have been previously published. Bradley (1993 and 1995, private communication), however, has run some models based on the results of this

[3]Some might argue otherwise, since the existing models matched the first asteroseismological test put to it, the WET observations of PG 1159–035, incredibly well. I maintain that the success of this match was the surprise. That the DAV models don't exactly match their first critical test this time, I do not find particularly surprising.

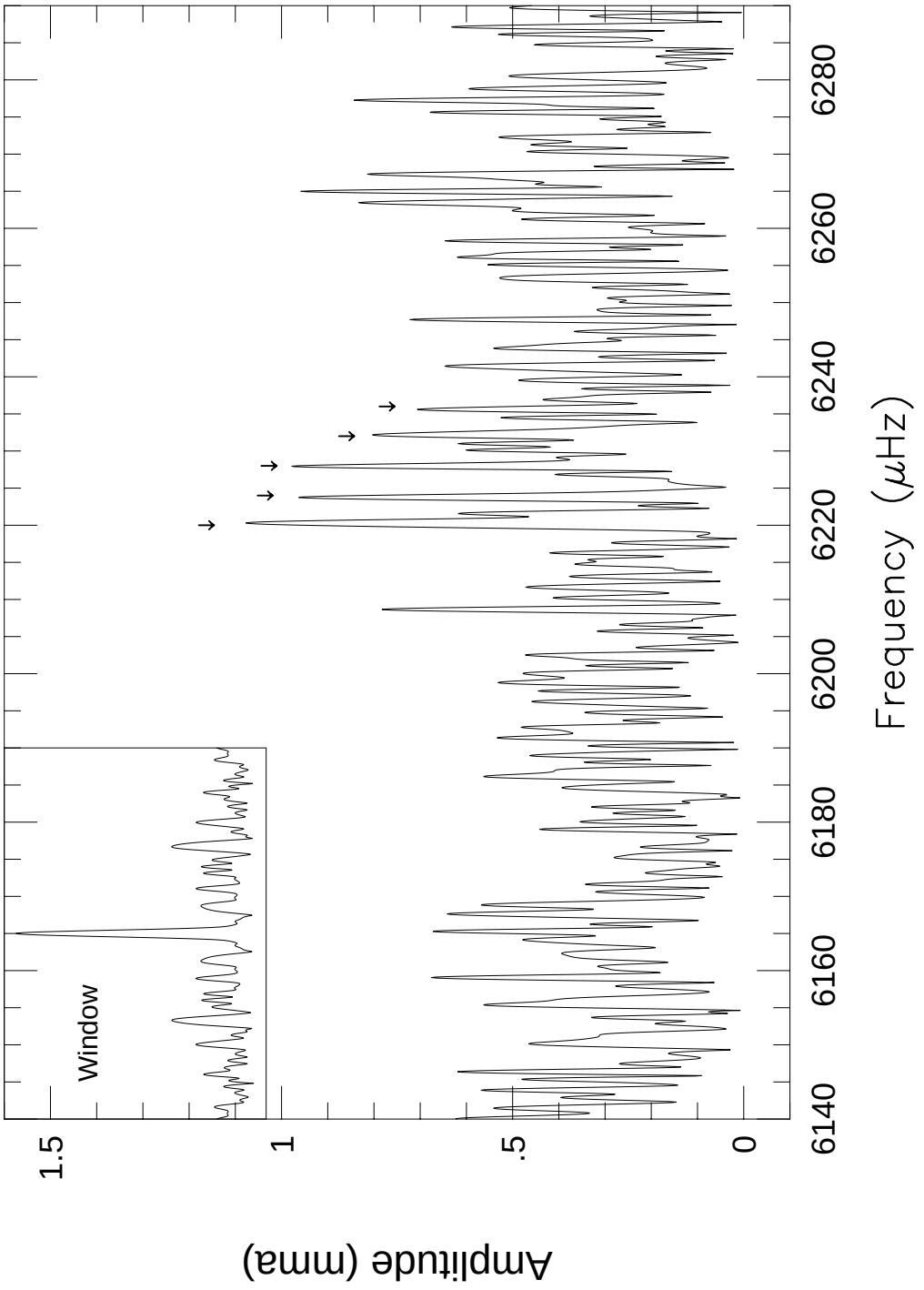

Fig. 4.5.— The X2N88 FT near the 6220 μHz possible power.

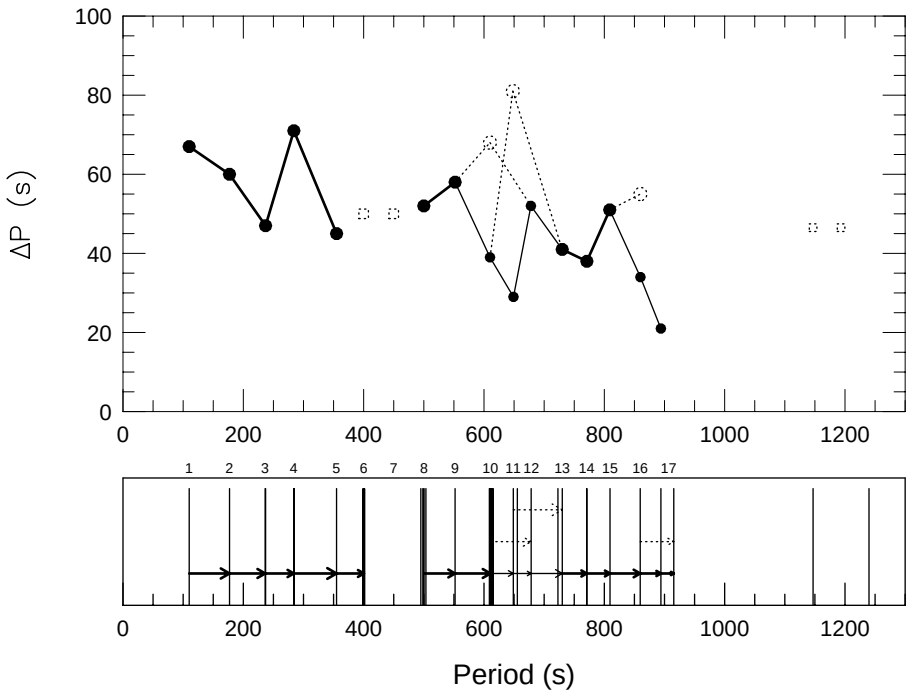

Fig. 4.6.— The observed ΔP vs. P diagram for G29–38.

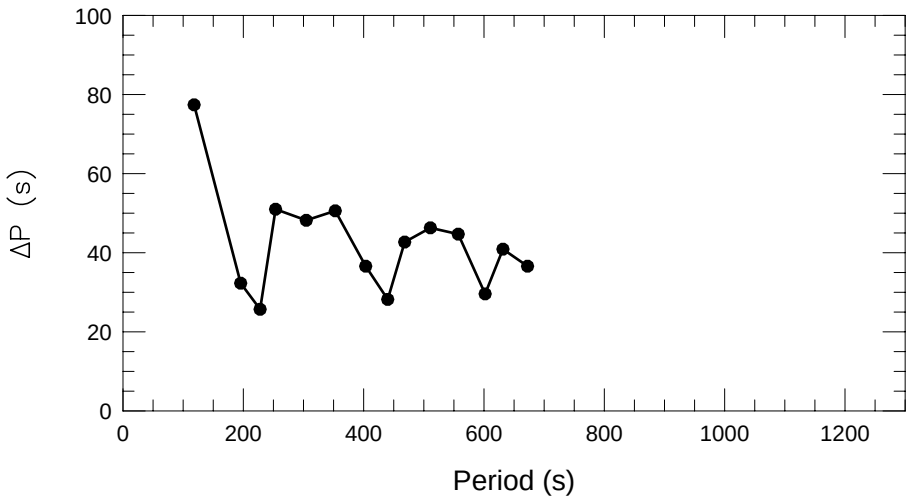

Fig. 4.7.— The ΔP vs. P diagram for a DAV model from Bradley (1995).

work. He has assumed a Hydrogen layer mass of $1.5 \times 10^{-4} M_\star$ and finds decreasing the Hydrogen layer increases the period spacing significantly. For a $0.6 M_\odot$ model, for example, P_o increases by roughly 15s when the Hydrogen layer mass is decreased from $10^{-4} M_\star$ to $10^{-13} M_\star$. Figure 4.8 shows, for a series of model masses, the relationship between π_o (the theoretician's equivalent of the observed mean period spacing, equal to $P_o \sqrt{\ell(\ell+1)}$) and the effective temperature of the star. Using the temperature of Bergeron et al. (1995) and our measured P_o (51s), we can estimate the mass of G29–38. As shown by the dotted lines in Figure 4.6, we get a mass near $0.55 M_\odot$. Bergeron et al. measure $0.69 M_\odot$. To get $0.7 M_\odot$ with our measured period spacing and these models would require a temperature well outside the instability strip — not very likely. The allowable mass range with temperature as a free parameter is about 0.5 — $0.6 M_\odot$. To get $0.7 M_\odot$ using the Bergeron temperature would require lowering P_o by 10s, equally unlikely. While there could be missing modes in between those observed, they would skew the uniformity so much, it would no longer look like roughly equal period spacing. To increase the model π_o via the Hydrogen layer mass would require a much thinner H-layer, like $10^{-10} M_\star$.[4] If the modes were ℓ=2, incidentally, the resulting star would be an extremely low-mass object, with a π_o near 125s. The majority, at least, of the modes must be ℓ=1.

The mass discrepancy, however, is interesting. It says G29–38's mass is more near the norm of $0.6 M_\odot$ than most mass estimators have placed it.

---

[4]This is the only piece of evidence that suggests a thin H-layer. If we go this thin, current models cannot match the location of the k=1 and k=2 ℓ=1 modes. In addition, we would have to explain why the other DAVs we have observed (presented in Chapter 6) are all similar and consistent with thick ($\approx 10^{-4} M_\star$) H-layers. Still, the result should raise a warning flag.

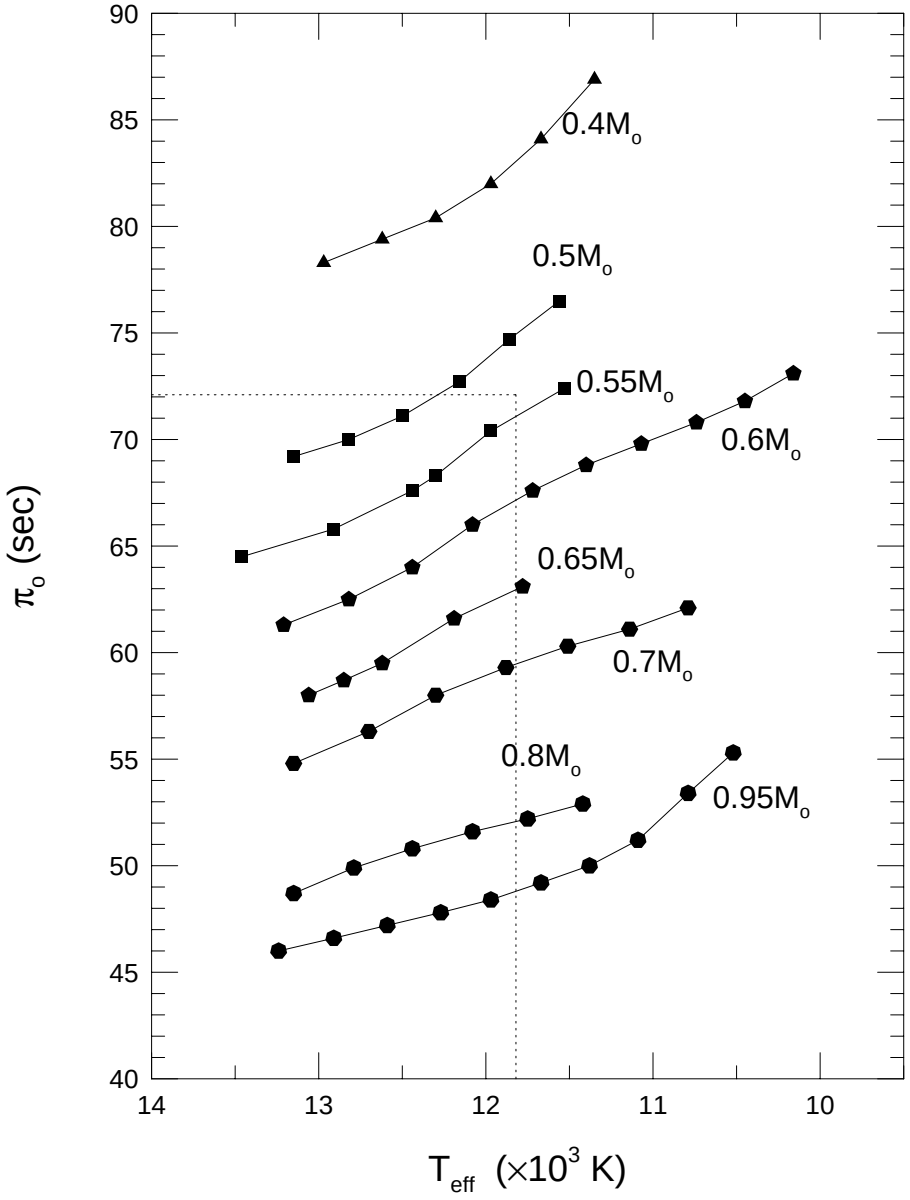

Fig. 4.8.— Model fits of π_o ($P_o(\ell(\ell+1))^{1/2}$) for a variety of DA masses. The assumed H-layer was $1.5 \times 10^{-4} M_\star$.

G29–38 historically comes out on the high end of the mass scale. I suggest one of two (or both) things may be the cause:[5]

1. The asteroseismological models are incomplete. We know this is true from the ΔP *vs.* P diagram, but the mean period spacing should be less sensitive to model details than are the details of mode trapping.

2. Something strange is happening to G29–38's envelope due to its large and highly non-linear pulsations which affect the spectroscopic estimates.

Either way, the field of individual DAV asteroseismology is off and running.

[5]Another alternative will be discussed in Chapter 6.

Chapter 5

G29–38 Multiplets

Picture a bright blue ball just spinning, spinning free.
It's dizzying, the possibilities.
—Bob Weir & John Barlow, *Throwing Stones*

A sub-theme of this work is that we see variations in the white dwarf pulsators on almost every timescale on which we look. The previous chapter discussed the g-mode variations with periods on the order of tens of minutes (and implicitly displayed their variability on timescales of months to years). The next most dramatic timescale for variability is that of the rotation timescale: days. Through asteroseismology, we have direct evidence of rotation through the m-splitting accompanying it. Under strictly uniform rotation (and in the asymptotic limit where $C_{\ell,k} \approx \frac{1}{\ell(\ell+1)}$), we expect a constant set of splittings for each ℓ present in the star. The ratio of an ℓ=2 to an ℓ=1 splitting is 1.67. Other effects, however, can make the observed m-splitting deviate from this nice orderly behavior. First, if the star is differentially rotating (in the radial direction) then each mode, which samples a different part of the stellar interior, will feel a different rotation rate and thus will have

a slightly different splitting, although to first order,[1] within each multiplet, the spacing will still be uniform.

The uniform spacing within a multiplet can be destroyed by the presence of magnetic fields. By creating an extra force to inhibit mass motions on the surface of the star, magnetic fields shift modes with different m values to higher frequencies. For a simple dipole field aligned with the pulsation/rotation axis, the shift is proportional to m^2 (Jones et al. 1989). Thus, in the absence of rotation, an ℓ=1 mode is split into a doublet; an ℓ=2 into a triplet. With rotation playing the dominant role and the magnetic field a perturbation on it, the equal-frequency splitting is skewed slightly so the higher-frequency mode (which I am calling positive m) is split slightly more from the central m=0 component than is the m=–1 mode. Such is the case in the WET observations of the DBV, GD 358 (Winget et al. 1994) which shows evidence for both differential rotation (with the surface rotating almost twice as fast as the core) and the presence of a magnetic field on the order of 1200 Gauss. No similar measurements have ever been made on a DAV. There simply have not been enough observed multiplets. Prior to this work, there had been no evidence of multiplets on G29–38 in particular. To those concerned with such things, the marked lack of DAV multiplets was a small mystery.

Here, I solve this one mystery by showing G29–38 does have the expected multiplets, but introduce a few more: the observed multiplets do not quite fit the standard picture. We see two sets of multiplet spacings, but they

[1]For an example of observed second order rotation effects, see O'Donoghue & Warner (1982, 1987). For the theoretical framework, see Chlebowski (1978) and Saio (1981).

are not entirely consistent with ℓ=1 and ℓ=2 spacings. We also see multiplet spacings that change significantly from year to year, possibly periodically. Only twice do we see identical multiplet spacings in the same data set.

The purpose of discussing the multiplets in G29–38 is two-fold: 1) show the star does have the expected multiplets and derive a rotation rate based on them, and 2) use this additional source of information to improve the mode identifications made in the previous chapter. As in the previous chapter, I will be referring to only the best data sets from each observing season. Here, however, the X2N88 data set includes follow-up single-site observations taken at McDonald immediately after the WET run in November, 1988.

1. The 400s Region

The best example of a rotationally split multiplet in G29–38 comes from the modes near 400s (2500 μHz). Unlike most of the other power which comes and goes in each yearly data set, there is always power present in this region. The triplet is nearly evenly-spaced and has an average spacing around 5μHz. Assuming this is an ℓ=1 triplet, and not 3 components of a higher-ℓ multiplet, the largest-amplitude peak is always the m=–1 or m=+1 but never the m=0 mode. In some cases, the m=0 mode is not seen at all. The equally-spaced triplet supports the ℓ=1 assignments made earlier.

It is possible to use the relative amplitudes of the $|m| = 1$ modes to the m=0 mode to calculate an angle of inclination if we are willing to assume each member of the multiplet is excited to the same physical amplitude and only the geometry of how the modes appear on the surface, combined with

our aspect angle, causes the observed amplitudes to be non-uniform (Pesnell 1985). This is an assumption I am not willing to make. WET observations of PG 1159–035, GD 358, as well as those presented here, all show multiplets with variable amplitudes. Each multiplet in the star does *not* have the same relative amplitude structure. The multiplet amplitudes change not only from mode to mode, but also from year to year. These observational facts call into question *any* theory which demands the multiplet components be excited to the same physical amplitude.

The spacing between each member of the multiplet measures a star's rotation rate, but another problem arises here: the observed frequency splitting is not constant from year to year. Figure 5.1 is a schematic diagram which shows the position of each multiplet member in each of the yearly data sets. In two cases, the m= ± 1 modes were seen, but not the m=0, so I plot a smaller line segment at the mean of the two observed modes. The data in Oct90 do not have a high enough signal to noise ratio or resolution to detect but one mode, although more may be present, but not detected — hidden in the noise.

The central m=0 (or median of the $|m| = 1$) mode remains at roughly the same position, 2497.32$\pm$ 0.17μHz, based on the three times it was observed. The spacing between the m=–1 and m=+1 changes by nearly 2.0μHz(each m moving about 1.0μHz). Since the changes are nearly symmetric with respect to the m=0 mode (although this is a little uncertain since the m=0 is not always seen), the cause can not be a changing simple magnetic field; it must be a change in rotation. An immediate explanation came to mind in light of the reported radial velocity variation of Barnbaum & Zuckerman (1992). If

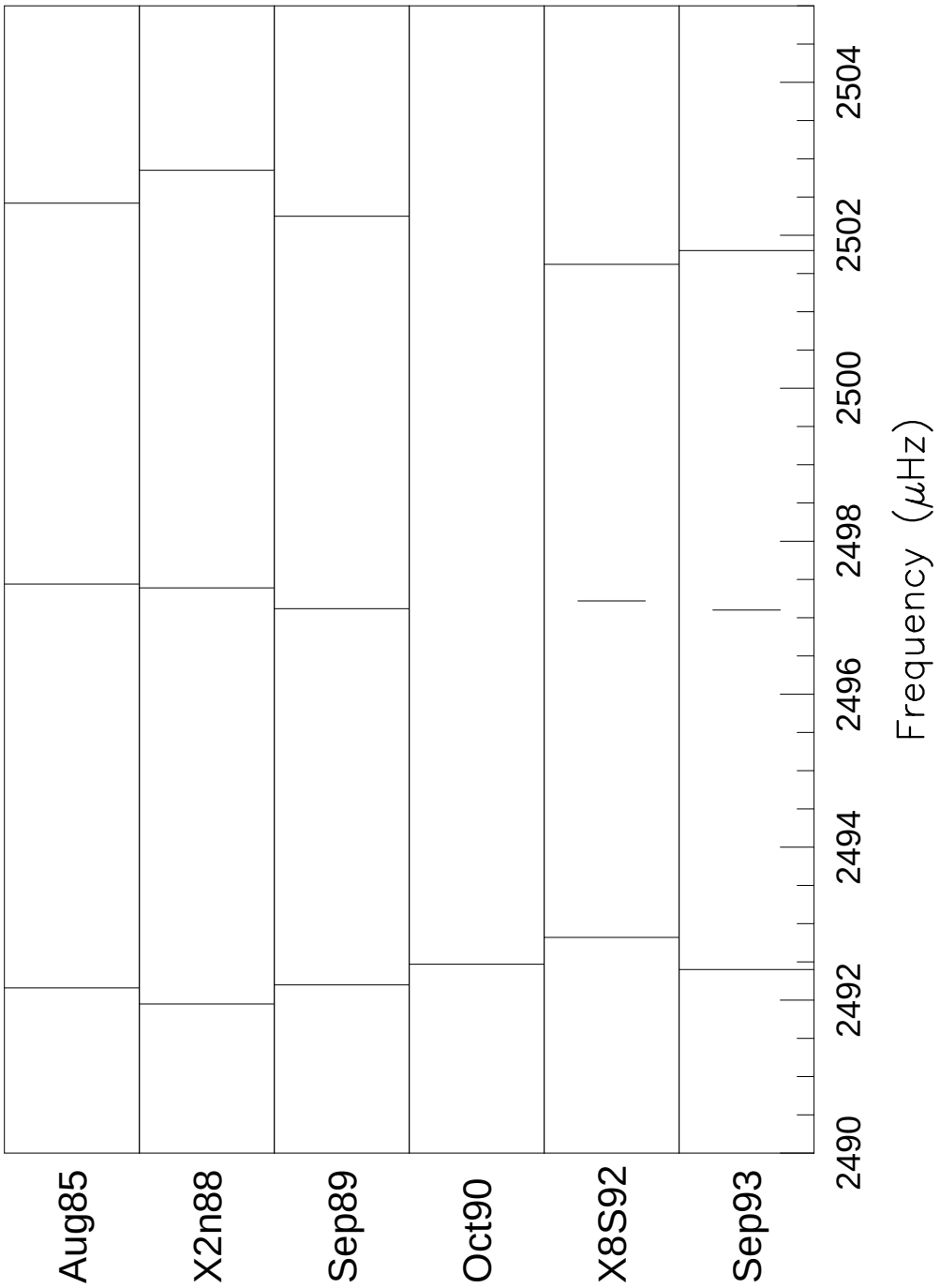

Fig. 5.1.— Schematic diagram of the 400s multiplet over time.

this variation is due to radial motion of material on the star itself, then the star's rotation speeds up or slows down as the result of conserving angular momentum. Assuming a year period, however (consistent with the Barnbaum & Zuckerman result), the required radial velocity variation would be on the order of 10^{-2}cm/s, many orders of magnitude less than the Barnbaum & Zuckerman measurements.

Although not yet in the published literature, these sorts of multiplet irregularities are not completely new. During the XCOV10 run on GD 358, we saw severe changes in the multiplet structure both as the run went on and as compared to the previous WET run on the star. During the run, for example, many of the triplets actually looked more like quintuplets for a time, but then came back to a triplet state. These changes occurred on timescales as short as a few days. While we cannot apply our explanation of these phenomena to G29–38 (only because we don't have one), it is worth noting that there is additional evidence for some fundamental flaws in our simple picture of ever-lasting equally-spaced multiplets.

Figure 5.2 shows the FTs of the 400s region in each of the data sets. The m=0 mode in Sep89 was only visible after pre-whitening by the other two triplet components. Pre-whitening in other seasons failed to find any more unambiguous peaks than those listed in Table 5.1 which gives the frequencies and amplitudes for the triplet in each data set. The average spacing of 4.9μHz corresponds to a rotation period of 1.2d. The range of spacings correspond to rotation periods from 1.1 to 1.3d, assuming the asymptotic expression for $C_{\ell,k}$ is valid.

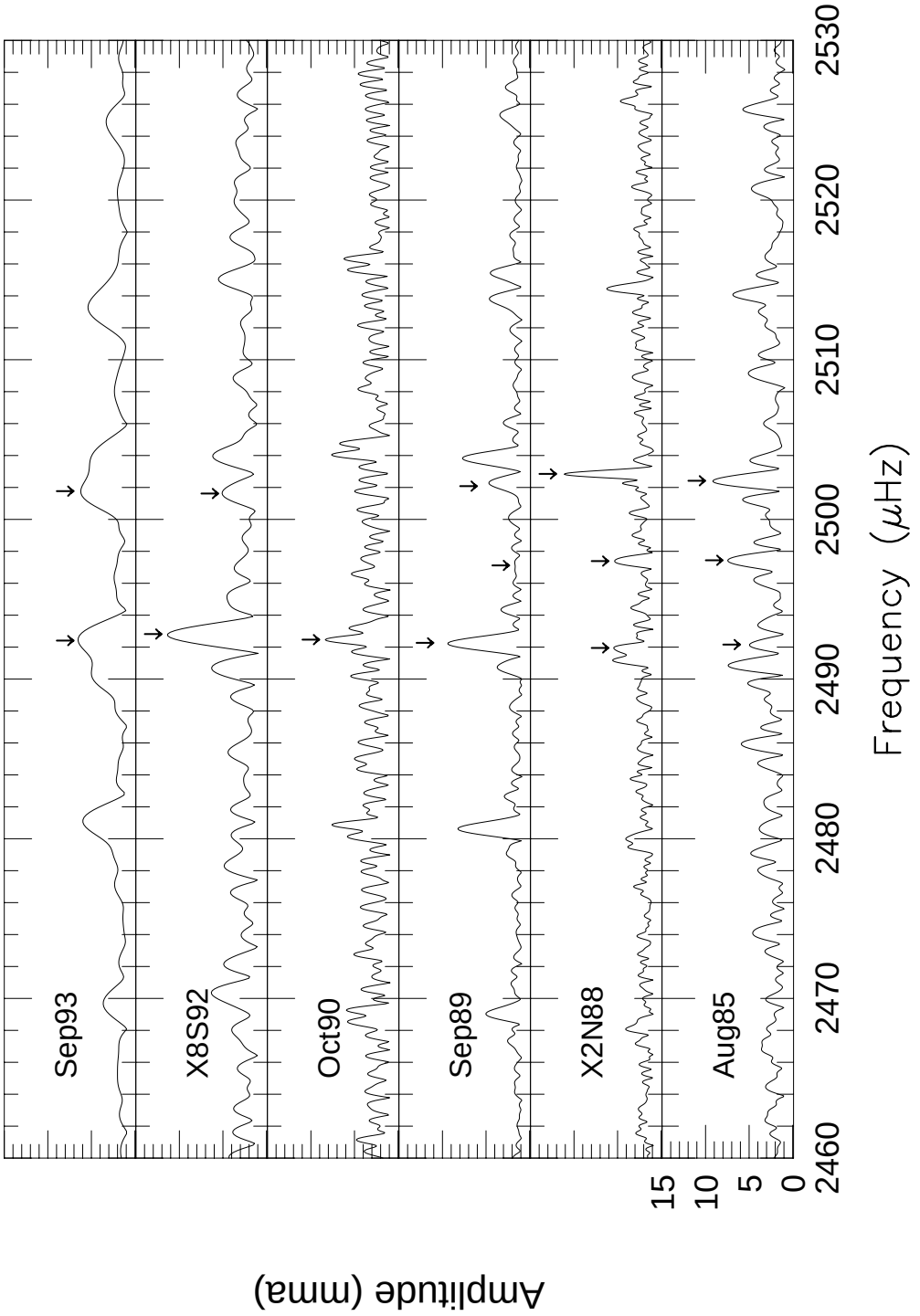

Fig. 5.2.— Fourier transform of the 400s multiplet over time.

Table 5.1. G29–38's 400s triplet over time.

Data Set	Frequency (μHz)	Amplitude (mma)	Spacing (μHz)
Aug85	2492.16	4.4	5.28
	2497.44	7.0	
	2502.42	8.8	4.98
X2N88	2491.95	4.9	5.44
	2497.39	4.8	
	2502.85	10.9	5.46
Sep89	2492.268	9.7	4.85
	2497.118	1.3	
	2502.083	4.9	4.97
Oct90	2492.47	8.0	
X8S92	2492.82	11.2	4.40
	2497.22	Average	
	2501.62	4.5	4.40
Sep93	2492.41	6.0	4.68
	2497.09	Average	
	2501.77	5.7	4.68

2. The 284s Mode

Besides the 400s multiplet, the only consistently recurring area of power in G29–38 is the 284s mode, which does not, unfortunately, show similar multiplet characteristics. Only once, in the Sep89 data, is another peak clearly seen in the transform. Figure 5.3 shows an additional peak spaced 5.9 μHz to the right of the 284s mode. In the remaining data sets there are some cases with a slight excess of power near this mode, but it is never conclusive. In Aug85, there is clearly excess power in this region and it is consistent with a multiplet component at the same place as seen in Sep89, but not well-resolved. Since the spacing observed in 1989 is similar, although not equal, to that in the 400s mode, there is some support for labeling the 284s mode and the 400s multiplet as the same ℓ although we still have to account for the slight, but significant, difference in splitting. (Slightly differential radial rotation rates could explain it.)

3. The 500s Region

While not as stable as the 284s and 400s regions, there is recurring power near 500s. The exact periods seen in any given year vary and the region is not always completely resolved. Figure 5.4 shows the FT of this region in each of the primary data sets. I conservatively pre-whitened and synthesized the FT and lightcurve around this region and mark what peaks I believe are real with arrows in Figure 5.4. There are no arrows in Sep89 despite there being obvious power there because it is very unclear which modes are real — they are not at all resolved. The Aug85 and X2N88 data sets show fairly obvious

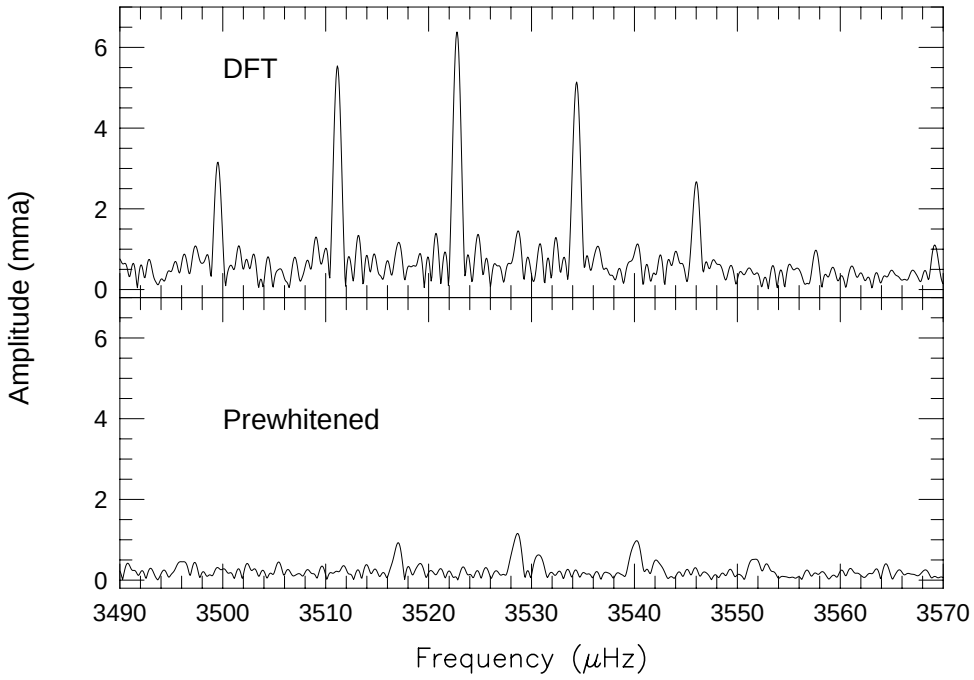

Fig. 5.3.— Fourier transform of the 284s region of G29–38 in Sep89.

triplets with near equal (but different in each data set) spacings. The only identified peak in the Sep93 data set matches the central (m=0) component of these two triplets, but the power seen in the Oct90 and X8S92 data sets do not match at all. Table 5.2 lists the identified frequencies and their spacings.

Twice this region has been resolved into a triplet that shows similar behavior to the 400s triplet. The central m=0 peaks appears to remain stable while the $m \neq 0$ peaks move symmetrically about the m=0 mode. With only two measured spacings, I cannot say quantitatively if the same phenomena are happening here as with the 400s mode, but I do note the direction of the frequency change form Aug85 to X2N88 is the same as in the 400s mode, but with a larger absolute (and relative) magnitude. The spacing observed here averages to 7.8μHz compared to 4.9μHz for the 400s modes. If the 400s and 500s triplets are the same ℓ, then there must be radially differential rotation in the star. (Models of Bradley [private communication] show $C_{\ell,k}$s that only vary by at most 30% when not in the asymptotic limit. This is too small a change to be the cause here.) If this splitting represents an ℓ=1 rotationally split mode, the rotation rate is 0.7d.

The ratio of the average 500s splitting to the average 400s splitting[2] splittings is 1.59, close to the expected value of 1.66 for the ℓ=2 to ℓ=1 ratio, suggesting therefore, that the 500s mode is ℓ=2 and the 400s mode is ℓ=1. That we only see triplets and not quintuplets cannot rule out an ℓ=2 identification, although it is suggestive. This ratio may, however, just be a coincidence. Taking each season separately, the splitting ratio for Aug85 is

[2]These are averages of the splittings seen each year.

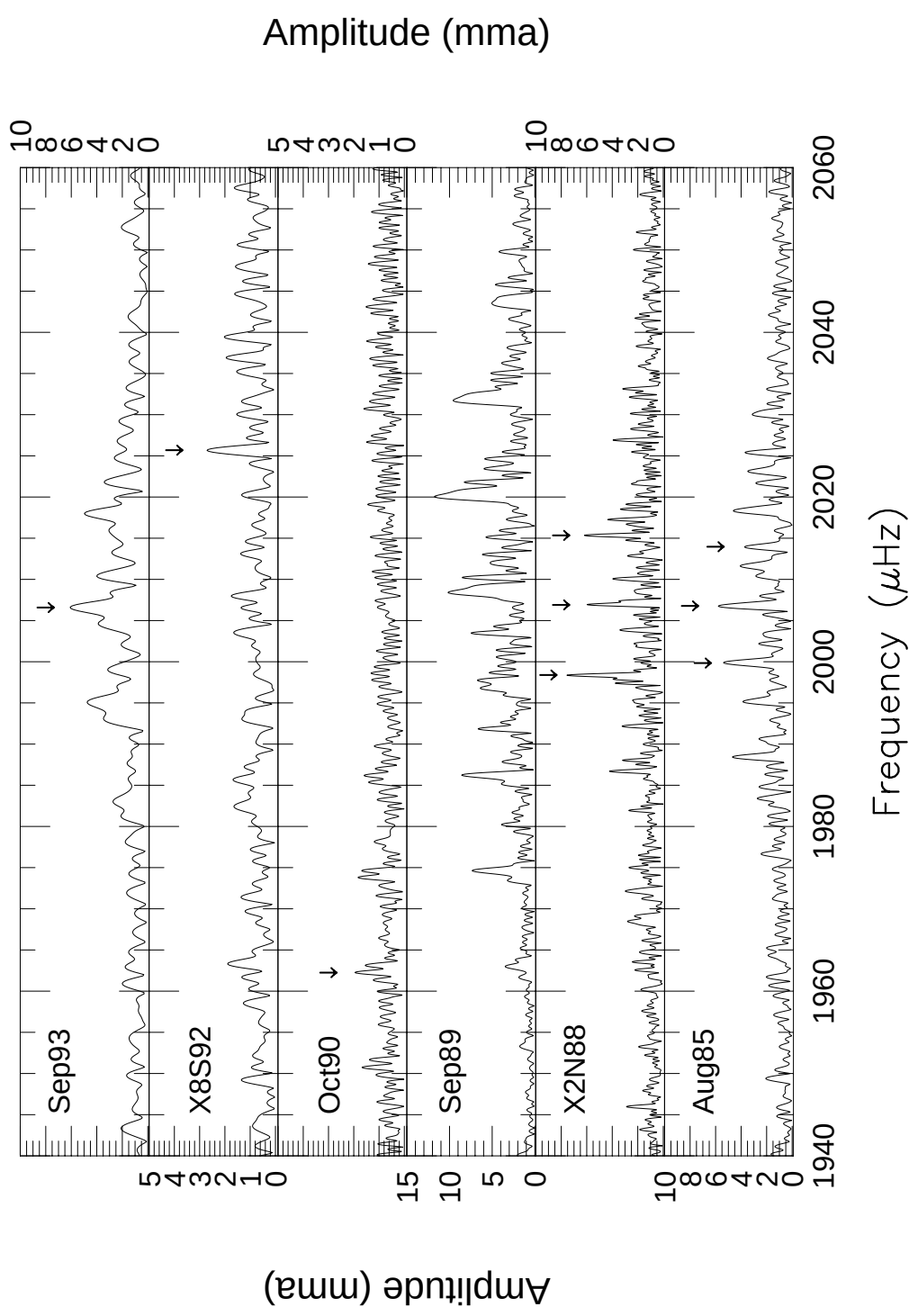

Fig. 5.4.— Fourier transform of the 500s region in G29–38 data.

Table 5.2. Identified power in the 500s region of G29–38's FTs.

Data Set	Frequency (μHz)	Amplitude (mma)	Spacing (μHz)
Aug85	1999.84	5.3	6.94
	2006.78	5.7	
	2013.97	3.1	7.19
X2N88	1998.39	7.5	8.51
	2006.91	5.7	
	2015.34	6.2	8.43
Sep89	???		
Oct90	1962.25	1.9	
X8S92	2025.69	2.7	
Sep93	2006.58	6.1	

1.38 and for X2N88 it is 1.55. These ratios, which may be more meaningful as they are ratios taken in the same seasonal data set, are not as close to the predicted ℓ=2 to ℓ=1 ratio as the overall average ratio is. The multiple-ℓ explanation does not fit any better.

The modes seen in X8S92 and Oct90 are of low signal to noise, and therefore hard to classify. There is clearly something happening in the Sep89 data set as well, but the data are simply not resolved. There may be instances of both the high (near 8μHz) and low (near 5μHz) spacings at once in this data set, but it is very hard to to see the forest for the grass.

4. The 615s Mode

The dominant power in the X2N88 data was a mode at 615.15s. Winget et al. (1990) claimed this mode was single, isolated and showed a strange, unexplained phase variation. Their plot of the observed FT and spectral window convincingly shows there are no nearby peaks. A similar figure from my re-reduced data is seen in Figure 5.5. However, upon pre-whitening the data by the 615s mode, I found there is indeed another mode nearby — spaced 8.53μHz to the right. The 615s mode's first harmonic also shows the same structure. Both of these modes are seen in Figure 5.6. The 8.5μHz spacing here is the same as seen in the 500s triplet in this same data set. The simplest explanation of this mode therefore, is it is the same ℓ as the 500s modes and at least one component of the multiplet is missing.

The beat period between the dominant mode and this new companion is almost 33 hours, so during a single run the two modes will not be resolved.

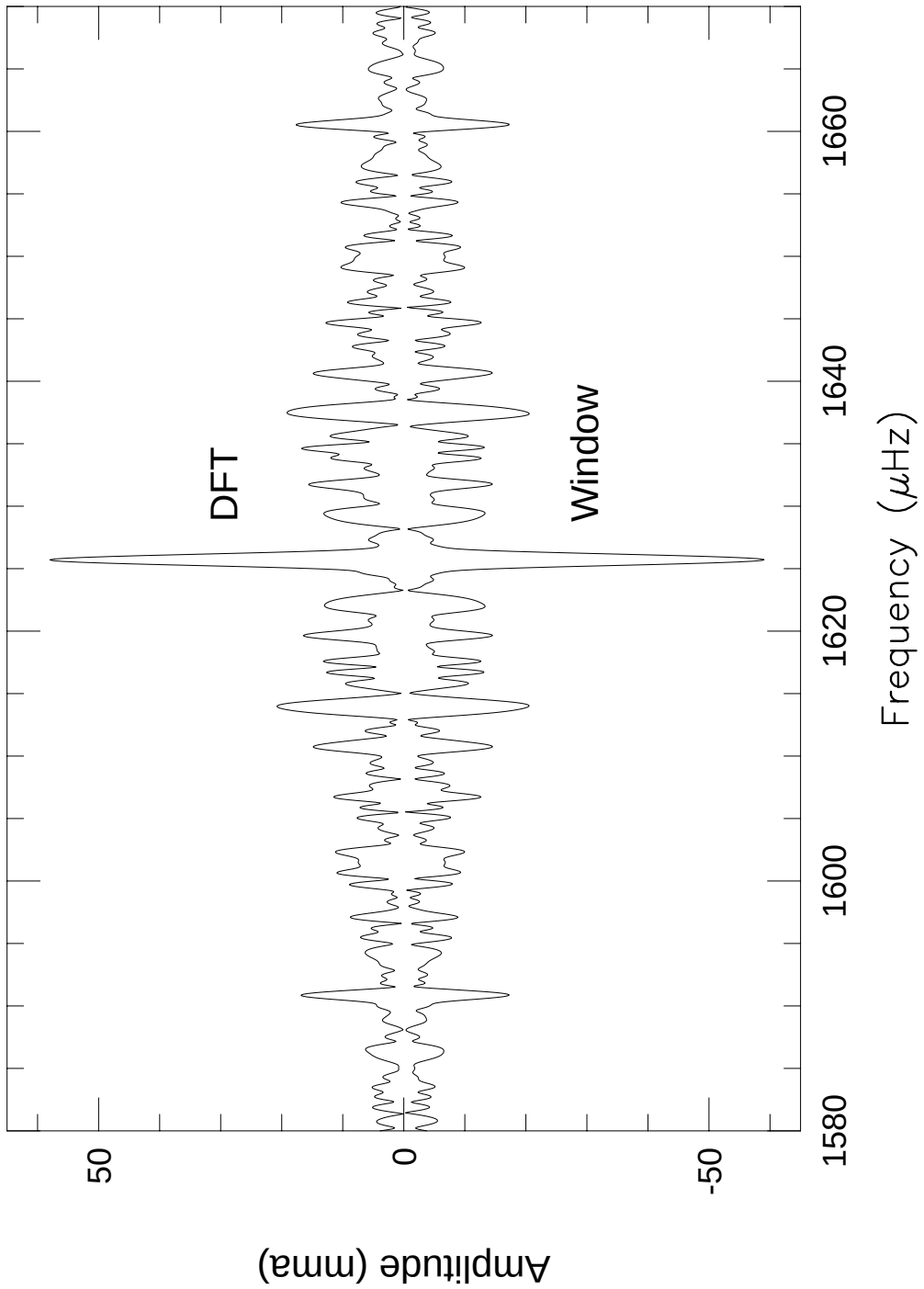

Fig. 5.5.— The FT and window of the 615s mode in G29–38 during the X2N88 run.

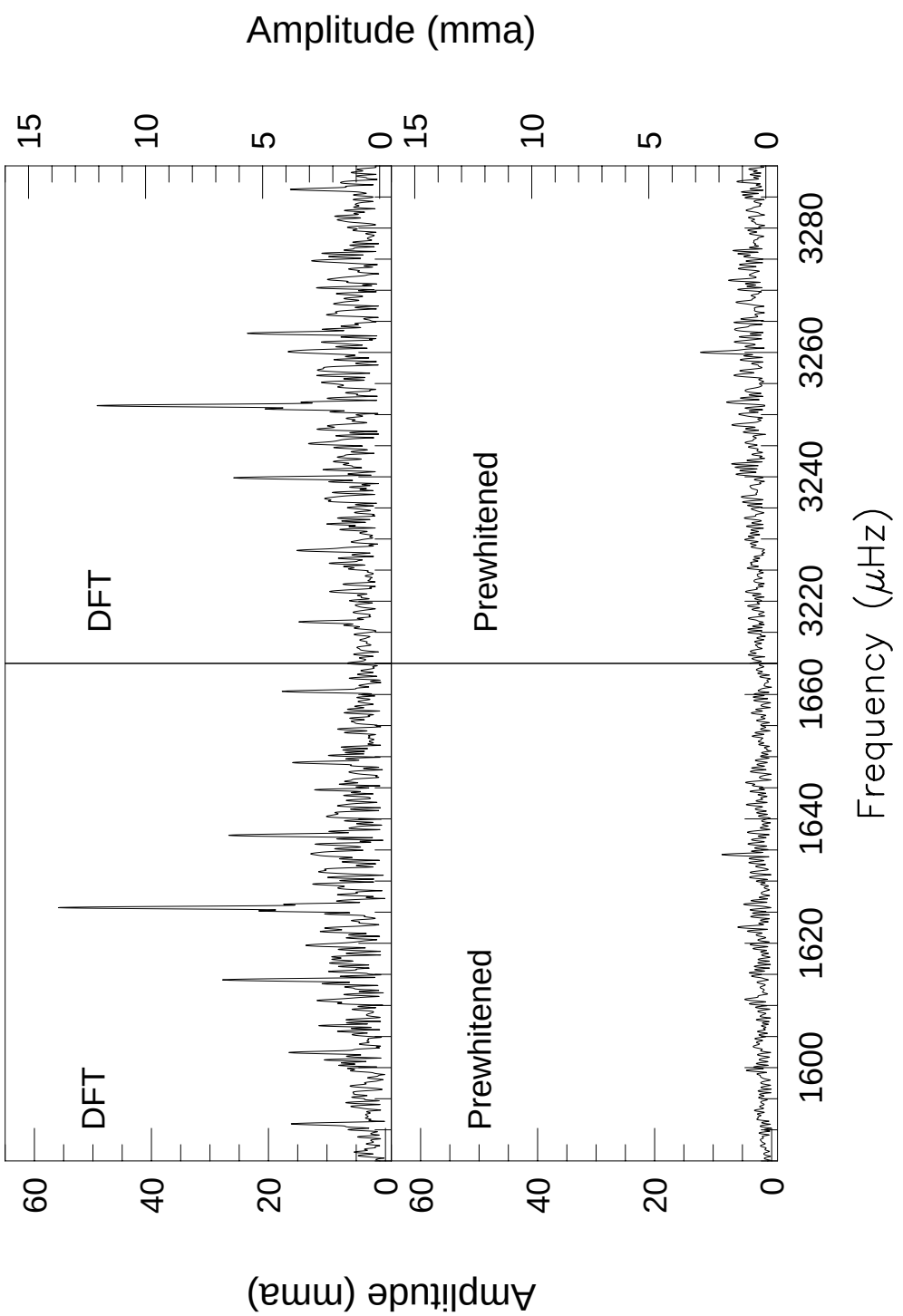

Fig. 5.6.— The 615s and first harmonic region with the main peak removed from the data (X2N88 data).

What affect will this have on the phase of the 615? Could this previously unseen mode be the cause of the 615s phase variation? Or could it be an artifact produced by the FT to accommodate the observed (but perhaps real) phase variation?

To answer these questions, I simulated a light curve containing only the two peaks near 615s and then did a linear least squares (fixed period) $O-C$ fitting only the 615s mode. The resulting $O-C$ showed no sign of the previously observed variation, proving the new observed mode is neither the cause nor effect of the observed phase variation. Not accounting for this mode's presence had roughly a 10% effect on the phase of the 615s mode. Kepler et al. (1995) give a formula ($\tan\phi_{max} = \frac{A_1/A_0}{[1-(A_1/A_0)^2]^{\frac{1}{2}}}$ where ϕ_{max} is the expected phase wander and A_0 and A_1 are the amplitudes of the largest and smallest peaks, respectively) for the phase variation caused by an unresolved doublet. For these two modes, we expect only a few percent variation in phase and a fairly short beating timescale — slightly over one day. The variation of Winget et al. was over a much longer timescale and had a much larger amplitude.

In 1989, the 615s mode disappeared, but by the end of the 1992 season, power near there started to reappear. By Sep93, its amplitude had grown to 33mma and clear multiplet structure emerged. Figure 5.7 shows the FT in this region. The frequency spacing this time is 4.7μHz (as opposed to the 8.5μHz splitting seen in the X2N88 data) — identical to that seen in the 400s mode this season, suggesting (if the different splittings are due to different ℓs) this is the same ℓ as the 400s mode and different ℓ from the 500s region. This is in direct contradiction with the two modes found in the X2N88 data which

suggest the 615 power is the same ℓ as the 500s region and different from the 400s power. It is possible there is a missing mode in the X2N88 doublet so the spacing is really 4.2μHz, much closer to that seen in Sep93. It is difficult, however, to call the match between the 8.5μHz spacing in these two modes and that of the 500s triplet in the same data set as a coincidence. Figure 5.8 schematically shows all the main multiplets in each data set and readily shows which multiplets "agree" with each other when.

The 615s period in the X2N88 data set is roughly 7μHz away from the nearest peaks seen in Sep93; its companion peak falls right in between the left-most and central Sep93 components. This difference is not easy to explain and suggests we may not be seeing the same normal mode in the star. The phase (or period) of the 615s peak in the X2N88 data was changing rather dramatically. When nearby power reappeared in 1992 and grew in amplitude through Sep93, its frequency again changed significantly, from about 1638μHz to 1630μHz. Given the mode's large amplitude in addition to this frequency change, we suspect there is a strong resonance or trapping here and these two sets of modes are probably the same normal mode of the star.[3] As the mode grows in amplitude, it may be pulled more and more into the trap. We observed the 600s mode's period increasing as it grew in 1992 — 1994, just the direction it would need to go to match the larger X2N88 mode. It is also the direction we expect (from the ΔP *vs.* P diagram of Chapter 4) trapping to pull the mode. Incidentally, this observation has important implications to mode-trapping. It shows the strength of the trap is proportional to the

[3]Actually, this is more than a suspicion. The ΔP *vs.* P diagram presented in Chapter 4 shows the 615s mode is near a deep trap.

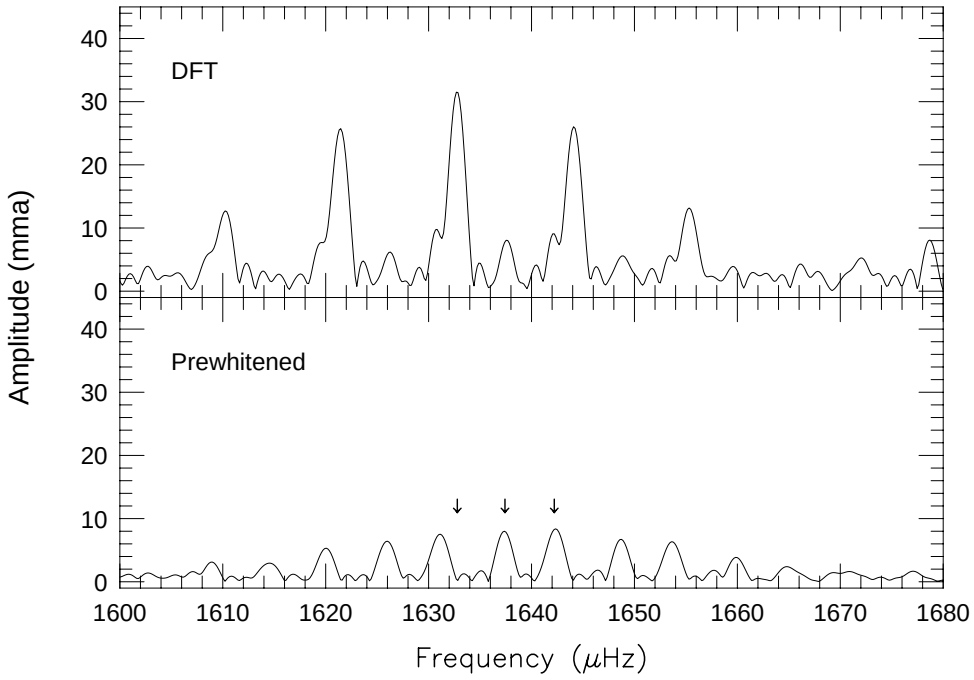

Fig. 5.7.— The Sep93 G29–38 FT near 612s with arrows indicating the multiplet components.

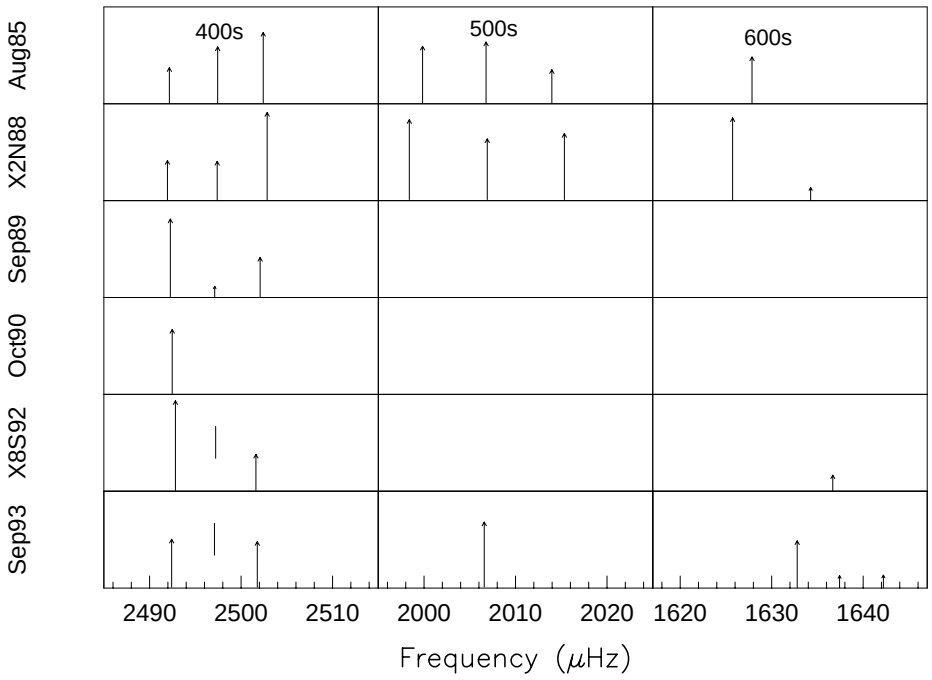

Fig. 5.8.— A schematic plot of all the major observed multiplets. The short line segments are not real modes, but averages of the two flanking modes.

amplitude of the trapped mode. While this correlation may be intuitive, it is certainly not included in the linear trapping theory and could be used to calibrate non-linear models.

The different m-splittings of the two sets of 600s modes, however, still remain a problem. This apparent contradiction could be explained in at least two ways (a good theorist, and even many bad ones, can always come up with an explanation after the fact): a change in the (differential) rotation in the star, or the existence of an ℓ=1 and a ℓ=2 mode near 615s which "take turns" being excited to observable amplitude.

The Aug85 and X8S92 data sets show some evidence of excess power in the 615s region, but the data are not good enough to resolve it. In Aug85, there is possibly a peak about 9μHz away from the dominant peak and in X8S92, there is excess power in one of the alias sidelobes of the main peak, split about 2.5μHz to the left. Table 5.3 lists all the identified power in the 600s region.

5. Conclusion

There are many other regions in the FTs with excess power, but none that can be unambiguously identified as a multiplet of any sort. The power in the 800s region, when present, often shows excess power, but is never resolved well enough to say exactly what is going on. So we are left having to explain only the modes already presented.

There are two classes of multiplets seen, both triplets, but with spacings either near 5, or 8 μHz. The 400s mode is always of the first class; the 500s

of the second (plus some unexplained excess power perhaps) and the 615s alternately falls into both. The 284s mode once showed a nearby mode with a slightly larger splitting than seen in the 400s mode the same year. Only twice are there two modes with the same splitting in the same year: 1) X2N88: the 500s and 615s modes (large spacing) and 2) Sep93: the 400s and 612s modes (small spacing). There are two possible explanations for these matches.

If we maintain all modes are ℓ=1, then in addition to a time variable rotation rate to explain the 400s multiplet variability, there must be differential rotation (to provide the two sizes of splittings) which in itself is also time variable (hence the 615 falling into both camps). A nice test to this theory would have been to measure a 615s splitting in Aug85 (where the 400s was low and the 500s, high) or a 500s splitting in Sep93 where both the 400s and 615s were low. In the former case, I would expect the 615s splitting to be high, and in the latter, the 500s to be low. Although the current data do not permit such measurements, future data may provide such an opportunity if only the star cooperates and shows the needed multiplets at the same time.

Allowing for ℓ=2 in addition to ℓ=1 modes does not do any better since the splitting ratios are not quite right. We would still have to employ time-dependent differential rotation to get things to work. Another possibility is for the 615s mode to be near an accidental degeneracy where an ℓ=1 and ℓ=2 each have modes in the same place. As such, if the ℓ=1 mode were excited, the ℓ=2 mode could be as well, or perhaps, could take over and wipe out the ℓ=1 mode. Thus, we could be seeing sometimes an ℓ=1 and other times an ℓ=2. This has the additional benefit of maintaining the period spacing described in the previous chapter, as only the ℓ=2 modes near ℓ=1

modes would be excited thereby leaving the ℓ=1 period spacing relatively intact. Such a mixture of modes could also explain why there is often an excess of power observed which is not easily resolved.

We have now had to resort to time-varying, radially differential rotation, or precise accidental degeneracies to explain the observed multiplet components. While such a model may indeed work, it is starting to become weighed down with modifications and amendments.[4] Measured a new and different multiplet splitting? No problem, we'll just adjust the rotation rate at that radius at that instant in time to account for it. Next. What may be more likely than the uncomfortable set of requirements above, is that there is simply more to this than existing theory considers; we may not fully understand all the components that go into the multiplet structure (in amplitude-space, we already know this is true). While I am loathe to resort to new physics having made an unexplainable observation, the large number of parameters in the current model required for a reasonable explanation makes me equally uncomfortable.

The primary purpose of this study was to further improve the mode identifications made earlier. But like everything in this star, nothing is spelled out exactly as we would have it. While we see only triplets (and not quintuplets, for example), the variable splittings are not easily explained by any simple model. While we could use some ℓ=2 modes in a model to these observations, the fit would be a bit worse than the ℓ=1 only model. It will take some time, and some modelling to sort everything out, but I suspect we

[4]Shades of epicycles ....

will find there are additional parameters not included in our stellar models.

Table 5.3. Identified power in the 600s region of G29–38's FTs.

Data Set	Frequency (μHz)	Amplitude (mma)	Spacing (μHz)
Aug85	1627.85	31.3	
X2N88	1625.73	55.5	8.53
	1634.26	8.6	
X8S92	1638.68	10.6	
Sep93	1632.79	31.6	4.63
	1637.42	8.2	
	1642.21	8.5	4.79

Chapter 6

Other Cool DAV Stars

We can share what we have of yours
'cause we done shared all of mine.
—Bob Weir & Robert Hunter, *Jack Straw*

Having successfully explored the period spectra of G29–38 and noted a few unsolved mysteries along the way, it is now time to look at other, similar stars to see what observed characteristics are specific to G29–38 and what are universal to the particular subclass of DA pulsators. If G29–38 is simply a weird duck, producing a model that explains all its behavior merely explains a single star. If, however, there are similar affectations in other stars of the same class, whatever we learn about G29–38 will teach us about the class of stars to which it belongs, and hopefully, in the process, a little bit about how these stars got to where they are. In addition, if there is similar behavior in these stars, we can use each star as an additional source of information, an additional clue to the puzzle.

Clemens's (1993, 1994) work, which first made DAV asteroseismology possible made a bold statement: all DA pulsators are the same; variations in

their pulsation spectra are primarily due to variations in total stellar mass, nothing more. In arriving at this conclusion, he studied the hotter DAVs and did not include the cool DAVs in much of the analysis. Here, we have a unique opportunity to test Clemens's conclusions with a different sample of stars from the ones he used.

It would have been nearly impossible to obtain as much data on all stars similar to G29–38 as I did on G29–38 itself, so I concentrated on only a few, and even then, have much less data on each of them than I do on G29–38. Nonetheless, the data will show, at least with respect to its pulsations, that G29–38 is not simply a weird duck, despite its unique infrared excess (Zuckerman & Becklin 1987). It will also show the cool DAVs agree with the result that the hotter DAVs form a very uniform class of objects.

1. Long Period Variability and Stability

As a glance through FTs shown in Chapter 4 (and Appendices A and B) will indicate, G29–38's power spectrum varies, sometimes dramatically, from year to year. Correspondingly, there are less dramatic, but nonetheless substantial changes occurring on monthly timescales. The other stars I present here, G38–29, G191–16, and HL Tau 76 also show similar changes, but to slightly different degrees. The most dramatic, like the change seen in G29–38 from the X2N88 to Sep89 data sets, is G191–16, between January and November, 1991. My best data set is from November, 1990 (Figure 6.1) and shows a very large-amplitude ($\approx 70mma$) pulsation near 1200μHz. Data in January, 1991, show roughly the same power spectra, but by November that year, the 1200μHz power had completely disappeared with the largest power, now

near 1675μHz, down by more than a factor of four (two in amplitude) (see Figure 6.2). The next data set I have, February, 1994, looks very similar to the lower-amplitude states of November, 1991 with no indication of the once dominant 1200μHz power. Power near 2000μHz remains in the transform each season.

While not quite as dramatic as G191–16 (mainly because its amplitude wasn't as high to begin with), G38–29 showed a set of similar changes. In October, 1990 (Figure 6.3), the largest power was near 1000μHz with an amplitude of 24mma. By December, 1993 (the next available data set), the same peaks had an amplitude of 36mma (Figure 6.4). It is clear that this area is not resolved, so part of the problem could be beating between closely-split modes due to rotational splitting. The nightly transforms, however, show consistent peaks near 24mma in 1990, and wildly varying peaks in 1993, with amplitudes ranging from 18mma to 75mma, all for runs about the same length. While 1993 showed evidence of beating, the constant 1990 amplitudes suggest there was a significant change in power over this time period. Further evidence of such change is the power at 1800μHz absent in 1990, but with an amplitude over 20mma in 1993. Power near 2000μHz remains relatively constant.

HL Tau 76 has power with variable amplitudes near 900 and 1600μHz. Power at 900μHz in October and November, 1990 is completely absent by February, 1991, but reappears in November, 1993 (see Figures 6.5—6.8). While power near 1675μHz varies from 30mma in 1990 to near zero in the 1993 data set. It reasserts itself the following season, by January, 1992. Power near 1800, 2000, and 2600μHz remain present an nearly equal amplitude in all

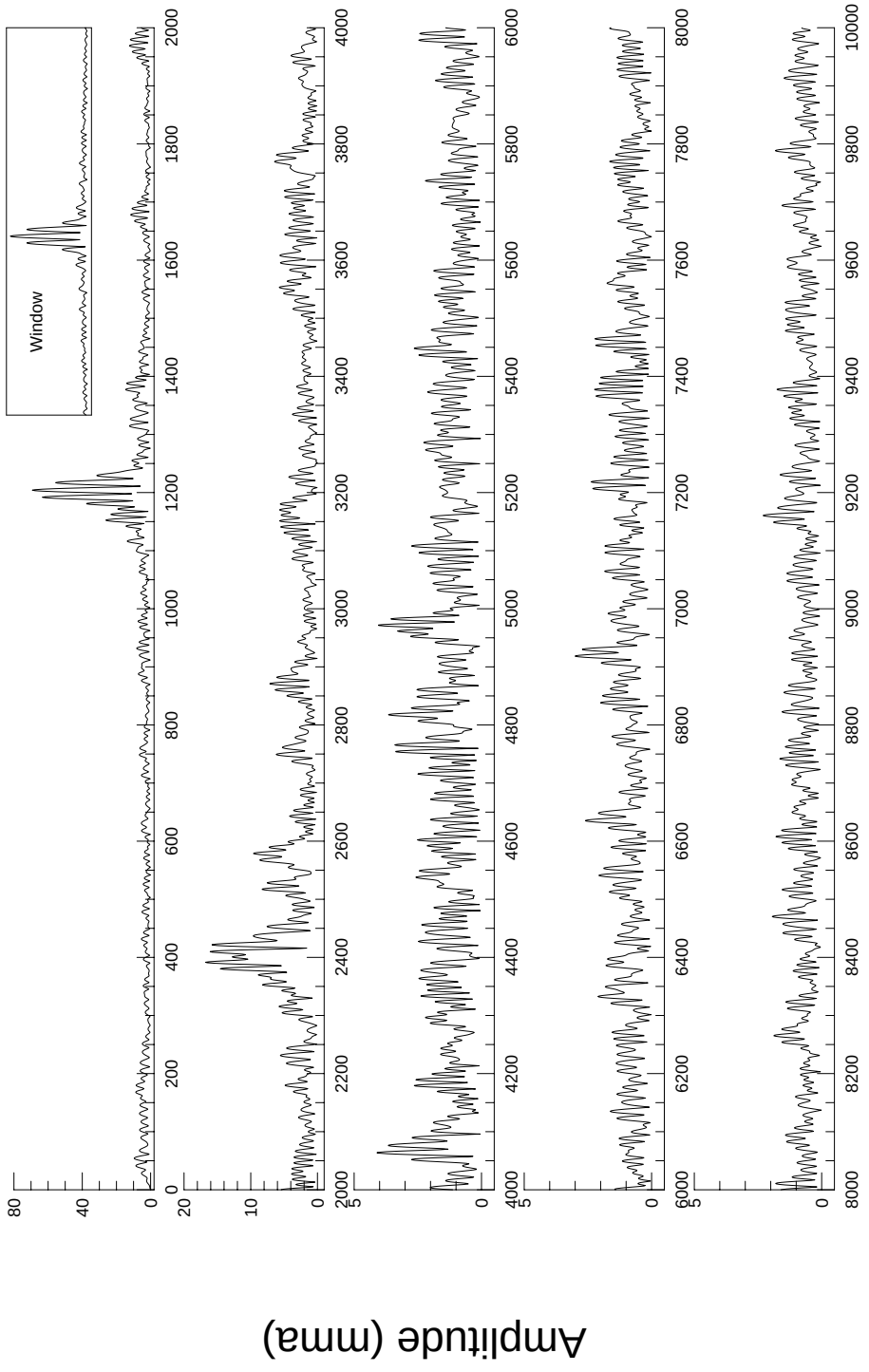

Fig. 6.1.— The FT for the November, 1990 data on G191–16.

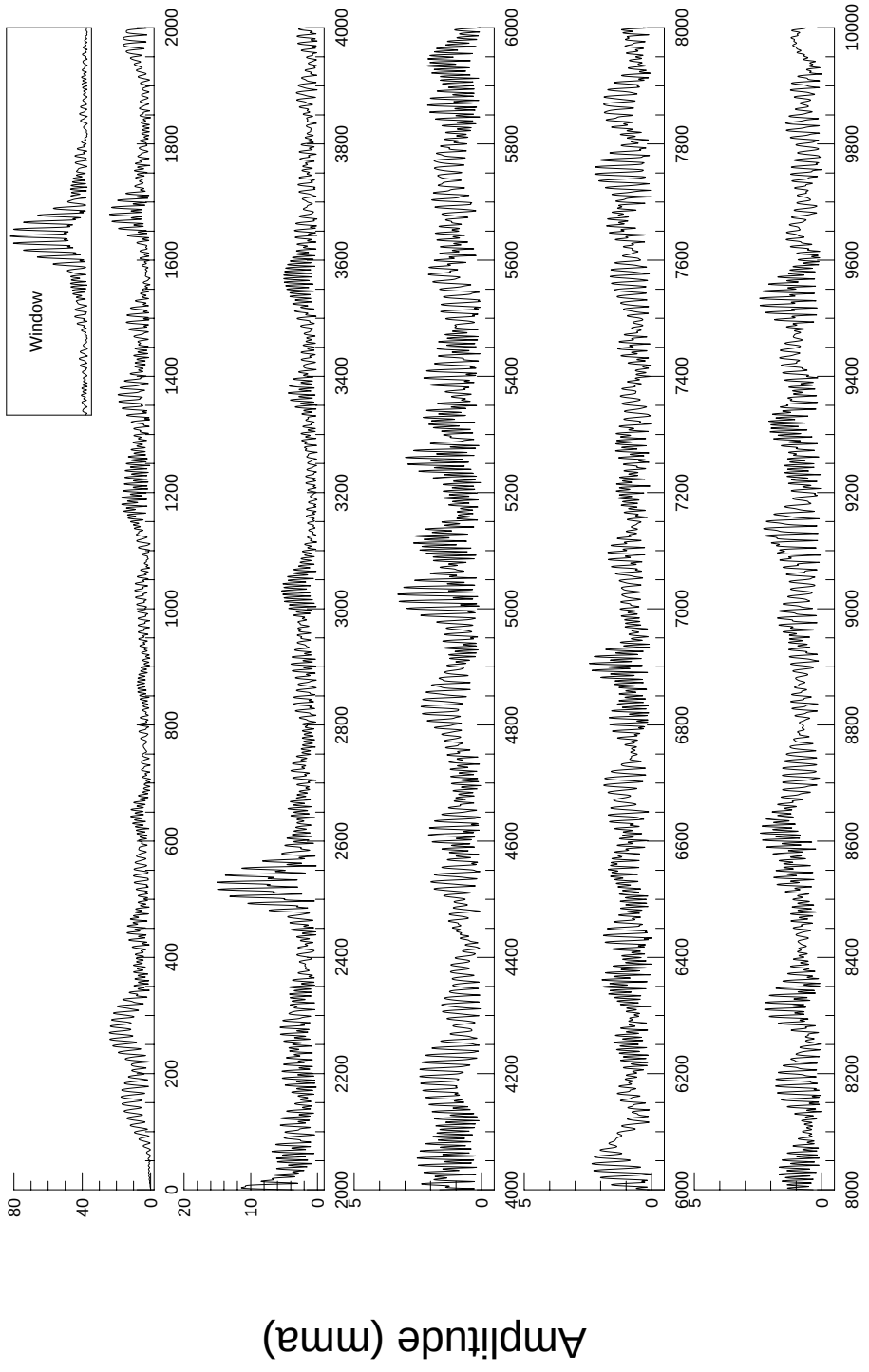

Fig. 6.2.— The FT for the November, 1991 data on G191–16.

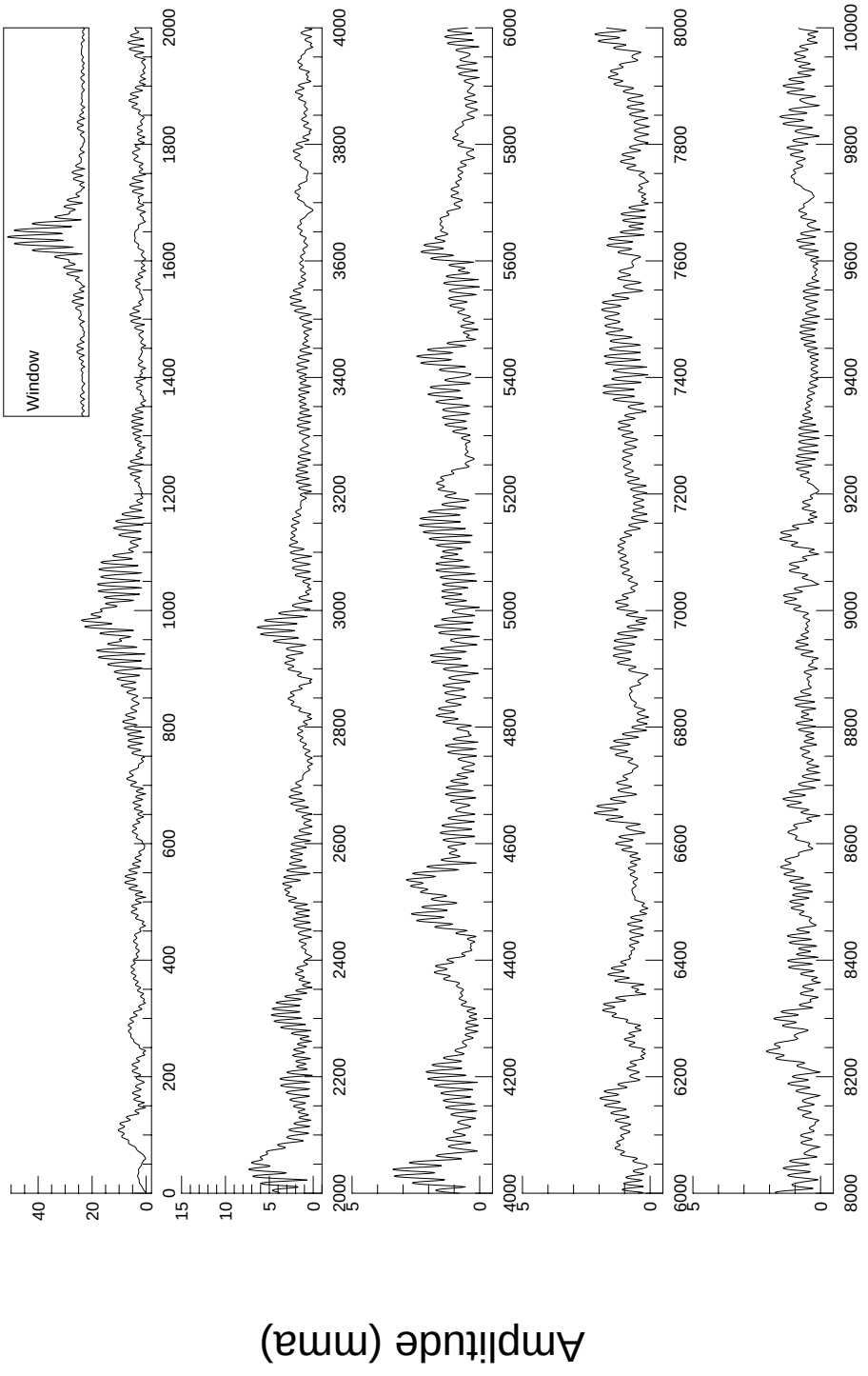

Fig. 6.3.— The FT for the October, 1990 data on G38–29.

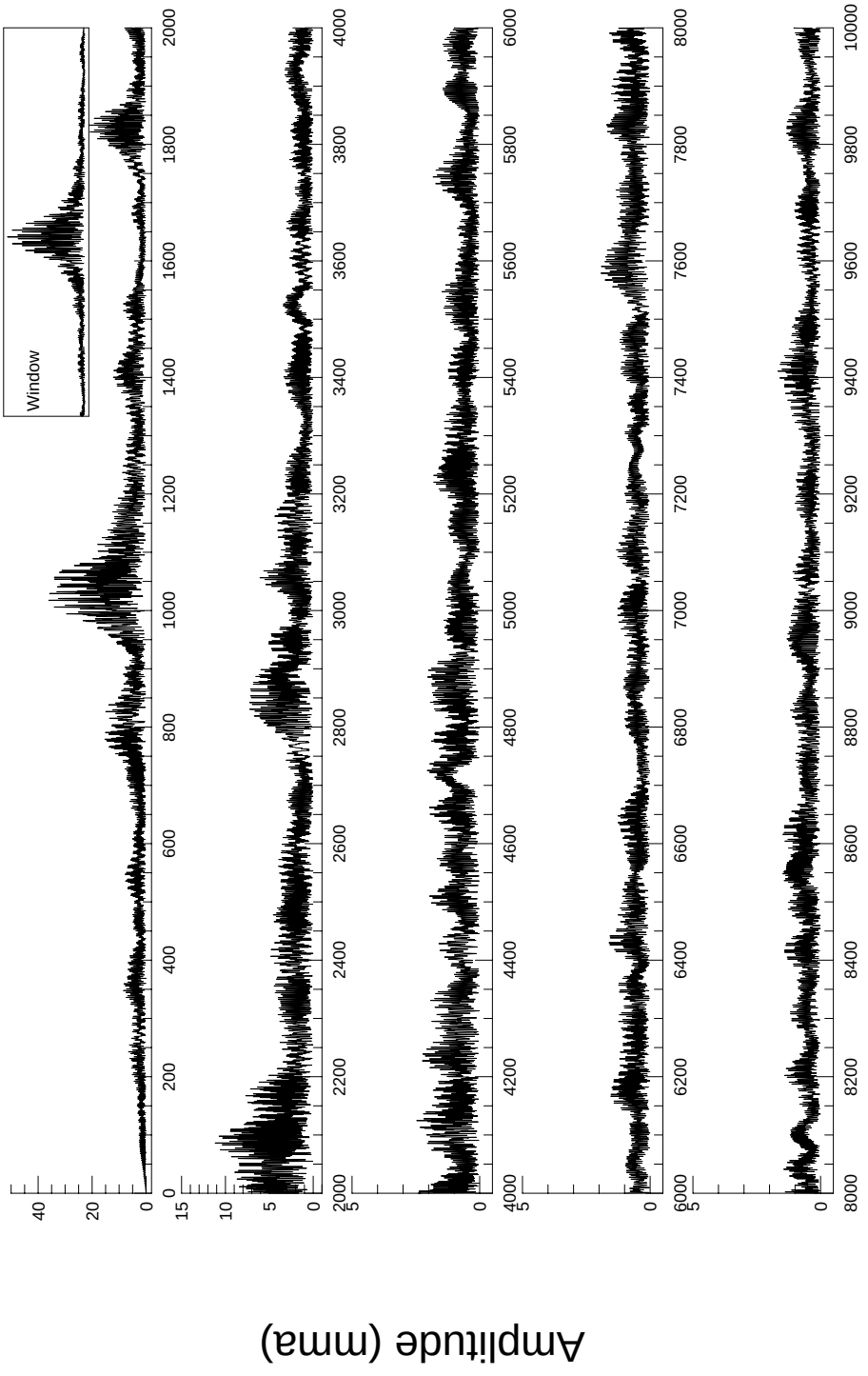

Fig. 6.4.— The FT for the December, 1993 data on G38–29.

the data sets.

Additional FTs of these stars, and G29–38 which were not discussed here are presented in Appendix B for archival purposes. In general, their quality is lower than those presented here, but they can show very gross features in the power spectra.

There is a startling amount of similarity in these stars (and G29–38). We see very dramatic power changes, modes coming, going, and reappearing, and the frequent recurrence of variable power near 1600μHzand stable power near 2000μHz. Interestingly, all three stars show power near the constant 3523μHz peak in G29–38. Unfortunately, the data are not good enough to examine the stability of this mode in these stars, but I suggest future studies may reveal some more interesting clues as to why this particular mode is so stable in G29–38.

I cannot explain the large power changes and stability observed within them, but I am pleased, nonetheless to find them, for it means time spent studying and understanding any one of these stars will benefit the understanding of all of them. The similarities and differences, I am convinced, will be crucial to exploring their variable nature. It is also encouraging to see power come and go and reappear; it means, with data similar to what we have collected on G29–38, we can study additional individual DAVs asteroseismologically.

2. Class Mode Structure

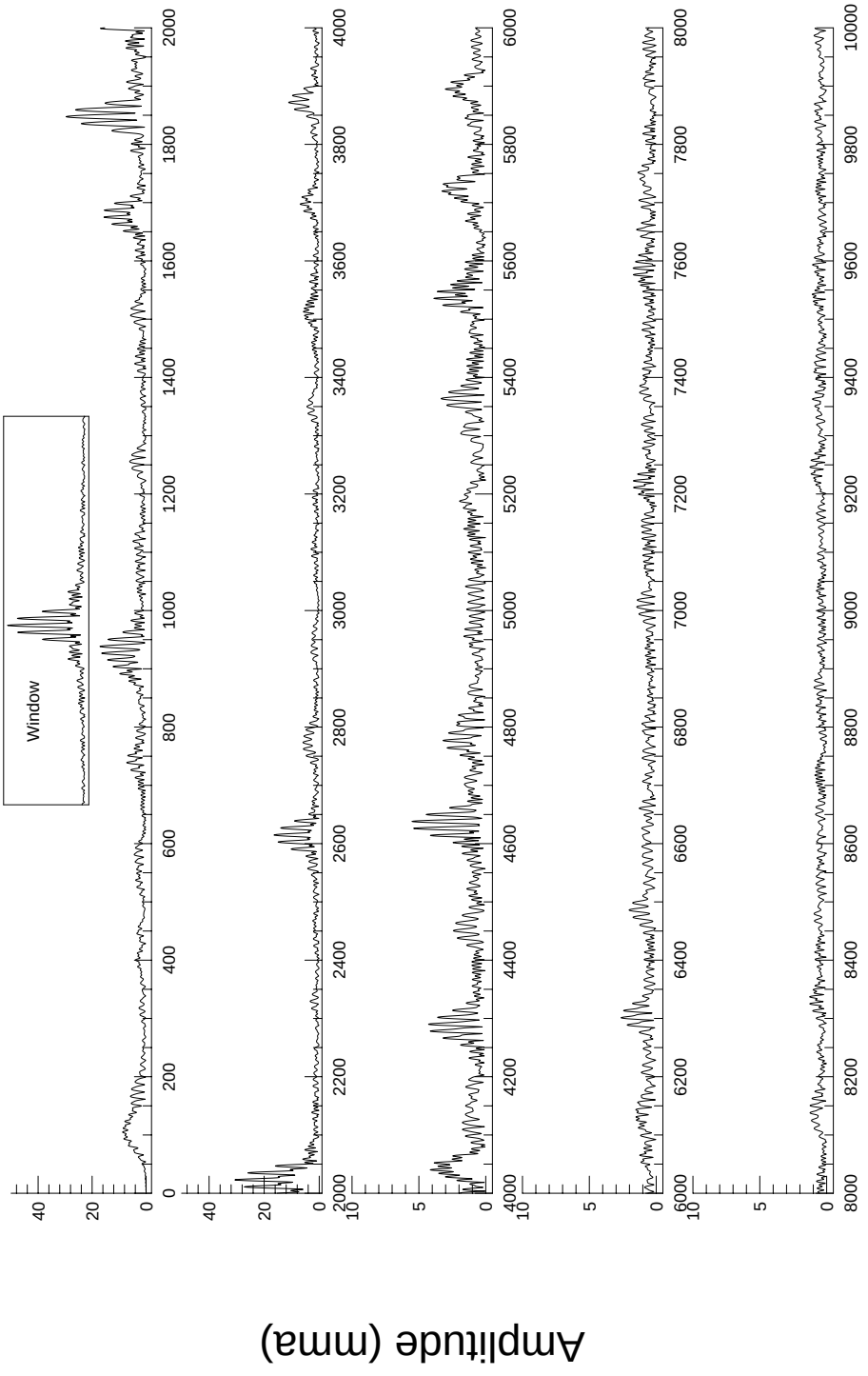

Fig. 6.5.— The FT for the October, 1990 data on HL Tau 76.

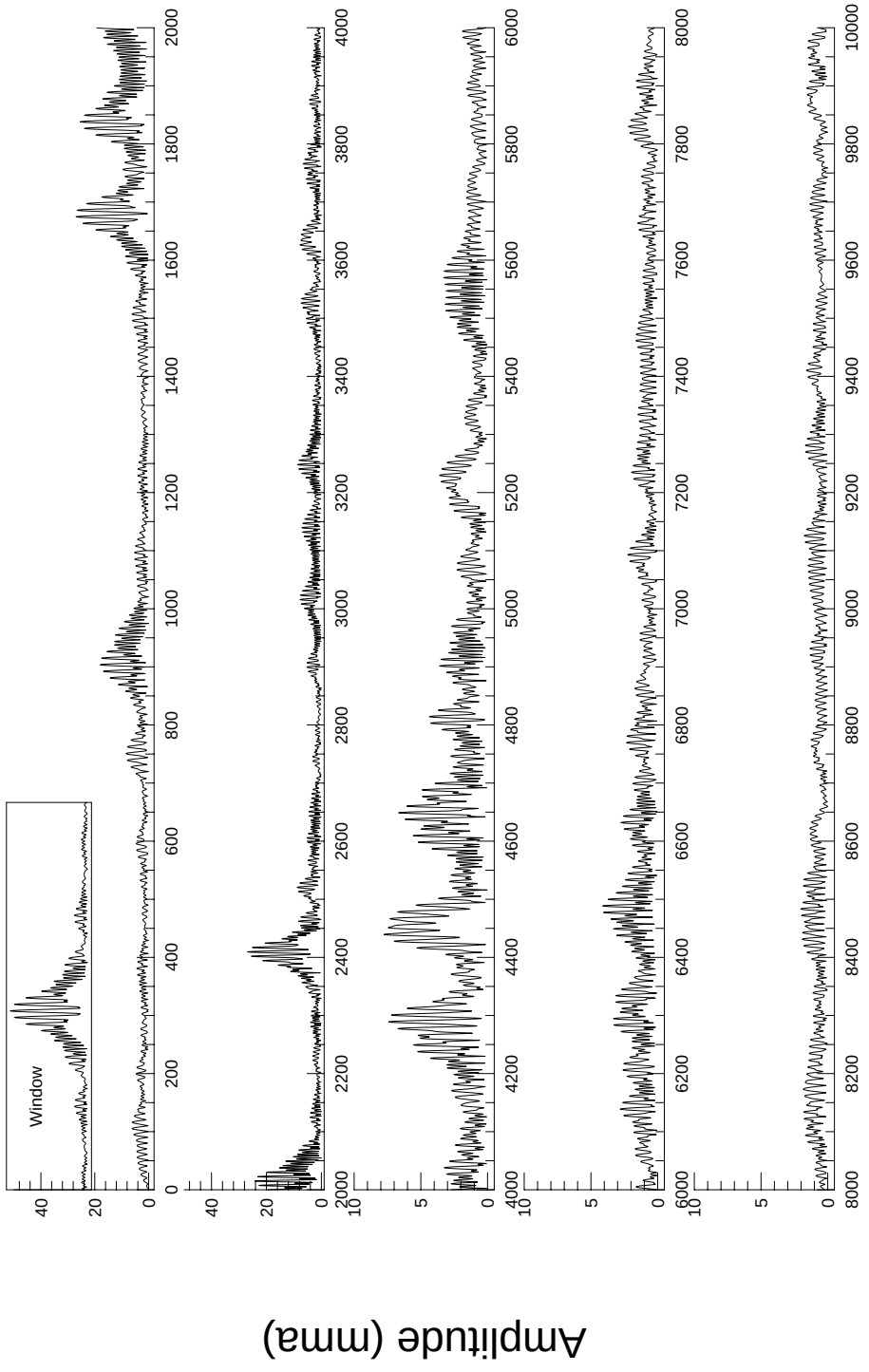

Fig. 6.6.— The FT for the November, 1990 data on HL Tau 76.

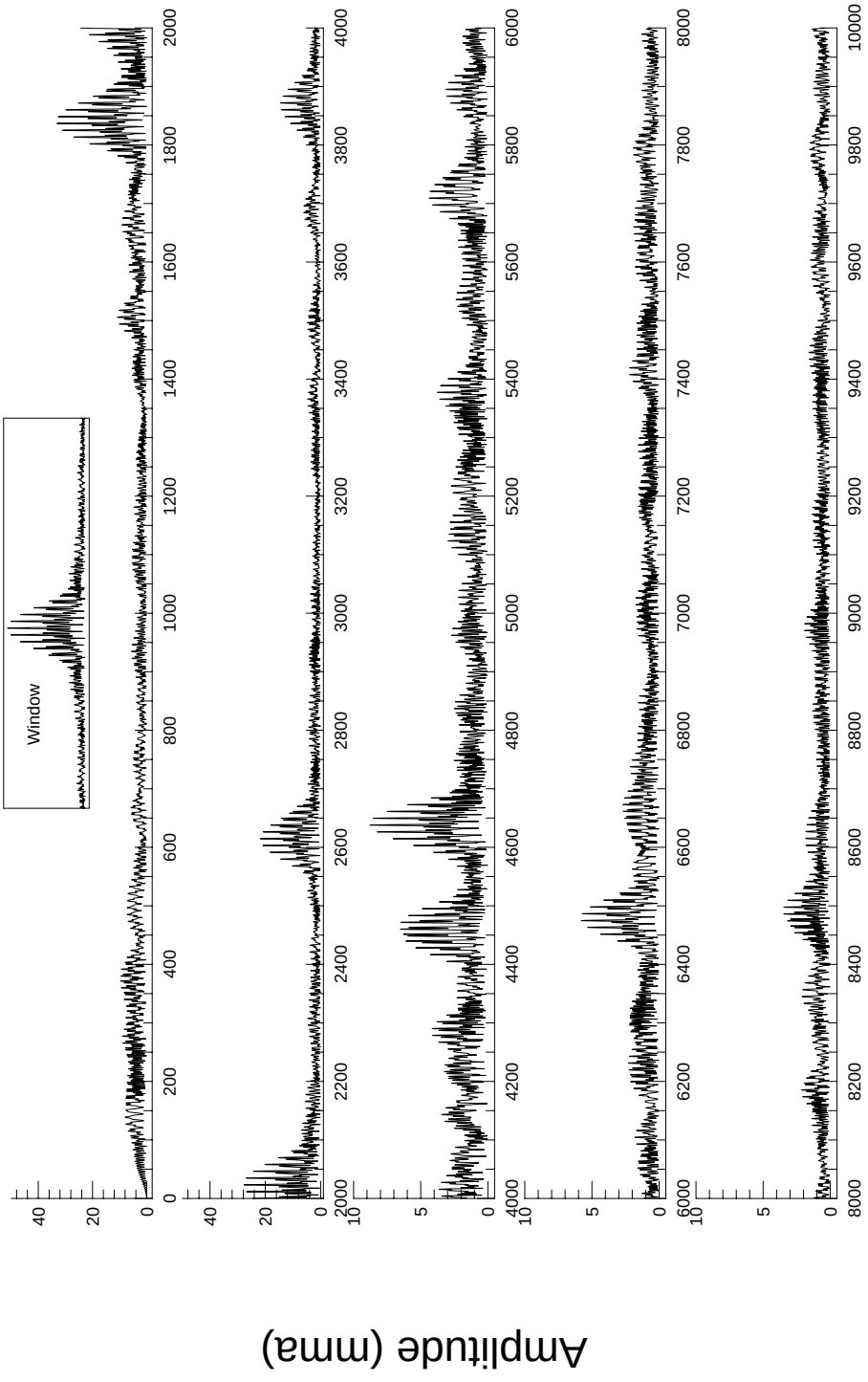

Fig. 6.7.— The FT for the February, 1991 data on HL Tau 76.

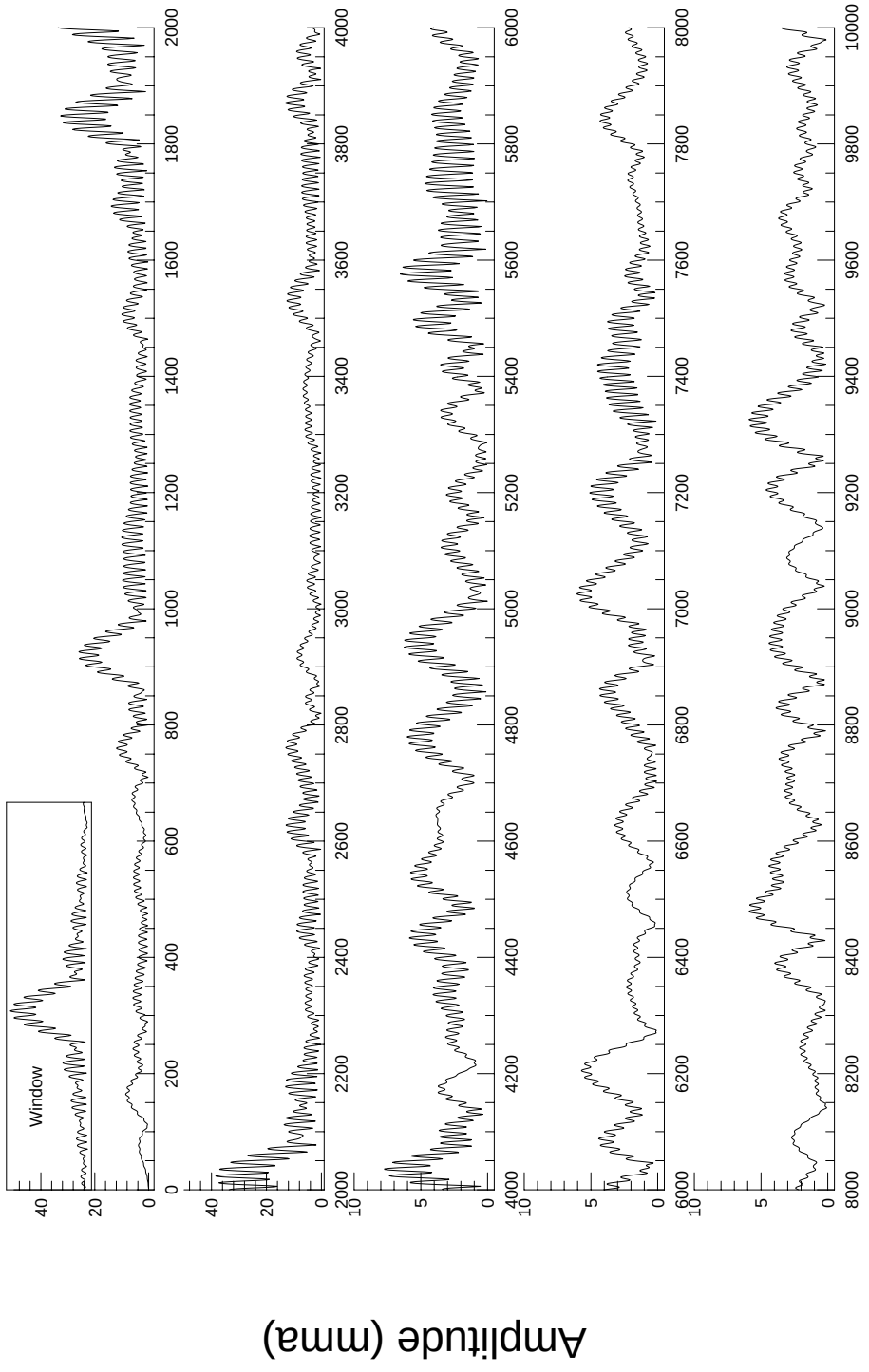

Fig. 6.8.— The FT for the November, 1993 data on HL Tau 76.

With sparse data sets, it is very difficult to identify modes in these complicated pulsators. In addition to signal to noise constraints and rotationally-split multiplet beating, the other major difficulty is the identification and removal of linear combinations. To best avoid these problems, I once again concentrate only on my best data sets: HL Tau 76: October, 1990 and G191–16: November, 1990 and November, 1991. For the first pass, at least, I don't feel any of the data on G38–29 are good enough to allow reliable peak identification.

I start, as in G29–38, by identifying major power in the spectrum, then removing linear combinations as best as possible (see discussion in Chapters 3 and 4 for how this is done) and seeing what's left. I have been very conservative and only listed peaks I am sure are real and sure they are not combination modes. In some cases, I have a three mode combination (A+B=C) and know that one mode is real, but cannot determine which of the other modes is real and which is the combination mode (does A+B=C or does C-A=B?). In such cases, I left both the uncertain modes out. Even so, there were two modes which I was not completely sure about, but felt strongly enough not to discard them; they are plotted as dashed arrows in Figure 6.9 along with the other modes from this analysis. The bottom panel in the figure shows the union of all the modes above it.

Since G29–38 has many more identified modes than the other stars do, the important thing to see in this plot is if G29–38 modes exist where there are G191–16 and HL Tau 76 modes. Indeed, there are obvious groupings at 400, 500, 550, and 600 seconds with two smaller groups at 350 and 650 seconds. Taken at face value, these groups, with their characteristic 50s

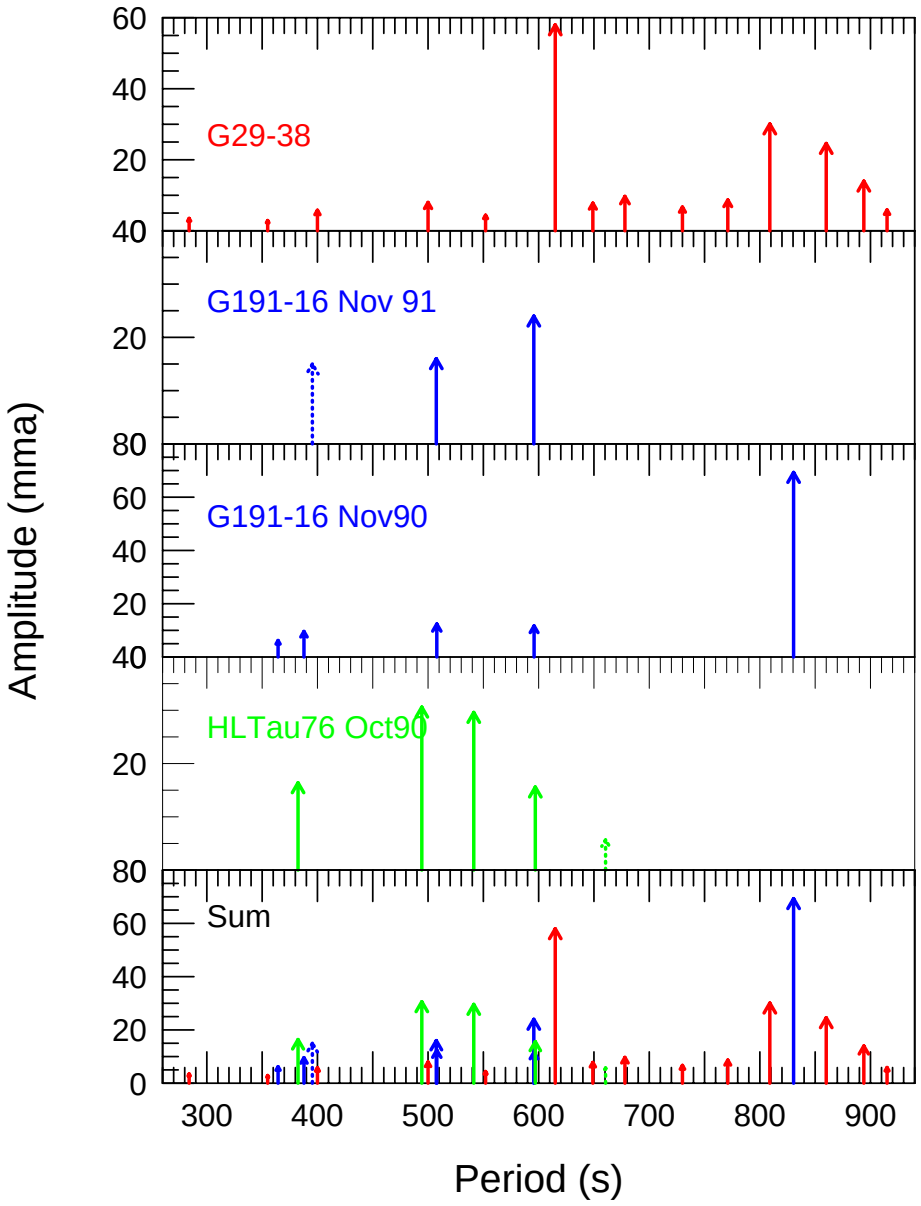

Fig. 6.9.— The non-combination modes of the cool DAVs.

spacing, strongly support the successive-k, ℓ=1 identification made in G29–38. These stars really are very similar. The group widths are between 10 — 20s. Even if all the stars had modes in exactly the same place, there would be some natural width to the groups due to the uncertainty of which m-value the modes are. For a characteristic frequency splitting of 10μHz (corresponding to a rotation period near 0.6d) the expected widths vary from 3s for the 400s group to 7s for the 600s group (remember, the spacing is constant in *frequency* not period). So the groups are only a few times the minimum possible width, given a typical m-splitting.

As Clemens (1993, 1994) showed, there will also be some width to these groups due to the various masses of the stars involved. Ignoring mode-trapping for the moment, increasing the overall stellar mass has two effects: 1) the first (k=1) ℓ=1 mode is at a lower period and 2) the spacing between adjacent ℓ=1 modes will be smaller. The mass of the H-layer, however, also plays a role in the inter-mode spacings (decreasing the H-layer mass increases the spacing). Clemens (private communication) has found the H-layers in the hotter DAs are anti-correlated with mass: the larger the stellar mass, the smaller the H layer, so his observed groups are actually tighter than they would be otherwise. (This correlation is exactly what one would expect for a nuclear-burning based H layer forming mechanism.) With these caveats in mind, I calculated the average of the 400, 500, 550, and 600s groups and the deviation of each star's modes from the group average. I then shifted each mode of each star by the average deviation. This is different from the method used by Clemens, but justified by the sparsity of modes given the uncertain m-values. The resultant shifted modes are shown in Figure 6.10

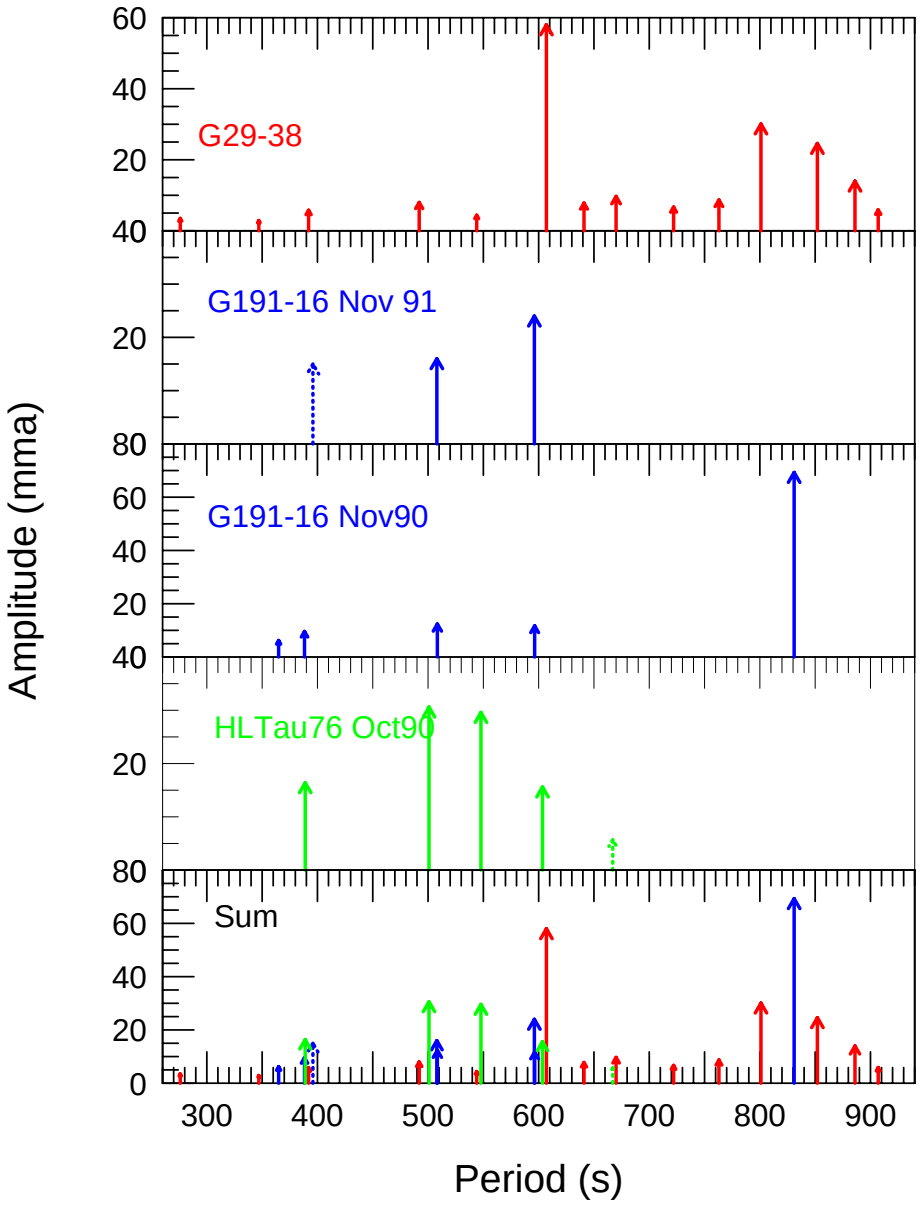

Fig. 6.10.— The shifted non-combination modes of the cool DAVs.

With the exception of the 500s group, the width of each group has narrowed with the shift, as expected. Now, taking the masses from Bergeron et al. (1995), we can now see if the shifts are consistent with the observed masses. The masses and temperatures from Bergeron et al. are in Table 6.1. In order of increasing masses, the stars are HL Tau 76, G191–16, and G29–38. If things works as they did with the hot DAVs (and as theory predicts), the ordering of applied shifts from smallest to largest should follow the same pattern. In order, the shifts applied were: G29–38: -8s, G191–16: 0.5s, HL Tau 76: 6.5s. The shifts are in precisely the *wrong* order. This result is certainly unexpected and suggests that either first order shift (versus a change in scale due to a changing mean period spacing) is not enough, or the group widths are dominated by m-splitting and not by any effects due to changing mass or composition. Hopefully, more precise model-fitting attempts, which will yield both the overall mass and H-layer mass, and better data which can resolve the multiplet splitting will shed some light on this mystery.

This is, however the *second* piece of evidence that says the asteroseismological and spectroscopic masses of G29–38 disagree. The first came from the period-spacing fits of Chapter 4. There, I proposed two possibilities; I'd like to mention a third one here. If we accept the asteroseismological mass estimates, then the spectroscopic mass is too high. Assuming the observed line profiles are correct, then perhaps something else is broadening them that mimics an increased gravity. Whatever it is, though, needs to be unique to G29–38 as there appears to be no systematic errors in the spectroscopic masses. So, what is unique about G29–38? It's infrared excess is the obvious answer. In their study of He in cool ($T_{eff} \approx 11500$K)

DA white stars, Bergeron et al. (1990) state the following: *It is not possible to separate the pressure effects originating from increased helium abundance from those stemming from an increased surface gravity.* If the observed infrared excess (see Chapter 1) is He-dominant and some of the matter is accreted onto G29–38, the result may be a small presence of surface He detected only by its increasing the H-line widths.

Why would there be He in the system, though? Perhaps G29–38 is related to the interacting binary white dwarf system, G61–29 (Nather, Robinson & Stover 1981), where a pure low mass ($\approx 0.02 M_{\odot}$) He white dwarf is losing mass to its more massive companion. For the first time, we have used the IR excess to explain other aspects of G29–38's behavior. If there is still some of this He remnant, careful IR photometry and phase analysis may reveal its orbit. This is a testable hypothesis.

3. Model Fits

The average of the four observed groups are 390s, 500s, 547s, and 603s. For an average period spacing (between successive ℓ=1 modes) of 50s, these periods are consistent with a series of consecutive-k (save 1)[1] ℓ=1 modes. If so, it would be nice to see what the pulsation models, which have proven so successful for PG 1159–035 and GD 358, say about the structure of a star with these modes.

After Clemens's work on the hot DAVs, Bradley (1995) published a set

[1]The missing mode, presumably near 450s, is the same mode missing in the G29–38 data. What is this telling us about the stars' common structure?

of DAV models with thick (near $10^{-4}M_\star$) H-layers. Previously, Bradley (1993) had already published models with thinner H-layers, from 10^{-5} — $10^{-13}M_\star$. I will first take the average star (a fictional star with modes at the group averages) of average mass ($0.6M_\odot$) at a temperature near 11750K (where Bradley's grids are calculated and quite close to the observed temperatures of Bergeron as well) and see what constraints can be placed on the H-layer mass.

For this fictional mass of $0.6M_\odot$, there are two models that fit reasonably well: one with a $10^{-4}M_\star$ H-layer and one with a $10^{-9}M_\star$ H-layer. The model fits are summarized in Table 6.2.

Clearly, neither model is an exact fit, but given the coarseness of the search grid, both are good indications that a more exact fit could be found with suitable parameter adjustment. Unfortunately however, based on this model star alone, we cannot distinguish well between the thick and thin H-layer cases. Using the individual stars, with their own periods and Bergeron et al. masses, however, may help limit our choices.

Starting with G29–38, I can find no thin layer models from Bradley (1993) that can match the observed group modes. Amongst the thick H-layer choices, a model with a $1.0 \times 10^{-4}M_\star$ layer is the best fit with a $1.5 \times 10^{-4}M_\star$ layer a close second. The model match is in Table 6.3. The fit is quite good[2] and could certainly be improved by using more modes and a finer grid in parameter space.

Matching models to HL Tau 76 and G191–16 present a little more of

[2]Although the $k$values of the model fit are different than those assigned in Chapter 4. This is further evidence for the spectroscopic mass (with it's smaller period spacing) being incorrect.

Table 6.1. Masses and temperatures of the cool DAVS from Bergeron et al. (1995).

Star	Temperature (K)	Mass ($M_\odot$)
G29–38	11820	0.69
G191–16	11420	0.64
HLTau 76	11440	0.55
G39–29	11180	0.55

Table 6.2. Bradley (1993,1995) ℓ=1 model fits to fictional 0.6$M_\odot$ cool DAV.

Observed Period (s)	$M_H = 10^{-4} M_\star$ Periond (k) (s)	$M_H = 10^{-9} M_\star$ Period (k) (s)
390	406 (6)	419 (4)
500	493 (8)	502 (6)
547	538 (9)	540 (7)
603	599 (10)	610 (8)

Table 6.3. Bradley (1995) ℓ=1 model fit to G29–38 group modes. The observed $k$values are those assigned in Chapter 4.

Observed Period (k) (s)	Model Period (k) (s)
355 (5)	353 (6)
400 (6)	403 (7)
500 (8)	511 (10)
552 (9)	557 (11)
609—615 (10)	602 (12)

a challenge, only because the Bradley (1995) grids are not very complete for modes with their masses (0.55 and 0.65$M_{\odot}$) and the thin layer Bradley (1993) models do not cover these masses at all. Nonetheless, one can get reasonable fits in the thick layer range of 10^{-4} for HL Tau 76, the least massive of the two, and 10^{-5} for G191–16. If two can be called a trend, this trend of thinner H-layers with increasing mass agrees with what we expect. G29–38, however, with its higher mass should have the smallest H-layer, but it has one of the largest, instead. Perhaps this is tied in with G29–38's other peculiarities, or perhaps it is just highlighting the tentative nature of these model assignments. Or, given the incompleteness of the lower-mass models, we may be seeing a correlation of the H-layer with overall mass opposite that seen by Clemens. If so, the dominant H-layer determining mechanism may still be nuclear burning, but winds, which would decrease the H-layer for less massive white dwarfs, may also play a significant role.

The important thing to come out of this search through model space is that these results, based only on the observed groupings of three cool DAVs are consistent with the results of Clemens on the hotter DAVs. All the DAVs, now, are consistent with thick H-layer masses. Once further observations and models arrive, we'll be able to explore these points in more detail, but for now, a direction is indicated, and there is no reason to concentrate solely on thin H-layer models any more. We have provided an independent sample of DAVs from the Clemens sample and get similar results.

Chapter 7

The Rug

Once in a while you get shown the light
In the strangest of places if you look at it right.
—Robert Hunter & Jerry Garcia, *Scarlet Begonias*

Here is where everything that would normally be swept under the rug is proudly displayed and presented. We may not know the full explanation or story behind some of the observations presented here, but we do not for a moment doubt their significance and ability to help us in the future. Nature is shouting at us; we just do not always understand the language.

There are often surprises underneath the rug. Sometimes it's that long lost favorite comb; it may also be the missing diamond from Aunt Lulu's old necklace. Other times there's nothing there but bits and pieces of lint, thread, and general muck. Through careful sorting, however, even this motley collection of items can sometimes be woven into a breathtaking tapestry.

1. Non-linearities

One of the striking things about Chapter 4 is how much information we had to discard to get to the information we can use and understand. Fortunately, for the work done in that chapter at least, the periodicities we leave strewn across the highway to asteroseismology all have something in common: they are linear combinations, sums and differences, of other periodicities in the star.

The theory behind such combination modes is both complicated and poorly constrained. Non-linearities abound in the full pulsation problem. Which effects are important? Which ones need to be included to accurately reproduce the modes we see? Brassard et al. (1993) include only the T^4 dependence of luminosity on temperature and a purely sinusoidal temperature variation in their treatment of non-linearities. Brickhill (1992), however, uses sinusoidal pressure variations which result in non-sinusoidal temperature variations. In Winget et al. (1994), they use the results of a WET run on the DBV, GD 358, to show that neither of these effects, by themselves, can account for the observed non-linearities and suggest some combination of these, with perhaps others, will be needed to fully explain the observations. Clearly, it is a difficult problem.

Were we to clean up our littered highway, gather these combination modes and identify them and their components by their amplitude, frequency, k, ℓ, and m, we would have an observed constraint on the process; we could produce observational selection rules. The 2500μHz power, for example, nearly always combines. The other stable power at 3500μHz rarely combines. In addition, since some modes come and go in the power spectrum, sometimes with different amplitudes, we have a unique chance to study just when (at

what amplitudes) modes combine with what other modes. With our extensive data sets, we have accurate phase measurements and thus can add phases to our combination peak identifiers. All these parameters will provide important constraints on non-linear theory.

2. Variability

The very feature of G29–38 which allowed us to proceed as we did, its time-variable power spectrum, is completely unexplained theoretically. From year to year, there are dramatic changes in the power spectra; from month to month there are less subtle, but still significant changes. There are also signs of changes on daily and weekly scales. On every timescale we examine in this star, we see variability. Why?

The data on the other cool DAVs (Chapter 6) show that at least most of these changes are universal to this particular subclass of pulsating white dwarfs. They are *not* unique to G29–38. This is an important piece of information, but it also serves to highlight how global our ignorance of this particular facet of white dwarf asteroseismology is. Strike a bell now and strike it again in 10 years, it will sound the same. Watch G29–38 over two consecutive seasons and see what looks like two different stars.

3. $\dot{\mathrm{P}}$

As discussed in Kleinman et al. (1994), the 284s (3523μHz) mode in G29–38 is extremely stable and remains in the power spectrum year after year after year. Because of this stability, we were able to use it in the above paper, to

place limits on the existence of orbital companions to G29–38, ruling out all but the most inclined, or least massive, short period companions.

The remaining trend in the 284s $O-C$ could be indicative of a long period orbital companion as discussed in the paper, or could be a measurement of the rate of period change of this mode. If we take the observed trend in the $O-C$ at face value, then $\dot{\mathrm{P}} \approx -10^{-12}$s/s. This value is some three orders of magnitude larger, and the wrong sign, from the expected rate due to secular cooling. Even mode trapping, which changes $\dot{\mathrm{P}}$s from their expected values, cannot explain a $\dot{\mathrm{P}}$ of this magnitude, let alone sign. It appears as if we are measuring a different phenomenon, at a different timescale, and have not gotten to the highly prized evolutionary $\dot{\mathrm{P}}$ measurement. Exactly what we are measuring is unclear, but it is something at a new timescale.

4. The 615s Mode

The phase variation of the dominant (615s) peak of the Xcov2 (Winget et al. 1990) run on G29–38 has still not been explained. In their paper, Winget et al. show the 615s peak changed its phase dramatically while maintaining a near-constant amplitude. The significant curvature to the phase, or $O-C$, diagram of this mode is easily fit by a binary orbit model producing reflex orbital motion of the white dwarf. This model was eliminated, however, by the discovery of another mode in the star whose phase was constant over the same period. Reflex orbital motion must affect the phases of all modes simultaneously. There were some small errors in the $O-C$ values in that paper which are corrected in Kleinman (1990) although the overall shape remains unchanged and the cause, a mystery. Since the mode went away the

following season, we suspect the observed phase variation may be related to the amplitude changes taking place in the star. Someday, this too will be an important observational constraint.

By the middle of the 1989 observing season, the 615s mode vanished completely. It gave away no sign of its continued existence until the Xcov8 campaign, in 1992. When it reappeared, however, it was not at the same frequency as before, preferring instead to be near 610s. Its multiplet structure (see chapter 5) also changed.

5. The Future Underneath the Rug

A favorite new set of plots of mine starts with one similar to Figure 4.3, except with the height of each peak reflecting its true amplitude. From there, I show Figure 4.3 itself, having now thrown out the amplitude information. Then, I move to Figure 4.4, throwing out most of the monthly FTs and all the combination modes in the process. It is this small subset of the initial set of information that we can analyze and explain. The fortunate thing is, of course, so much science can come from this small subset. Having gone ahead and lifted the rug, I think it only appropriate to point out how much we must stuff underneath it to get to what we understand and how much more we could do were we able to use all the available information.

Why do these stars' spectra change so dramatically? Why are the low-period modes generally more stable? Why does the multiplet structure of G29–38 appear so irregular and is it that way in all the cool DAVs? With additional data, we can begin to answer some of these questions. They will be crucial in our understanding of the detailed physics of these objects.

Watching modes dominate the power spectrum, disappear, and then grow back in, we are certain to learn about the growth rate of these modes, as well as something about how and why they are changing so much. Is the G29–38 615s phase variation related to its disappearance sometime later? Our hunch is yes, but it is difficult to prove. Someday, we will see a star change while we watch. The reappearance of the 615s mode happened partially while we were watching. We have not yet analyzed the phase of the mode as it grew in, nor of other modes as they come and go, but we have noted a substantial frequency change (Chapter 5). Clearly, these additional measurements must also be made.

Does mode-coupling occur? Are there selection rules? At what amplitudes do modes begin to couple? Non-linear theory is unlikely to provide us these answers without observational constraints. Observations such as those presented here will be those constraints. When we understand the cause of the combination modes (often more abundant than the "linear" normal modes) we will have a whole new way of looking at the processes and energetics of non-radial pulsations. We may eventually be able to use all the information on that first plot I like to pull out. For now, however, it's a rather lumpy rug.

6. The Tapestry

Bits and pieces of evidence have now been presented on the nature of G29–38's (and the other complex cool DA pulsators') modes of oscillation. At stake is the entire notion of making asteroseismological measurements with the DAVs. Is there stability amidst the very large changes in the stars' pulsation spectra?

Are they normal-mode pulsators? Are they the same as the hotter DAVs except for their temperatures? What can they tell us about stellar evolution?

Before addressing these questions, let me first comment on the observations needed for this work: a WET run is not enough for individual cool DAV asteroseismology. Their very nature, their long term variability, means an extended baseline of observations is essential for their study. We only see a few non-combination modes at once. On the timescale of months, we are likely to see quite similar (in gross terms) power spectra. The major power spectra changes happen on yearly timescales. We therefore need several years of data. Nevertheless, we need the advantages of the WET to identify multiplet structure, a key element in solidly identifying each observed mode. Since we can't run the WET all the time for the same object,[1] we need extremely good, high resolution, single-site data so aliases can be separated from any nearby multiplet peaks. High temporal resolution is also essential to identify and separate out the linear combinations.

The bright side of these requirements, however, is that at least for the brighter targets, small telescopes (of order 1m) are quite suitable for these observations. For the dimmer stars, we could still use the smaller telescopes if we had a more efficient detector, such as a CCD on it (the WET is currently looking into the next generation high-speed photometer which will be based on high blue quantum efficiency CCDs). Large telescopes will help lower the limit at which we can find modes, but without the long baseline for the high temporal resolution, this increased signal to noise ratio doesn't do much good.

---

[1] Or can we...?

By the time we have enough temporal resolution, we probably have a high enough signal to noise ratio.

6.1. G29–38

Many of the results of this work strongly depend on the mode identification made at the end of Chapter 4. In that chapter, we postulated (and supported with observations) the non-combination modes are a succession (in k) of ℓ=1 normal g-modes. In subsequent chapters, we presented additional evidence of this assignment. In each case, however, the evidence presented was not 100% conclusive.[2] The ideal method of mode-identification was only once realized, in the PG 1159–035 WET observations. There we found a series each of triplets and quintuplets. We found the triplet spacings and ratios agreed with theory for ℓ=1 and ℓ=2. We also measured period spacings, and found they too agreed precisely with theory. We derived a mass and parallax consistent with, but more accurate than, existing measurements. We measured a rate of period change, consistent with the evolutionary timescale.[3] Theorists say it is because of mode trapping, but until we measure the $\dot{\text{P}}$of a non-trapped mode, we will not know for sure. Every asteroseismological test we threw at the observations solidly confirmed our mode identification. It was a glorious success, but has yet to be repeated with such success for any other variable white dwarf.

In our G29–38 analysis, we weren't so lucky. We did not have many

[2]But then in astronomy, few things are.

[3]But of the wrong sign.

instances of multiplets and can find no convincing evidence for an ℓ=2 set of modes. Everything points to the ℓ=1 identifications, but we do not have the redundancy of proofs that PG 1159–035 so graciously provided us. The primary items of evidence we do have include:

- There is a fairly regular 50s observed period spacing. The value is too high to be ℓ=2 and maintain a reasonable mass for G29–38.
- We see only triplets.
- The cool DAVs as a class share many common modes.
- Modes disappear and reappear at precise locations.

Were the evidence as simple as stated above, I probably would not be recapping them here. To nearly each of the above items can be added a caveat or two. Are they sufficient, however, to call into doubt our identifications? I have listed four pieces of evidence, none of which, by themselves leave us completely convinced of our analysis. Taken together, however, they make an extremely strong case. If we are going to label these modes as something other than normal ℓ=1 g-modes, we have to explain these four observations as coincidences. One accidental agreement is relatively easy to dismiss; four are much more difficult. In addition to supporting our model, many of the above items point the way for new understanding of the DA white dwarfs. Our current model stars are too simplistic to accurately reflect our observations. Some of these new areas for understanding include:

- The ΔP *vs.* P diagram is not well-matched by existing models. The P_o of G29–38 corresponds to a mass significantly lower than current

spectroscopic estimates, but quite close to the observed average white dwarf mass.

- The observed triplets show strange behavior and variable splittings.
- The possible $\dot{P}$for the 284s mode is too large, and the wrong sign, to be evidence of secular cooling.

In the appropriate chapters, I discuss possible explanations using existing theory, where available, for these observations. It is equally likely that there is some parameter, some missing physics in our model, that when discovered, will explain these observations and increase our understanding of these stars. Asteroseismology has had a blessed existence; its theory and observations have generally been in remarkable agreement.[4] It is surprising, therefore, only in this light, that our observations present some new mysteries. Were it not for our being accustomed to these past successes, we would hardly bat an eyelash if new observations failed to confirm every facet of a previously untested theory. With the DA white dwarf variables, this is exactly what we are doing. This is the first time we have such detailed asteroseismological information on an individual DA pulsator.

6.2. The Cool DAVs

The asteroseismological information presented on the other cool DAVs also has profound implications. We have long since noticed the difference between

[4]The DBVs, for example, are the only class of variable stars whose variability was predicted before their discovery (Winget et al. 1982).

the hotter and the cooler DAVs (McGraw 1977, Clemens 1993, 1994). The hotter group has shorter periods, lower amplitudes, and greater stability. The cooler group has longer period, higher-amplitude modes and variable power spectra dominated by linear combination modes. The tacit assumption is that these two groups represent the same underlying physics and that only the temperature of an individual star determines what group it belongs to. But this has never really been proved. Does a hot, low amplitude, stable DAV eventually become a cool, large-amplitude, unstable DAV? These results say yes, the two groups are separated only by temperatures. When combined with the masses, H-layer, and mode structure of Clemens (1994) for the hot DAVs, the values derived here for the cooler DAVs show the entire DAV class is uniform. There is nothing preventing a stable, hot DAV like G117 B15A from becoming a star like G29–38. This may seem an obvious statement,[5] but were it not for these results, this issue would remain a tacit assumption, and were it found not so, would have serious repercussions in the field. It is something we have been taking on faith. We now have proof.

The rough asteroseismological analysis of the different cool DAVs performed in Chapter 6 had a few surprise of its own. Since the data coverage on these stars was not as complete as it was on G29–38, the actual model-fitting results are less certain, but may be implying the H-layer mass is directly correlated with the overall stellar mass. That is, the more massive

[5]This is far from obvious when we consider that the cooling time across the instability strip is $\approx 0.5 \times 10^9 yr$ (Wood 1990). Any change in the star formation history of our galaxy over this time period may eventually reveal itself to us through differences in the physical parameters derived for the cooler vs. the hotter DAVs. We do not see any signs of such differences now, but our models and data are rather sparse. Future explorations may pay off handsomely here.

white dwarfs have the most massive H-layers. In the broadest sense, all the DAVs observed are consistent with thick H-layers, near 10^{-5}—$10^{-4}M_{\star}$. This values agrees with that of Clemens for the hot DAVs and supports his conclusion that nuclear burning plays the dominant role in setting the H-layer size. The G29–38 observations (which may imply a heavier H-layer), however, suggest that winds, which are expected to be stronger on less massive, "fluffier" white dwarfs, also play a role. When we begin to have models that better match G29–38 and better data on the other cool DAVs, we will be better able to explore this hypothesis. The results here, however, are certainly suggestive and quite intriguing.

7. The Big Picture

The modern era of white dwarf asteroseismology, in its full glory, began with the WET observations of of the DOV, PG 1159–035. Some time later, the first DBV, GD 358, was analyzed in a similar manner. The detailed picture emerging from these two sets of observations was astounding. It may appear as if we started with the hottest class of white dwarf pulsators and worked our way down the cooling track, just now getting to the coolest of the white dwarf pulsators, the DAVs. In actuality, however, we observed a DAV, G29–38 as it turns out, with the WET before any of the ground-breaking measurements of PG 1159–035 and GD 358 were ever taken. The fact of the matter is we did not understand the DAVs. We did not know how to attack their analysis.

We now know what we need to get valuable asteroseismological measurements for the DAVs. Implicit in that statement is that we now know the DAVs are normal-mode pulsators; they are not simply weird ducks.

When combined with the recent, and currently unpublished, work on the PNNV pulsators, which suggests their previously mysterious pulsation spectra can be understood in terms of mode trapping, the entire range of white dwarf pulsators are now open for analysis. We can make mass, structure, composition, and rates of cooling measurements all over the white dwarf cooling track. These dead corpses, the white dwarfs, are revealing themselves, and their past history, to us through their pulsations. We now have the observational tools to listen to them. All of them.

Appendices

Appendix A

G29–38 Lightcurves, FTs, and Mode Lists

In this Appendix, I present, for both archival and verification purposes, the lightcurves, FTs and mode lists for each of the primary G29–38 data sets studied in Chapters 4 and 5. As a reminder, the data sets are named by the month and year in which the data were taken. This said, X2N88 is the WET XCOV 2 observations in November, 1988 and X8S92 is from XCOV 8, September, 1992.

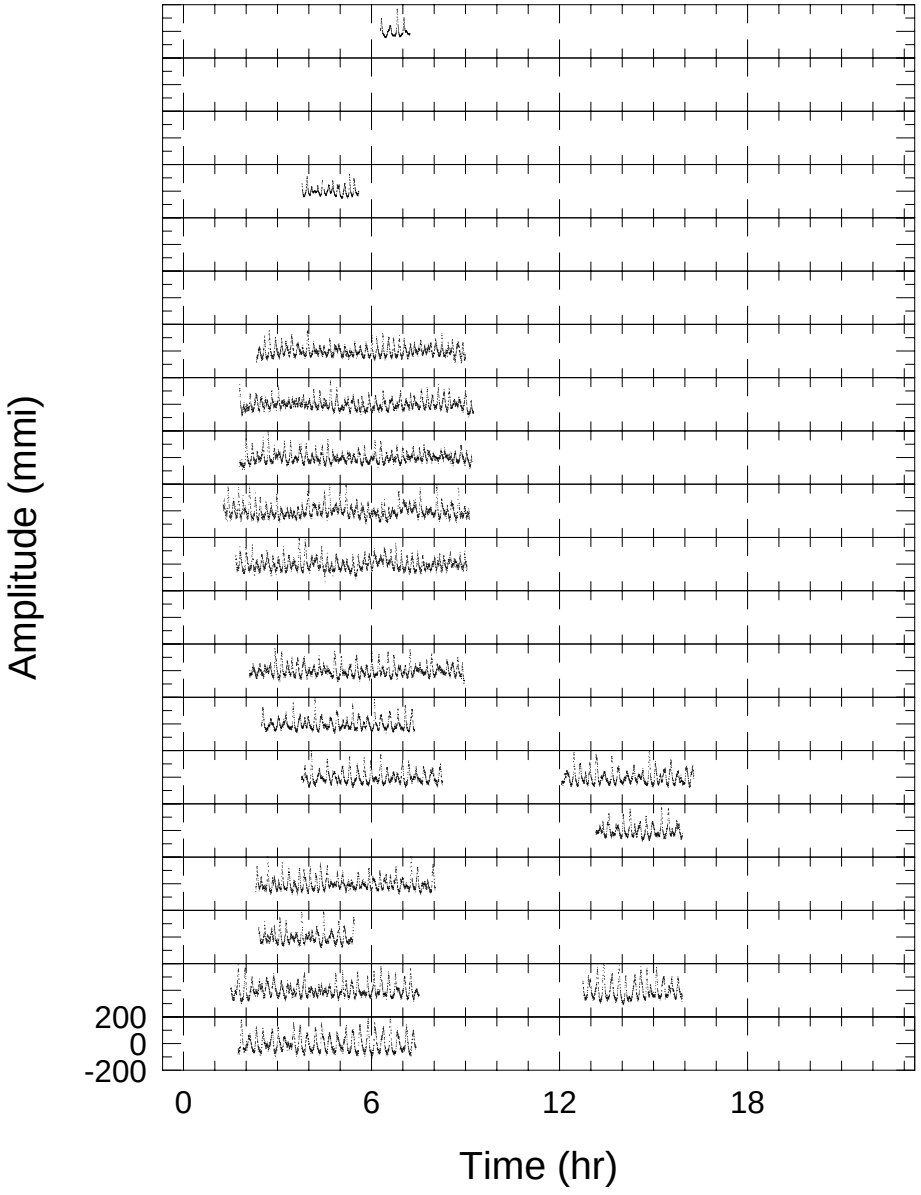

Fig. A.1.— The lightcurve for the Aug85 data on G29–38.

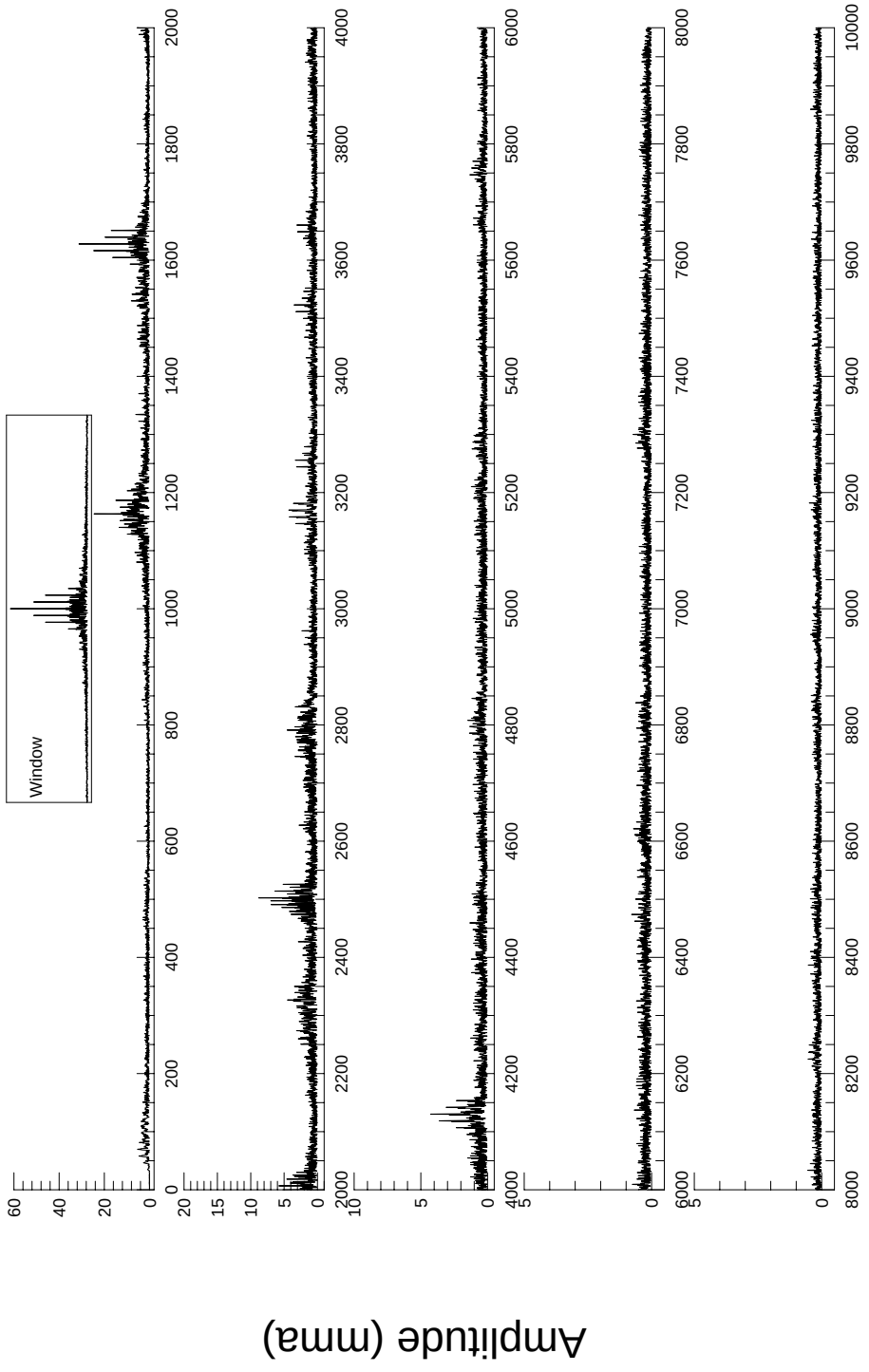

Fig. A.2.— The FT for the Aug85 data on G29–38.

Table A.1. Periodicities contained in the Aug85 G29–38 data set.

Frequency (μHz)	Period (s)	Amplitude (mma)	Comments
843.42	1185.649	3.4	DP
1163.28	859.638	24.6	R
1334.34	749.434	6.1	D
1464.36	682.892	5.5	?P
1541.46	648.736	7.8	RP
1627.86	614.303	31.3	R
2006.76	498.316	5.8	R
2326.68	429.797	4.5	S
2492.16	401.258	4.4	RM
2497.44	400.410	7.0	RM
2502.52	399.613	8.8	RM
2627.46	380.596	2.8	?P
2791.20	358.269	4.6	S
2962.02	337.607	2.3	SP
3169.80	315.477	4.3	S
3255.78	307.146	3.3	S
3522.90	283.857	3.5	R
3660.36	273.197	3.1	S
4130.16	242.121	4.3	S
5758.50	173.656	1.2	S

Note. — The Comments are encoded as follows: R=Real peak, S=linear combination Sum peak, D=linear combination Difference peak, M=Multiplet member, P=Probable — mode is not cleanly identified, A=Alias — this peak is an alias of another peak and we are not sure which is real, and ?=Unknown.

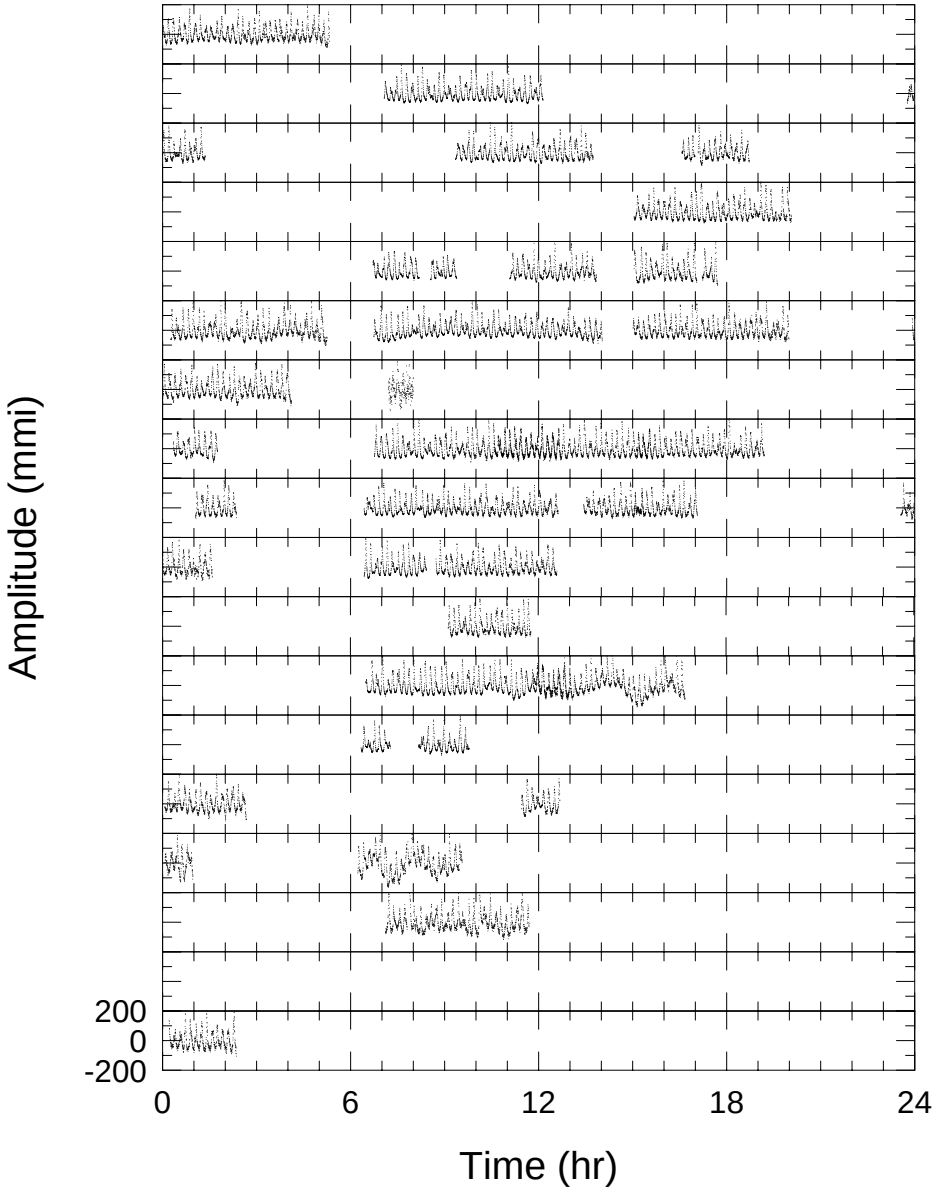

Fig. A.3.— The lightcurve for the X2N88 data on G29–38.

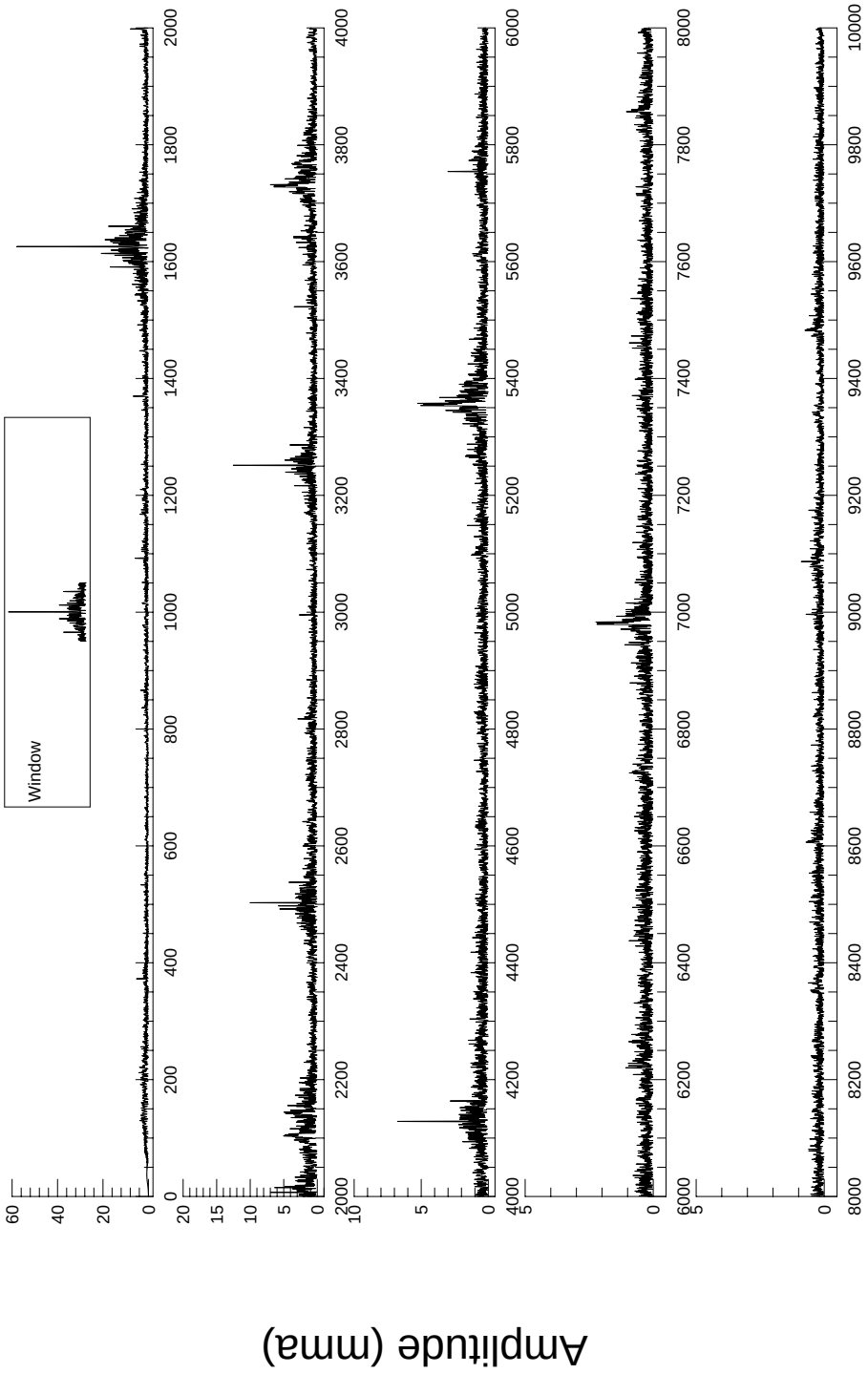

Fig. A.4.— The FT for the X2N88 data on G29–38.

Table A.2. Periodicities contained in the X2N88 G29–38 data set.

Frequency (μHz)	Period (s)	Amplitude (mma)	Comments
372.570	2684.059	5.3	DP
533.346	1874.955	3.3	DP
866.250	1154.401	3.5	DP
1092.366	915.444	5.9	R
1369.632	730.123	6.7	D?
1625.712	615.115	58.0	R
1998.282	500.430	8.0	R
2105.664	474.910	4.8	RP
2492.094	401.269	5.6	RM
2497.440	400.410	5.8	RM
2502.786	399.555	10.0	RM
2817.408	354.936	2.9	RP
2995.278	333.859	2.7	R?
3251.358	307.564	12.6	S
3522.816	283.864	3.5	R
3731.640	267.979	7.0	S
4128.498	242.219	6.8	S
5148.396	194.235	1.6	SP
5357.352	186.659	5.3	SP
5754.210	173.786	3.0	S
6983.064	143.204	2.2	SP

Table A.2—Continued

Frequency (μHz)	Period (s)	Amplitude (mma)	Comments
9086.616	110.052	0.9	RP

Note. — The Comments are encoded as follows: R=Real peak, S=linear combination Sum peak, D=linear combination Difference peak, M=Multiplet member, P=Probable — mode is not cleanly identified, A=Alias — this peak is an alias of another peak and we are not sure which is real, and ?=Unknown.

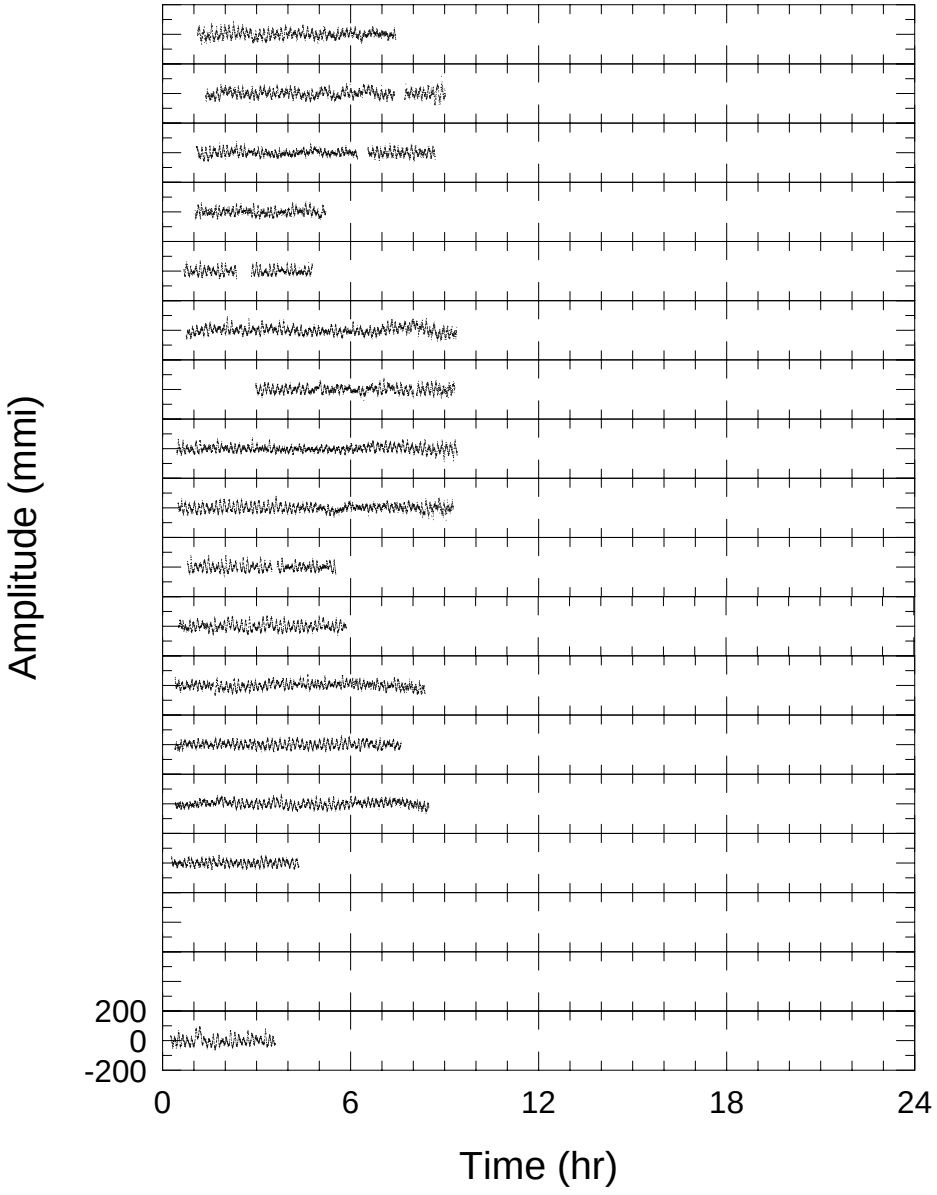

Fig. A.5.— The lightcurve for the Sep89 data on G29–38.

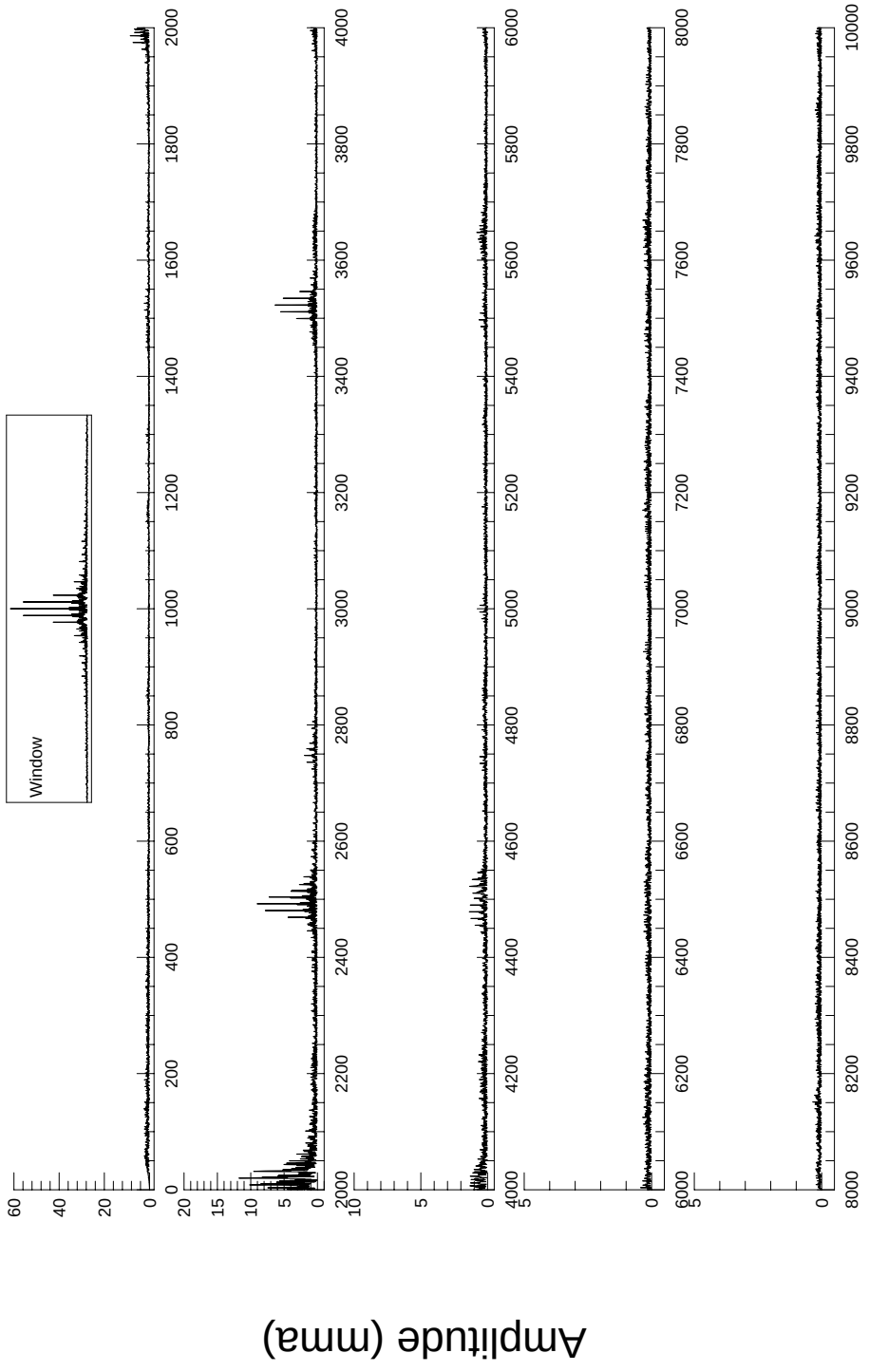

Fig. A.6.— The FT for the Sep89 data on G29–38.

Table A.3. Periodicities contained in the Sep89 G29–38 data set.

Frequency (μHz)	Period (s)	Amplitude (mma)	Comments
1297.589	770.660	1.5	R
1525.724	655.427	2.4	R?
1986.215	503.470	8.6	R
2020.050	495.037	11.8	R
2492.268	401.241	9.7	RM
2497.118	400.462	1.3	RM
2502.083	399.667	4.9	RM
2747.536	363.962	2.0	?
3522.726	283.871	6.4	R
3972.564	251.727	0.8	S
4006.801	249.576	1.3	S?P
4478.481	223.290	1.4	S
4522.232	221.130	1.3	S
4733.818	211.246	0.6	?
4984.72	200.613	0.3	S
4989.32	200.428	0.3	S
4994.46	200.222	0.6	S
5497.283	181.908	0.6	S
5647.698	177.063	0.8	RP

Note. — The Comments are encoded as follows: R=Real peak, S=linear combination Sum peak, D=linear combination Difference peak, M=Multiplet member, P=Probable — mode is not cleanly identified, A=Alias — this peak is an alias of another peak and we are not sure which is real, and ?=Unknown.

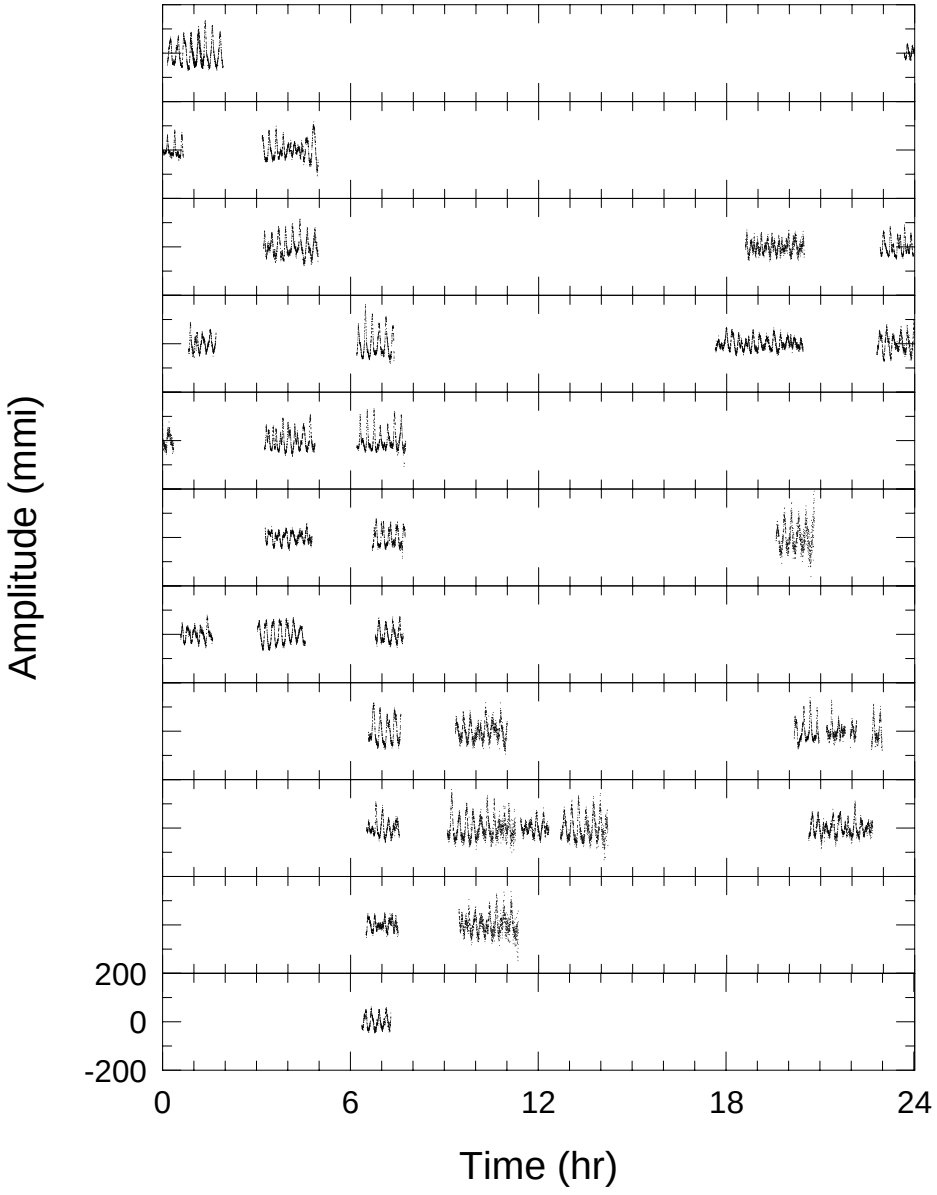

Fig. A.7.— The lightcurve for the X8S92 data on G29–38.

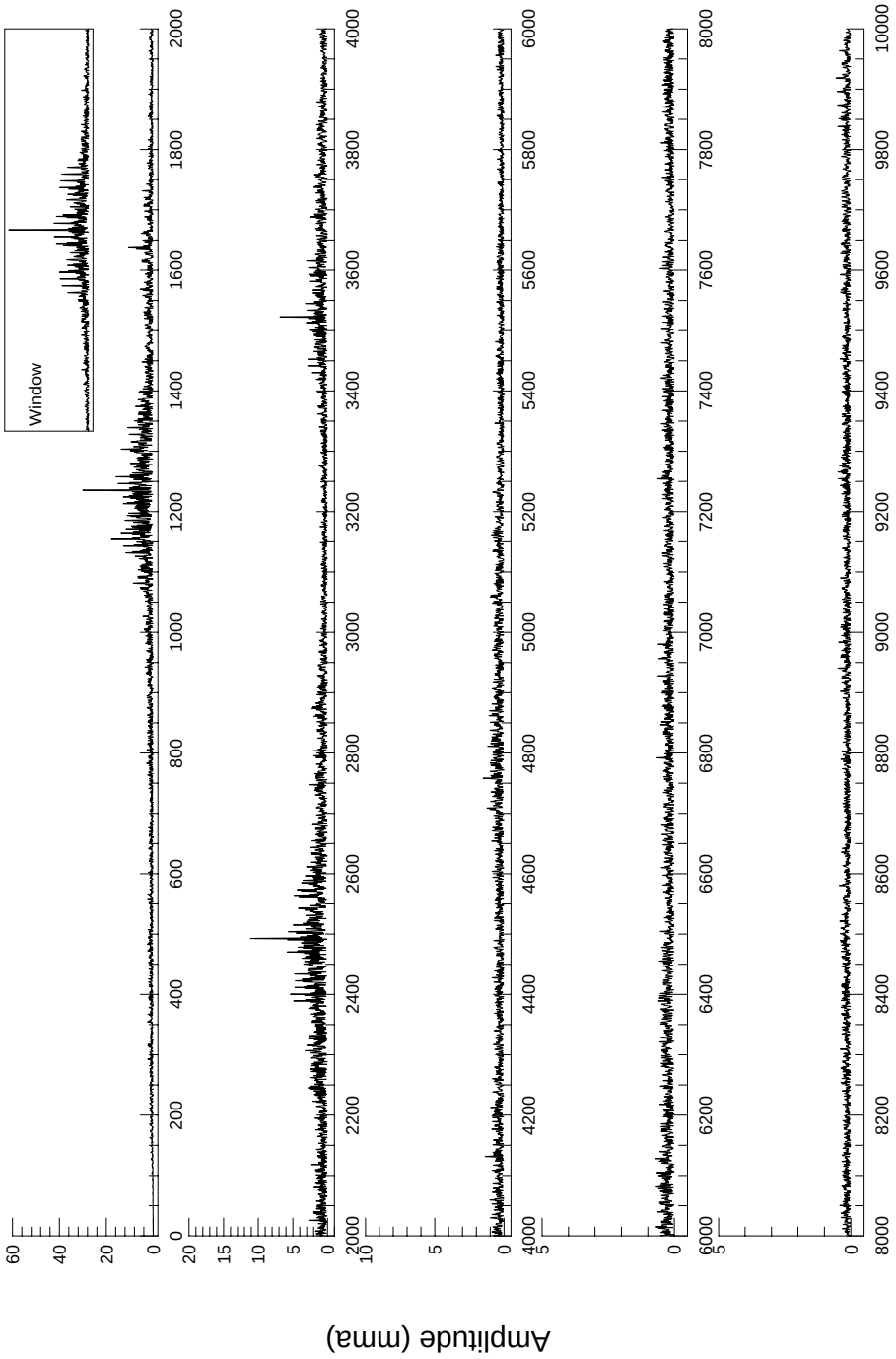

Fig. A.8.— The FT for the X8S92 data on G29–38.

Table A.4. Periodicities contained in the X8S92 G29–38 data set.

Frequency (μHz)	Period (s)	Amplitude (mma)	Comments
1235.41	809.448	30.1	R
1638.67	610.251	10.6	R
2025.65	493.669	2.7	P
2492.82	401.152	11.2	RM
2501.62	399.741	4.5	RM
3522.75	283.869	6.9	R

Note. — The Comments are encoded as follows: R=Real peak, S=linear combination Sum peak, D=linear combination Difference peak, M=Multiplet member, P=Probable — mode is not cleanly identified, A=Alias — this peak is an alias of another peak and we are not sure which is real, and ?=Unknown.

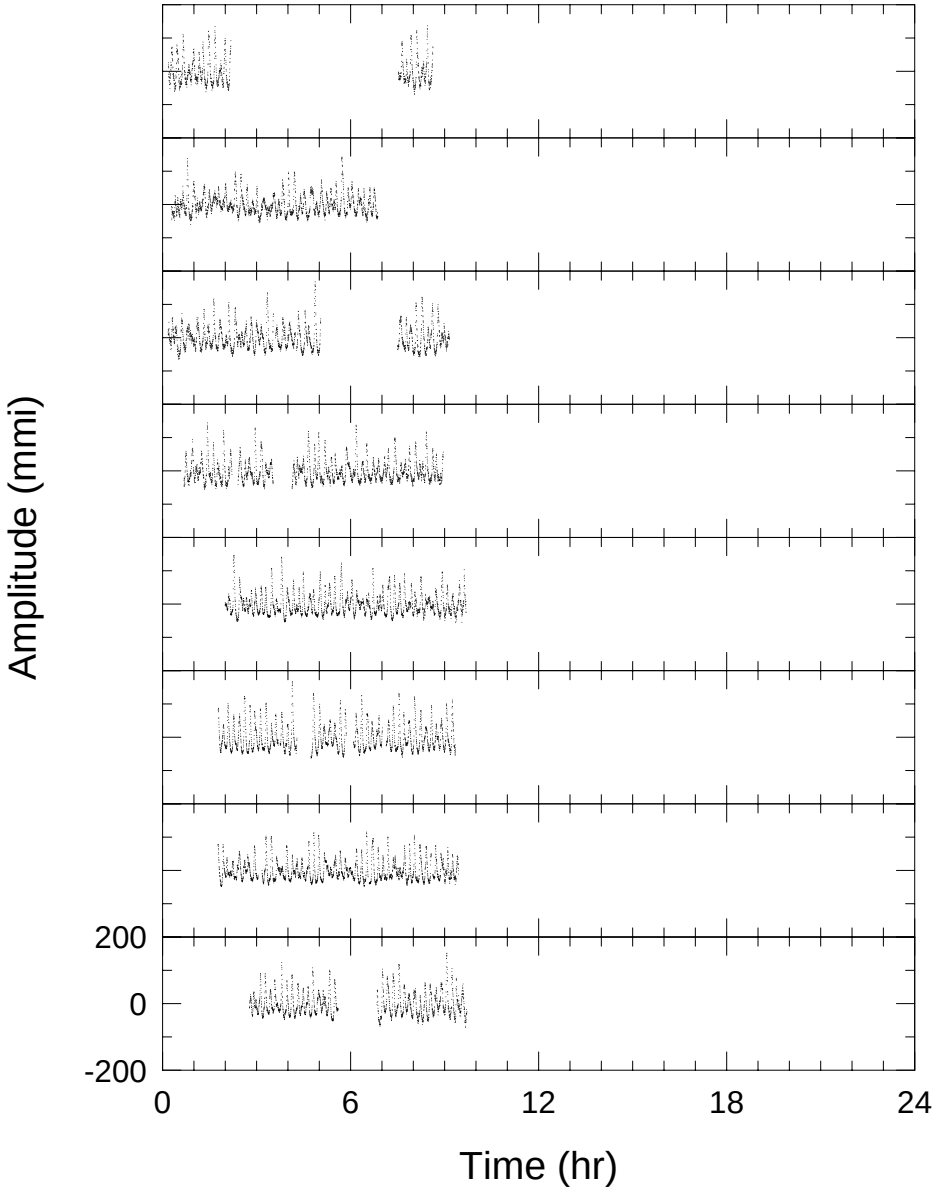

Fig. A.9.— The lightcurve for the Sep93 data on G29–38.

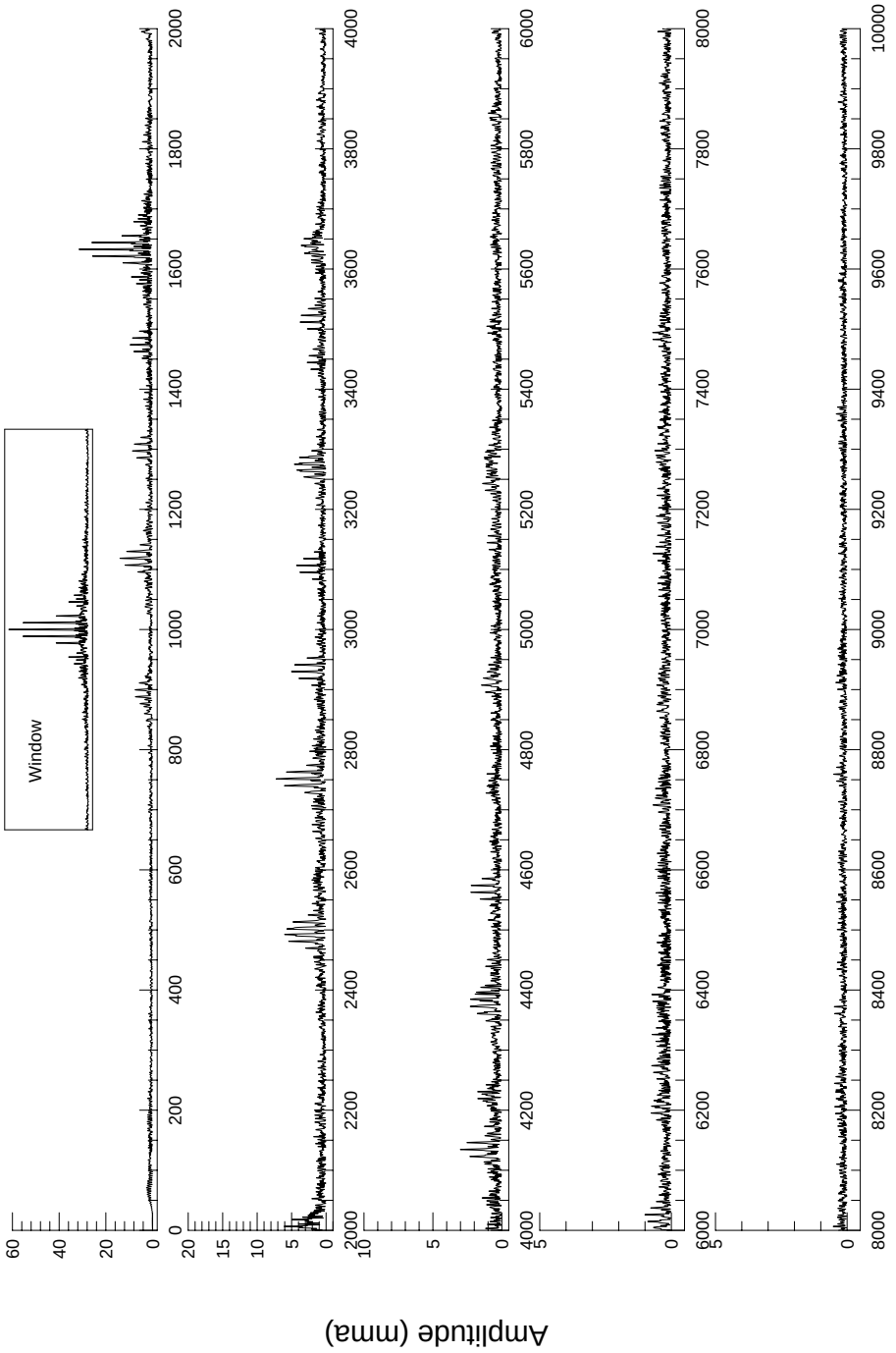

Fig. A.10.— The FT for the Sep93 data on G29–38.

Table A.5. Periodicities contained in the Sep93 G29–38 data set.

Frequency (μHz)	Period (s)	Amplitude (mma)	Comments
806.520	1239.895	1.9	R
871.884	1146.942	3.7	RM
888.108	1125.898	7.4	D?M
1118.520	894.039	14.0	R
1297.296	770.834	8.7	R
1367.184	731.430	2.4	RM?
1383.252	722.934	3.8	RM?
1474.044	678.406	9.7	R
1632.788	612.449	31.6	RM
1637.420	610.717	8.2	RM
1642.210	608.935	8.5	RM
1811.784	551.942	4.4	R
2006.628	498.348	6.1	RS?
2492.412	401.218	6.0	RM
2501.772	399.717	5.7	RM
2751.372	363.455	7.3	S
2929.992	341.298	5.0	S
3106.584	321.897	4.3	S
3265.392	306.242	4.3	SM
3270.047	305.806	2.0	SM
3274.952	305.348	4.6	S?

Table A.5—Continued

Frequency (μHz)	Period (s)	Amplitude (mma)	Comments
3444.480	290.320	2.8	S
3522.948	283.853	3.6	R?M?
3539.796	282.502	1.6	PM?
3639.168	274.788	3.6	S
4134.624	241.860	3.0	S
4219.332	237.004	1.8	RPA
4230.876	236.358	1.8	RPA
4384.536	228.212	2.3	S
4393.272	227.621	1.9	PM?
4439.448	225.253	1.2	S
4562.688	219.169	2.3	S
4907.448	203.772	1.5	S

Note. — The Comments are encoded as follows: R=Real peak, S=linear combination Sum peak, D=linear combination Difference peak, M=Multiplet member, P=Probable — mode is not cleanly identified, A=Alias — this peak is an alias of another peak and we are not sure which is real, and ?=Unknown.

Appendix B

Archival Cool DAV FTs

In this Appendix, I present, for both archival and verification purposes, the FTs for each of the non-primary G29–38 data sets presented in Chapter 4. I also include FTs from the other observed cool DAVs. Some months I only have one or two runs on a star. In these cases, I did not bother to present the DFT here.

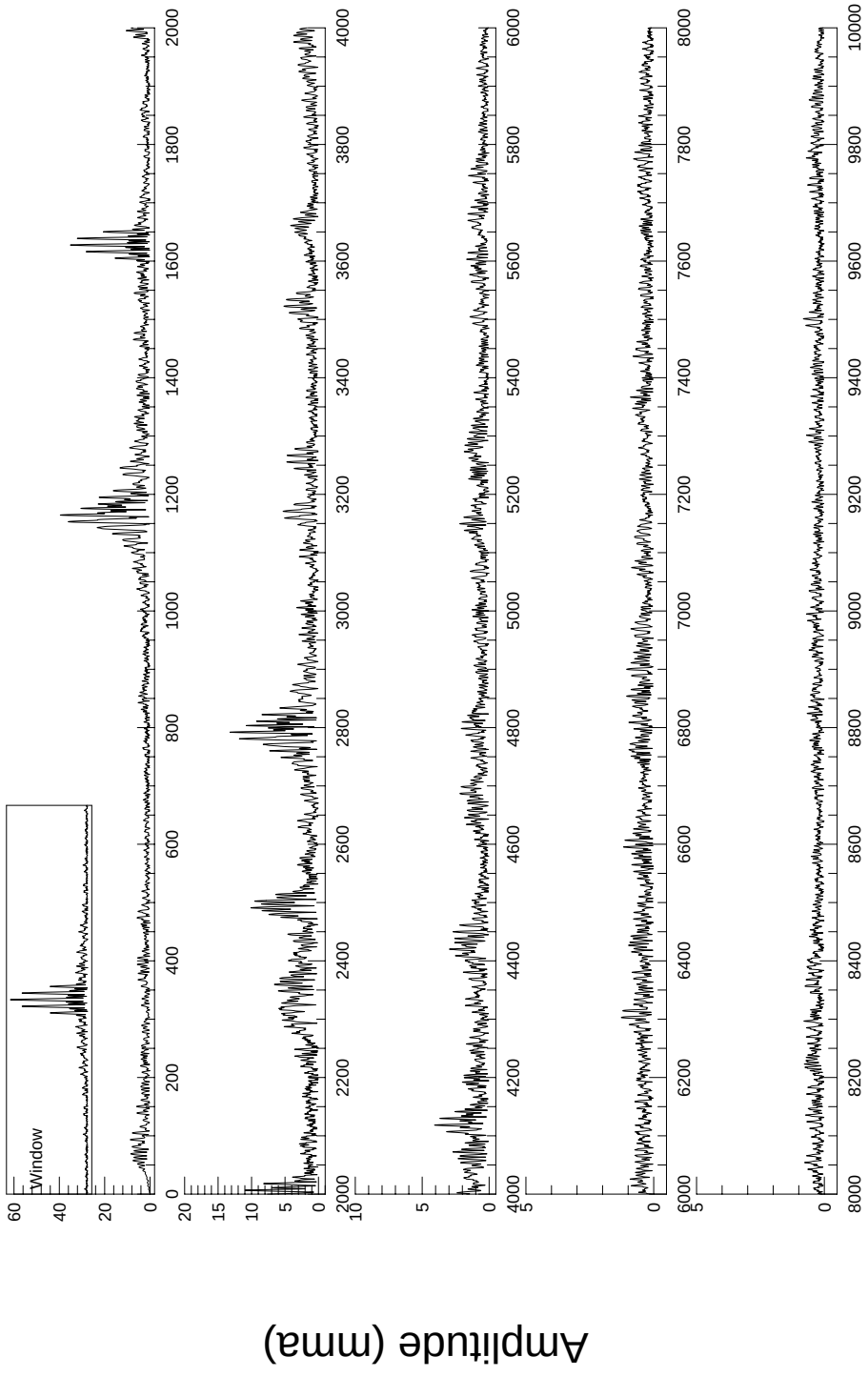

Fig. B.1.— The FT for the September 1985 data on G29–38.

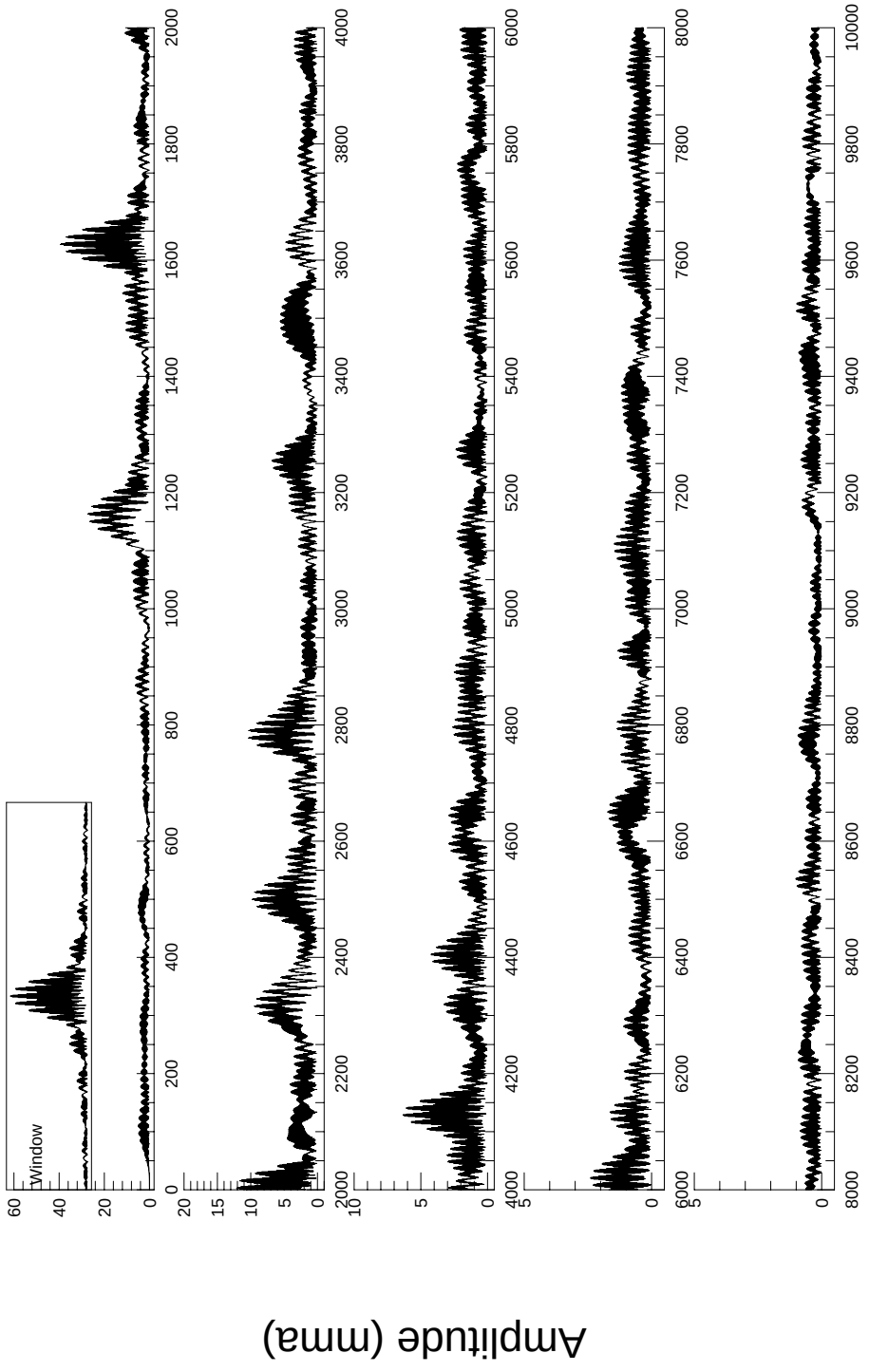

Fig. B.2.— The FT for the October 1985 data on G29–38.

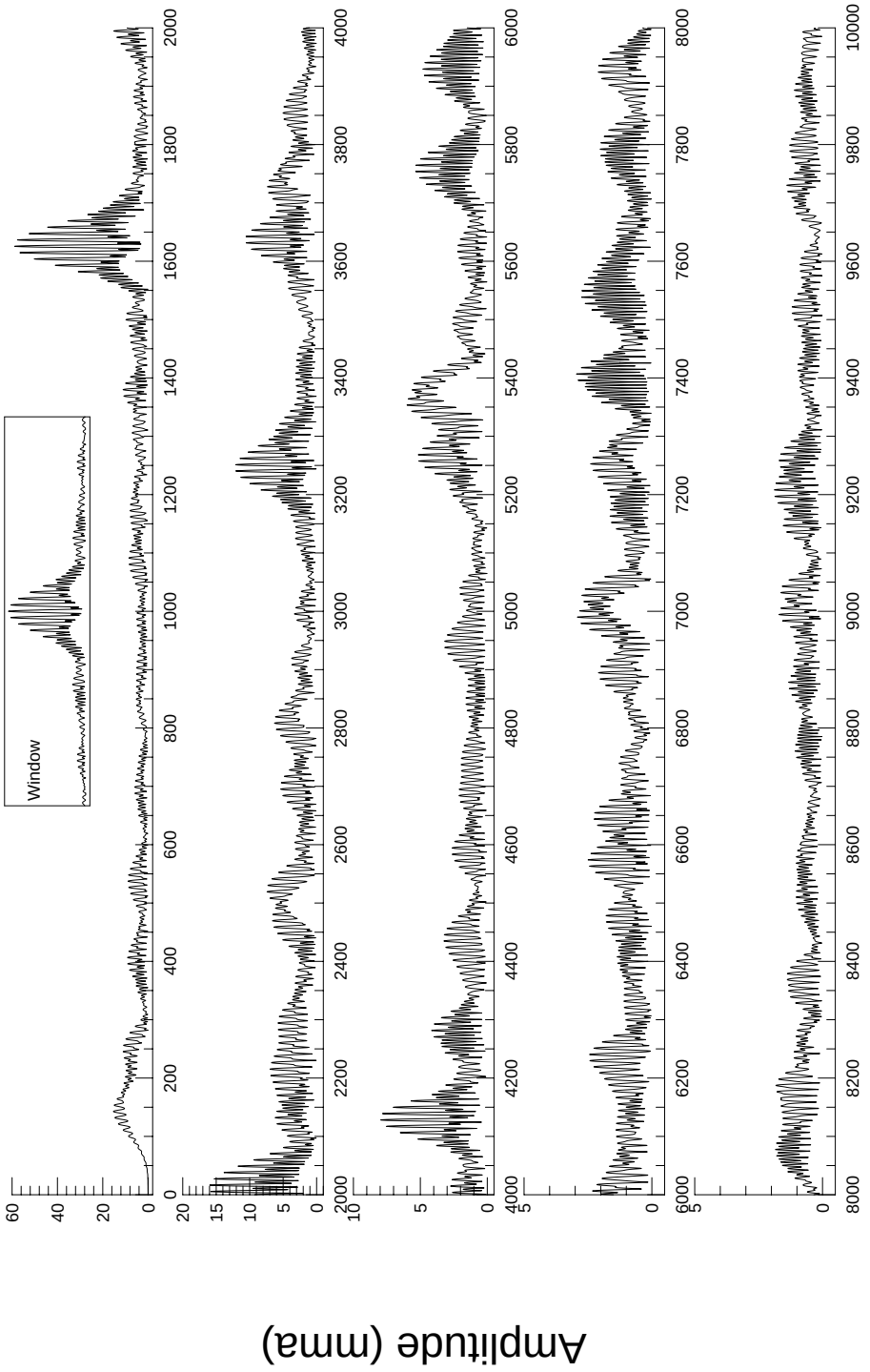

Fig. B.3.— The FT for the October 1988 data on G29–38.

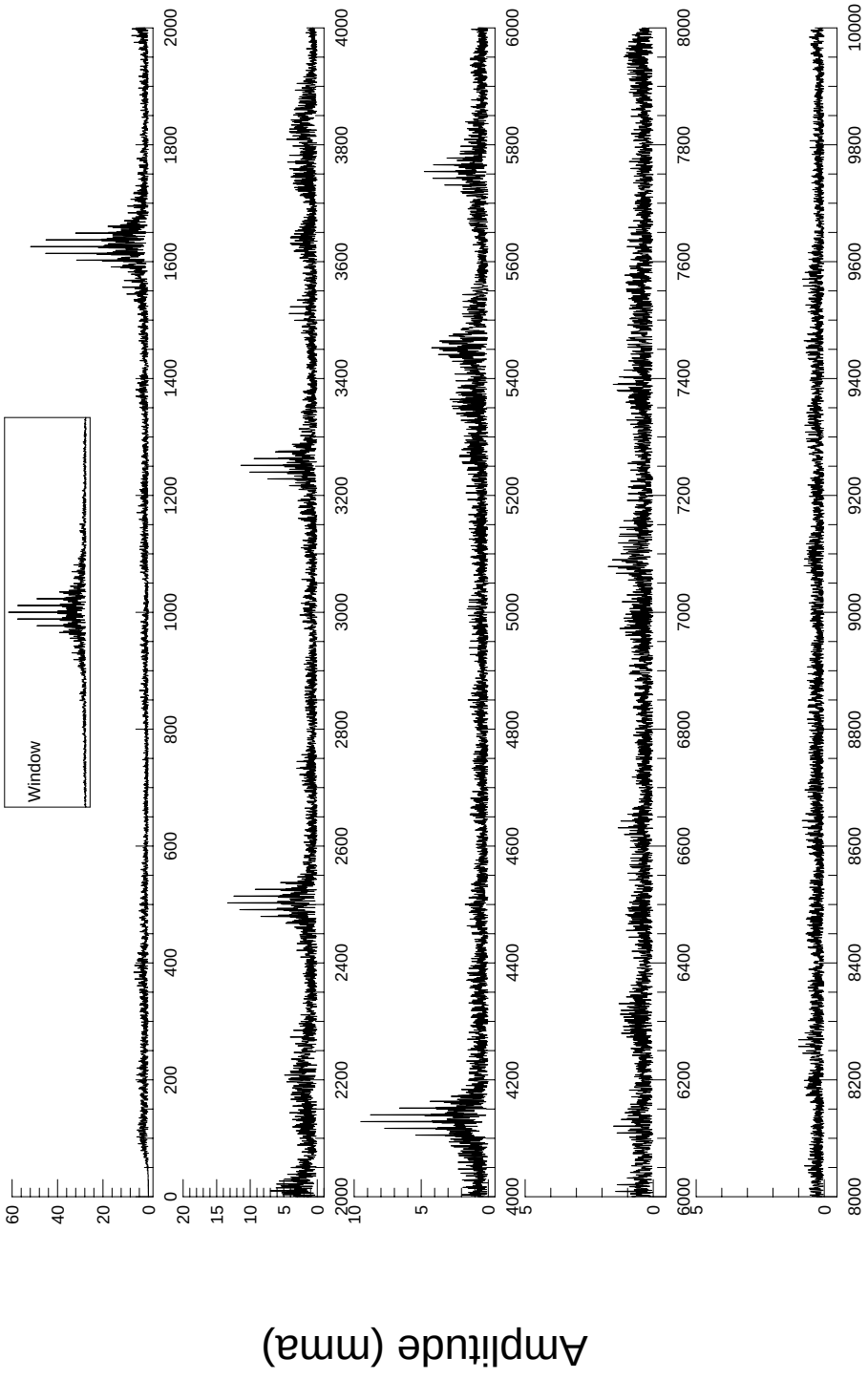

Fig. B.4.— The FT for the November 1988 data on G29–38.

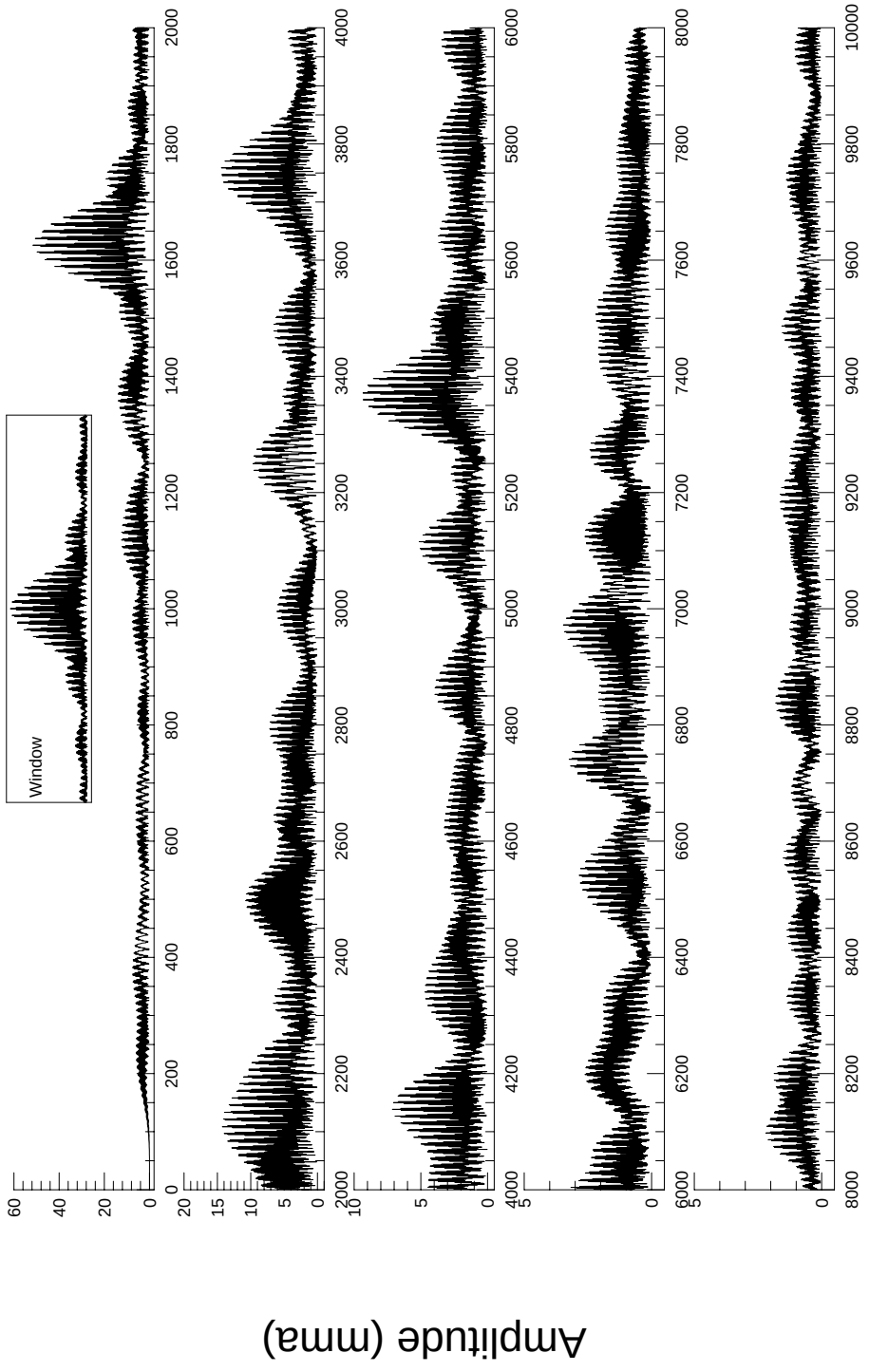

Fig. B.5.— The FT for the December 1988 data on G29–38.

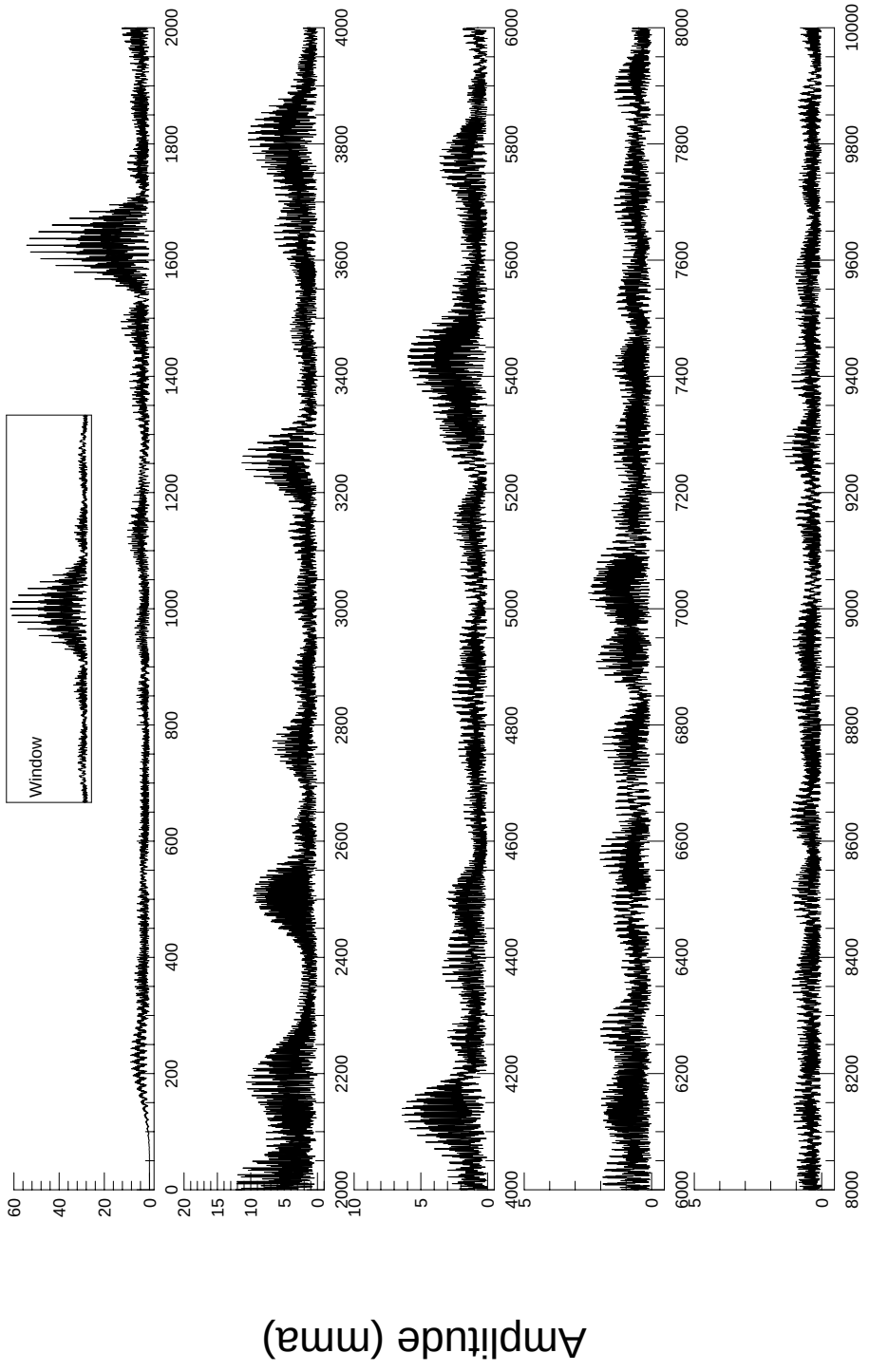

Fig. B.6.— The FT for the January 1989 data on G29–38.

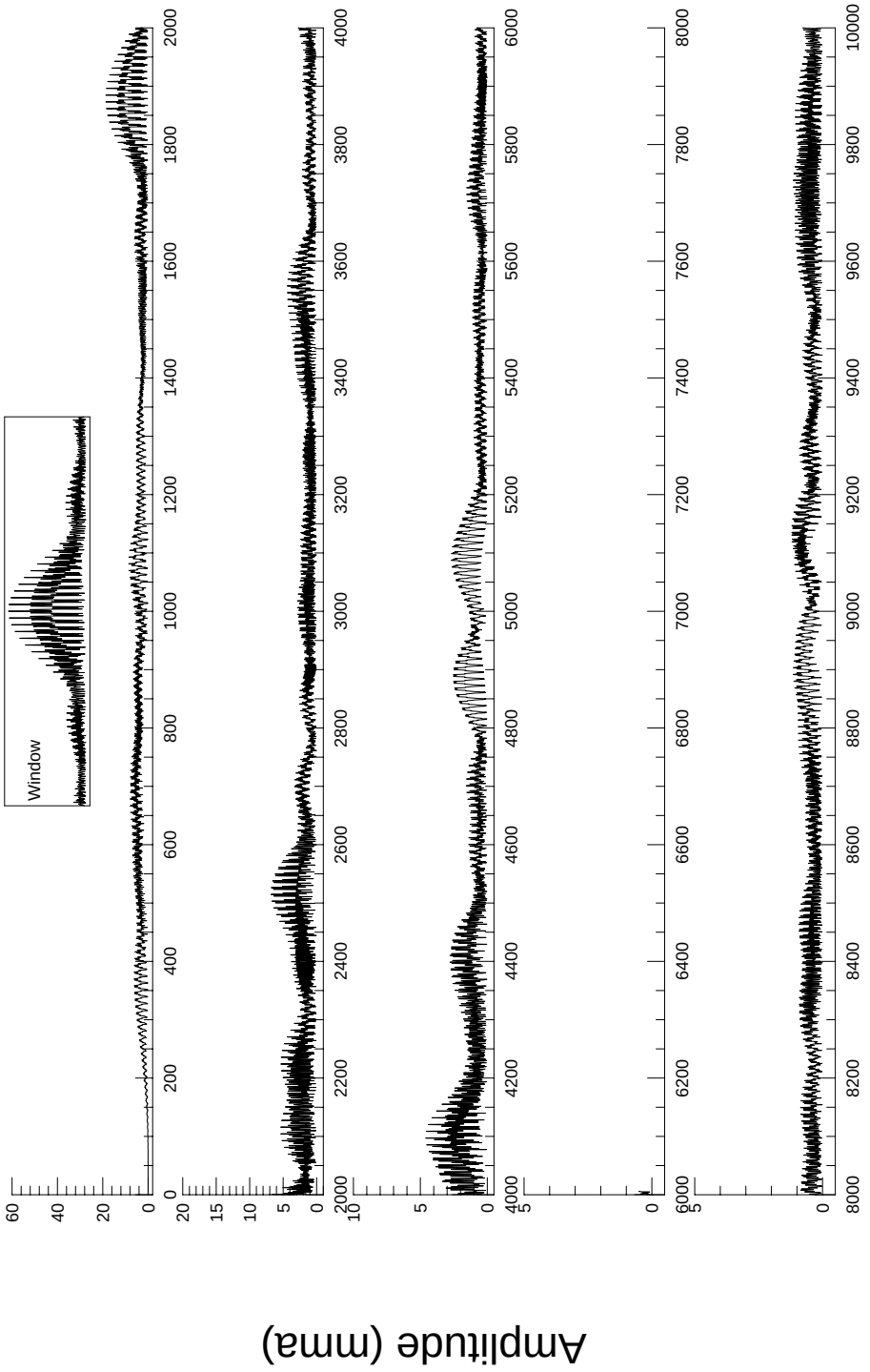

Fig. B.7.— The FT for the June 1989 data on G29–38.

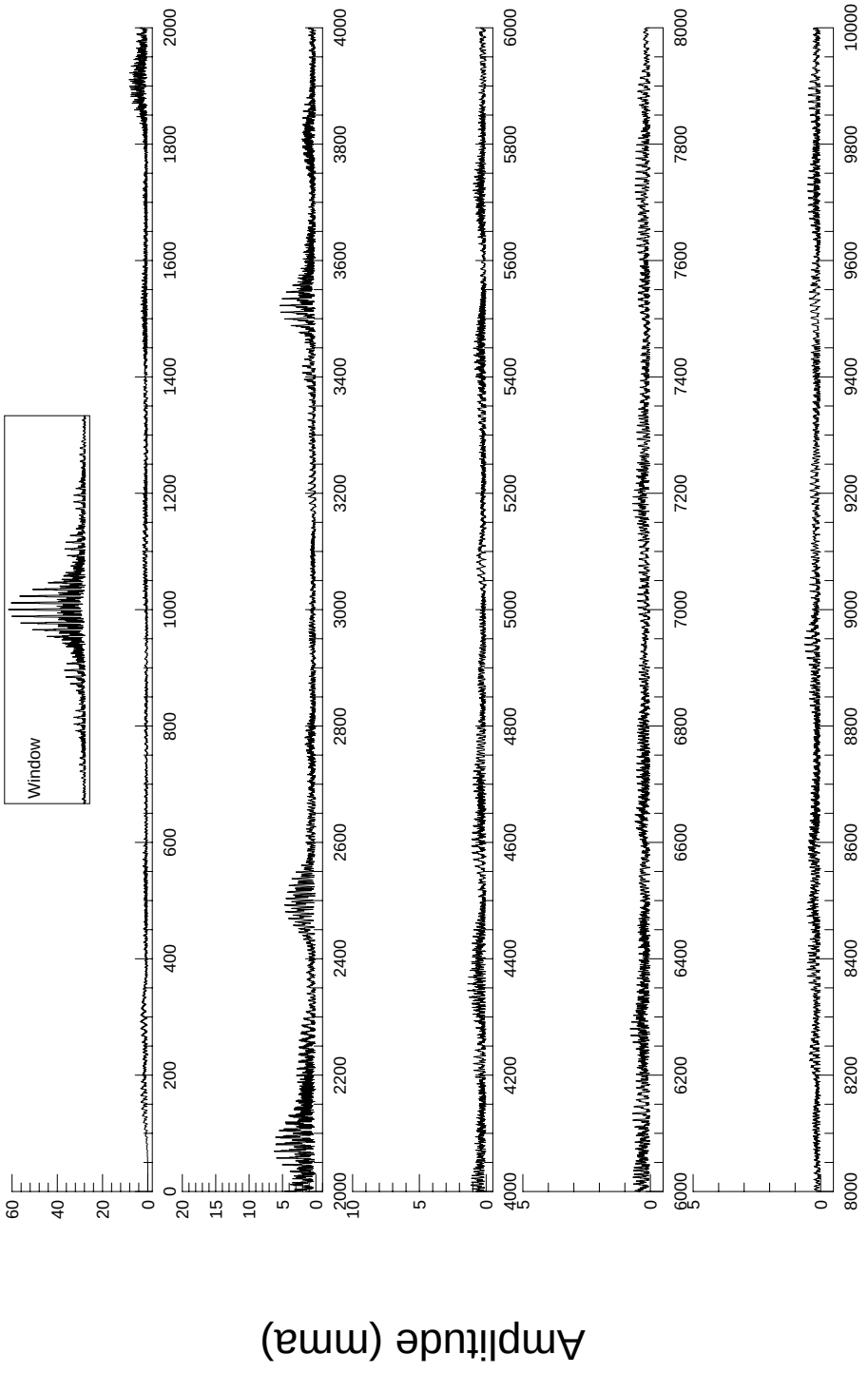

Fig. B.8.— The FT for the July 1989 data on G29–38.

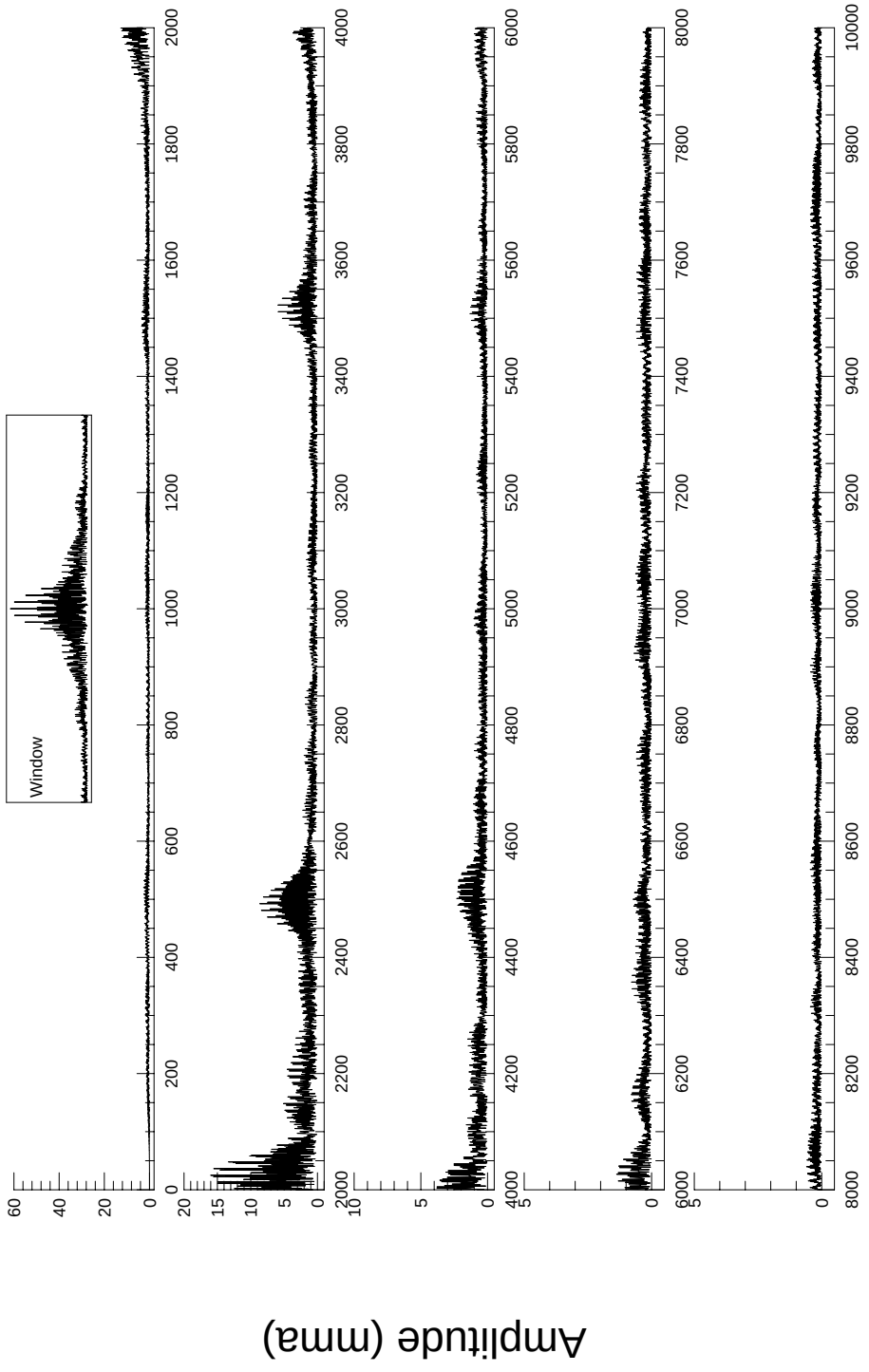

Fig. B.9.— The FT for the first August 1989 data on G29–38.

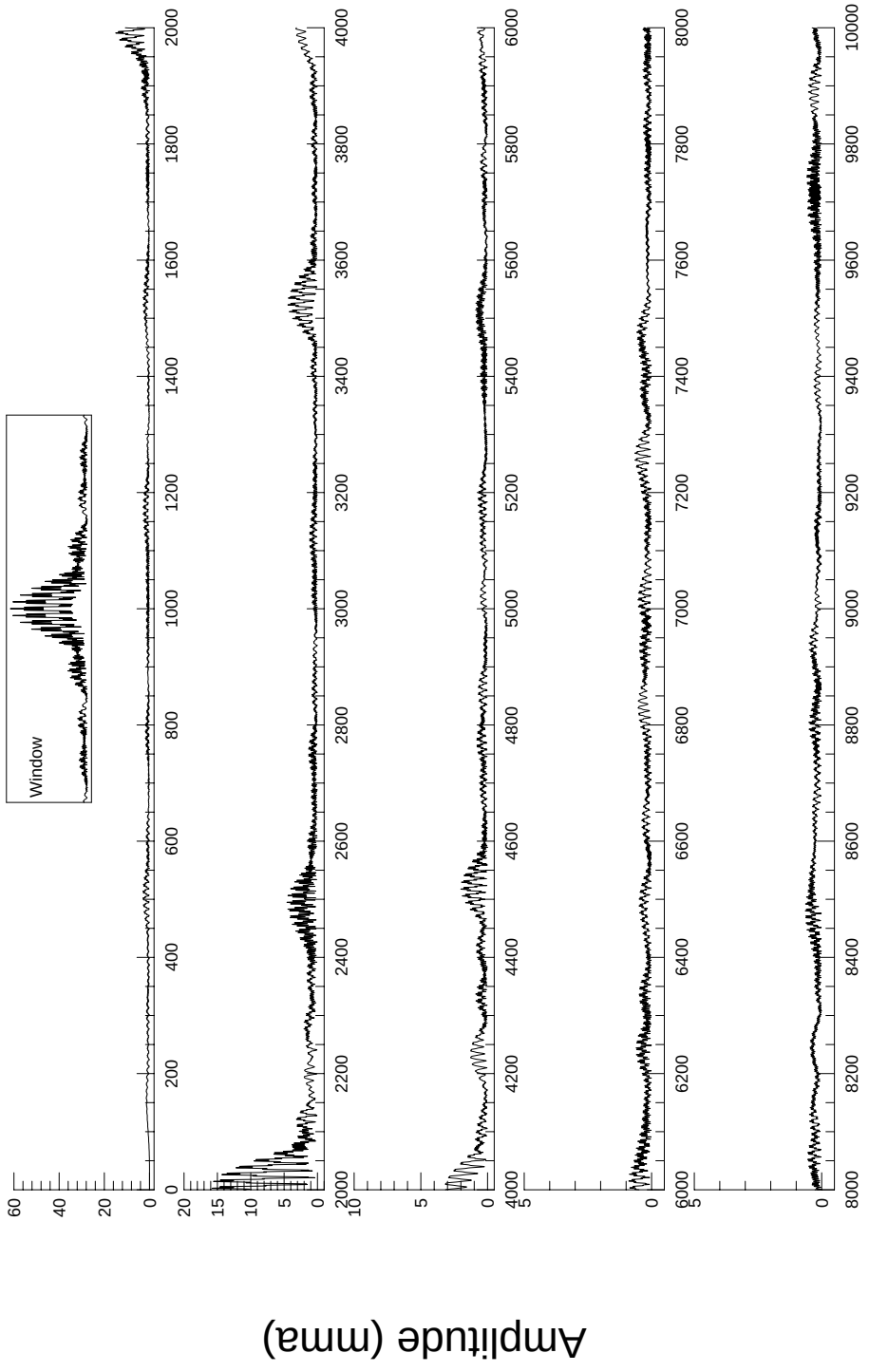

Fig. B.10.— The FT for the second August 1989 data on G29–38.

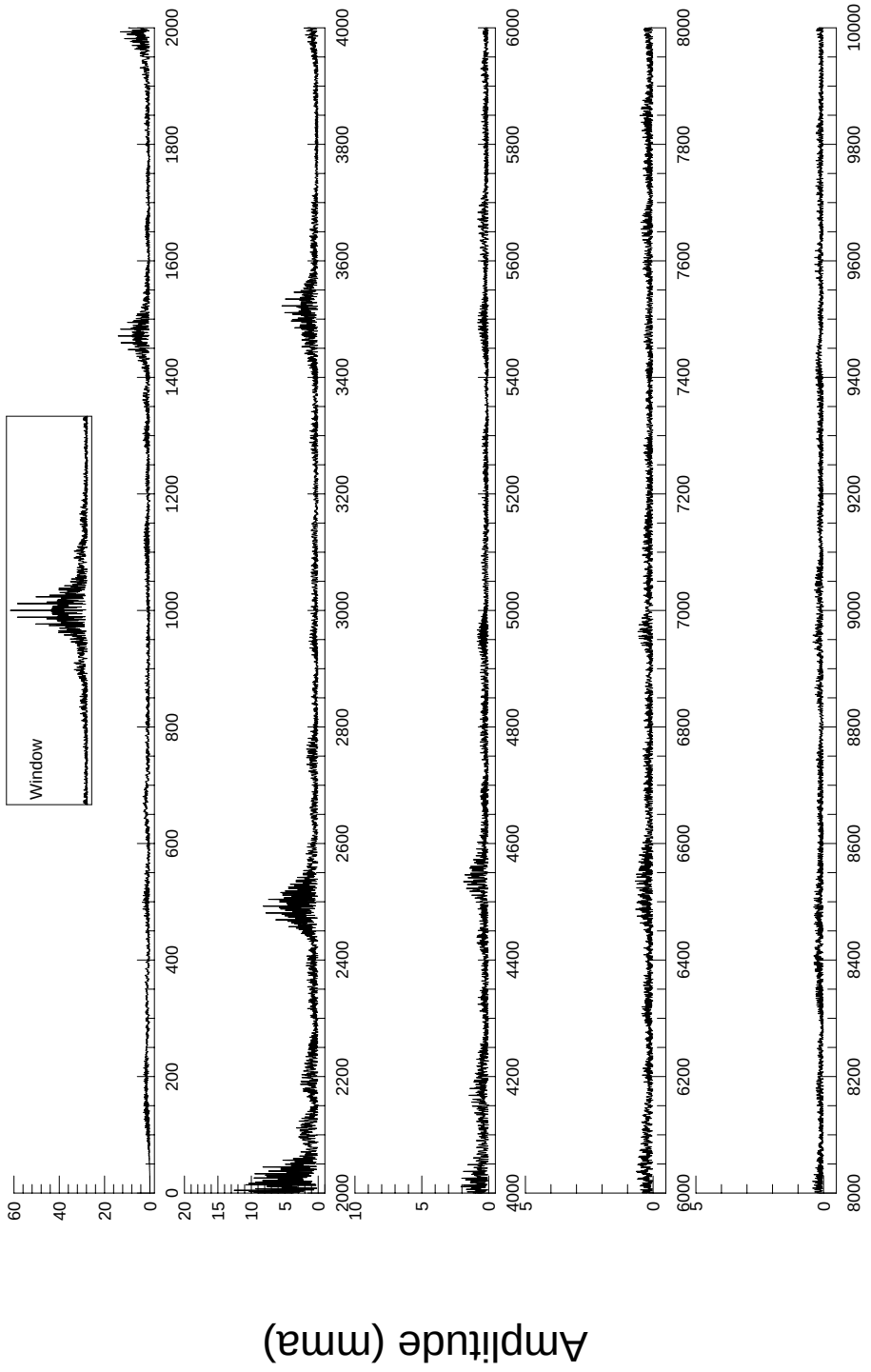

Fig. B.11.— The FT for the October 1989 data on G29–38.

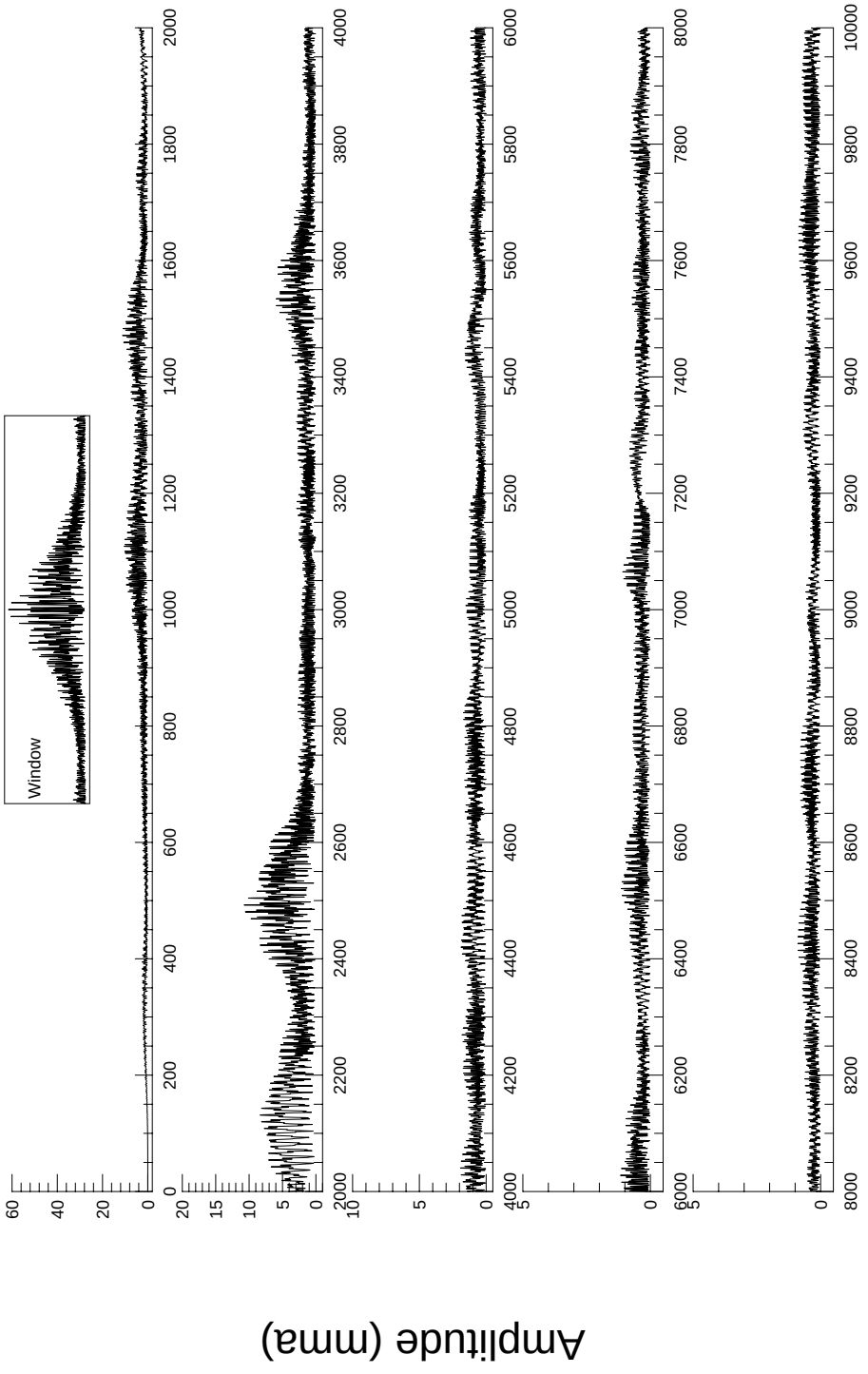

Fig. B.12.— The FT for the November 1989 data on G29–38.

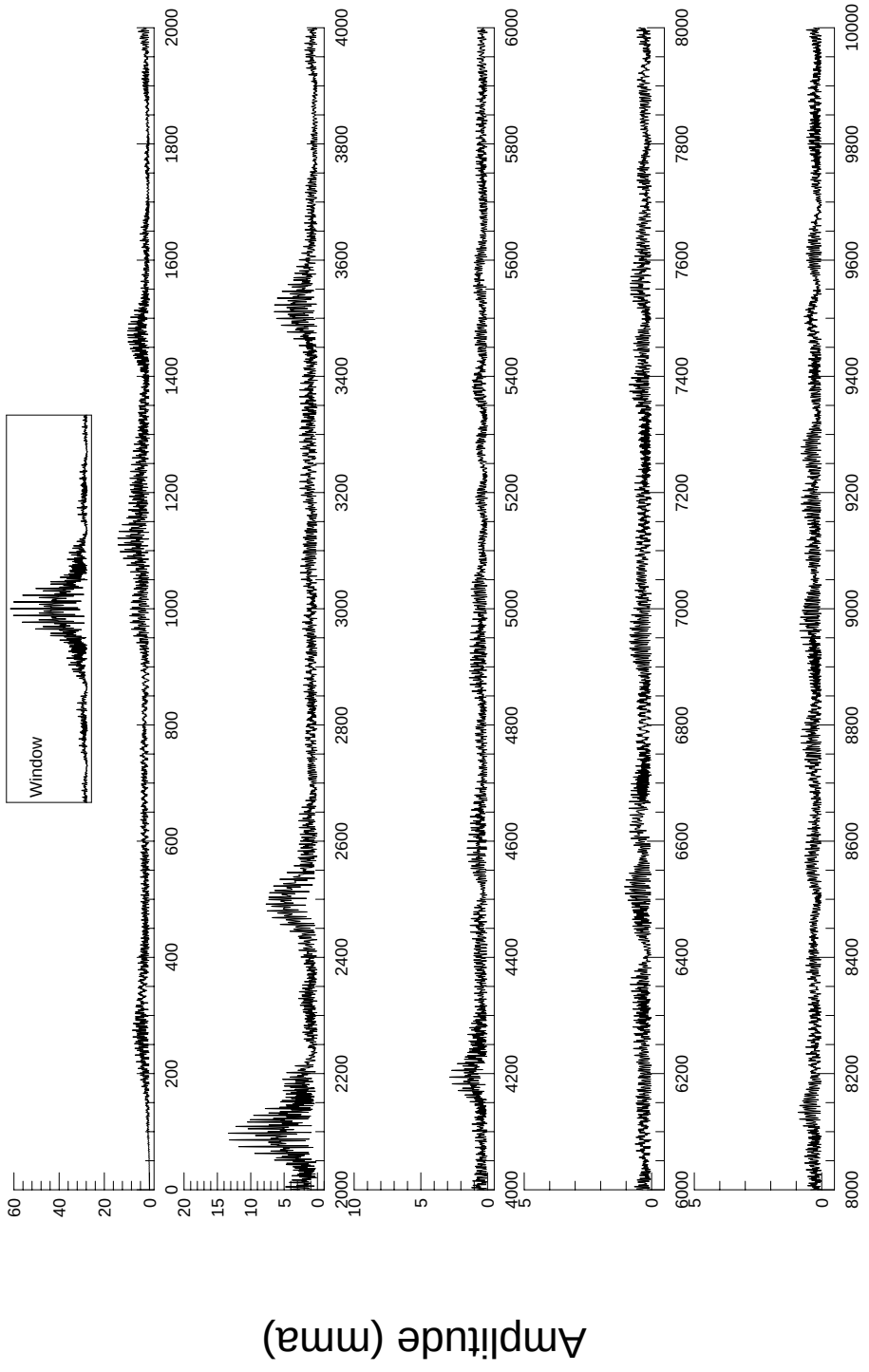

Fig. B.13.— The FT for the December 1989 data on G29–38.

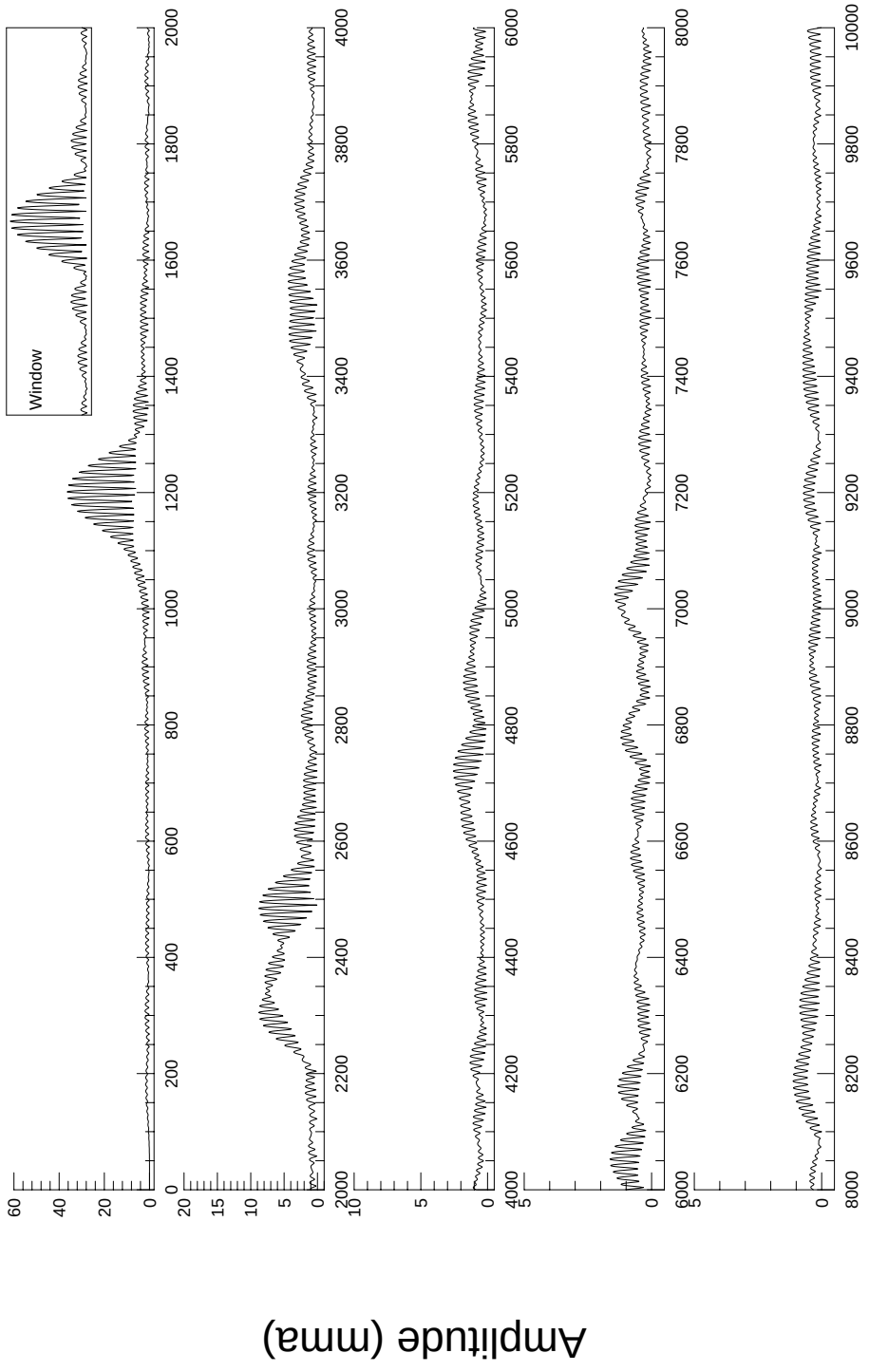

Fig. B.14.— The FT for the June 1990 data on G29–38.

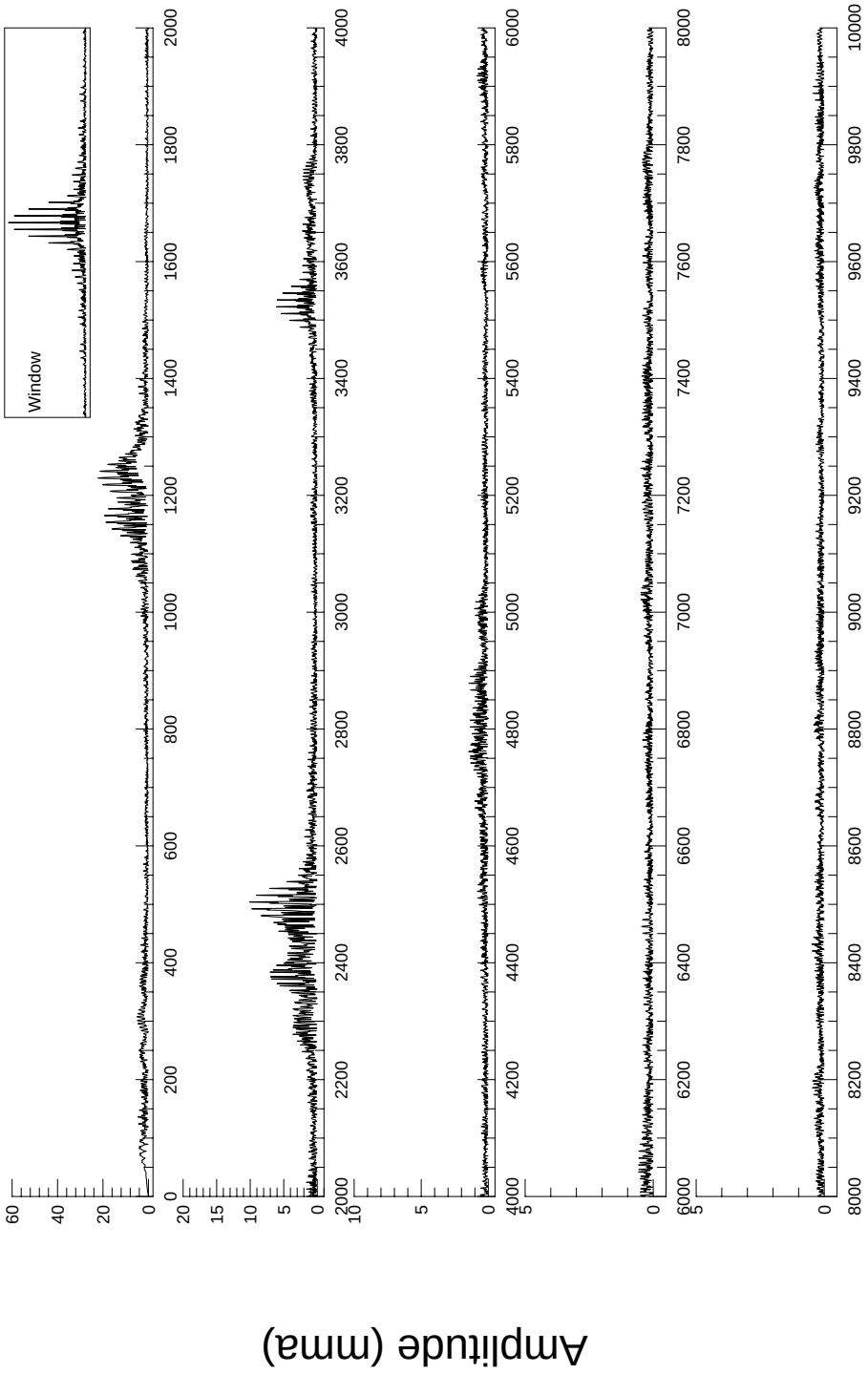

Fig. B.15.— The FT for the August 1990 data on G29–38.

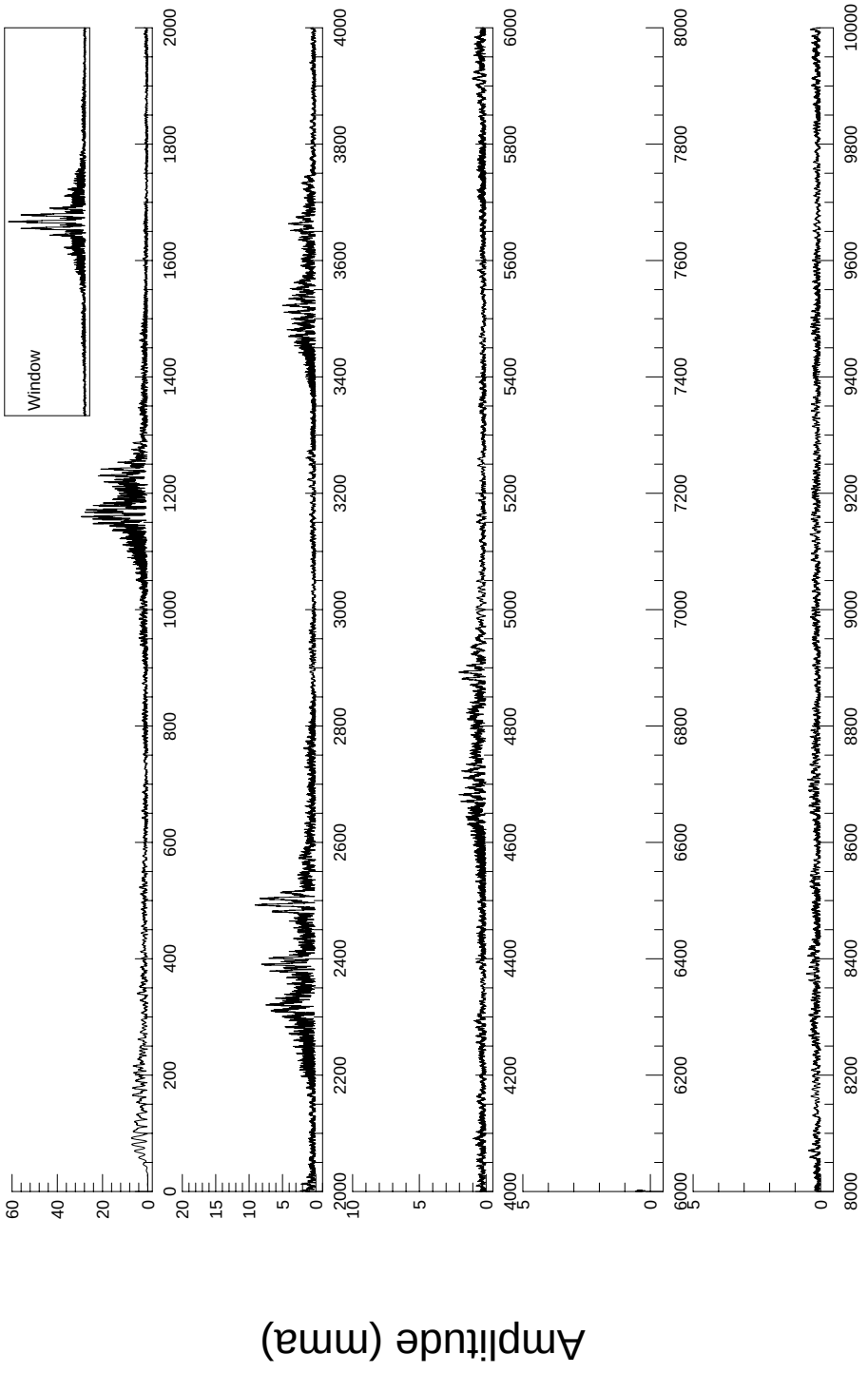

Fig. B.16.— The FT for the September 1990 data on G29–38.

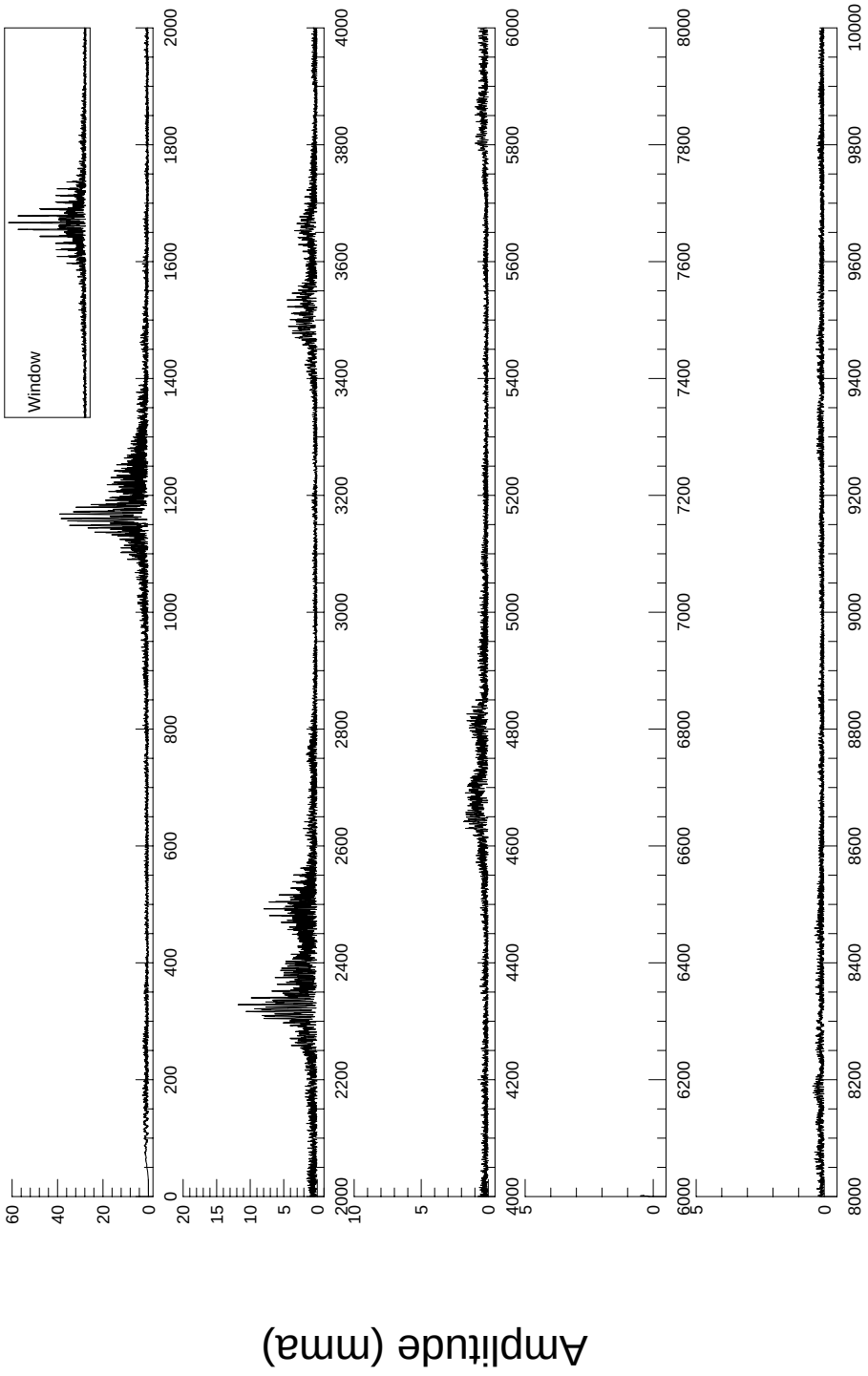

Fig. B.17.— The FT for the October 1990 data on G29–38.

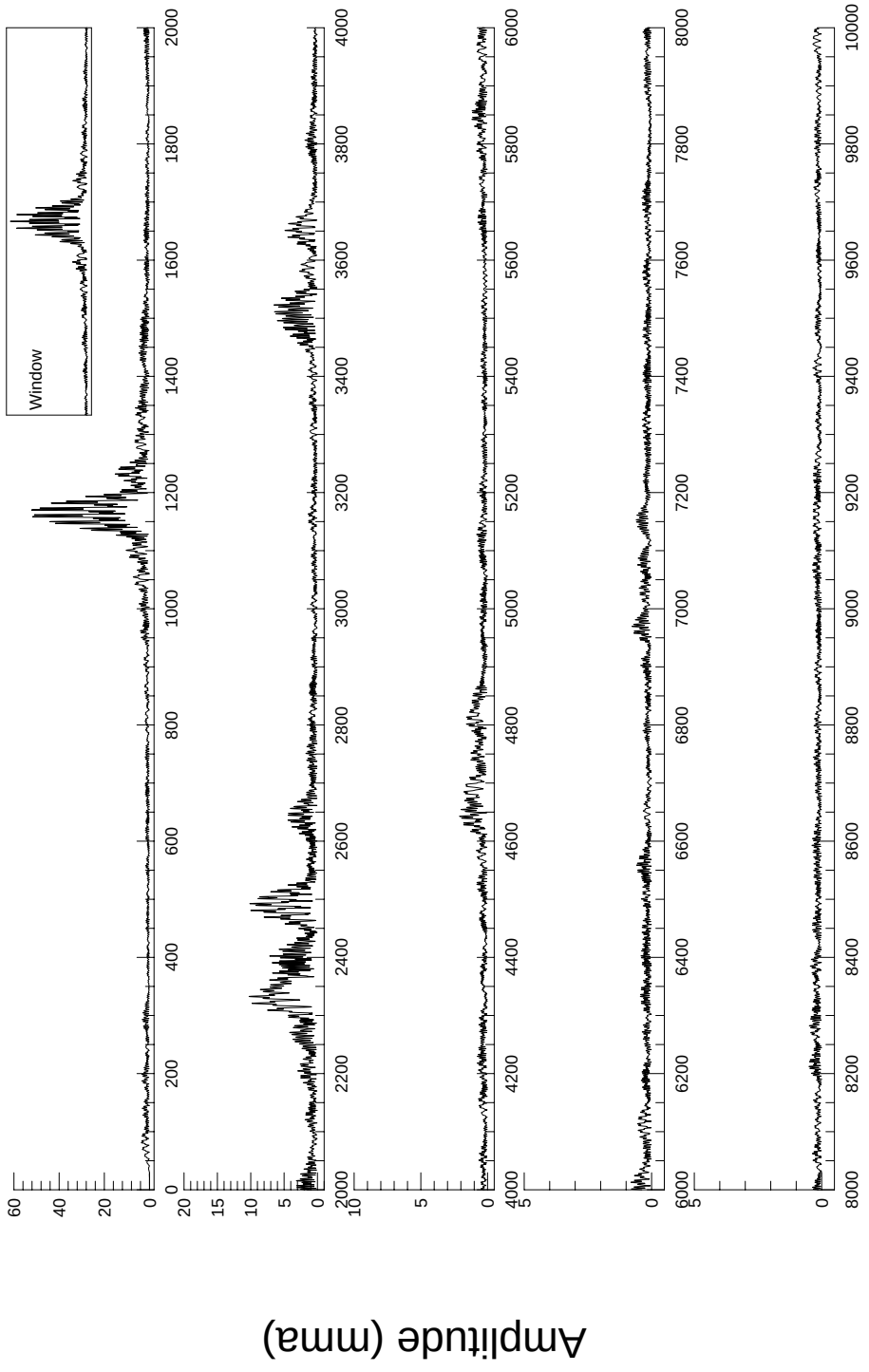

Fig. B.18.— The FT for the November 1990 data on G29–38.

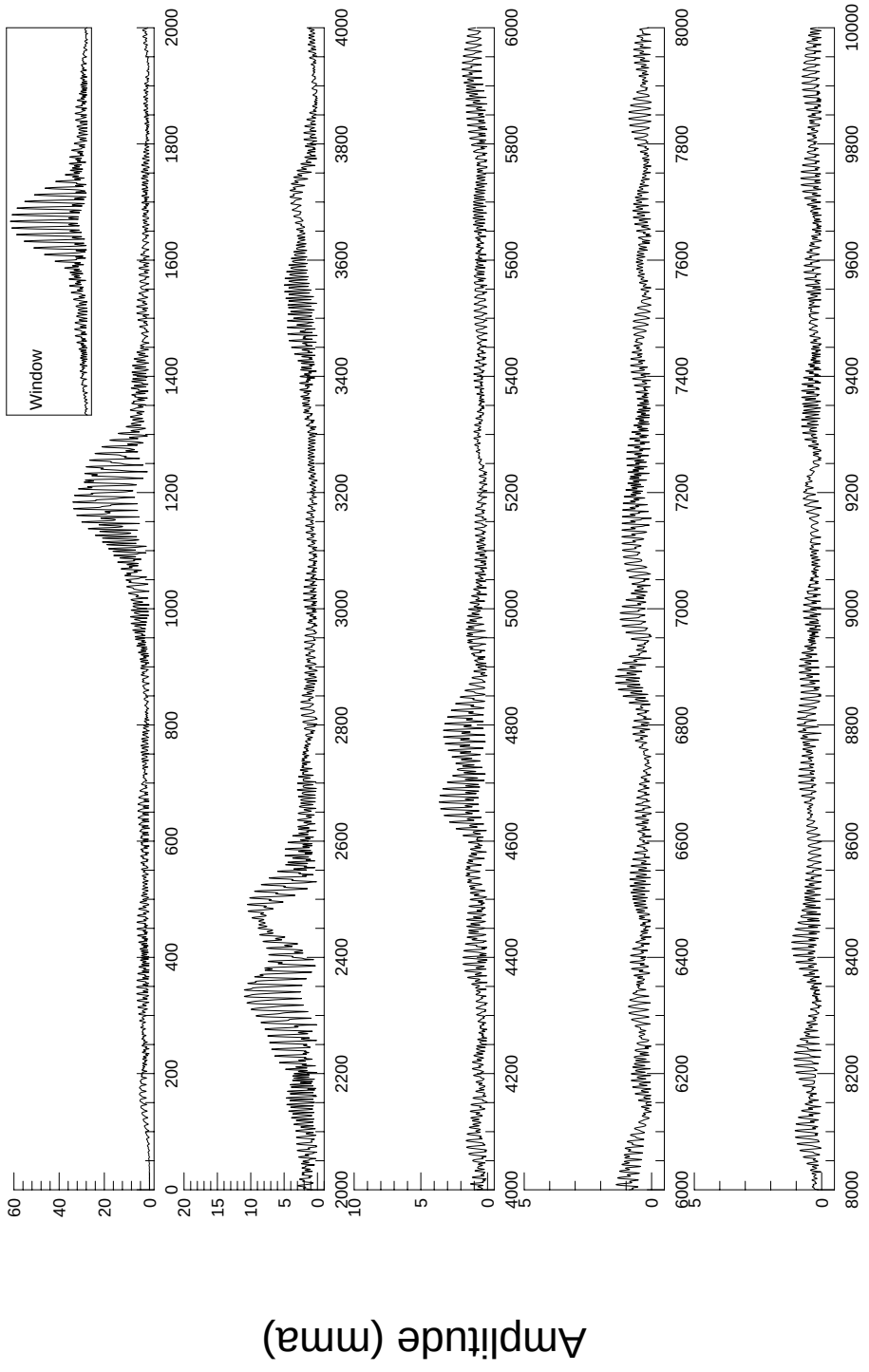

Fig. B.19.— The FT for the December 1990 data on G29–38.

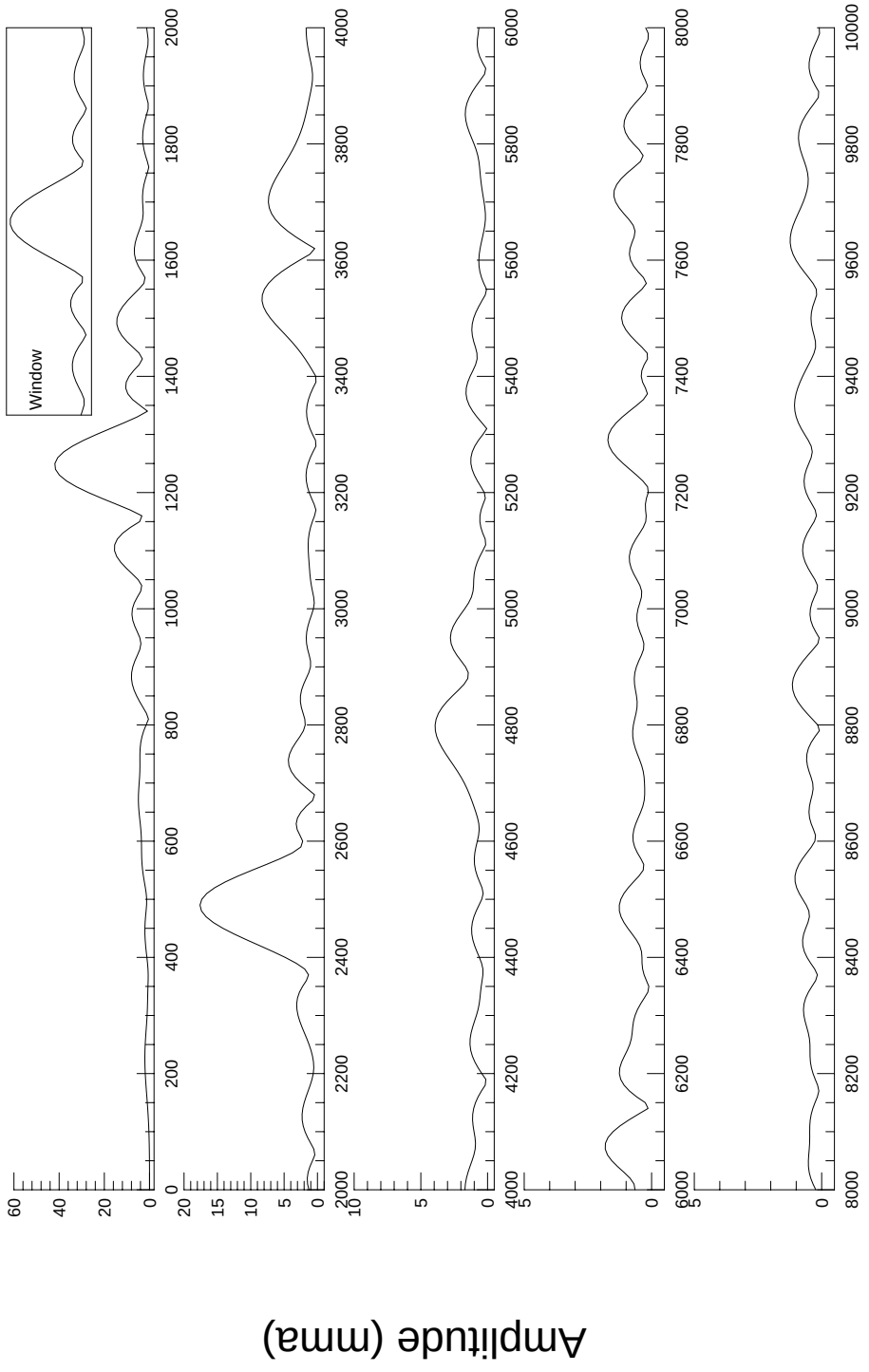

Fig. B.20.— The FT for the July 1991 data on G29–38.

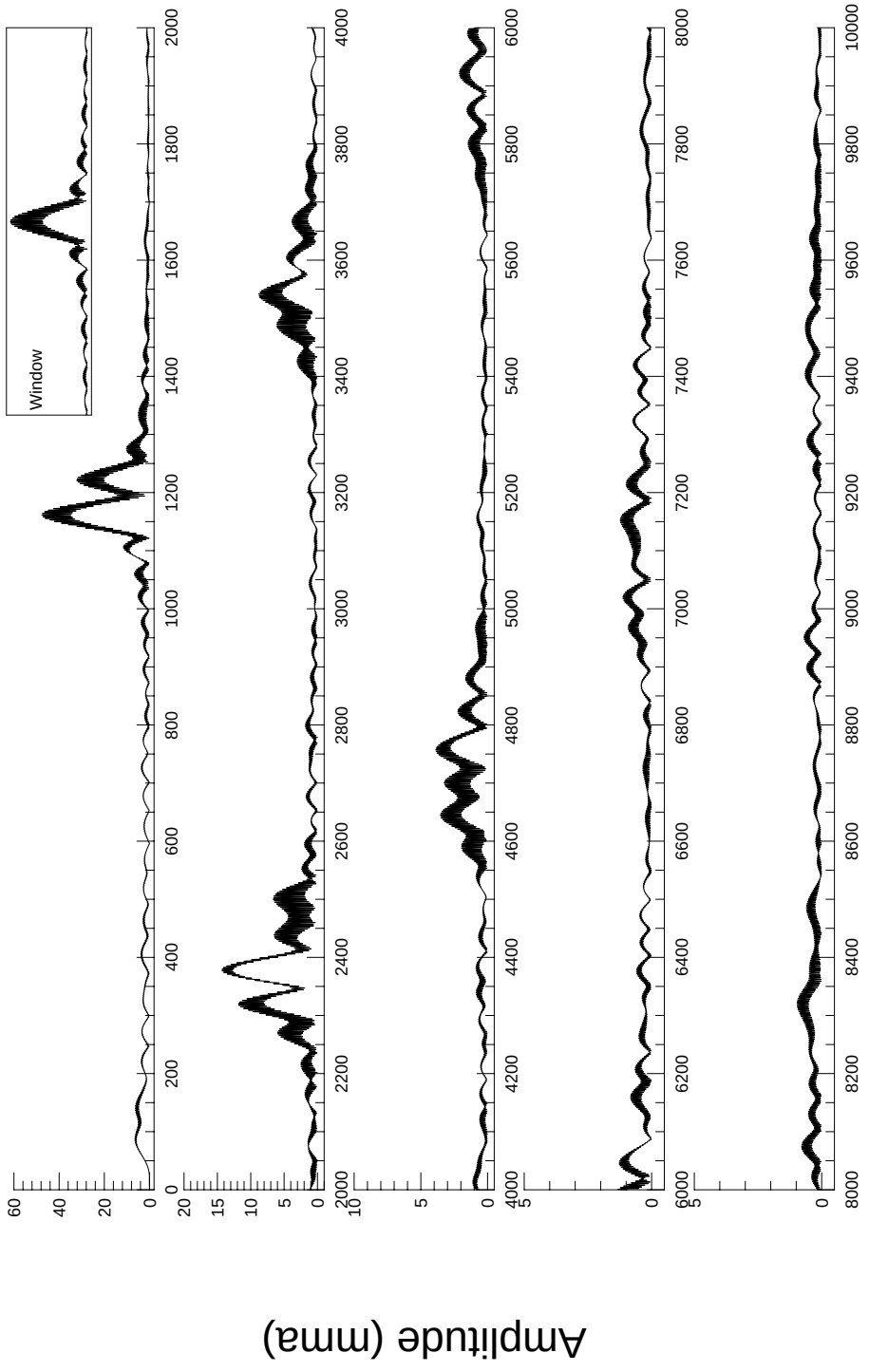

Fig. B.21.— The FT for the September 1991 data on G29–38.

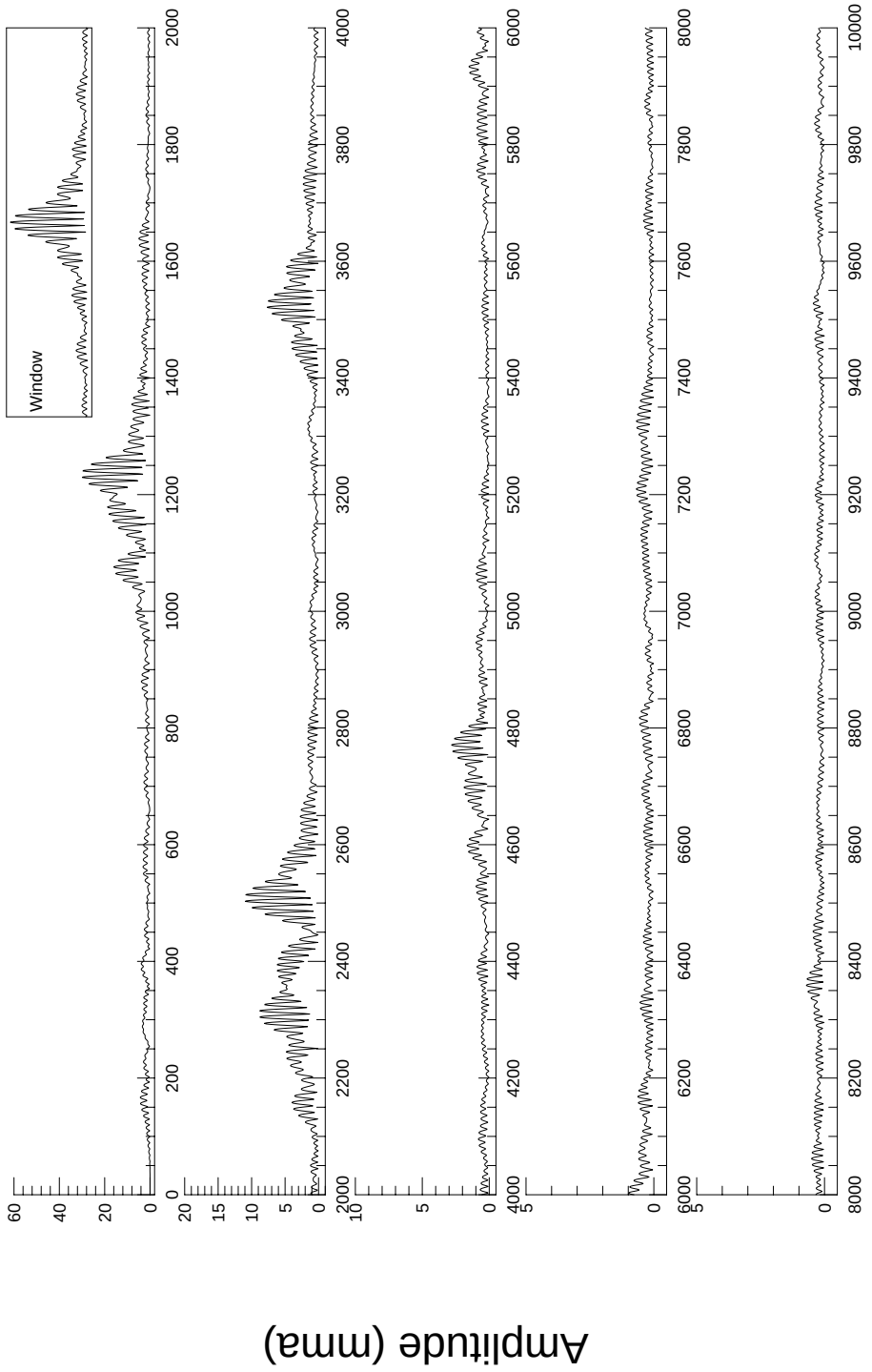

Fig. B.22.— The FT for the October 1991 data on G29–38.

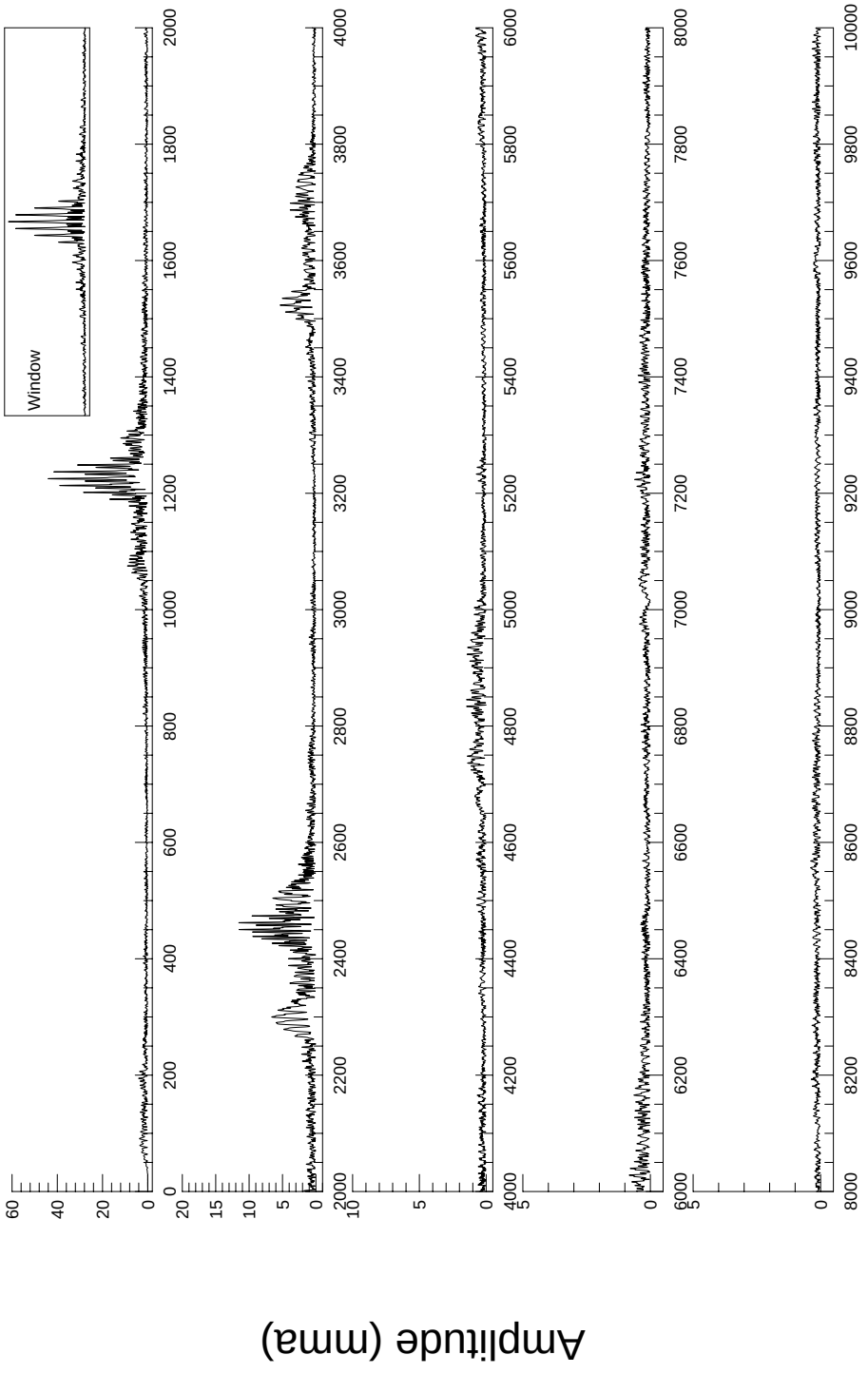

Fig. B.23.— The FT for the November 1991 data on G29–38.

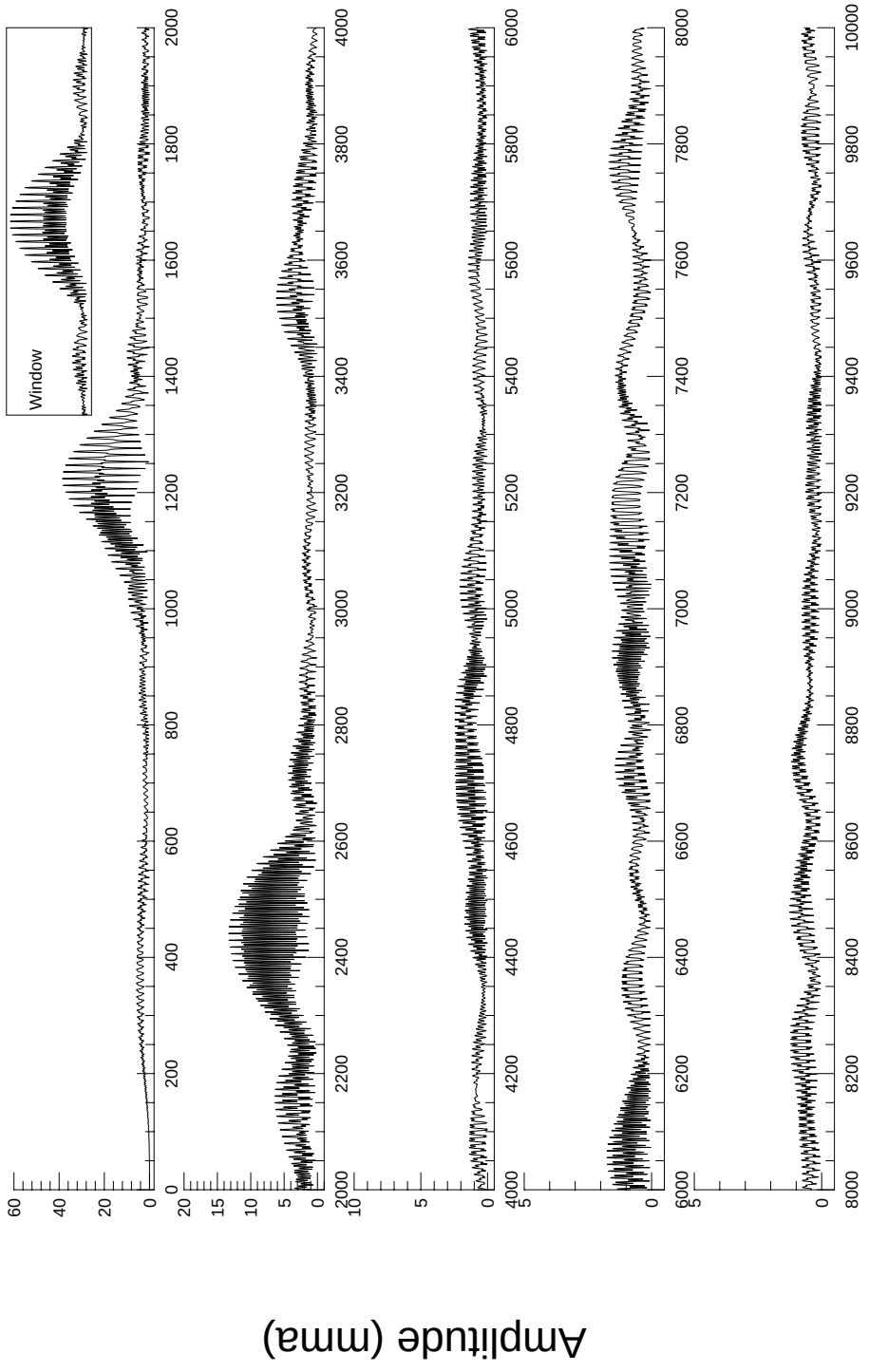

Fig. B.24.— The FT for the December 1991 data on G29–38.

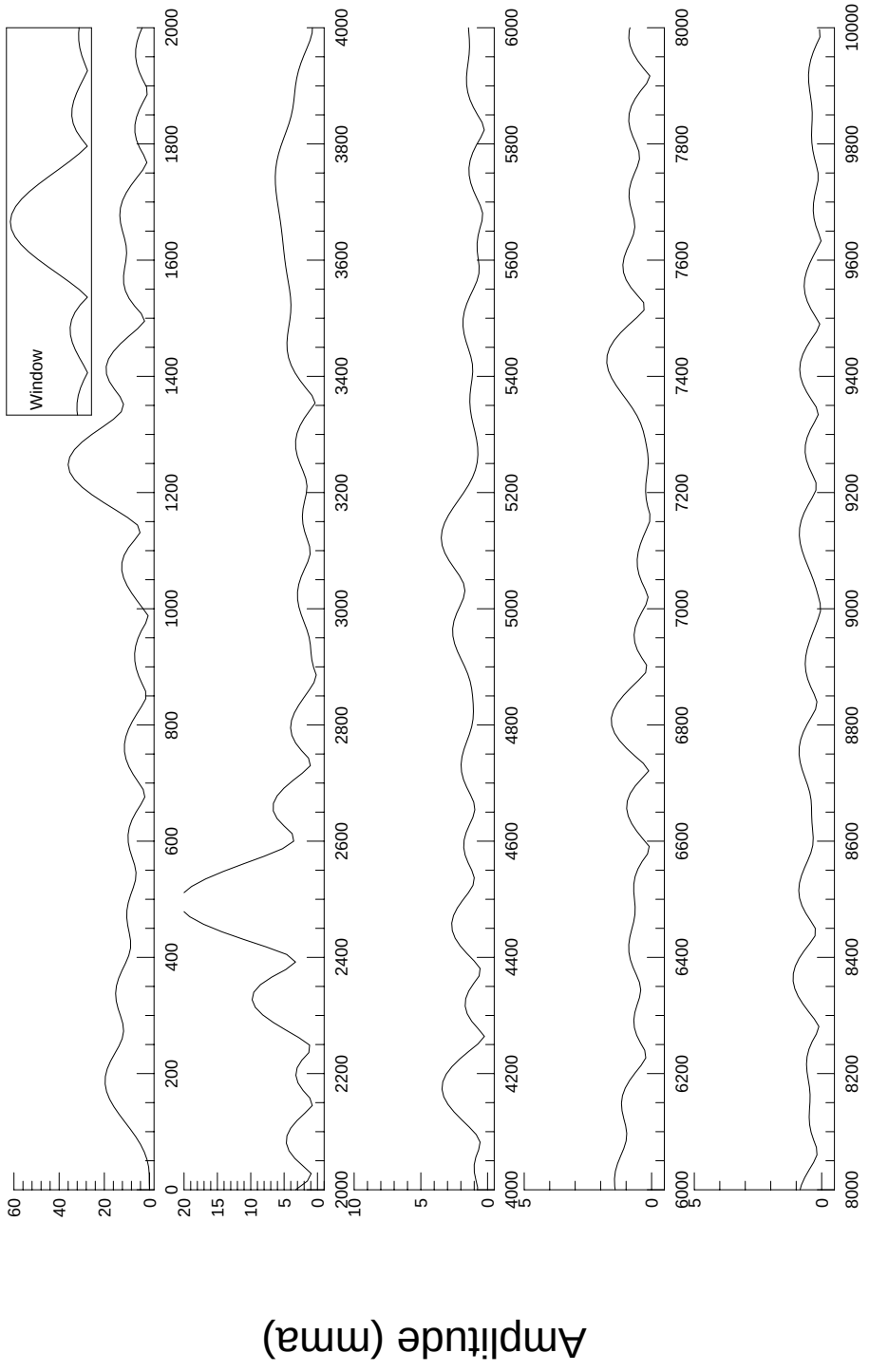

Fig. B.25.— The FT for the August 1992 data on G29–38.

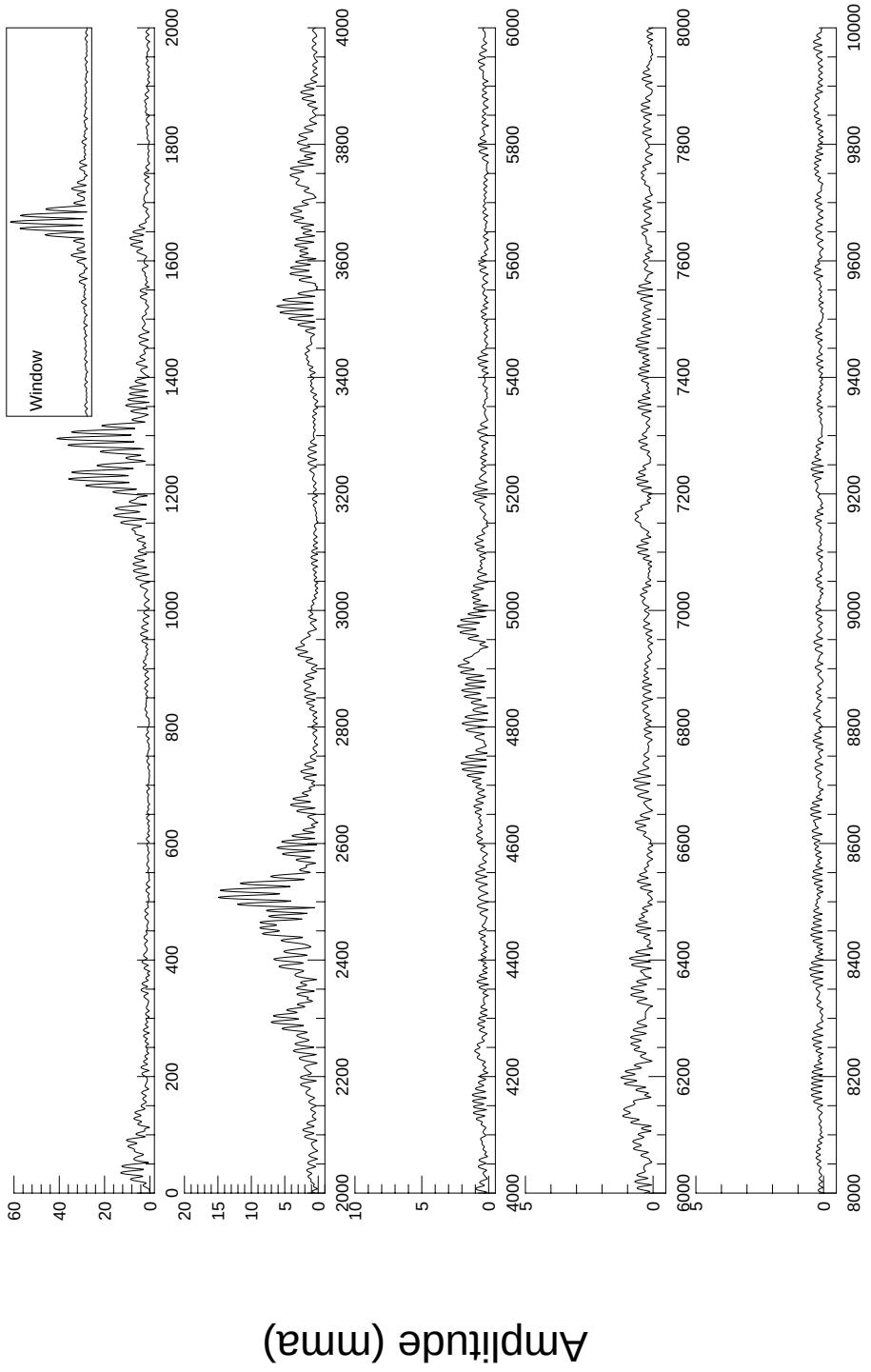

Fig. B.26.— The FT for the October 1992 data on G29–38.

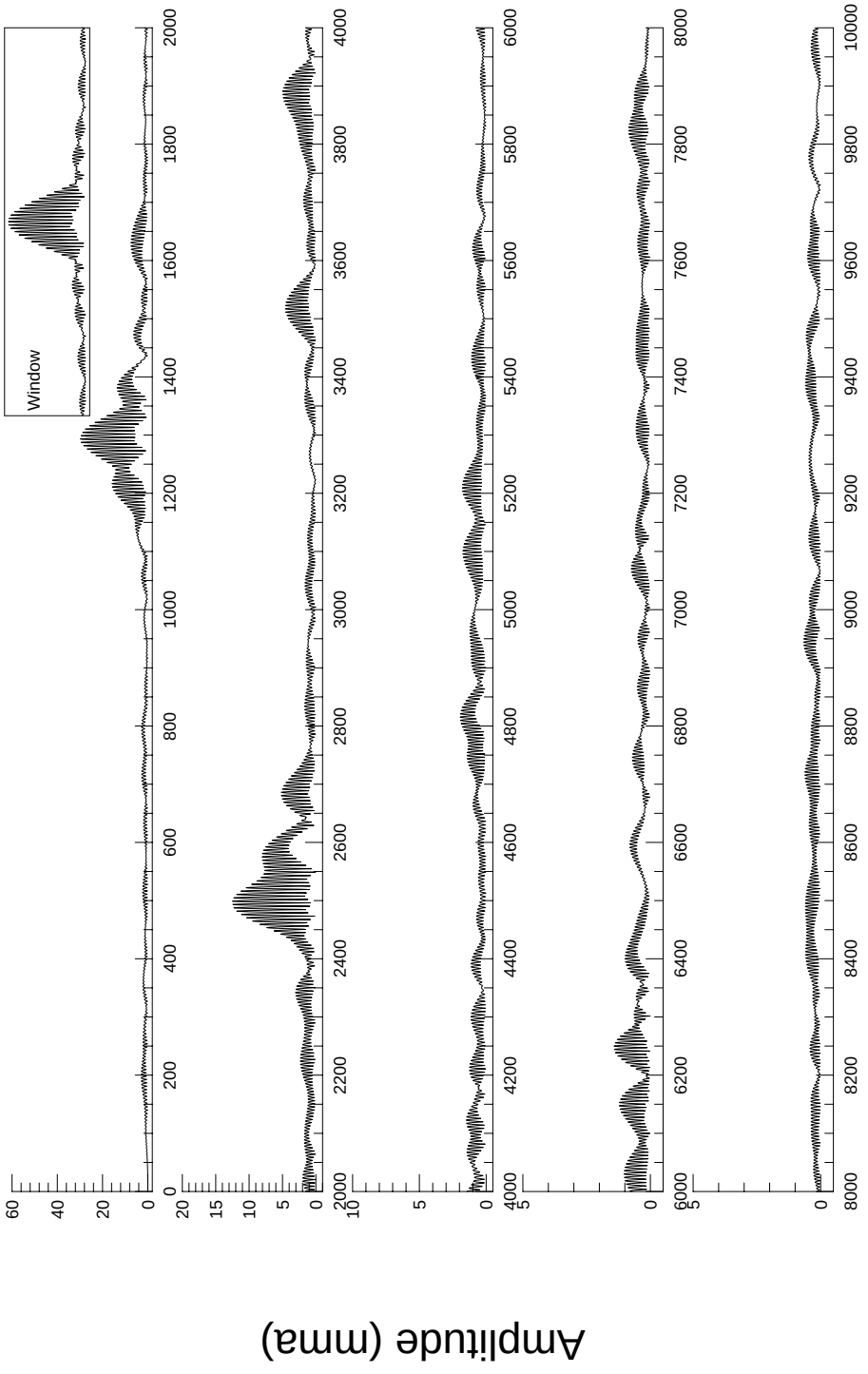

Fig. B.27.— The FT for the November 1992 data on G29–38.

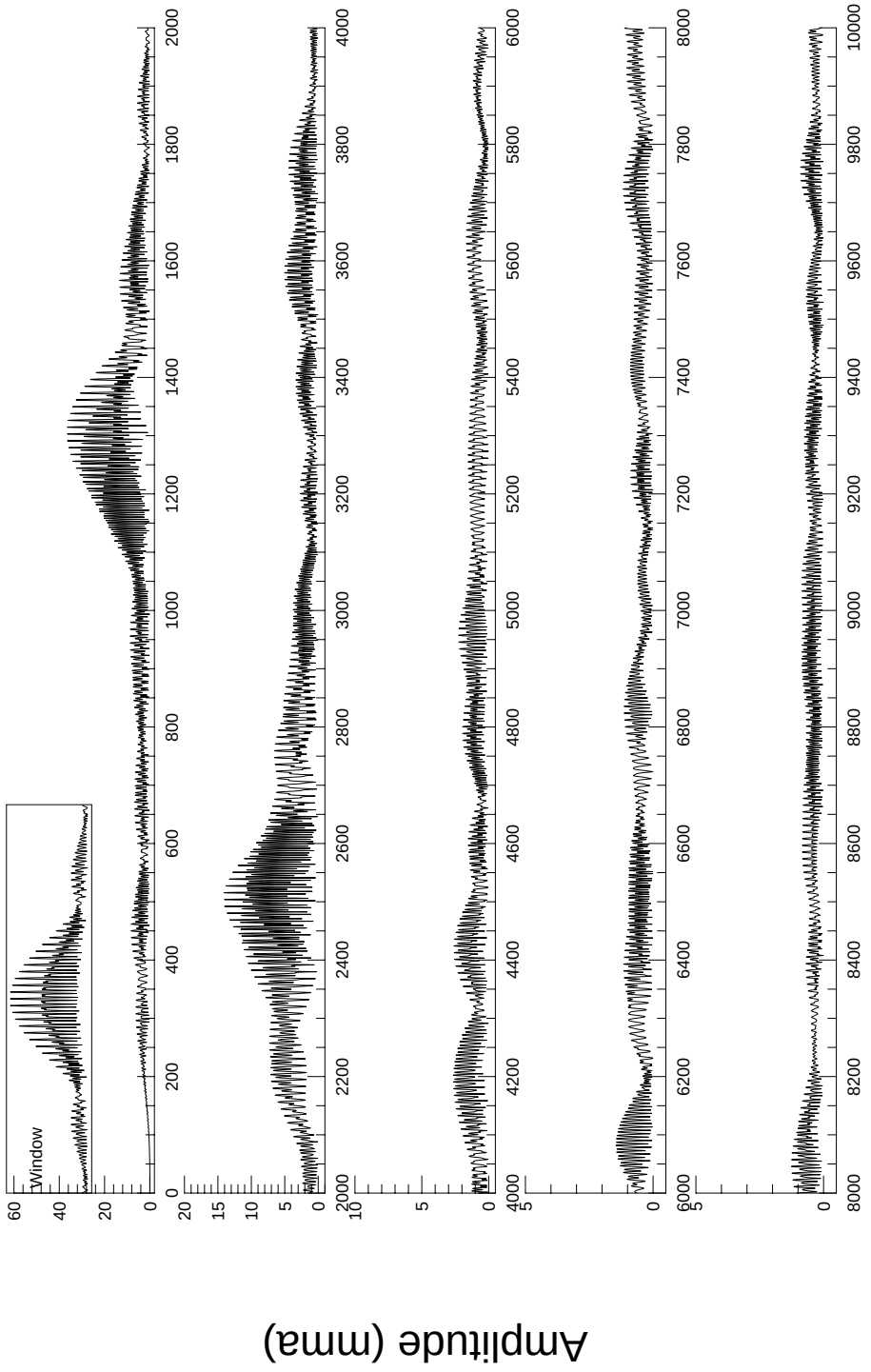

Fig. B.28.— The FT for the January 1993 data on G29–38.

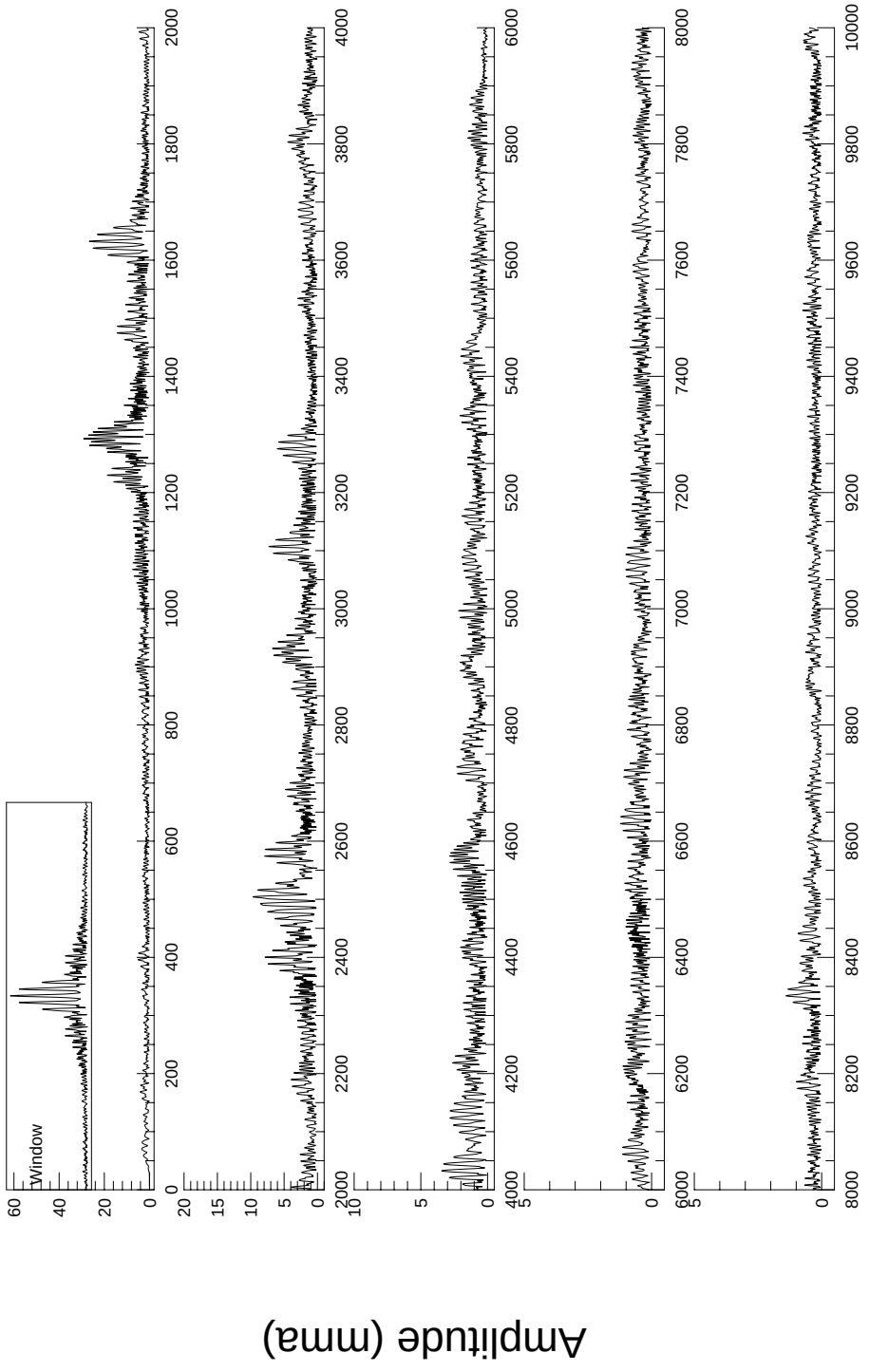

Fig. B.29.— The FT for the November 1993 data on G29–38.

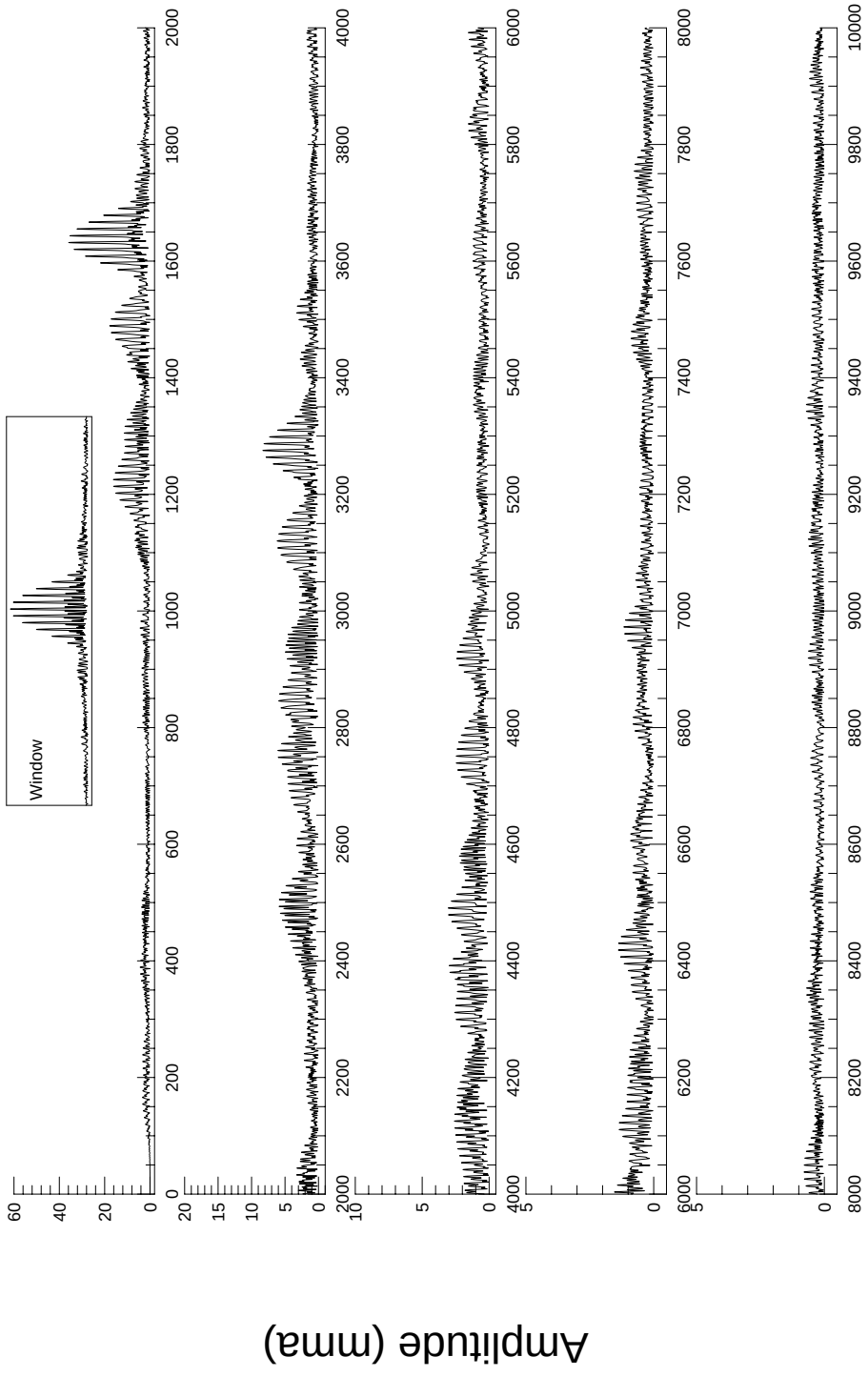

Fig. B.30.— The FT for the December 1993 data on G29–38.

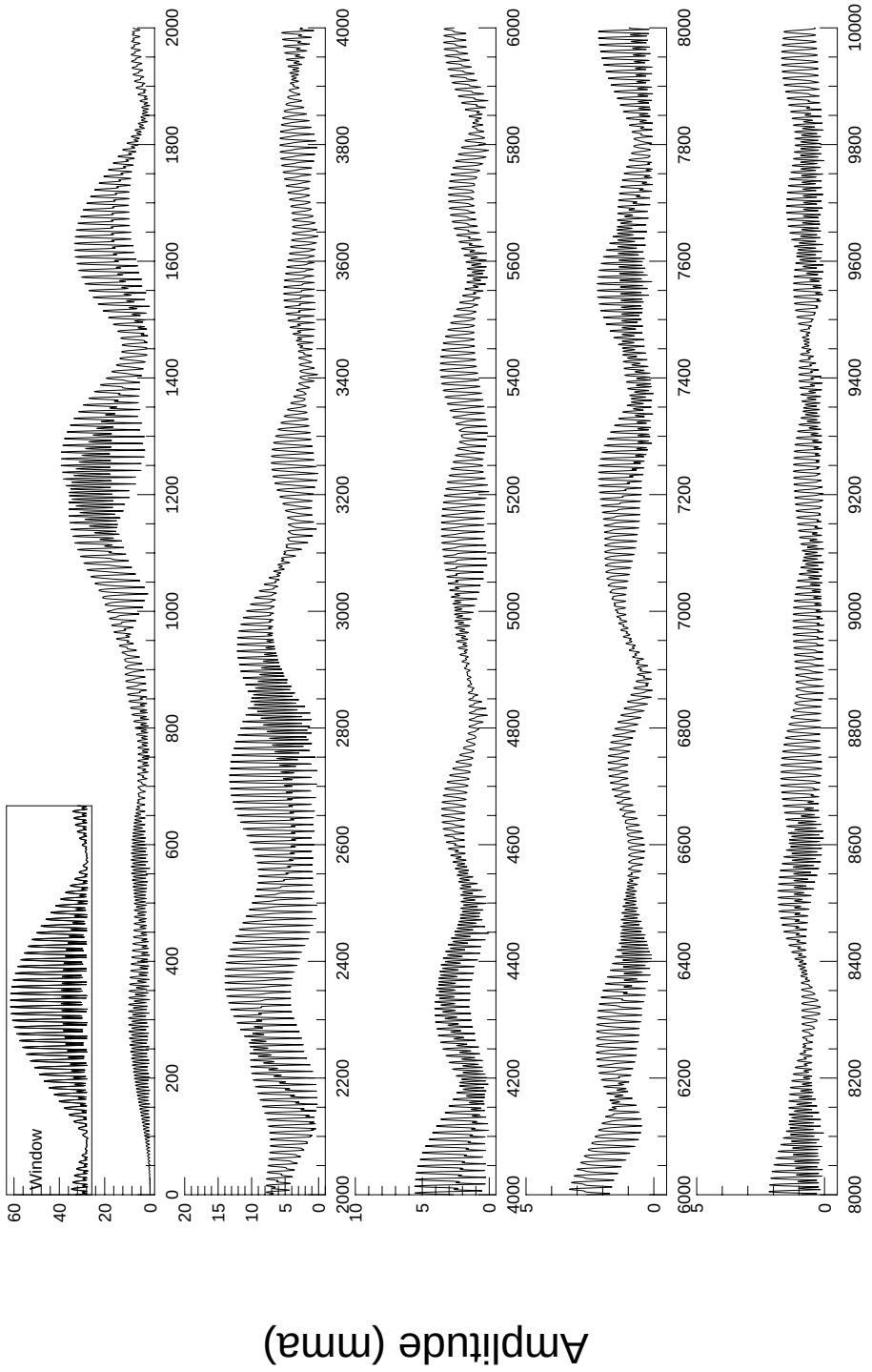

Fig. B.31.— The FT for the May 1994 data on G29–38.

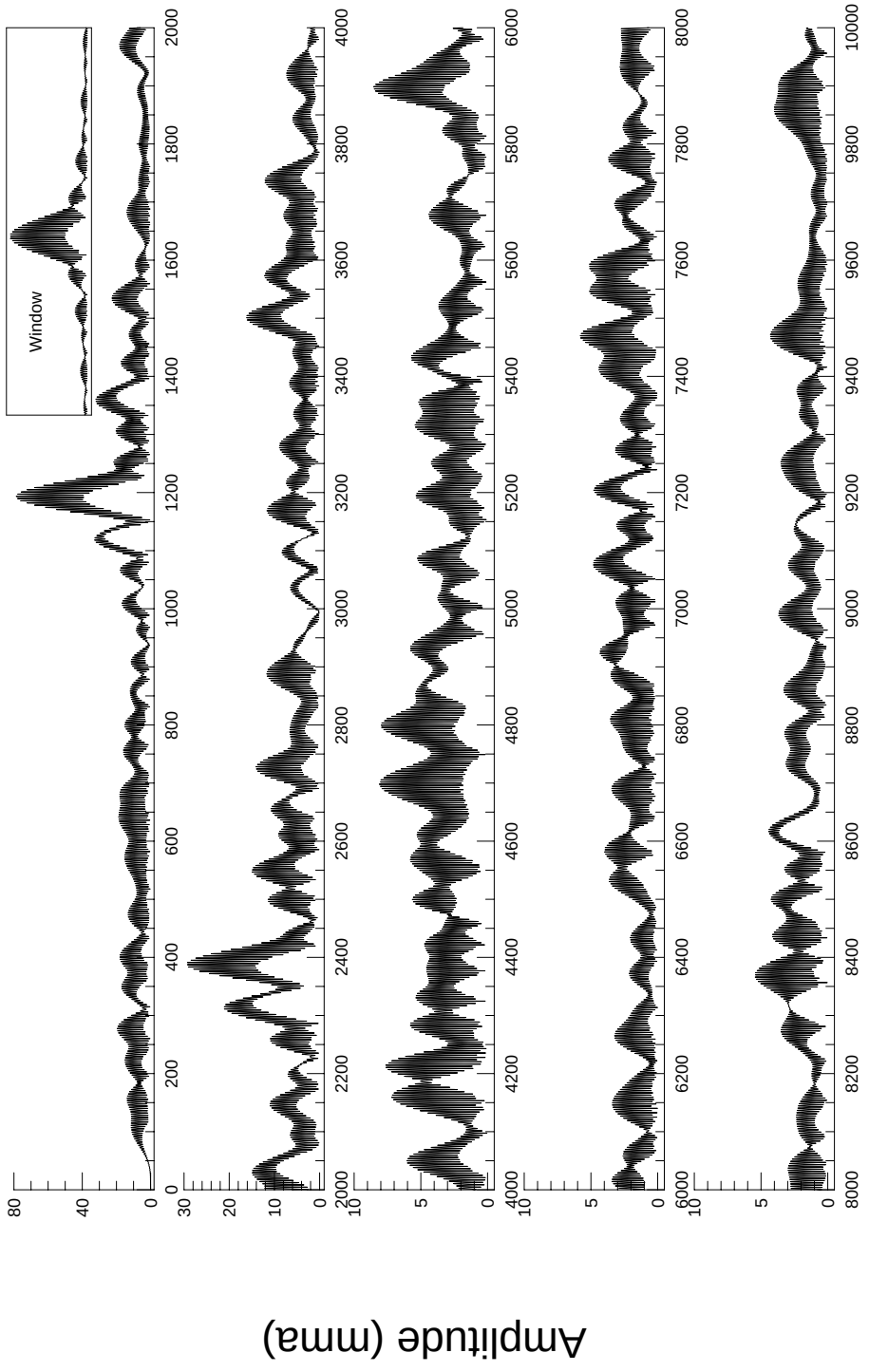

Fig. B.32.— The FT for the January 1991 data on G191–16.

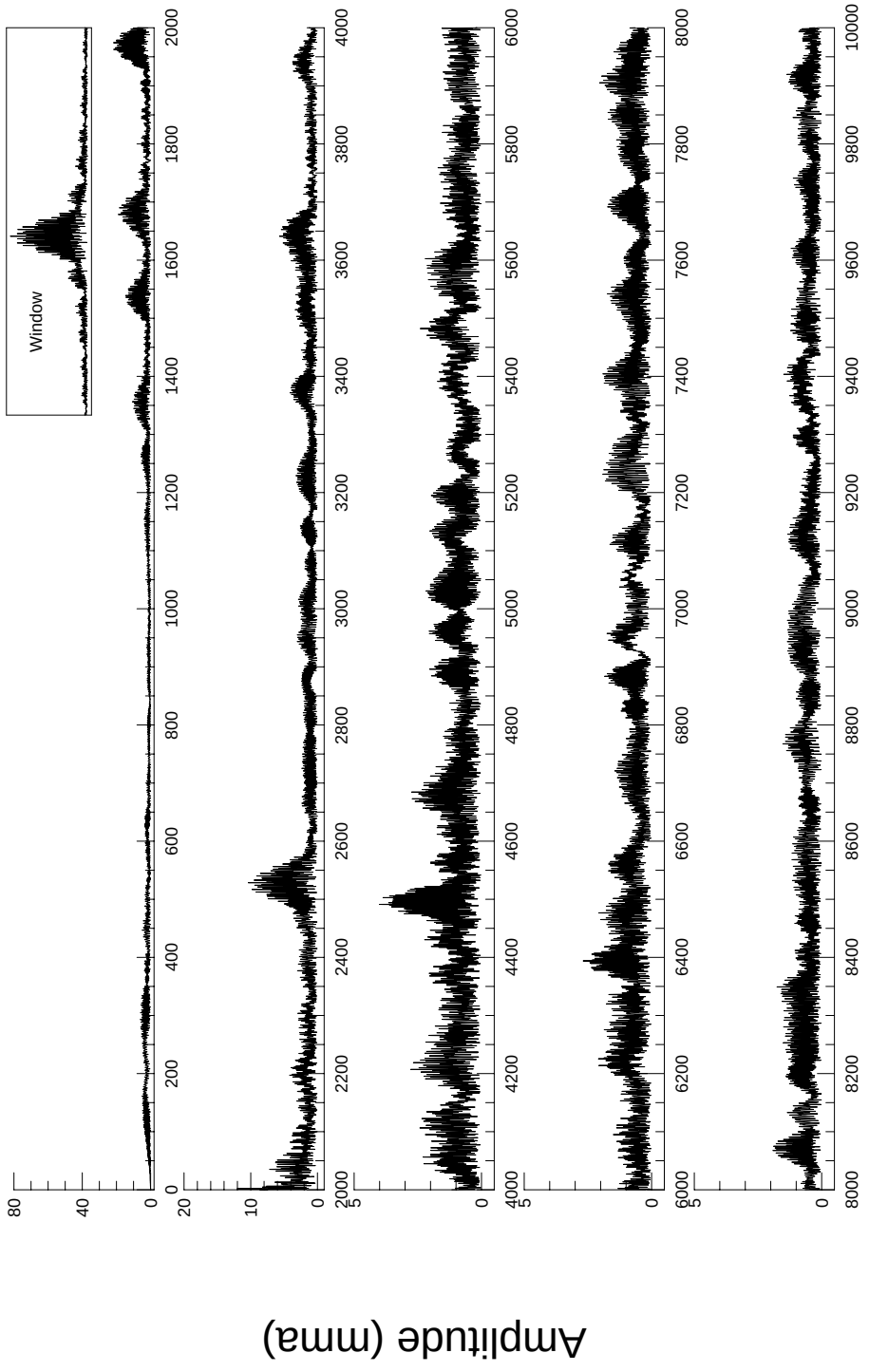

Fig. B.33.— The FT for the February 1994 data on G191–16.

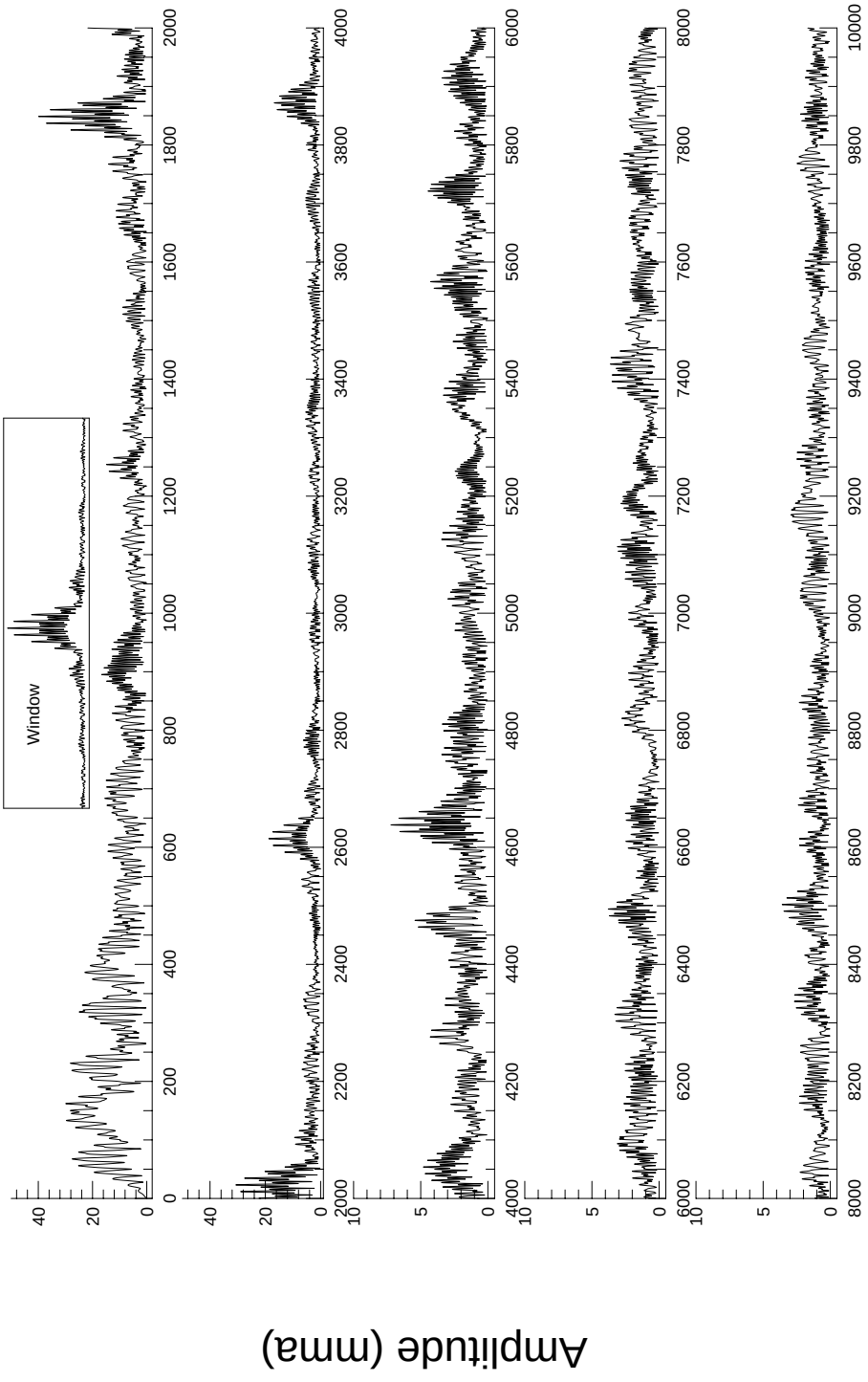

Fig. B.34.— The FT for the December 1990 data on HL Tau 76.

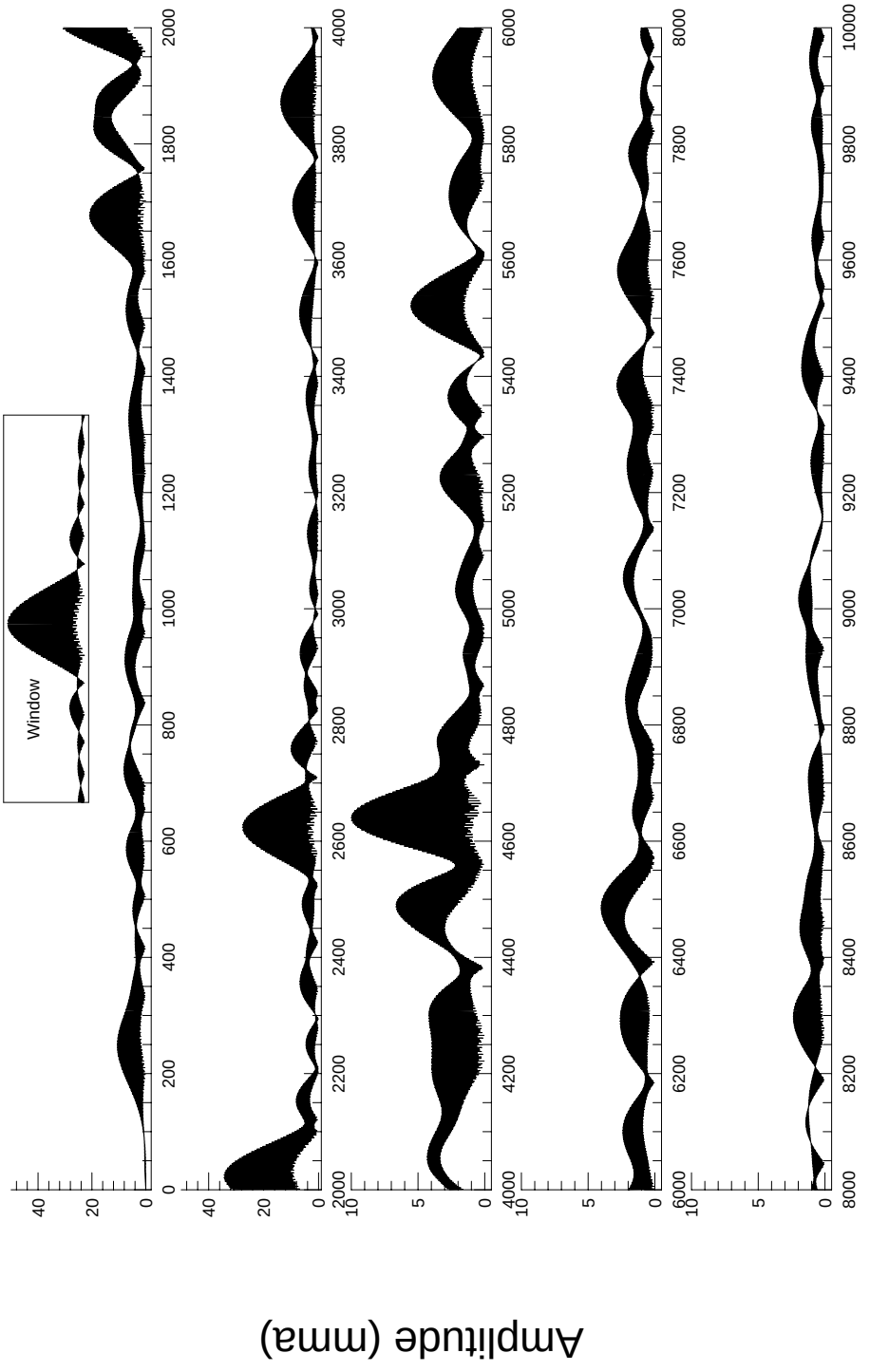

Fig. B.35.— The FT for the January 1992 data on HL Tau 76.

Bibliography

Barnbaum, C., and Zuckerman, B., 1992 ApJ, 396, L31

Bergeron, P., Wesemael, F., Fontaine, G., & Liebert, J., 1990, ApJ, 351, L21

Bergeron, P., et al., 1995, ApJ, 449, 258

Bradley, P.A., 1993, Ph.D. Thesis, University of Texas at Austin

Bradley, P.A., Winget, D.E., 1994, ApJ, 421, 236

Bradley, P.A., 1995, ApJ, in press

Brassard, P., Fontaine, G., Wessemael, F., & Talon, A., 1993, in White Dwarfs: Advances in Observations and Theory, ed., M.A. Barstow (Dordrecht:Kluwer), 485

Brickhill, A.J., MNRAS, 259, 529

Chlebowski, T., 1978, Acta Astron., 28, 441

Clemens, J. C., Nather, R.E., 1987, BAAS, 19, 1130

Clemens, J.C., et al., 1992, ApJ, 391, 773

Clemens, J.C., 1993, Baltic Astronomy, 2, 407

Clemens, J.C., 1994, Ph.D. Thesis, University of Texas at Austin

Deeming, T.J., 1975, Ap&SS, 36, 137

Dolez, N., Vauclair, G., & Koester, D., 1991, in White Dwarfs, ed., G. Vauclair & E. Sion (Dordrecht:Kluwer). 361

Dziembowski, W.A., 1977, Acta Astron., 27, 203

Dziembowski, W.A., 1982, Acta Astron., 32, 147

Graham, J. R., Matthews, K., Neugebauer, G., Soifer, B. T., 1990a, ApJ, 357, 216

Graham, J. R., McCarthy J. K., Reid, I. N., Rich, R. M., 1990b, ApJ, 357, L21

Grauer, Albert D., Bond, Howard E., 1981, ApJ, 93, 388

Greenstein, J. L., 1988, AJ, 95, 1494

Handler, G., 1995, private communication

Harrington, R.S., Dahn, C.C., 1980, AJ, 85, 454

Harrington, R.S., et al., 1985, AJ, 90, 123

Holm, Albert V., et al., 1985, ApJ, 289, 774

Johnson, H., 1962 in *Astronomical Techniques*, ed. A. Hiltner, (U. Chicago Press)

Jones, Philip W., Pesnell, W. Dean, Hansen, Carl J., Kawaler, Steven D., 1987, ApJ, 336, 403

Kawaler, Steven D., Bradley, Paul A., 1994, ApJ, 427, 415

Kawaler, Steven D., et al., 1994, ApJ, 107, 298

Kepler, S.O., et al., 1991, ApJ, 378, L45

Kepler, S.O., 1993, Baltic Astronomy, 2, 444

Kepler, S.O., Nelan, E.P., 1993, AJ, 105, 608

Kepler, S.O., et al., 1995, submitted to Baltic Astronomy

Kleinman, S. J., 1990, Master's Thesis, Univ. Texas at Austin

Kleinman S. J., et al., 1994, ApJ, 436, 875

Landolt, A.U., 1968, ApJ, 153,151

Ledoux, P. & Walraven, Th., 1958, Handbuch der Physik, 51, 353

Liebert, J., Dahn, C.C., & Monet, D.G., 1988, ApJ, 332, 891

Liebert, J., Saffer, R. A., Pilachowski, C. A., 1989, AJ, 97, 182

McGraw J. T., and Robinson E. L., 1975, ApJ, 200, l89

McGraw, J.T., 1977, Ph.D. Thesis, Univ. Texas

Michlovic, Joe, 1972, Applied Optics, v.11, no.2, 490

Nather, R. Edward, Warner, Brian, 1971, MNRAS, 152, 209

Nather, R.E., 1973, Vistas in Astronomy, 15, 91

Nather, R.E., Robinson, E.L., & Stover, R.J., 1981, ApJ, 244, 269

Nather, R. E., Winget, D. E., Clemens, J. C., Hansen, C. J., Hine, B. P., 1990, ApJ, 361, 309

O'Donoghue, D., Warner, B., 1982, MNRAS, 200, 563

O'Donoghue, D., Warner, B., 1987, MNRAS, 228, 949

Pesnell, W.D., 1985, ApJ, 292, 238

Robinson, E.L., Kepler, S.O., Nather, R.E., 1982, ApJ, 259, 319

Robinson, E.L., 1984, AJ, 89, 1732

Saio, Hideyuki, 1981, ApJ, 244, 299

Scargle, Jefferey D., 1982, ApJ, 263, 835

Schwarzschild, Bertram, 1995, Physics Today, 48, 5, 19

Shipman, Harry L., 1979, ApJ, 228, 240

Shulov, O. S., and Kopatskaya, E. N. 1974, Astrofizika, 10, 117

Stringfellow, Guy S., Black, David C., & Bodenheimer Peter, 1990, ApJ, 349, L59

Telesco, C. M., Joy, M., Sisk, C., 1990, ApJ, 358, L17

Tokunaga, A.T., etal., 1988, ApJ, 332, L71

Tokunaga, A. T., Becklin, E. E., Zuckerman, B., 1990, ApJ, 358, L21

Unno, W., Osaki, Y., Ando, H., Shibahashi,H., 1979, Nonradial Oscillation of Stars, (Tokyo: Univ. of Tokyo Press)

Unno, W., Osaki, Y., Ando, H., Saio, H., Shibahashi, H., 1989, Nonradial Oscillations of Stars, (2nd ed.; Tokyo: Univ. of Tokyo Press)

Vauclair, G., Goupil, M.J., Baglin, A., Auvergne, M., Chevreton, M., A&A, 215, L17

Vauclair, G., et al., 1993, A&A, 267, L35

Watson, T.K., 1992, IAU Circular # 5603

Werner, K., Heber, U., & Hunger, K., 1991, A&A, 244, 437

Winget, D.E., Van Horn, H.M., & Hansen, C.J., 1981, ApJ, 245, L33

Winget, D.E., Robinson, E.L., Nather, R.E., & Fontaine, G., 1982, ApJ, 262, L11

Winget, D.E., et al., 1988, ApJ, 315, L77

Winget, D. E., 1988, in IAU Symp. 123, Advances in helio- and Asteroseismology, ed. J. Christensen-Dalsgaard & S. Frandsen (Dordrecht: Reidel), 305

Winget, D.E., et al., 1990, ApJ, 357, 630

Winget, D. E., 1991, in Proc. 7th European Workshop on White Dwarfs, ed. G. Vauclair & E. M. Sion, (NATO ASI Ser.), (Dordrecht: Kluwer), 129

Winget, D.E., et al., 1991, ApJ, 378, 326

Winget, D.E., et al., 1994, ApJ, 430, 839

Wood, M.A., 1990, Ph.D. Thesis, University of Texas at Austin

Zuckerman, B. and Becklin, E. E., 1987, Nature, 330, 138

Vita

I, Scot James Kleinman, was born on 29 July 1965, in San Mateo, California to Joann Lee and Bruce Roy Kleinman and grandparents Art and Fran Smothers and Raymond and Martha Kleinman. I graduated from the same high school as my mother, Hillsdale High in San Mateo, in 1983 and proceeded to a small, unknown private college named Harvey (*not* Harry) Mudd. From there I received a B.S. in Physics with a minor in Spanish. I also started observing at Table Mountain Observatory with (William) Sandy Sandmann, doing mostly photometry of flare and spotted stars. During this time, I worked at NASA/Ames during breaks with Bill Borucki and Lori Allen on a project to detect extra-solar planets. I also spent a summer working in Geneva, Switzerland thanks to trustee Dudley Wright. I came to the University of Texas at Austin Astronomy Department in 1987 and stumbled across the beginnings of the Whole Earth Telescope. Since that time, I have travelled to 6 continents in the guise of science and somehow still managed to finish this work. And now, there's *Nothing left to do, but smile, smile, smile.*

Permanent address: 611 9th ave.
San Mateo, CA 94402

This dissertation was typeset with LaTeX[‡] by the author.

[‡] LaTeX is a document preparation system developed by Leslie Lamport as a special version of Donald Knuth's TeX Program.